1972

Elastic and inelastic analysis of pretensioned cable-roof structures.

T. Kumanan
University of Windsor

ELASTIC AND INELASTIC ANALYSIS OF PRETENSIONED CABLE-ROOF STRUCTURES

BY

T.KUMANAN

A Dissertation
Submitted to the Faculty of Graduate Studies in Partial
Fulfillment of the Requirements for the Degree of
Doctor of Philosophy in Civil Engineering
At Univeristy of Windsor

Windsor, Ontario, Canada

1971

ABSTRACT

Equations have been derived to determine the displacements and tensions under load, of a general non-orthogonal cable network with reference to a set of oblique axes. The derivation is based on the displaced geometry of the structure and second-order displacement terms are included. The Newton-Raphson method is suitably adapted for the solution of the resulting nonlinear equations. A theoretical model for the material stress-strain curve is used to simulate the material behaviour in the elastic and inelastic regions.

The general behaviour of cable networks having hyperbolic paraboloid shapes is studied in the elastic and inelastic regions and their ultimate capacities are determined. Numerical investigations have been carried out for two types of roofs: (i) a simple hyperbolic paraboloid shape formed by two non-orthogonal sets of cables and referred to as a 'single-roof'; (ii) a compound shape formed by two hyperbolic paraboloids of two orthogonal sets of cables and referred to as a 'double roof'. The theoretical solutions are substantiated by experimental results obtained by testing models of cable networks.

From this study the following conclusions can be drawn:

(1) Linearized equations are inadequate to predict actual

cable-network behaviour. The linear solution does not always give a conservative estimate of the true values. It can also underestimate the deflections and tension changes in some cases.

(2) The use of a high pretension decreases the deformations considerably without significantly increasing the final tensions. The use of a higher pretension in the prestressing cables is also shown to result in efficient use of the cables.

(3) When the network is non-orthogonal, the deflections are increased, whereas the cable-tensions remain practically unchanged.

(4) The elastic and inelastic behaviour and the ultimate capacity are considerably influenced by the slope of the roof structure. It is shown that there exists a critical roof height at which the tension changes are maximum. On the basis of this definition, roofs can be classified as flat and steep. The steep slope is advantageous to use in practice since the deflections and tension changes are small and drainage is easy; although its ultimate capacity is not large, its factor of safety against failure is quite high in comparison to a conventional structure and therefore its use is justified.

(5) By a comparison of a non-orthogonal single roof and an orthogonal double roof covering the same area in plan, it is found that the latter has a higher ratio of load

intensity to amount of steel used in the net.

(6) Theoretical solutions of practical roofs with very large number of joints may be obtained by analyzing an equivalent sparser net without much loss of accuracy.

(7) Good agreement between theory and experiment indicates that the procedure developed herein could be used successfully when the nonlinearity is high or when a discontinuity occurs in the structure.

ACKNOWLEDGEMENTS

The writer wishes to express his sincere gratitude to his supervisor Dr. J. B. Kennedy for his valuable guidance throughout the duration of this study. The helpful suggestions of the other members of the thesis committee are also appreciated.

Thanks are also due to the laboratory technicians in the Department of Civil Engineering for their assistance in the experimental work and to the Computer Centre for providing the many hours of computer time required for the theoretical analysis.

The writer is also grateful for the financial assistance provided by the Canadian Commonwealth Scholarship Committee in the form of a Commonwealth Scholarship and wishes to thank the Government of Ceylon for selecting him for this award. The financial assistance provided by the University of Windsor during the completion of this study is also very much appreciated.

Finally, the writer would like to thank his wife Imayam and daughter Kothai for their patience and moral support during the past years.

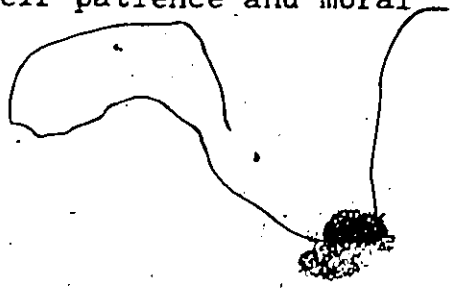

TABLE OF CONTENTS

LIST OF FIGURES

LIST OF TABLES

LIST OF PHOTOGRAPHS

List of Symbols

A	- Effective area of cross-section of cable.
A_ξ, A_η	- Area of cross-section of cable in the ξ and η directions.
α	- Angle made by cable with the ξ direction.
β	- Angle made by cable with the η direction.
γ	- Angle made by cable with the z direction.
c, f, g	- Constants in the theoretical equation for stress-strain curve (equation 2-26).
C_1, C_2, C_3	- Constants defined in equation 2-35.
D	- Deflection.
$\delta\alpha$, $\delta\beta$, $\delta\gamma$	- Increments in angles α, β, γ
$\delta\xi$, $\delta\eta$, δz	- Displacements.
$\delta\delta\xi$, $\delta\delta\eta$, $\delta\delta z$	- Increments in displacements $\delta\xi$, $\delta\eta$, δz
δl	- Change in length.
δx, δy	- Increments in x, y.
δT_{ij}	- Tension increment.
Δ	- Displacement matrix.
e	- Thermal coefficient of expansion.
E	- Elastic modulus.
ϵ	- Strain.
ϵ_p, ϵ_y, ϵ_u	- Strain at proportional limit, yield and ultimate stress.
ξ, η	- Oblique coordinates.
H	- Horizontal component of cable tension.
H_ξ, H_η	- Horizontal components of cable tensions in the ξ, η directions.

i, j	- Joint numbers.
l	- Length of cable segment.
λ, μ	- Defined in equations (2-16).
NJ	- Number of joints.
NTYP	- Type of roof as defined in section 3.1.2.
INDS	- No. of internodes as defined in section 3.1.2.
$P_{i\xi}$, $P_{i\eta}$, P_{iz}	- Loads in ξ, η, z directions.
R	- Ratio of sides.
R_r	- Residual matrix in the r^{th} cycle.
S_r	- Stiffness matrix in the r^{th} cycle.
S_1, S_2	- Matrices of linear and nonlinear terms.
σ	- Stress.
σ_p, σ_y, σ_u	- Proportional limit, yield stress and ultimate stress.
t	- Temperature change.
T	- Cable tension.
θ	- Angle between y and η axes.
x, y, z	- Cartesian coordinates.

CHAPTER I

INTRODUCTION

1.1 General

1.1.1 Cable Structures - Their Utilization in Modern Building Design

The suspended cable has been almost exclusively used in bridge construction until two decades ago. The cable in the form of rope and chains was used in suspension bridges in China and the Far East even before their history was recorded (11). During the last two centuries it has been used in modern suspension bridges. Even though the world's longest bridges were built with suspension cable as the primary load carrying member, the use of the cable in building design was limited to only temporary structures such as tents. The State Fair Arena at Raleigh, North Carolina was the first major cable roof structure in the United States when it was completed in 1953. Since then several roofs of this type have been built in the United States and in Europe.

The cable structure has a number of advantages over the conventional form of construction. One is its esthetic value - it offers an infinite number of forms and shapes. Another advantage is that it is more economical than conventional structures since the load is carried in pure tension thereby utilizing the entire cross-section of the cable to

the maximum. The economy is enhanced by the use of high-tensile steel in the manufacture of cables and the very light self-weight of the roof when constructed. The West German Pavilion at Expo '67, Montreal was covered with a cable roof whose self-weight was only 1½ psf. (37). Cable roofs also make very long spans possible and provide an unobstructed interior which makes them suitable for large exhibition halls and sport stadiums.

The cable roof, like any other structure, has its disadvantages too. Its inherent flexibility makes it deform considerably under load. This change in geometry, itself undesirable in a structure, also makes the theoretical analysis complicated. With the development of numerical methods and the use of modern high-speed electronic computers, it is now possible to analyze cable roofs and design them economically. Cable roofs are more susceptible to wind forces than conventional structures. Prestressing of cables decreases the possibility of flutter in cable roofs (35). Cable roofs require heavy anchorages to transfer the tensile forces to the ground and often what is gained in the actual roof may be lost in the anchorages. But the supporting frame could be judiciously designed to take up most of these forces. For example, in the circular bowl-shaped roof covering the entertainment centre at Madison Square Garden, New York, the inner and outer rings to which the cables were anchored, were designed as tension and compression rings respectively.

1.1.2 Classification of Cable Roofs

Cable roofs may be broadly classified into two groups: (i) Cable-suspended roofs, and (ii) cable-supported roofs. In cable-suspended roofs, the cables carry the load directly. The roof may or may not be stiffened by flexural members but the primary load-carrying members are the cables themselves. In cable-supported roofs, cables are used as supplemetary support to rigid members carrying the load. Such a structure is an office building in Vancouver, B.C., where cables, suspended from a central core, support the cantilevering floors and roof (22). Roofs known as 'bubbles' supported mainly by airpressure (49), may also be classified in this category when they use a cable network as supplementary support. The difference between cable-suspended and cable-supported roofs may be likened to that between suspension bridges and cable-stayed bridges.

The cable-suspended roofs can be further classified into the following:

(i) Single curvature roofs with single set of cables

Catenary roofs fall into this category (Fig. 1-1a). These roofs have little resistance to wind and require heavy roof decking to eliminate flutter. Sometimes the rigidity is increased by prestressing the roof decking by applying a temporary load while precast concrete elements are kept in place and the space between adjacent panels are filled with concrete. The passenger terminal at Dulles International Airport in Virginia, U.S. is an example of this type of

construction.

(ii) Single-curvature roofs with double set of cables

In this case, the two sets of cables are prestressed against each other with uniformly spaced ties (Fig. 1-1b) or struts (Fig. 1-1c) between them. This arrangement is called a cable-truss and is generally known as the Jawerth system. The prestressing of the cables, stiffens the roof and also eliminates flutter due to the damping effect of the secondary cables (89).

(iii) Double-curvature roofs with positive Gaussian curvature

Bowl-shaped circular roofs with a single set of cables placed radially in vertical planes belong to this category (Fig. 1-1d). This type also has a low resistance to flutter unless the roof deck is prestressed as mentioned in (i) in which case it acts like an inverted dome. Instead of a single set of cables, cable trusses may also be used (Fig. 1-1e). This will reduce the chances of flutter. Bowl-shaped roofs may also be formed with rectangular or other boundaries with two sets of cables intersecting to form a network (Fig. 1-1f). The two sets of cables, cannot be prestressed against each other and the rigidity of the system will depend on the weight of the deck and the cables. Another disadvantage with all bowl-shaped roofs is their drainage which invariably has to be provided at the centre of the roof.

(iv) Double-curvature roofs with negative Gaussian curvature

This group consists of what is commonly known as saddle-

shaped roofs with two sets of cables intersecting systematically (Fig. 1-1g) to form a network. The advantage here is that the two sets of cables can be prestressed against each other without the necessity for temporarily applied loads. Numerous different shapes can be formed with these roofs by varying the boundary frame and the prestress in the cables. The boundary itself is a space frame and the two sets of cables may be either orthogonal or non-orthogonal. With proper boundary and pretensions, hyperbolic paraboloid shapes may be obtained with this roof. Orthogonal hyperbolic paraboloid roofs are commonly constructed with a square plan-form. A square or a rectangular plan-form may not be very economical from a point of view of transmitting the anchorage forces, unlike the circular plan-form where most of the anchorage forces are balanced internally. Nevertheless, a rectangular boundary frame may be designed as a closed rigid frame capable of resisting bending moments. Sometimes the thrusts are transmitted to the ground by means of anchor cables or even some part of the structure such as spectator stands etc.

1.2 Literature Survey and Review of Prior Work

One of the most valuable references on the subject of cable-roof structures is 'Hanging Roofs', the proceedings of the IASS Colloquium on Hanging Roofs, Continuous Metallic Shell Roofs and Superficial Lattice Roofs held in Paris in July 1962 (26). This consists of a collection of papers on cable-roof design and theory presented at the colloquium and

represents a comprehensive survey of the knowledge that existed on cable roofs prior to 1962. A more recent survey of the state of cable-suspended roof construction has been published as a report entitled 'Cable-Suspended Roof Construction State-of-the-Art' by a subcommittee on Cable-suspended Structures of the American Society of Civil Engineers (13). This report deals with the existing knowledge on the shapes of suspension systems, the structural analysis of suspension systems, the manufacture of wire cables and their physical properties and the design and erection of cable-suspended structures. A complete bibliography on all aspects of the structural applications of steel cable systems to 1969 has been compiled by Shore and Chaudhari and published by the American Iron and Steel Institute (4).

Methods of analyzing a single isolated cable due to changes in loading have long been available. Papers on single cable analysis published recently are by Buchanan (17), Jennings (40), Michalos and Birnstiel (50), O'Brien (54, 55) and O'Brien and Francis (56). Work on cable-roof structures can be grouped into two categories - cable trusses and cable nets. Studies on cable trusses have been published by Buchholdt (20, 21), Krishna and Sparkes (46, 47), Poskitt (58) and Zetlin (89).

Several studies on cable networks have been published but they have almost exclusively been on orthogonal networks of hyperbolic paraboloid shape and based on linearly-elastic material behaviour. The equations to determine the initial

unloaded shape of an orthogonal hyperbolic paraboloid cable net were derived in a paper by Siev and Eidelman (71). Those for a non-orthogonal cable net were derived by the writer (48) with respect to an oblique set of coordinate axes.

Siev and Eidelman also published a paper (72) which described an approximate method of analysis of prestressed roofs, neglecting the horizontal displacements [redacted]ints. Another paper by Siev (67) gave a general method taking the horizontal displacements into account. The equations derived in both cases were linear and a correction for nonlinearity by iteration using the force imbalance at the joints, was suggested. Similar linearized equations based on a system of oblique coordinates were derived by the writer (48) for non-orthogonal nets with and without the horizontal displacements taken into account. Correction for nonlinearity was applied by an incremental load method and by an iterative method where the calculations were based on a configuration which is half-way between the initial and deformed configurations. The difference between solutions obtained by the approximate iterative method and the more accurate incremental load method was small.

Thornton (77) derived equations for a general three-dimensional unstiffened suspension structure and presented two numerical methods, the method of continuity and an incremental load method for the solution of the resulting non-linear simultaneous algebraic equations. In the method of continuity, the nonlinear set of simultaneous algebraic

equations were transformed into a set of nonlinear differential equations that was numerically integrated. The incremental load method consisted of increasing the applied loads incrementally and solving the equations at each step by means of an iterative technique. During the iteration, the nonlinear terms were added to the load vector and using this an improved solution was obtained. Thornton also presented numerical studies of isolated cables, counter-stressed dual cable structures and an orthogonal prestressed net. His dissertation (76) included studies on suspension systems stiffened by an orthogonal gridwork of flexural members in addition to studies presented in his paper.

Buchholdt (18, 19) developed a theory for prestressed cable-nets based on the minimization of the total potential energy and solved the resulting equations by the method of steepest descent. Avent (7) used a field analysis for structural nets and a walk-through method to solve them. As opposed to the discreet method used by the authors hitherto mentioned, Bathish (9) used a continuous method, treating the cable network as a membrane without shear rigidity. He assumed a deflection function in the form of a double Fourier series to solve the governing differential equations.

The methods of analysis of suspension structures reviewed above were based on the assumption of linearly-elastic material behaviour. However, very little work has been done on cable-suspended structures stressed into the inelastic region or with nonlinear material properties. A dissertation

by Greenberg (32) is the first known published work on cable-roofs including nonlinear material properties. He assumed a second-degree parabola between the origin and a strain of 1.8% with an initial modulus of 25,000 ksi reducing to one-tenth its value at the latter strain. Between this point and the assumed ultimate strain of 3%, the modulus remained constant. In a subsequent paper (31), Greenberg improved the theoretical model he used to represent the material stress-strain curve. He used a compound curve which is initially linear up to the elastic limit followed by an exponential curve to the ultimate stress at which point the modulus reduced to zero. It does not appear, however, that in either case the effect of unloading in the inelastic region (when the modulus will be different from that during loading) has been taken into account. Hence the method is applicable only when the components are subjected to monotonically increasing loads in the inelastic region.

Jonatowski and Birnstiel (41) presented a numerical procedure for determining the inelastic behaviour of three-dimensional suspension structures. They used a continuous smooth curve fitted to test results for the cable stress-strain relationship. Like Greenberg, they used a load-increment procedure and determined the ultimate capacity as the load at which the first cable ruptures. While Greenberg's study was limited only to orthogonal cable-nets, Jonatowski and Birnstiel presented numerical studies of both stiffened and unstiffened suspension structures. They also included the

effect of strain reversal in the inelastic region of cables. However, this effect was not considered for the flexural members used in the stiffening frameworks.

Saafan (59) also included nonlinear material behaviour in his study of suspension roofs. The stress-strain curve used by Saafan has a variable modulus with an unspecified equation between stresses of approximately 160 ksi and 207 ksi, the former being the elastic limit. There appears to be a discontinuity at the latter stress with the modulus remaining zero thereafter until the ultimate stress.

Several papers have also been published on experimental studies of cable roof models. Krishna (42) has tested a small scale model of a counter-stressed cable-truss. In a recently published paper (43), Krishna and Agarwal reported the testing of a model of an orthogonal hyperbolic paraboloid net. Siev published the experimental study (70) of a model of a prestressed suspended roof bounded by main cables. The writer tested a model of a non-orthogonal net (48). Results of experimental study on orthogonal nets by Bathish has been presented in his dissertation (9).

Although an appreciable amount of work has been done on the behaviour of cable roofs under static loads, very little work has been carried out to determine its dynamic behaviour. Zetlin (89) described a procedure by which flutter in cable suspended roofs constructed with cable-trusses could be eliminated. The paper did not deal mathematically with the behaviour of a suspension roof during flutter. A few

studies on the vibration of cable networks and the determination of their natural frequencies have been reported (33, 73). Siev has performed an experimental study of flutter in suspended roofs and concluded that flutter was likely in structures of daring design. He also concluded that a closed structure was safer than an open one. While no adequate procedures are available to determine the frequencies of forced and free vibrations of cable-suspended roofs, it is also not possible to avoid close-to-resonance frequencies by designing since data on dynamic wind loading is presently insufficient to specify what frequencies to avoid (13).

1.3 Objective of the Present Study

The displacement equations developed by authors such as Siev and Thornton (67, 76) for cable networks are general and could theoretically be used for any kind of nets. However, the use of these equations becomes cumbersome when applied to non-orthogonal nets, where the two sets of cables intersect at an angle other than a right angle. This is probably why the numerical studies hitherto published are almost exclusively on orthogonal nets. On the other hand, equations derived with respect to an oblique set of axes coinciding with the directions of the cables in plan are convenient to use with non-orthogonal nets. Once these equations are derived, the study of orthogonal nets becomes a special case where the angle between the two sets of cables is a right angle. One

objective of the present study is to derive such equations. A linearized form of these equations were derived by the writer in a previous work (48). In this dissertation, these equations are derived taking the nonlinear terms into account. The Newton-Raphson method is adapted to provide convenient numerical solution of the equations in a manner similar to that shown by Poskitt for cable trusses.

In hyperbolic paraboloid roofs with cables running diagonally in two directions, the network is orthogonal when the plan shape is a rhombus or a square. When the area to be covered is a rectangle or a less common parallelogram, the cables are no longer orthogonal. Using the equations derived for such non-orthogonal roofs, an attempt is made to study their behaviour since very little work has been done in this direction. Furthermore, a more in-depth investigation is undertaken into the behaviour of hyperbolic paraboloid roofs in general by means of parametric studies. Since not much work has been done on the inelastic behaviour of cable roofs (research confined to only orthogonal networks), the study is extended to include the inelastic behaviour and ultimate load capacities of general non-orthogonal networks. Unlike Greenberg's work on orthogonal networks (31,32), the actual material behaviour is simulated when strain-reversal takes place in the inelastic region.

The concept of a new compound roof-shape composed of two commonly used hyperbolic paraboloids is introduced here. The latter is referred to in this dissertation as the 'single'

roof (Fig. 1-2a) while the former is referred to as the 'double' roof (Fig. 1-2b). The double roof itself may be orthogonal or non-orthogonal. In practice it may, by itself, be used to replace a single roof, that is, to cover the same area that can be covered by a single roof or it may be extended to form a continuous multi-roof (Fig. 1-2c) consisting of several of such roofs connected together. A theoretical and experimental study of a double roof and its performance in comparison to the single roof is also included in this dissertation.

CHAPTER II

MATHEMATICAL FORMULATION

2.1 Nonlinear Displacement Equations for a General Non-orthogonal Cable Net

2.1.1 Introduction

The nonlinear displacement equations for a general non-orthogonal cable net consisting of two sets of cables intersecting at an angle of (90-θ), are derived in this section. The equation to determine the initial shape in the unloaded state of such a net was derived in reference (48) as,

$$H_{\xi}(z_{m,n+1}-2z_{m,n}+z_{m,n-1})+H_{\eta}(z_{m+1,n}-2z_{m,n}+z_{m-1,n}) = 0 \quad . \quad . \quad 2\text{-}1$$

where H_{ξ}, H_{η} are the horizontal component of the tensions in the ξ and η directions respectively and z's are the vertical ordinates.

It is seen that the vertical ordinates are independent of the non-orthogonality of the cables. It is dependent only on the ratio of the horizontal components of tensions in the two directions and the shape of the boundary frame. The derivation of equation (2-1) is given in Appendix (A). It is also shown that when the horizontal components of tensions in the two directions are equal, horizontal sections of the initial

shape are rectangular hyperbolas irrespective of the non-orthogonality of the cables.

2.1.2 Assumptions

The following assumptions are made in deriving the displacement equations:

(i) the cables are weightless and the applied load acts at the joints between cables. In cases where the weight of the cable becomes appreciable, it can be assumed to be concentrated at the joints as part of the dead load.

(ii) the cables are straight between joints and have constant cross-sectional area.

(iii) any change in cross-sectional area of the cables due to stressing is neglected.

(iv) the cables do not take any compressive or bending loads.

(v) the joints are perfectly smooth.

(vi) the material stress-strain relationship remains linear within the range of load considered. This assumption is good as long as the stress is below the proportional limit. When the proportional limit is exceeded, the load has to be applied in small increments to ensure reasonable accuracy.

2.1.3 Derivation

The displacement equations are derived from first principles considering the equilibrium of the system. Fig. 2-1 shows the equilibrium of a joint i in the initial and

displaced positions and Fig. 2-2 shows the plan of a cable segment between joints i and j. An oblique set of axes ξ and η has been used in the horizontal plane with an angle of $(90-\theta)$ between them, the same as the obliquity between the two sets of cables. The (x,y) coordinates and the (ξ,η) coordinates can be related by the equations,

$$x = \xi+\eta\sin\theta \qquad \ldots \quad 2\text{-}2a$$

$$y = \eta\cos\theta \qquad \ldots \quad 2\text{-}2b$$

Increments $(\delta x, \delta y)$ in the (x,y) coordinates can be related to increments $(\delta\xi, \delta\eta)$ in the (ξ,η) coordinates by,

$$\delta x = \delta\xi+\delta\eta\sin\theta \qquad \ldots \quad 2\text{-}3a$$

$$\delta y = \delta\eta\cos\theta \qquad \ldots \quad 2\text{-}3b$$

The initial direction cosines of the cable segments between joints i and j can be expressed by

$$\cos\alpha_{ij} = \frac{(\xi_j-\xi_i)+(\eta_j-\eta_i)\sin\theta}{l_{ij}} \qquad \ldots \quad 2\text{-}4a$$

$$\cos\beta_{ij} = \frac{(\eta_j-\eta_i)+(\xi_j-\xi_i)\sin\theta}{l_{ij}} \qquad \ldots \quad 2\text{-}4b$$

$$\text{Cos}\gamma_{ij} = \frac{(z_j - z_i)}{l_{ij}} \qquad \ldots 2\text{-}4c$$

where α_{ij}, β_{ij}, γ_{ij} are angles made by the cable segment with the ξ, η, z axes respectively and l_{ij} is the length of the cable segment.

The direction cosines in the displaced position are given by,

$$\text{Cos}(\alpha_{ij}+\delta\alpha_{ij}) = \frac{(\xi_j+\delta\xi_j-\xi_i-\delta\xi_i)+(\eta_j+\delta\eta_j-\eta_i-\delta\eta_i)\sin\theta}{l_{ij}+\delta l_{ij}} \qquad \ldots 2\text{-}5a$$

$$\text{Cos}(\beta_{ij}+\delta\beta_{ij}) = \frac{(\eta_j+\delta\eta_j-\eta_i-\delta\eta_i)+(\xi_j+\delta\xi_j-\xi_i-\delta\xi_i)\sin\theta}{l_{ij}+\delta l_{ij}} \qquad \ldots 2\text{-}5b$$

$$\text{Cos}(\gamma_{ij}+\delta\gamma_{ij}) = \frac{(z_j+\delta z_j-z_i-\delta z_i)}{l_{ij}+\delta l_{ij}} \qquad \ldots 2\text{-}5c$$

considering equation (2-5a), dividing the numerator and denominator of the right hand side by l_{ij} and substituting from equation (2-4a) we get,

$$\text{Cos}(\alpha_{ij}+\delta\alpha_{ij}) = \frac{\text{Cos}\alpha_{ij} + \dfrac{(\delta\xi_j-\delta\xi_i)+(\delta\eta_j-\delta\eta_i)\sin\theta}{l_{ij}}}{1+\dfrac{\delta l_{ij}}{l_{ij}}}$$

Since $(\frac{\delta l_{ij}}{l_{ij}})$ is small compared to 1, higher order terms involving it may be neglected. Taking the term $(1+\frac{\delta l_{ij}}{l_{ij}})$ to the numerator, expanding in a Taylor series and retaining only second order terms, we get,

$$\cos(\alpha_{ij}+\delta\alpha_{ij})=[\cos\alpha_{ij}+\frac{(\delta\xi_j-\delta\xi_i)+(\delta\eta_j-\delta\eta_i)\sin\theta}{l_{ij}}][1-\frac{\delta l_{ij}}{l_{ij}}+\tfrac{1}{2}(\frac{\delta l_{ij}}{l_{ij}})^2] \quad \ldots 2\text{-}6a$$

Similarly,

$$\cos(\beta_{ij}+\delta\beta_{ij})=[\cos\beta_{ij}+\frac{(\delta\eta_j-\delta\eta_i)+(\delta\xi_j-\delta\xi_i)\sin\theta}{l_{ij}}][1-\frac{\delta l_{ij}}{l_{ij}}+\tfrac{1}{2}(\frac{\delta l_{ij}}{l_{ij}})^2] \quad \ldots 2\text{-}6b$$

$$\cos(\gamma_{ij}+\delta\gamma_{ij})=[\cos\gamma_{ij}+\frac{(\delta z_j-\delta z_i)}{l_{ij}}][1-\frac{\delta l_{ij}}{l_{ij}}+\tfrac{1}{2}(\frac{\delta l_{ij}}{l_{ij}})^2] \quad \ldots 2\text{-}6c$$

Now, considering the equilibrium of joint i, the equations of equilibrium before loading, in the ξ, η and z directions respectively are,

$$\Sigma(T_{ij}\cos\alpha_{ij}) = 0 \quad \ldots 2\text{-}7a$$

$$\Sigma(T_{ij}\cos\beta_{ij}) = 0 \quad \ldots 2\text{-}7b$$

$$\Sigma(T_{ij}\cos\gamma_{ij}) = 0 \qquad \ldots 2\text{-}7c$$

where the summation is over all segments connecting joint i to adjoining joints j. The corresponding equations after loading are,

$$\Sigma[(T_{ij}+\delta T_{ij})\cos(\alpha_{ij}+\delta\alpha_{ij})]+P_{i\xi} = 0 \qquad \ldots 2\text{-}8a$$

$$\Sigma[(T_{ij}+\delta T_{ij})\cos(\beta_{ij}+\delta\beta_{ij})]+P_{i\eta} = 0 \qquad \ldots 2\text{-}8b$$

$$\Sigma[(T_{ij}+\delta T_{ij})\cos(\gamma_{ij}+\delta\gamma_{ij})]+P_{iz} = 0 \qquad \ldots 2\text{-}8c$$

where $P_{i\xi}$, $P_{i\eta}$, P_{iz} are the external loads acting at joint i in the ξ, η, z directions respectively, and δT_{ij} is the increment in T_{ij}.

Substracting equations (2-7) from (2-8), we get,

$$\Sigma[T_{ij}(\cos(\alpha_{ij}+\delta\alpha_{ij})-\cos\alpha_{ij})+\delta T_{ij}\cos(\alpha_{ij}+\delta\alpha_{ij})]+P_{i\xi} = 0. \qquad 2\text{-}9a$$

$$\Sigma[T_{ij}(\cos(\beta_{ij}+\delta\beta_{ij})-\cos\beta_{ij})+\delta T_{ij}\cos(\beta_{ij}+\delta\beta_{ij})]+P_{i\eta} = 0. \qquad 2\text{-}9b$$

$$\Sigma[T_{ij}(\cos(\gamma_{ij}+\delta\gamma_{ij})-\cos\gamma_{ij})+\delta T_{ij}\cos(\gamma_{ij}+\delta\gamma_{ij})]+P_{iz} = 0. \qquad 2\text{-}9c$$

Considering equation (2-9a) and substituting for $\cos(\alpha_{ij}+\delta\alpha_{ij})$ from equation (2-6a) we obtain,

$$\Sigma\Big[T_{ij}\Big\{\frac{(\delta\xi_j-\delta\xi_i)+(\delta\eta_j-\delta\eta_i)\sin\theta}{l_{ij}}\Big(1-\frac{\delta l_{ij}}{l_{ij}}+\tfrac{1}{2}\Big(\frac{\delta l_{ij}}{l_{ij}}\Big)^2\Big)$$

$$-\cos\alpha_{ij}\Big(\frac{\delta l_{ij}}{l_{ij}}-\tfrac{1}{2}\Big(\frac{\delta l_{ij}}{l_{ij}}\Big)^2\Big)\Big\}+\delta T_{ij}\Big\{\cos\alpha_{ij}$$

$$+\frac{(\delta\xi_j-\delta\xi_i)+(\delta\eta_j-\delta\eta_i)\sin\theta}{l_{ij}}\Big\}\Big(1-\frac{\delta l_{ij}}{l_{ij}}+\tfrac{1}{2}\Big(\frac{\delta l_{ij}}{l_{ij}}\Big)^2\Big)\Big]+P_{i\xi}=0 \qquad \ldots\ 2\text{-}10a$$

Now, the extended length of cable segment between joints i and j is given by,

$$(l_{ij}+\delta l_{ij})^2=(x_j+\delta x_j-x_i-\delta x_i)^2+(y_j+\delta y_j-y_i-\delta y_i)^2+(z_j+\delta z_j-z_i-\delta z_i)^2 \qquad \ldots\ 2\text{-}11a$$

and the original length is given by,

$$l_{ij}^2=(x_j-x_i)^2+(y_j-y_i)^2+(z_j-z_i)^2 \qquad \ldots\ 2\text{-}11b$$

Subtracting equation (2-11b) from equation (2-11a) we get,

$$2l_{ij}\delta l_{ij}+\delta l_{ij}^2=2(x_j-x_i)(\delta x_j-\delta x_i)+2(y_j-y_i)(\delta y_j-\delta y_i)$$

$$+2(z_j-z_i)(\delta z_j-\delta z_i)+(\delta x_j-\delta x_i)^2+(\delta y_j-\delta y_i)^2+(\delta z_j-\delta z_i)^2 \ldots\ 2\text{-}12a$$

The left hand side of equation (2-12a) can be written in the form,

$$l_{ij}^2 \frac{\delta l_{ij}}{l_{ij}}\left(2+ \frac{\delta l_{ij}}{l_{ij}}\right)$$

Since $\frac{\delta l_{ij}}{l_{ij}} << 2$ for steel cable, which is almost exclusively used in cable roof construction, the term $\frac{\delta l_{ij}}{l_{ij}}$ in the brackets can be neglected.

Equation (2-12a) can therefore be rewritten as,

$$\frac{\delta l_{ij}}{l_{ij}} = \frac{(x_j-x_i)(\delta x_j-\delta x_i)+(y_j-y_i)(\delta y_j-\delta y_i)+(z_j-z_i)(\delta z_j-\delta z_i)}{l_{ij}^2}$$

$$+ \frac{(\delta x_j-\delta x_i)^2+(\delta y_j-\delta y_i)^2+(\delta z_j-\delta z_i)^2}{2l_{ij}^2} \quad \ldots \text{2-12b}$$

Substituting now for x, δx, y, δy from equations (2-2) and (2-3) into equation (2-12b), we get,

$$\frac{\delta l_{ij}}{l_{ij}} = [(\xi_j-\xi_i+\eta_j\sin\theta-\eta_i\sin\theta)(\delta\xi_j-\delta\xi_i+\delta\eta_j\sin\theta-\delta\eta_i\sin\theta)$$

$$+(\delta\eta_j-\delta\eta_i)(\eta_j-\eta_i)\cos^2\theta+(z_j-z_i)(\delta z_j-\delta z_i)]\frac{1}{l_{ij}^2}+[((\delta\xi_j-\delta\xi_i)$$

$$+(\delta\eta_j-\delta\eta_i)\sin\theta)^2+(\delta\eta_j-\delta\eta_i)^2\cos^2\theta+(\delta z_j-\delta z_i)^2]\frac{1}{2l_{ij}^2} \quad \ldots \text{2-12c}$$

Simplifying and substituting from equations (2-4),

$$\delta l_{ij} = (\delta\xi_j-\delta\xi_i)\cos\alpha_{ij}+(\delta\eta_j-\delta\eta_i)\cos\beta_{ij}+(\delta z_j-\delta z_i)\cos\gamma_{ij}$$

$$+\frac{1}{2l_{ij}}[(\delta\xi_j-\delta\xi_i)^2+2(\delta\eta_j-\delta\eta_i)(\delta\xi_j-\delta\xi_i)\sin\theta+(\delta\eta_j-\delta\eta_i)^2+(\delta z_j-\delta z_i)^2] \quad \ldots 2\text{-}12d$$

The total extension δl_{ij} of the cable segment is made up of the extension due to the increase in tension and the thermal extension due to any change in temperature. Hence,

$$\delta l_{ij} = \frac{\delta T_{ij}}{EA} l_{ij} + etl_{ij} \quad \ldots 2\text{-}13$$

where E is the elastic modulus,

A is the area of cross-section

e is the coefficient of thermal expansion of the cable and t is the change in temperature.

With the substitution for δT_{ij} from equation (2-13), equation (2-10a) becomes,

$$\Sigma[T_{ij}\frac{(\delta\xi_j-\delta\xi_i)+(\delta\eta_j-\delta\eta_i)\sin\theta}{l_{ij}}+\frac{\delta l_{ij}}{l_{ij}}(EA(1+et)-T_{ij})\cos\alpha_{ij}+$$

$$\frac{(\delta\xi_j-\delta\xi_i)+(\delta\eta_j-\delta\eta_i)\sin\theta}{l_{ij}}-EAet\cos\alpha_{ij}+\frac{(\delta\xi_j-\delta\xi_i)+(\delta\eta_j-\delta\eta_i)\sin\theta}{l_{ij}}$$

$$-EA(1+\tfrac{1}{2}et)\left(\frac{\delta l_{ij}}{l_{ij}}\right)^2\cos\alpha_{ij}+\tfrac{1}{2}T_{ij}\left(\frac{\delta l_{ij}}{l_{ij}}\right)^2\cos\alpha_{ij}]+P_{i\bar{3}}=0 \quad . \quad . \quad 2\text{-}14$$

where third and higher order terms have been neglected.

Substituting now for δl_{ij} from equation (2-12d), rearranging terms and neglecting third and higher order terms, we obtain,

$$\Sigma\Big[\frac{(\delta\bar{3}_j-\delta\bar{3}_i)}{l_{ij}}\Big\{(EA(1+et)-T_{ij})\cos^2\alpha_{ij}+T_{ij}-EAet\Big\}$$

$$+\frac{(\delta\eta_j-\delta\eta_i)}{l_{ij}}\Big\{(EA(1+et)-T_{ij})\cos\alpha_{ij}\cos\beta_{ij}+(T_{ij}-EAet)\sin\theta\Big\}$$

$$+\frac{(\delta z_j-\delta z_i)}{l_{ij}}\Big\{(EA(1+et)-T_{ij})\cos\alpha_{ij}\cos\gamma_{ij}\Big\}$$

$$+\frac{(\delta\bar{3}_j-\delta\bar{3}_i)^2}{l_{ij}^2}\Big\{(EA(1+et)-T_{ij})\tfrac{3}{2}\cos\alpha_{ij}-(EA(1+\tfrac{et}{2})-\tfrac{T_{ij}}{2})\cos^3\alpha_{ij}\Big\}$$

$$+\frac{(\delta\eta_j-\delta\eta_i)^2}{l_{ij}^2}\Big\{(EA(1+et)-T_{ij})(\tfrac{1}{2}\cos\alpha_{ij}+\cos\beta_{ij}\sin\theta)$$

$$-(EA(1+\tfrac{et}{2})-\tfrac{T_{ij}}{2})\cos\alpha_{ij}\cos^2\beta_{ij}\Big\}$$

$$+\frac{(\delta z_j-\delta z_i)^2}{l_{ij}^2}\Big\{(EA(1+et)-T_{ij})\tfrac{1}{2}\cos\alpha_{ij}-(EA(1+\tfrac{et}{2})-\tfrac{T_{ij}}{2})\cos\alpha_{ij}\cos^2\gamma_{ij}\Big\}$$

$$+\frac{(\delta\xi_j-\delta\xi_i)(\delta\eta_j-\delta\eta_i)}{l_{ij}^2}\left\{(EA(1+et)-T_{ij})(2\sin\theta\cos\alpha_{ij}+\cos\beta_{ij})\right.$$

$$\left.-2(EA(1+\frac{et}{2})-\frac{T_{ij}}{2})\cos^2\alpha_{ij}\cos\beta_{ij}\right\}$$

$$+\frac{(\delta\eta_j-\delta\eta_i)(\delta z_j-\delta z_i)}{l_{ij}^2}\left\{(EA(1+et)-T_{ij})\cos\gamma_{ij}\sin\theta\right.$$

$$\left.-2(EA(1+\frac{et}{2})-\frac{T_{ij}}{2})\cos\alpha_{ij}\cos\beta_{ij}\cos\gamma_{ij}\right\}$$

$$+\frac{(\delta z_j-\delta z_i)(\delta\xi_j-\delta\xi_i)}{l_{ij}^2}\left\{(EA(1+et)-T_{ij})\cos\gamma_{ij}\right.$$

$$\left.-2(EA(1+\frac{et}{2})-\frac{T_{ij}}{2})\cos^2\alpha_{ij}\cos\gamma_{ij}\right\}$$

$$-EAet\cos\alpha_{ij}\ ]\ +P_{i\xi}=0 \qquad \ldots 2\text{-}15$$

To simplify equation (2-15), the following substitutions are used:

$$\lambda_{ij}=EA(1+et)-T_{ij} \qquad \ldots 2\text{-}16a$$

$$\mu_{ij}=EA(1+\frac{et}{2})-\frac{T_{ij}}{2} \qquad \ldots 2\text{-}16b$$

from which,

$$EAet\text{-}T_{ij} = 2(\lambda_{ij}-\mu_{ij})$$

Using these substitutions, equation (2-15) can be rewritten as,

$$\Sigma\Big[\frac{(\delta\xi_j-\delta\xi_i)}{l_{ij}}(\lambda_{ij}\cos^2\alpha_{ij}-2(\lambda_{ij}-\mu_{ij}))+\frac{(\delta\eta_j-\delta\eta_i)}{l_{ij}}(\lambda_{ij}\cos\alpha_{ij}\cos\beta_{ij}$$

$$-2(\lambda_{ij}-\mu_{ij})\sin\theta)$$

$$+\frac{(\delta z_j-\delta z_i)}{l_{ij}}(\lambda_{ij}\cos\alpha_{ij}\cos\gamma_{ij})+\frac{(\delta\xi_j-\delta\xi_i)^2}{l_{ij}^2}\left(\frac{3}{2}\lambda_{ij}\cos\alpha_{ij}-\mu_{ij}\cos^3\alpha_{ij}\right)$$

$$+\frac{(\delta\eta_j-\delta\eta_i)^2}{l_{ij}^2}(\lambda_{ij}(\tfrac{1}{2}\cos\alpha_{ij}+\cos\beta_{ij}\sin\theta)-\mu_{ij}\cos\alpha_{ij}\cos^2\beta_{ij})$$

$$+\frac{(\delta z_j-\delta z_i)^2}{l_{ij}^2}(\tfrac{1}{2}\lambda_{ij}\cos\alpha_{ij}-\mu_{ij}\cos\alpha_{ij}\cos^2\gamma_{ij})$$

$$+\frac{(\delta\xi_j-\delta\xi_i)(\delta\eta_j-\delta\eta_i)}{l_{ij}^2}(\lambda_{ij}(2\sin\theta\cos\alpha_{ij}+\cos\beta_{ij})-2\mu_{ij}\cos^2\alpha_{ij}\cos\beta_{ij})$$

$$+\frac{(\delta\eta_j-\delta\eta_i)(\delta z_j-\delta z_i)}{l_{ij}^2}(\lambda_{ij}\sin\theta\cos\gamma_{ij}-2\mu_{ij}\cos\alpha_{ij}\cos\beta_{ij}\cos\gamma_{ij})$$

$$+\frac{(\delta z_j-\delta z_i)(\delta\xi_j-\delta\xi_i)}{l_{ij}^2}(\lambda_{ij}\cos\gamma_{ij}-2\mu_{ij}\cos^2\alpha_{ij}\cos\gamma_{ij})$$

$$-EA_{et}\cos\alpha_{ij}\ ]\ +P_{i\xi}=0 \qquad \ldots\ 2\text{-}17a$$

Proceeding in a similar manner from equations (2-9b) and (2-9c), the following equations can be derived for the η and z directions:

$$\Sigma[\frac{(\delta\xi_j-\delta\xi_i)}{l_{ij}}(\lambda_{ij}\cos\alpha_{ij}\cos\beta_{ij}-2(\lambda_{ij}-\mu_{ij}))$$

$$+\frac{(\delta\eta_j-\delta\eta_i)}{l_{ij}}(\lambda_{ij}\cos^2\beta_{ij}-2(\lambda_{ij}-\mu_{ij}))+\frac{(\delta z_j-\delta z_i)}{l_{ij}}(\lambda_{ij}\cos\beta_{ij}\cos\gamma_{ij})$$

$$+\frac{(\delta\xi_j-\delta\xi_i)^2}{l_{ij}^2}(\lambda_{ij}(\sin\theta\cos\alpha_{ij}+\tfrac{1}{2}\cos\beta_{ij})-\mu_{ij}\cos^2\alpha_{ij}\cos\beta_{ij})$$

$$+\frac{(\delta\eta_j-\delta\eta_i)^2}{l_{ij}^2}(\tfrac{3}{2}\lambda_{ij}\cos\beta_{ij}-\mu_{ij}\cos^3\beta_{ij})+\frac{(\delta z_j-\delta z_i)^2}{l_{ij}^2}(\tfrac{1}{2}\lambda_{ij}\cos\beta_{ij}$$

$$-\mu_{ij}\cos\beta_{ij}\cos^2\gamma_{ij})$$

$$+\frac{(\delta\xi_j-\delta\xi_i)(\delta\eta_j-\delta\eta_i)}{l_{ij}^2}(\lambda_{ij}(\cos\alpha_{ij}+2\sin\theta\cos\beta_{ij})-2\mu_{ij}\cos\alpha_{ij}\cos^2\beta_{ij})$$

$$+\frac{(\delta\eta_j-\delta\eta_i)(\delta z_j-\delta z_i)}{l_{ij}^2}(\lambda_{ij}\cos\gamma_{ij}-2\mu_{ij}\cos^2\beta_{ij}\cos\gamma_{ij})$$

$$+\frac{(\delta z_j-\delta z_i)(\delta\xi_j-\delta\xi_i)}{l_{ij}^2}(\lambda_{ij}\sin\theta\cos\gamma_{ij}-2\mu_{ij}\cos\alpha_{ij}\cos\beta_{ij}\cos\gamma_{ij})$$

$$-EA\varepsilon_{ij}\cos\beta_{ij}\Big] + P_{i\eta} = 0 \qquad \ldots 2\text{-}17b$$

$$\Sigma_L \frac{(\delta\xi_j-\delta\xi_i)}{l_{ij}}(\lambda_{ij}\cos\alpha_{ij}\cos\gamma_{ij})+\frac{(\delta\eta_j-\delta\eta_i)}{l_{ij}}(\lambda_{ij}\cos\beta_{ij}\cos\gamma_{ij})$$

$$+\frac{(\delta z_j-\delta z_i)}{l_{ij}}(\lambda_{ij}\cos^2\gamma_{ij}-2(\lambda_{ij}-\mu_{ij}))+\frac{(\delta\xi_j-\delta\xi_i)^2}{l_{ij}^2}(\tfrac{1}{2}\lambda_{ij}\cos\gamma_{ij}$$

$$-\mu_{ij}\cos^2\alpha_{ij}\cos\gamma_{ij})$$

$$+\frac{(\delta\eta_j-\delta\eta_i)^2}{l_{ij}^2}(\tfrac{1}{2}\lambda_{ij}\cos\gamma_{ij}-\mu_{ij}\cos^2\beta_{ij}\cos\gamma_{ij})$$

$$+\frac{(\delta z_j-\delta z_i)^2}{l_{ij}^2}(\tfrac{3}{2}\lambda_{ij}\cos\gamma_{ij}-\mu_{ij}\cos^3\beta_{ij})$$

$$+\frac{(\delta\xi_j-\delta\xi_i)(\delta\eta_j-\delta\eta_i)}{l_{ij}^2}(\lambda_{ij}\sin\theta\cos\gamma_{ij}-2\mu_{ij}\cos\alpha_{ij}\cos\beta_{ij}\cos\gamma_{ij})$$

$$+\frac{(\delta\eta_j-\delta\eta_i)(\delta z_j-\delta z_i)}{l_{ij}^2}(\lambda_{ij}\cos\beta_{ij}-2\mu_{ij}\cos\beta_{ij}\cos^2\gamma_{ij})$$

$$+\frac{(\delta z_j-\delta z_i)(\delta\xi_j-\delta\xi_i)}{l_{ij}^2}(\lambda_{ij}\cos\alpha_{ij}-2\mu_{ij}\cos\alpha_{ij}\cos^2\gamma_{ij})-EA\epsilon t\cos\gamma_{ij}\Big]$$

$$+P_{iz}=0 \qquad \ldots\ 2\text{-}17c$$

Equations (2-17) can be written at each joint of the cable net. They take into account changes in geometry, the horizontal displacements of the joints and the stresses induced by temperature changes. The effect of deformation in the bounding frame can also be taken into account when writing the equations at joints adjacent to the bounding frame. The displacements of the joints lying on the bounding frame are expressed in terms of the cable tensions and the influence coefficients for the frame at each joint. Additional equations can be written to express the influence coefficients in terms of the elastic constants of the frame. These will provide sufficient number of equations to solve for the displacements of all the joints.

When equations (2-17) are written at each joint of the

net, a set of nonlinear simultaneous equations equal to thrice the number of joints, results. These equations cannot be solved directly to obtain the displacements. Consequently, a numerical method will have to be used. This is discussed in the following section.

2.2 Numerical Solution of Displacement Equations

2.2.1 Introduction

The numerical solution of equations (2-17) is achieved by an adaption of the Newton-Raphson process by Poskitt (58). This iterative method illustrated by Poskitt in the case of a cable-suspended truss, avoids the neqessity of actually forming the partial derivatives at each step. The basic theory given by Hartree (34), on iterative processes and their convergence will be briefly summarized here. The Newton-Raphson method and its adaptation to solve equations (2-17) will be discussed subsequently.

2.2.2 Iterative Processes and Their Convergence

The nonlinear equation $f(x) = 0$ to be solved is expressed in the form,

$$x = F(x)$$

The iterative scheme consists of constructing a sequence,

$$x_{n+1} = F(x_n) \qquad \ldots 2\text{-}18$$

When the difference between x_{n+1} and x_n becomes smaller than some predetermined value, the value of x_{n+1} is the solution of the equation.

Let X be the exact solution of the equation and δ_n, δ_{n+1} be the errors in x_n and x_{n+1} respectively. Substituting for x_n, x_{n+1} into equations (2-18) and expanding the right hand side in a Taylor's series, we have,

$$X+\delta_{n+1} = F(X)+F'(X)\delta_n + \tfrac{1}{2}F''(X)\delta_n^2+ \ldots \quad \ldots 2\text{-}19$$

and since $X = F(X)$, equation (2-19) becomes,

$$\delta_{n+1} = a_1\delta_n+a_2\delta_n^2+ \ldots \quad \ldots 2\text{-}20$$

where $a_1 = F'(X)$, $a_2 = \tfrac{1}{2}F''(X)$, ...

Case 1 $a_1 \neq 0$

As $\delta_n \longrightarrow 0$, equation (2-20) gives

$$\delta_{n+1} = a_1\delta_n$$

For convergence $|\delta_{n+1}/\delta_n|<1$ or $|a|< 1$. Here, at any stage of the iteration, the number of cycles to get a new figure is always the same and the convergence is called 'first-order'.

covergence.

Case 2 $a_1 = 0, \quad a_2 \neq 0$

As $\varepsilon_n \longrightarrow 0$, equation (2-20) gives,

$$\varepsilon_{n+1} = a_2 \varepsilon_n^2$$

Here the convergence is much more rapid than in case 1 and is called 'second-order' convergence.

2.2.3 Newton-Raphson Method

To construct the Newton-Raphson sequence of iteration for the nonlinear equation $f(x) = 0$, let ε be the error in x_n so that,

$$X = x_n + \varepsilon$$

Hence,

$f(X) = f(x_n+\varepsilon)$ becomes,

$$0 = f(x_n)+f'(x_n)\varepsilon + \ldots$$

Neglecting higher orders,

$$\varepsilon = - \frac{f(x_n)}{f'(x_n)}$$

Hence,

$$x_{n+1} = x_n - \frac{f(x_n)}{f'(x_n)} \qquad \ldots 2\text{-}21$$

which is the well known Newton-Raphson method. This is a 'second-order' process since,

$$F(x) = x - \frac{f(x)}{f'(x)}$$

from which,

$$F'(x) = \frac{-f(x)f''(x)}{[f'(x)]^2}$$

and since $f(X) = 0$, it follows that $F'(X) = 0$.

This method has the disadvantage that it requires evaluation of the derivative $f'(x)$ at each stage which becomes tedious when the variables involved are large in number. In order to avoid setting up the partial derivatives, a variational technique is used in which a small variation is introduced into equations (2-17) and all but the linear components of the variation are neglected in the subsequent expanded form.

2.2.4 Method of Solution

Suppose $\delta\xi'$, $\delta\eta'$, $\delta z'$ are approximate solutions of

equations (2-17). Let increments $\delta\delta\xi$, $\delta\delta\eta$, $\delta\delta z$ be added to give exact solutions $\delta\xi$, $\delta\eta$, δz.

Substituting now into equation (2-17a), we have,

$$\Sigma\Bigg[\frac{(\delta\xi'_j+\delta\delta\xi_j-\delta\xi'_i-\delta\delta\xi_i)}{l_{ij}}(\lambda_{ij}\cos^2\alpha_{ij}-2(\lambda_{ij}-\mu_{ij}))$$

$$+\frac{(\delta\eta'_j+\delta\delta\eta_j-\delta\eta'_i-\delta\delta\eta_i)}{l_{ij}}(\lambda_{ij}\cos\alpha_{ij}\cos\beta_{ij}-2(\lambda_{ij}-\mu_{ij})\sin\theta)$$

$$+\frac{(\delta z'_j+\delta\delta z_j-\delta z'_i-\delta\delta z_i)}{l_{ij}}(\lambda_{ij}\cos\alpha_{ij}\cos\gamma_{ij})$$

$$+\frac{(\delta\xi'_j+\delta\delta\xi_j-\delta\xi'_i-\delta\delta\xi_i)^2}{l_{ij}^2}(\tfrac{3}{2}\lambda_{ij}\cos\alpha_{ij}-\mu_{ij}\cos^3\alpha_{ij})$$

$$+\frac{(\delta\eta'_j+\delta\delta\eta_j-\delta\eta'_i-\delta\delta\eta_i)^2}{l_{ij}^2}(\lambda_{ij}(\tfrac{1}{2}\cos\alpha_{ij}+\cos\beta_{ij}\sin\theta)-\mu_{ij}\cos\alpha_{ij}\cos^2\beta_{ij})$$

$$+\frac{(\delta z'_j+\delta\delta z_i-\delta z'_i-\delta\delta z_i)}{l_{ij}^2}(\tfrac{1}{2}\lambda_{ij}\cos\alpha_{ij}-\mu_{ij}\cos\alpha_{ij}\cos^2\gamma_{ij})$$

$$+\frac{(\delta\xi'_j+\delta\delta\xi_j-\delta\xi'_i-\delta\delta\xi_i)(\delta\eta'_j+\delta\delta\eta_j-\delta\eta'_i-\delta\delta\eta_i)}{l_{ij}^2}(\lambda_{ij}(2\sin\cos\alpha_{ij}+\cos\beta_{ij})$$

$$-2\mu_{ij}\cos^2\alpha_{ij}\cos\beta_{ij})$$

$$+\frac{(\delta\eta_j'+\delta\delta\eta_j-\delta\eta_i'-\delta\delta\eta_i)(\delta z_j'+\delta\delta z_j-\delta z_i'-\delta\delta z_i)}{l_{ij}^2}(\lambda_{ij}\sin\theta\cos\gamma_{ij}$$

$$-2\mu_{ij}\cos\alpha_{ij}\cos\beta_{ij}\cos\gamma_{ij})$$

$$+\frac{(\delta z_j'+\delta\delta z_j-\delta z_i'-\delta\delta z_i')(\delta\xi_j'+\delta\delta\xi_j-\delta\xi_i'-\delta\delta\xi_i)}{l_{ij}^2}(\lambda_{ij}\cos\gamma_{ij}$$

$$-2\mu_{ij}\cos^2\alpha_{ij}\cos\gamma_{ij})$$

$$-EAe_{tc}\cos\alpha_{ij}\,] + P_{i\xi} = 0 \qquad \ldots 2\text{-}22a$$

The increments $\delta\delta\xi$, $\delta\delta\eta$, $\delta\delta z$ are considered to be sufficiently small so that their second order terms may be neglected. Simplifying equation (2-22a) gives,

$$\Sigma\Big[\frac{(\delta\delta\xi_j-\delta\delta\xi_i)}{l_{ij}}(\lambda_{ij}\cos^2\alpha_{ij}-2(\lambda_{ij}-\mu_{ij}))$$

$$+\frac{(\delta\delta\eta_j-\delta\delta\eta_i)}{l_{ij}}(\lambda_{ij}\cos\alpha_{ij}\cos\beta_{ij}-2(\lambda_{ij}-\mu_{ij})\sin\theta)$$

$$+\frac{(\delta\delta z_j-\delta\delta z_i)}{l_{ij}}(\lambda_{ij}\cos\alpha_{ij}\cos\gamma_{ij})$$

$$+\frac{(\delta\bar{3}'_j-\delta\bar{3}'_i)(\delta\delta\bar{3}_j-\delta\delta\bar{3}_i)}{l_{ij}^2}(3\lambda_{ij}\cos\alpha_{ij}-2\mu_{ij}\cos^3\alpha_{ij})$$

$$+\frac{(\delta\eta'_j-\delta\eta'_i)(\delta\delta\eta_j-\delta\delta\eta_i)}{l_{ij}^2}(\lambda_{ij}(\cos\alpha_{ij}+2\cos\beta_{ij}\sin\theta)-2\mu_{ij}\cos\alpha_{ij}\cos\beta_{ij})$$

$$+\frac{(\delta z'_j-\delta z'_i)(\delta\delta z_j-\delta\delta z_i)}{l_{ij}^2}(\lambda_{ij}\cos\alpha_{ij}-2\mu_{ij}\cos\alpha_{ij}\cos^2\gamma_{ij})$$

$$+\frac{(\delta\bar{3}'_j-\delta\bar{3}'_i)(\delta\delta\eta_j-\delta\delta\eta_i)+(\delta\eta'_j-\delta\eta'_i)(\delta\delta\bar{3}_j-\delta\delta\bar{3}_i)}{l_{ij}^2}$$

$$(\lambda(2\sin\cos\alpha_{ij}+\cos\beta_{ij})-2\mu_{ij}\cos^2\alpha_{ij}\cos\beta_{ij})$$

$$+\frac{(\delta\eta'_j-\delta\eta'_i)(\delta\delta z_j-\delta\delta z_i)+(\delta z'_j-\delta z'_i)(\delta\delta\eta_j-\delta\delta\eta_i)}{l_{ij}^2}$$

$$(\lambda_{ij}\sin\theta\cos\gamma_{ij}-2\mu_{ij}\cos\alpha_{ij}\cos\beta_{ij}\cos\gamma_{ij})$$

$$+\frac{(\delta z_j'-\delta z_i')(\delta\delta\xi_j-\delta\delta\xi_i)+(\delta\xi_j'-\delta\xi_i')(\delta\delta z_j-\delta\delta z_i)}{l_{ij}^2}$$

$$(\lambda_{ij}\cos\gamma_{ij}-2\mu_{ij}\cos^2\alpha_{ij}\cos\gamma_{ij})\ ]+R_{i\xi}=0 \quad \ldots \text{2-23a}$$

where $R_{i\xi}$ is the residual obtained by substituting $\delta\xi'$, $\delta\eta'$, $\delta z'$ into equation (2-17a). This residual must be reduced to zero by iteration.

Similar equations can be developed from equations (2-17b) and (2-17c) for the η and z directions.

$$\Sigma[\frac{(\delta\delta\xi_j-\delta\delta\xi_i)}{l_{ij}}(\lambda_{ij}\cos\alpha_{ij}\cos\beta_{ij}-2(\lambda_{ij}-\mu_{ij})\sin\theta)$$

$$+\frac{(\delta\delta\eta_j-\delta\delta\eta_i)}{l_{ij}}(\lambda_{ij}\cos^2\beta_{ij}-2(\lambda_{ij}-\mu_{ij}))$$

$$+\frac{(\delta\delta z_j-\delta\delta z_i)}{l_{ij}}(\lambda_{ij}\cos\beta_{ij}\cos\gamma_{ij})$$

$$+\frac{(\delta\xi_j'-\delta\xi_i')(\delta\delta\xi_j-\delta\delta\xi_i)}{l_{ij}^2}(\lambda_{ij}(2\sin\theta\cos\alpha_{ij}+\cos\beta_{ij})-2\ _{ij}\cos^2\alpha_{ij}\cos\beta_{ij})$$

$$+\frac{(\delta\eta_j'-\delta\eta_i')(\delta\delta\eta_j-\delta\delta\eta_i)}{l_{ij}^2}(3\lambda_{ij}\cos\beta_{ij}-2\mu_{ij}\cos^3\beta_{ij})$$

$$+\frac{(\delta z_j'-\delta z_i')(\delta\delta z_j-\delta\delta z_i)}{l_{ij}^2}(\lambda_{ij}\cos\beta_{ij}-2\mu_{ij}\cos\beta_{ij}\cos^2\gamma_{ij})$$

$$+\frac{(\delta\xi_j'-\delta\xi_i')(\delta\delta\eta_j-\delta\delta\eta_i)+(\delta\eta_j'-\delta\eta_i')(\delta\delta\xi_j-\delta\delta\xi_i)}{l_{ij}^2}$$

$$(\lambda_{ij}(\cos\alpha_{ij}+2\sin\theta\cos\beta_{ij})-2\mu_{ij}\cos\alpha_{ij}\cos^2\beta_{ij})$$

$$+\frac{(\delta\eta_j'-\delta\eta_i')(\delta\delta z_j-\delta\delta z_i)+(\delta z_j'-\delta z_i')(\delta\delta\eta_j-\delta\delta\eta_i)}{l_{ij}^2}$$

$$(\lambda_{ij}\cos\gamma_{ij}-2\mu_{ij}\cos^2\beta_{ij}\cos\gamma_{ij})$$

$$+\frac{(\delta z_j'-\delta z_i')(\delta\delta\xi_j-\delta\delta\xi_i)+(\delta\xi_j'-\delta\xi_i')(\delta\delta z_j-\delta\delta z_i)}{l_{ij}^2}$$

$$(\lambda_{ij}\sin\theta\cos\gamma_{ij}-2\mu_{ij}\cos\alpha_{ij}\cos\beta_{ij}\cos\gamma_{ij})\ ]$$

$$+R_{i\eta}=0 \qquad \ldots\ 2\text{-}23b$$

$$\Sigma\Big[\frac{(\delta\delta\xi_j-\delta\delta\xi_i)}{l_{ij}}(\lambda_{ij}\cos\alpha_{ij}\cos\gamma_{ij})+\frac{(\delta\delta\eta_j-\delta\delta\eta_i)}{l_{ij}}(\lambda_{ij}\cos\beta_{ij}\cos\gamma_{ij})$$

$$+\frac{(\delta\delta z_j-\delta\delta z_i)}{l_{ij}}(\lambda_{ij}\cos^2\gamma_{ij}-2(\lambda_{ij}-\mu_{ij}))$$

$$+\frac{(\delta\xi_j'-\delta\xi_i')(\delta\delta\xi_j-\delta\delta\xi_i)}{l_{ij}^2}(\lambda_{ij}\cos\gamma_{ij}-2\mu_{ij}\cos^2\alpha_{ij}\cos\gamma_{ij})$$

$$+\frac{(\delta\eta_j'-\delta\eta_i')(\delta\delta\eta_j-\delta\delta\eta_i)}{l_{ij}^2}(\lambda_{ij}\cos\gamma_{ij}-2\mu_{ij}\cos^2\beta_{ij}\cos\gamma_{ij})$$

$$+\frac{(\delta z_j'-\delta z_i')(\delta\delta z_j-\delta\delta z_i)}{l_{ij}^2}(3\lambda_{ij}\cos\gamma_{ij}-2\mu_{ij}\cos^3\gamma_{ij})$$

$$+\frac{(\delta\xi_j'-\delta\xi_i')(\delta\delta\eta_j-\delta\delta\eta_i)+(\delta\eta_j'-\delta\eta_i')(\delta\delta\xi_j-\delta\delta\xi_i)}{l_{ij}^2}$$

$$(\lambda_{ij}\sin\theta\cos\gamma_{ij}-2\mu_{ij}\cos\alpha_{ij}\cos\beta_{ij}\cos\gamma_{ij})$$

$$+\frac{(\delta\eta_j'-\delta\eta_i')(\delta\delta z_j-\delta\delta z_i)+(\delta z_j'-\delta z_i')(\delta\delta\eta_j-\delta\delta\eta_i)}{l_{ij}^2}$$

$$(\lambda_{ij}\cos\beta_{ij}-2\mu_{ij}\cos\beta_{ij}\cos^2\gamma_{ij})$$

$$+ \frac{(\delta z'_j-\delta z'_i)(\delta\delta\xi_j-\delta\delta\xi_i)+(\delta\xi'_j-\delta\xi'_i)(\delta\delta z_j-\delta\delta z_i)}{l_{ij}^2}$$

$$(\lambda_{ij}\cos\alpha_{ij}-2\mu_{ij}\cos\alpha_{ij}\cos^2\gamma_{ij}) \;] + R_{iz} = 0 \qquad \ldots \text{2-23c}$$

Equations (2-23) can be written in matrix form as,

$$\underline{S}.\underline{\Delta}+\underline{R} = 0$$

$$\text{or} \quad \underline{\Delta}_{r+1} = \underline{\Delta}_r - S_r^{-1}.R_r \qquad \ldots \text{2-24}$$

where $\underline{S}$ is the instantaneous stiffness matrix.

Thus the method of solution finally becomes one of a solution of a set of simultaneous linear equations to determine the correction for the displacements. Initial values to be used in the iteration are obtained by solving the linear part of the equations (2-17). Equations (2-24) is used to improve the values of the displacements obtained until the desired degree of convergence is reached. The tension increments in the cables are calculated using the final displacements and equations (2-12d) and (2-13).

The basic steps involved in solving equations (2-17) numerically to obtain the displacements are as follows:

1. Solve the linear part of equations (2-17) to obtain an initial value for the iteration.

2. Substitute the resultant displacements into equation (2-17) to obtain the residual matrix R.

3. Substitute into equations (2-23) to generate the instantaneous stiffness matrix S.

4. Obtain the correction for displacements from equation (2-24) and compute the corrected displacements.

5. Test for convergence and if not satisfactory go to step 2 and repeat.

In generating the residual matrix R and the stiffness matrix S, the latter is expressed as the sum of two matrices S_1 and S_2.

$$\text{ie} \quad \underline{S} = \underline{S}_1 + \underline{S}_2 \qquad \ldots 2\text{-}25$$

where $\underline{S}_1$ consists of the terms that do not involve the displacements $\delta\xi'$, $\delta\eta'$, $\delta z'$ and $\underline{S}_2$ consists of terms that do involve them (cf. equations (2-23)). By an inspection of equations (2-17) and equations (2-23), it is seen that the residual matrix R can be expressed by,

$$\underline{R} = (\underline{S}_1 + \underline{S}_2/2).\ \underline{\Delta} + \underline{P} \qquad \ldots 2\text{-}26$$

where $\underline{\Delta}$ is the displacement vector and $\underline{P}$ is the load vector. The matrices $\underline{S}_1$ and $\underline{S}_2$ correspond to the linear and nonlinear terms respectively. This procedure facilitates programming since, when $\underline{S}_1$ and $\underline{S}_2$ are computed separately, $\underline{S}$ and $\underline{R}$ are both found immediately by using the relations (2-25) and (2-26).

2.3 Inelastic Analysis

2.3.1 Material Properties of Cables

Cables used in suspended roof construction are usually wire ropes or wire strands. A strand is an assembly of wires formed helically around a centre wire in one or more symmetrical layers. A wire rope consists of a group of strands laid helically around a wire strand core or an independent wire rope core.

Because strands and ropes are fabricated from helically formed components, their behaviour is somewhat different from that of rods or even the individual wires from which they are made. When a tensile load is applied to a strand or a wire rope, the resulting elongation will consist of (i) a structural stretch which is caused by radial and axial adjustment of the wires and strands to the load, and (ii) the elastic stretch of the wires.

The structural stretch depends on the number of wires per strand, the number of strands per rope and the length of lay of the wires and strands. Most of the structural stretch can be removed by prestressing the wire rope to a predetermined load for a sufficient length of time to permit adjustment of the component parts to that load. The elastic modulus of a wire rope is generally lower than that of the material and varies throughout the life of the rope. It is dependent on the construction of the rope and the conditions under which it operates, and increases during the useful life of the rope. Prestressing of the wire rope increases and

stabilizes its modulus of elasticity. For prestressed galvanized bridge strands and ropes the modulus of elasticity lies between 20,000 to 24,000 ksi (85). The modulus is also reduced by 'galvanizing', a process by which a protective coating of zinc is applied to resist corrosion. When the coating is heavy it is recommended that the modulus be further reduced by 1000 ksi (12).

The high tensile strength of steel used in wire ropes is achieved by the process of cold-drawing. The wire is drawn through a series of decreasing diameter dies and this process realigns the crystal structure of the steel thereby increasing its tensile strength. Cold-drawing also produces a uniform, smooth surface and a greater degree of dimensional accuracy can be attained than by other methods (5).

Although the cold-drawing process increases the tensile strength of steel, it affects its other properties. The ductility of steel is reduced and it does not exhibit a definite yield point as the case with ordinary steel. A theoretical yield point is therefore defined and a widely accepted definition is on the basis of 0.2% permanent strain. It has also been defined as the proportional or elastic limit but this is difficult to determine accurately in practice. Wire ropes possessing ultimate strengths exceeding 250 ksi are not uncommon in present day cable structures. The elastic limit of a bridge wire rope is approximately 55% of its breaking strength; and for galvanized ropes it is approximately 50% (84).

In the following analysis, a mathematical model to represent the stress-strain curve for a high-tensile wire rope is presented, based on the elastic modulus, the 0.2% yield stress, the ultimate stress and the ultimate strain. These properties can be easily determined by properly testing a specimen.

2.3.2 Mathematical Model of Cable Stress-Strain Curve

The stress-strain curve is linear in the elastic region, that is, upto the proportional limit. Between the proportional limit and the point of ultimate stress, the curve is assumed to be a second-degree parabola. The parabola is assumed to have its axis parallel to the ϵ (strain) axis so that its equation is of the form,

$$\sigma^2 + 2g\epsilon + 2f\sigma + c = 0 \qquad \ldots 2\text{-}27$$

where σ is the stress and, g, f and c are constants to be determined.

Referring to fig. (2-3), $P(\sigma_p, \epsilon_p)$ represents the proportional limit, $Y(\sigma_y, \epsilon_y)$ represents the yield point and $U(\sigma_u, \epsilon_u)$ represents the point of ultimate stress. The initial straight line OP is tangential to the parabola at P.

The equation to the tangent to the parabola at P is given by,

$$\sigma\sigma_p + g(\epsilon + \epsilon_p) + f(\sigma + \sigma_p) + c = 0 \qquad \ldots 2\text{-}28$$

and since this tangent passes through 0, it has the equation $\sigma = E.\epsilon$. Equating the constant in equation (2-28) to zero and the gradient to E, we have,

$$g\epsilon_p+f\sigma_p+c = 0 \qquad \ldots 2\text{-}29$$

and,

$$\frac{-g}{f+\sigma_p} = E \qquad \ldots 2\text{-}30$$

Using the relation $\sigma_p = \epsilon_p.E$ and solving equations (2-29) and (2-30), we have,

$$c = \sigma_p^2 \qquad \ldots 2\text{-}31$$

Substituting back into equation (2-29) for σ_p and simplifying, we get,

$$g+Ef+E/c = 0$$

or $$E^2c = g^2+2Egf+E^2f^2 \qquad \ldots 2\text{-}32$$

Also since (σ_y, ϵ_y) and (σ_u, ϵ_u) are points on the parabola, they satisfy equation (2-27).

ie $$\sigma_y^2+2g\epsilon_y+2f\sigma_y+c = 0 \qquad \ldots 2\text{-}33$$

$$\sigma_u^2 + 2g\epsilon_u + 2f\sigma_u + c = 0 \qquad \ldots 2\text{-}34$$

Solving equations (2-33) and (2-34) for f and g, we get,

$$f = -\frac{(\epsilon_u\sigma_y^2 - \epsilon_y\sigma_u^2) + c(\epsilon_u - \epsilon_y)}{2(\epsilon_u\sigma_y - \epsilon_y\sigma_u)}$$

and,

$$g = -\frac{(\sigma_u\sigma_y^2 - \sigma_y\sigma_u^2) + c(\sigma_u - \sigma_y)}{2(\epsilon_u\sigma_y - \epsilon_y\sigma_u)}$$

Substituting these into equation (2-32), simplifying and rearranging terms result in,

$$c^2[(\sigma_u - \sigma_y) - E(\epsilon_u - \epsilon_y)]^2 + 2c[\{(\sigma_u - \sigma_y) - E(\epsilon_u - \epsilon_y)$$

$$(\sigma_u\sigma_y^2 - \sigma_y\sigma_u^2) - E(\epsilon_u\sigma_y^2 - \epsilon_y\sigma_u^2)\} - 2E^2(\epsilon_u\sigma_y - \epsilon_y\sigma_u)^2]$$

$$+[(\sigma_u\sigma_y^2 - \sigma_y\sigma_u^2) - E(\epsilon_u\sigma_y^2 - \epsilon_y\sigma_u^2)]^2 = 0$$

or,

$$c^2C_1 + 2cC_2 + C_3 = 0 \qquad \ldots 2\text{-}35$$

where,

$$C_1 = [(\sigma_u-\sigma_y)-E(\epsilon_u-\epsilon_y)]^2$$

$$C_2 = [\{(\sigma_u-\sigma_y)-E(\epsilon_u-\epsilon_y)\}\{(\sigma_u\sigma_y^2-\sigma_y\sigma_u^2)-E(\epsilon_u\sigma_y^2-\epsilon_y\sigma_u^2)\}$$

$$-2E^2(\epsilon_u\sigma_y-\epsilon_y\sigma_u)^2]$$

$$C_3 = [(\sigma_u\sigma_y^2-\sigma_y\sigma_u^2)-E(\epsilon_u\sigma_y^2-\epsilon_y\sigma_u^2)]^2$$

It is found that the admissible root of equation (2-35) is,

$$c = \frac{-C_2-\sqrt{C_2^2-C_1C_3}}{C_1} \qquad \ldots 2\text{-}36$$

the other root giving a value even greater than σ_y^2 for c and hence contradicting equation (2-31).

Also from the definition of yield point,

$$\sigma_y = (\epsilon_y-.002)E \qquad \ldots 2\text{-}37$$

Substituting this into equation (2-33) and solving with equation (2-30), we get,

$$g = -250(\sigma_y-\sigma_p)^2 \qquad \ldots 2\text{-}38$$

and from equation (2-30),

$$f = \frac{-g}{E} - \sigma_p \qquad \ldots 2\text{-}39$$

Hence the three constants g, f, c required to completely define the parabola can be expressed in terms of the known properties of the material. The tangent modulus corresponding to any stress value σ between points P and U is obtained by differentiating equation (2-27).

ie. $$2\sigma \cdot \frac{d\sigma}{d\epsilon} + 2g + 2f \cdot \frac{d\sigma}{d\epsilon} = 0$$

or,

$$\frac{d\sigma}{d\epsilon} = \frac{-g}{\sigma + f} \qquad \ldots 2\text{-}40$$

CHAPTER III

COMPUTER PROGRAM AND SOLUTION TECHNIQUE

3.1 Computer Program

3.1.1 Features of the Program

A computer program in Fortran IV has been developed for the theoretical analysis of cable networks with the aid of the IBM 360/50 computer. It could be used to analyze single or double roofs, rectangular in plan with cables running diagonally in two directions. The program is quite general in that it is suitable for networks with any degree of non-orthogonality, of any dimensions and with any number of joints that is dictated by the proper arrangement of the cables.

When the roof is a hyperbolic paraboloid, either single or double, with straight boundaries, the program calculates the initial ordinates of the joints. This step could be by-passed and the initial ordinates of the interior joints as well as those on the boundaries could be read in. This facilitates the use of the program for roofs with the edge beams arbitrarily curved in the vertical plane or for bowl-shaped roofs with known ordinates, with the boundary frame in the horizontal plane.

Using the preliminary data, the program calculates the displacements of the joints and the tension increments in

the cables for any given loading. The cable pretension in each direction can be independently defined. So can the steel area per cable in each direction. The load in one or more of the three directions and any temperature change can be applied in a specified number of increments. When the load is applied in a number of increments, the geometry of the roof and the cable tensions are updated and the nonlinear equations solved at each step. One or more loads or temperature changes can be added subsequent to a previous load or temperature change.

The program also takes into account the possibility of individual cable segments becoming slack. When this happens, the contribution to the stiffness of the roof, of those cable segments that became slack, is omitted and the calculations are repeated. The tensions in these cable segments are also set to zero. Slack cable segments are brought back into the system when they become taut, by keeping records of the distances between joints and the lengths of the cable segments between them.

The theoretical stress-strain curve for the cable is calculated by the program and when the proportional limit is exceeded in any one cable segment, the tangent modulus at the particular stress level is used. When unloading in a cable segment takes place after the proportional limit has been reached, the elastic modulus is used irrespective of the stress level.

When the ultimate load of the roof is desired, the load is increased repeatedly until the ultimate stress is

reached in the most highly stressed cable segment. This is considered failure of the roof and the ultimate load is computed by linear interpolation between the load just before the ultimate stress is reached and the final load. If desired, a different increment size of loading can be used after the first yielding takes place.

3.1.2 Input to the Program

The input data consists mainly of the dimensions of the roof, the pretensions, steel areas, properties of the cable material and the loading. It is provided in the following order:

The first card contains information on the type of roof, the number of internodes which defines the number of joints, the number of loadings to be analyzed, the number of sets of data, whether the joint ordinates have to be calculated or not and whether to print the intermediate values during calculations. The type of roof is defined by a '1' for a single roof and a '2' for a double roof. The number of joints is defined by the number of internodes which are the spaces between cable connections on the edge beam. In a double roof, the number of internodes on one side is double that on an adjacent side in which case the latter is specified. The joints are numbered from left to right starting from the top, in both types of roofs. The total number of joints is given by,

$$NJ = NTYP.INDS^2+(NTYP.INDS-1)(INDS-1) \quad \ldots \quad 3\text{-}1$$

where NTYP is the type number, and

INDS is the number of internodes.

Next the number of loadings per set of data which consists of the pretension, steel area etc., is given. When the loads are applied subsequent to existing load, they are all considered one loading. This is followed by the number of sets of data to be processed. If the ordinates of the joints are read in, a '1' is punched next. Lastly, if the intermediate values of the displacements and the residual matrix are desired to be printed, then a '1' is specified next.

The second and the following cards to a minimum of five cards, contain the ordinates when they are read in. The ordinates of the joints are punched in the order in which they are numbered followed by the ordinates of cable joints on the edge beams starting from the top left hand corner and proceeding clockwise. These cards are omitted when the ordinates are calculated in the program.

The next card contains the pretensions in the two directions, the ratio of the sides of the roof, which defines the non-orthogonality of the cables, the height and width of the roof and the thermal coefficient of expansion for the type of steel used. This is followed by a card containing the steel areas in the two directions, the elastic modulus, the yield stress, the ultimate stress and the ultimate strain.

Next comes a set of cards to define the loading. The

first card of this set contains the number of loads, that is, the first one and any subsequently added loads. The next card contains the load in all three directions at one joint. If this load is uniform then the next card contains a zero, otherwise it specifies the number of joints at which the load is different, followed by one or more cards containing the number corresponding to the joint and the magnitude of the load at each of those joints. The next card contains the number of increments the load should be divided into before and after the first yielding, the latter in the case of ultimate load. If the ultimate load is desired, a zero is punched next on the same card. Otherwise the number punched is 1. These are followed by similar sets of cards for subsequently added loads. More sets are provided for more loadings and there is no limit on the number of additional sets of data processed. Only the number of joints of the roof is limited by the size of the computer.

3.1.3 Working of the Program

The working of the program is best explained by means of the flow-chart given in Fig. (3-1). After the input is read in first, calculations to determine the stress-strain curve of the material are carried out and the work areas are initialized. The ordinates of the joints are calculated if necessary and the lengths of cable segments are calculated.*

* The length of the cable segment is calculated assuming that the cable is a flat parabola and that the lengths of two adjacent segments are equal. See reference (48), page 19.

If the load is applied subsequent to some previously added load, then these initial calculations are omitted. The direction cosines are then computed and the cable stresses and the corresponding modulii are determined. A check is also made on the proportional limit, yield and the ultimate loads. If the ultimate load is reached, the program is terminated. Otherwise, the program continues and the initial values of the displacements are calculated from the linearized version of equations (2-17). Using these values, tension increments in the cables are estimated. This helps to determine whether unloading or reloading takes place in a cable after the proportional limit has been exceeded, so that the proper modulus (which is the initial elastic modulus) could be used in the calculations. It also enables the use of a more accurate modulus in the inelastic region corresponding to an average stress rather than to the initial stress level and also reactivating any slack cables that become taut again.

Once these are done, the initial values are calculated again using the improved stiffnesses and the iteration cycle is started. The matrix of linear terms $\underline{S}_1$ and that of non-linear terms $\underline{S}_2$ are both generated by calling the subroutine ANMX. The instantaneous stiffness matrix $\underline{S}$ and residual matrix $\underline{R}$ are then generated and convergence is tested by checking each of the residuals against a predefined tolerance. When convergence is obtained, the tension increments are calculated using the final displacements and the cable tensions are adjusted and the procedure is repeated if necessary.

When the ultimate load is required, the external load is repeatedly increased until the ultimate stress is reached in the most highly stressed segment of the cables.

3.1.4 Subroutines

The main program described above was used in conjunction with two subroutines named ANMX and DGELB. The former generates the submatrices $\underline{S}_1$ and $\underline{S}_2$ which are combined to form the stiffness matrix and the residual matrix, and calculates the tension increments while the latter inverts the stiffness matrix $\underline{S}$ during iteration.

Subroutine ANMX when called first at each joint, generates the linear terms and the contribution of the temperature change to the load vector. When called again during the iteration, ANMX organizes the current values of the displacements and calculates the nonlinear terms. This is repeated when it is called again to calculate the tension increments.

Subroutine DGELB is taken from IBM System/360 Scientific Subroutine Package-Version III. It is used to solve a system of simultaneous equations with a coefficient matrix of band structure. The main program numbers the joints and arranges the coefficients so that the band width is kept to a minimum. The band matrix is stored rowwise in successive locations for solution by subroutine DGELB. The solution in this case yields $S_r^{-1}R_r$ which is the correction to the displacement vector in the r^{th} cycle (equation 2-24). The solution is carried out by means of Gauss elimination with

column pivoting only, in order to preserve the band structure in the remaining coefficient matrices. The use of this subroutine and the resultant saving in space enables roofs with large number of joints to be analyzed. For example, for a roof with 61 joints, the space required is about 25% of what it would have been if the entire matrix was stored. The execution time is also reduced in approximately the same ratio since unnecessary calculations involving zeros are eliminated.

Listings of subroutine ANMX and DGELB together with that of the main program are given in Appendix (C).

3.2 Solution Technique and Convergence

The solution of equations (2-17) involves the solution of their linearized form to obtain the starting values and of equation (2-24) during each iteration to obtain the correction terms. The solutions of simultaneous linear equations are obtained by the Gauss elimination process. This method has been found to be more advantageous than other iterative methods, for the solution of a large number of simultaneous equations in structural problems (86).

The stiffness matrix for a cable network based on the linear terms is a positive definite matrix since the strain energy U in the system is given by,

$$U = \frac{1}{2} \sum_{i=1}^{n} F_i u_i$$

where u_i is the displacement vector, and

F_i is the force vector,

or in matrix form by,

$$U = \tfrac{1}{2}\{u\}^T\{F\} \qquad \ldots 3\text{-}2$$

Substituting $[k]\{u\}$ for $\{F\}$ in equation (3-2) gives,

$$U = \tfrac{1}{2}\{u\}^T[k]\{u\} \qquad \ldots 3\text{-}3$$

Equation (3-3) is a quadratic form in u_i since the stiffness matrix $[k]$ is symmetric and since the strain energy U is always positive for any arbitrary value of u_i, the matrix $[k]$ is positive definite. The instantaneous stiffness matrix generated during the iteration cycle loses the positive definite property since it contains terms involving the displacements themselves and is no longer symmetric.

The stiffness matrix, however, is not well-conditioned. The ill-conditioning is inherent in analyzing suspension roof problems (31). Every third row of the stiffness matrix has the main diagonal term non-dominant and smaller than other terms in the same row. This is illustrated in Fig. (3-2) where the stiffness matrix for a cable network with five joints is given. The nondominance of diagonal terms is a characteristic of ill-conditioned matrices since it may introduce a certain amount of linear dependency between the

equations.

The matrix is stored in a band form to conserve memory space in the computer. Only column pivoting is used during the solution of equations since complete pivoting will destroy the band structure. Hence the round-off errors would be more than in the case of complete pivoting. To counteract this and the ill-conditioning of the matrix and improve the accuracy of the solution, double-precision arithmetic is used. This necessitates the use of more computer space and time but the appreciable saving in space by the use of the band matrix and in time by the elimination of computations involving zeros and the use of column pivoting only, more than compensates for the extra expenditure. It is also a necessity considering the large number of equations solved - 183 equations for the 61-joint single roof.

The convergence of the solution for displacements is fast - in most cases convergence is obtained in three or four iterations. Poskitt (58) suggests starting the iterations from zero but the starting values used in the program here are obtained by solving the linear portion of equations (2-17). No extra effort is needed to program this and the convergence is much faster from the linear values. When the nonlinearity is high and there is no convergence, Poskitt suggests using a more accurate starting value obtained by an incremental procedure. But it is found convenient in general, and necessary in the inelastic range, to use an incremental load method and solve the set of nonlinear equations at each step.

In the elastic range the step-by-step method is necessary only when there is no convergence but in the inelastic range it is essential that the step-by step method be used due to the constantly changing modulus.

It has been found that applying the load in a number of increments does not affect the final tensions and displacements very much. Fig. (3-3) shows the variation of the maximum tension increment in a non-orthogonal single roof of dimensions 120 ft x 240 ft x 12 ft high due to a uniform vertical load. The tension increment and the load are both expressed in dimensionless form as ratios of H, the horizontal component of the pretension. Graphs of the linear solution of the maximum tension increment and the nonlinear solutions obtained with the load applied in 6 and 12 increments respectively are shown. The difference between the linear and nonlinear solutions is as much as 15% while the difference between the two nonlinear solutions is only 1%. In the elastic range, keeping the number of increments to a minimum, provided there is convergence, results in a saving of computer time. This is borne out by the fact that when 6 increments were used, a complete solution involved 6 linear solutions and 15 iterations while 12 linear solutions and 24 increments were needed when 12 increments were used. This means an expenditure of approximately 70% more time for a gain of only 1% in the accuracy of the results.

To investigate the speed of convergence and check the accuracy of solutions obtained, comparisons were made with

the results obtained by Thornton for an orthogonal hyperbolic paraboloid net with 25 joints (Fig. 3-4). The orthogonal net is a special case of the general non-orthogonal net with $\theta = 0$. Four cases of loading were considered:

(i) vertical load of 1 kip at each joint with H, the horizontal component of cable pretension equal to 50 kips in all the cases,

(ii) vertical load of 1 kip at each joint plus additional load of 14 kips at joint 9, with H = 50 kips,

(iii) same loading as in (ii) with H = 25 kips, and

(iv) in addition to the load in (ii), a horizontal load of 10 kips at joint 9 in the $\bar{3}$ direction.

Thornton's results for loading cases (i), (ii) and (iv) are taken from reference (77), while that for loading case (iii) is from reference (76).

Thornton used the method of continuity and the solution in case (i) involved 41 solutions of the 75 simultaneous equations. The program developed in this study required only 3 solutions with the load applied in one increment. The maximum difference of 4% between the linear and nonlinear solutions for the displacements does not warrant even 3 solutions since one solution of the linear equations would have yielded sufficiently accurate results. Solution of case (ii) involved 30 solutions with the load applied in 10 increments in this study. The difference between the linear and nonlinear solutions in this case was 19% (77). Corresponding figures for loading case (iii) are 31 solutions, 10 increments and 56%.

Table(3-1). Comparison with Thornton's Results.

(a) Loading Cases (i), (ii) and (iii)

Joint No.	Vertical Displacement (feet)					
	Case (i)		Case (ii)		Case (iii)	
	Thornton	Writer	Thornton	Writer	Thornton	Writer
1	0.254	0.256	0.381	0.381	0.501	0.507
5	0.552	0.557	1.268	1.267	1.454	1.437
9	0.772	0.777	3.718	3.733	4.786	4.851
13	0.861	0.866	1.722	1.724	2.021	2.012
17	0.772	0.777	1.020	1.022	1.229	1.238
21	0.552	0.557	0.605	0.606	0.813	0.822
25	0.254	0.256	0.259	0.259	0.414	0.420

(b) Loading Case (iv)

Joint No.	Vertical Displacement (feet)		Cable	Horizontal Component of Cable Tension (kips)	
	Thornton	Writer		Thornton	Writer
A	0.000	0.000	(1,1)	45.947	46.069
1	0.445	0.446	(5,1)	46.056	46.145
5	1.368	1.368	(9,1)	46.264	46.351
9	3.750	3.765	(13,1)	36.657	36.743
13	1.664	1.665	(17,1)	36.679	36.061
17	0.963	0.964	(21,1)	36.697	36.073
21	0.558	0.559	(25,1)	36.710	36.702
25	0.228	0.228	(25,2)	37.706	36.736
C	0.0	0.0	-	-	-

Solution for loading case (iv) in the present analysis involved 30 solutions in 10 increments of loading. The linear and nonlinear solutions of the final cable tensions in this case differed by as much as 101% (77).

The results obtained by the present analysis are basically the same as those of Thornton's, as seen in tables (3-1a) and (3-1b). The difference is less than 1% in almost all the displacements. The number of solutions required for loading cases (ii), (iii) and (iv) have not been given by Thornton but it is reasonable to assume that they would have been at least equal to that of case (i). The procedure used here, therefore, can be said to give accurate results even when the nonlinearity is high, with less amount of computational work. The accuracy of the results when high nonlinearity exists is established later when results from the experimental work are discussed. Numerical studies on the elastic and inelastic behaviour of single and double hyperbolic paraboloid networks are presented in the following chapter.

CHAPTER IV

NUMERICAL STUDIES

4.1 Introduction

In order to determine the general behaviour of a non-orthogonal hyperbolic paraboloid cable-net, numerical investigations were carried out under various modes of loading. Several aspects of the roof including the effects of varying certain parameters were also studied. Similar studies were undertaken for an orthogonal double roof covering the same area in plan. This provided a comparison between the two types of roofs.

The two roofs are shown in plan in figures (4-1a) and (4-1b). The arrangements of the cables are also shown in these figures. The non-orthogonal single roof has 61 joints and the orthogonal double roof has 28 joints with these arrangements. The dimensions in plan of 120' x 240' and the height of the roof, which is defined as the rise from A to B, are the same in both cases. In both cases, the roof rises by 12 ft from A to B, dropping to the same level as A at C and again rising by 12 ft to D. The points B, C and D, however, do not refer to corresponding points on the boundary in the two cases. In the double roof, the boundary rises by 12 ft from D to E before dropping by the same height to F which

corresponds to point D on the single roof. The single roof is non-orthogonal with $\sin\theta = 0.60$ while the double roof is orthogonal with $\sin\theta = 0$.

Values of 24,000 ksi for the elastic modulus and 6.89×10^{-6} for the thermal coefficient of expansion were used in the calculations. Unless specified otherwise, horizontal components of tensions of 50 kips and a steel area of 1.25 in^2 in both directions were used. The total length of cable used is 3230 ft in the case of the single roof and 2040 ft in the case of the double roof.

The deflections and the tensions, tension increments and the applied load are plotted in dimensionless parameters, the first as a ratio of the height of the roof and the others as ratios of H, the horizontal component of the pretension. When the tension or tension increment in an individual cable segment is given, the cable segment is referred to as cable (J, I) where J is the joint number at one end of the segment and I is one of four directions, directions 1 and 2 being the negative and positive ξ directions respectively, and directions 3 and 4 being the negative and positive η directions respectively (Fig. 4-1c).

4.2 Elastic Analysis

4.2.1 Deflections and Tensions Under a Uniform Load

Initially the deflections and tension increments under a uniform load were calculated. A load of 1 kip/joint of the single roof corresponds to a uniformly distributed load of

5 psf of plan area. This in turn is equivalent to 2 kip/joint of the double roof. The variation of the maximum vertical deflection with the applied load in the two cases is shown in figures (4-2) and (4-3). The maximum deflection occurs at joint 31, the centre of the single roof and at joint 20 of the double roof. Deflection contours for the two roofs for a load of 30 psf of plan area have been drawn in figures (4-4) and (4-5). A comparison of the vertical displacement and the horizontal displacements is shown in figure (4-6) for the single roof and in figure (4-7) for the double roof. The deflections are shown at joint 22 for the former and at joint 8 for the latter. These joints were chosen since they exhibit the largest horizontal deflections - 5-10% of the vertical deflections at these joints. The maximum tension increment due to the uniform load in the single roof is given in figure (3-3) with both linear and nonlinear solutions plotted against the applied load. The maximum tension increment is developed in cable (17,4) of the single roof. The corresponding maximum tension for the double roof is plotted in figure (4-8) with both linear and nonlinear solutions shown. This is developed in cable (3,4).

4.2.2 Uniform Applied Load in More Than One Direction

In addition to the vertically applied load, loads were applied in one or both horizontal directions. The horizontal loads simulate the effect of wind loads on the roof. Wind loads of any magnitude and direction can be expressed in terms of

the loads in the three directions. Pure vertical load, vertical load combined with the horizontal load in each direction and loads in all three directions were applied uniformly and the maximum tension increment developed has been plotted against the load in figures (4-9) and (4-10) for the single and double roofs respectively. These figures illustrate the effect of windloads on the structure but several different combinations with loads acting over the entire area and on portions of it should be considered to determine the worst possible combination in any particular case.

To illustrate the fact that the linearized solution can sometimes lead to grossly misleading results, the reduction in tension in a prestressing or tie-down cable has been plotted against the load which was applied uniformly in the r and z directions with both linear and nonlinear solutions given. The reduction in tension in cable (1,1) of the single roof is shown in figure (4-11) while that in cable (6,4) of the double roof is shown in figure (4-12). The linearized solution predicts that the cables are slack in both cases at the maximum load, while in reality the tensions are close to the pretensions even though there was some relaxation at a lower load. It is apparent that the tensions in these cables will increase further on increasing the load.

4.2.3 Application of Concentrated Loads

The behaviour of the roofs under concentrated loads at specific joints were also studied. The nonlinearity can be

expected to be higher here than when uniformly distributed load is applied. Load concentrations can occur during the erection and fabrication of the roof-decking or even later as applied dead or live load. The concentrated loads were applied symmetrically and unsymmetrically.

(a) Single Roof

The concentrated load was applied at joint 9 in addition to a uniform load of 1 kip/joint and was increased from zero to 6 kips. This represents an unsymmetrical load while a similar concentrated load applied at joint 31 represents a symmetrical load. The vertical deflection at joint 9 due to the concentrated load there and the maximum tension increments are given in figures (4-13) and (4-14). The maximum tension increment is produced in cable (4,4). The vertical deflection at joint 31 and the maximum tension increment in cable (31,4) produced by a uniform load of 1 kip at each joint and a concentrated load at joint 31 are shown in figures (4-15) and (4-16) respectively. The deflection contours for the two cases of loading have been drawn in figures (4-17a) and (4-17b).

(b) Double Roof

Similar concentrated loads were applied on the double roof in addition to a uniform load of 2 kips at each joint (equivalent to 1 kip/joint on the single roof). A single concentrated load at joint 13 constituted an unsymmetrical

loading while two equal concentrated loads at joints 13 and 16 formed a symmetrical loading. The vertical deflection at joint 13 in the two cases of loading are plotted in figures (4-18) and (4-20) while the maximum tension increment, which is produced in cable (3,4) in both cases of loading, is plotted against the concentrated load in figures (4-19) and (4-21). The concentrated load here is increased from zero to 14 kips representing the same load per square foot of plan area as in (a) for the single roof. The deflection contours for the two cases of loading have been drawn in figures (4-22a) and (4-22b).

4.2.4 Temperature Effects

The effect of temperature changes on the deflections and tensions in a cable roof cannot be neglected as small due to the long spans made possible by the very use of cables themselves. This is particularly true in countries outside the tropics where large changes in temperatures take place within short periods of time. Cable roofs erected during one season of the year should be guarded against stresses introduced by temperature changes during the others.

The analysis including the temperature effects is also complicated by the fact that the behaviour of a cable roof is nonlinear. Examination of equations (2-17) suggests that the temperature terms are included even in the linear terms of the equations. This means that the temperature effects cannot be superposed as in a conventional structure even when only

a linear solution is sought. The presence of the temperature terms in the linear (and nonlinear) terms of the stiffness matrix stems from the fact that the equations were derived based on the deformed geometry of the structure (see derivation of equation (2-14) from equation (2-10a)). The linearized form of the nonlinear equations are, therefore, different from the small-deformation equations for conventional structures.

Temperature effects in the two cable roofs considered here are studied by applying a uniform load and at the same time imposing temperature changes of $-50^{\circ}F$, $0^{\circ}F$ and $+50^{\circ}F$. A value of 6.89×10^{-6} (84) for the thermal coefficient of expansion for steel is used. The maximum tension increment produced by the applied load and the temperature changes are shown in figure (4-23) for the single roof and in figure (4-24) for the double roof.

4.2.5 Effect of Non-orthogonality

Two-way cable networks having the particular shape studied here are rectangular hyperbolic paraboloids with the two sets of cables orthogonal, when the area covered in plan is a square or a rhombus. When the area covered is a rectangle, the cables are no longer orthogonal and the degree of non-orthogonality is a function of the ratio of the sides of the rectangle. The non-orthogonality is defined by the angle θ between the y and η axes when the ξ, η axes are chosen to coincide with the two directions of the cables. Angle θ is

given in the case of a single roof by,

$$\sin\theta = \frac{R^2-1}{R^2+1} \qquad \ldots 4\text{-}1$$

where R is the ratio of the sides. For a square, R=1 and $\sin\theta = 0$.

In the case of a double roof, the network is orthogonal when R = 2, i.e. when the side having the larger number of internodes is twice as long as the other. Angle θ in the case of the double roof is given by,

$$\sin\theta = \frac{R^2-4}{R^2+4} \qquad \ldots 4\text{-}2$$

or in general,

$$\sin\theta = \frac{R^2-NTYP^2}{R^2+NTYP^2} \qquad \ldots$$

where NTYP is the type number defined in section (3.1.2). The effect of non-orthogonality of cables was investigated by varying the ratio of the sides. In order to keep the applied load constant while changing R, the area in plan was kept constant so that the load per joint remained the same. The width and length of the roof for the different values of R are given in table (4-1) for both single and double roofs.

Table 4-1

Roof Dimensions with Constant Plan Area and Varying R

R		1.0	1.2	1.4	1.6	1.8	2.0
Roof width (feet)		169.7	154.8	143.4	134.0	126.2	120.0
Roof length (feet)		169.7	185.8	200.8	214.4	227.2	240.0
Sinθ	Single Roof	0.0	.1803	.3243	.4382	.5283	.6000
	Double Roof	-.6000	-.4706	-.3423	-.2195	-.1050	0.0

The maximum deflection is plotted against the load for values of R between 1.0 and 2.0 in figure (4-25) for the single roof and in figure (4-26) for the double roof. The variation in the tension increment due to the change in non-orthogonality is quite small as seen from tables (4-2a) and (4-2b) for the single and double roofs respectively.

4.2.6 Effect of Varying Cable Pretension

The behaviour of a cable roof depends to a great degree on the cable pretension. The pretensioning of the cables prevents uplift due to wind and increases the stability of the roof. It also prevents large deformations of the roof by stiffening it. A two-way cable net can be pretensioned,

(a) symmetrically, with equal horizontal tension components

Table (4-2). Effect of Changing Non-orthogonality on Tension Increments.

(a) Single Roof

Load/Jt (kips) / R	1.0	2.0	3.0	4.0	5.0	6.0
1.0	18.89	39.60	59.97	79.14	96.98	113.6
1.2	18.92	39.66	60.03	79.18	96.98	113.6
1.4	19.00	39.82	60.18	79.25	96.97	113.5
1.6	19.11	40.00	60.33	79.31	96.91	113.3
1.8	19.22	40.19	60.47	79.34	96.80	113.0
2.0	19.40	40.44	60.60	79.31	96.62	112.7

(b) Double Roof

Load/Jt (kips) / R	2.0	4.0	6.0	8.0	10.0	12.0
1.0	26.01	51.92	76.42	99.74	119.4	132.7
1.2	25.56	51.04	75.29	99.69	118.9	131.9
1.4	25.27	50.45	75.10	98.45	118.4	132.8
1.6	25.07	50.06	74.62	97.97	118.3	132.2
1.8	24.97	49.85	74.33	97.65	118.0	132.0
2.0	24.95	49.82	74.28	97.59	118.0	132.0

in cables in both directions, or

(b) unsymmetrically, with the pretension in cables in one direction different from that of the other.

(a) Symmetrical Pretension

When the pretension is symmetrical, the unloaded roof takes the form of a hyperbolic paraboloid. This shape is independent of the magnitude of the tension in the cables as long as the horizontal component of the tension is the same in all the cables. When the load is applied, the roof deforms into a new shape depending on the magnitudes of the load and cable pretension. The single and double roofs considered here are subjected to applied loads with pretensions ranging from values corresponding to H = 30 kips to H = 80 kips. The maximum deflection, maximum tension increment and the maximum cable tension are plotted against the applied load in figures (4-27), (4-28) and (4-29) for the single roof. Corresponding graphs for the double roof are given in figures (4-30), (4-31) and (4-32). The applied load is expressed in dimensionless form as a ratio of the stiffness of the cable since the pretension is a variable. The deflections and tension increments decrease with the increase of pretension as expected. The final cable tension increases with the pretension but as the load increases, the differences in cable tensions tend to become small.

(b) Unsymmetrical Pretension

When a roof with symmetrical pretension is loaded, the

deformed shape is no longer a hyperbolic paraboloid. The tensions in the load-carrying cables increase under the load while those in the prestressing cables decrease. This means that about half the number of cables are understressed during the entire life of the roof. This situation could be improved and all the cables could be utilized efficiently if an unsymmetrical pretensioning is used with a higher tension in the prestressing cables. When the load is applied, the tensions in all the cables tend to become equalized. This also enables a more even shape under the load. An optimum value of pretension could be determined by examining the effect of varying the pretension in the prestressing cables while keeping the tension in the load-carrying cables constant. Figure (4-33) shows the variation in maximum deflection due to change in pretension in the ξ direction. This deflection decreases with increase in ξ pretension. Figure (4-34) shows the final cable tension, both maximum and minimum, and the maximum pretension plotted against the ξ pretension for the single roof at a load of 6 kips/joint. It is seen that the final cable tensions lie within a narrow neck at pretensions of 120 kips and 50 kips in the ξ and η directions respectively. Similar graphs for the double roof are shown in figures (4-35) and (4-36). Due to the shape of the roof here, no particular advantage is gained by using unsymmetrical pretension.

4.2.7 Use of Unequal Steel Areas

The differential tension changes in the two sets of

cables can also be taken care of by providing unequal steel areas in the two directions. This will retain the initial shape of the roof while the final cable stresses will be more evenly distributed. Alternatively, the use of unequal areas may be combined with unsymmetrical pretensioning to further improve the efficient use of the material. This has been illustrated by the graph in figure (4-37) where the steel area in the ξ direction has been varied from 1.00 in^2 to 1.25 in^2 while keeping the steel in the η direction constant at 1.25 in^2. The optimum pretensions of 120 kips and 50 kips obtained in section (4.2.6) were used in the ξ and η directions. The maximum stress produced decreases with the steel area in the ξ direction with the minimum stress remaining almost unchanged. The minimum steel area that produces the maximum stress not in excess of the proportional limit can be taken as the ideal amount. As before, there will not be any advantage in using unequal areas in a double roof.

4.2.8 Effect of Roof Slope

The cable roof behaviour is also significantly influenced by the slope of the roof. The curvature or the slope of the roof is a function of the roof height as defined in section (4.1). To investigate the effect the roof height has on the resulting deflections and tension increments, roofs of different heights were analyzed under an increasing applied load. The maximum deflections in the single roof with heights varying from 1 foot to 60 feet are plotted against load in

figure (4-38). The deflections are expressed as ratios of the roof width W, since the roof-height is variable here. The deflections decrease gradually with the increase in roof-height. The nonlinearity is high when the height is small but it decreases as the height increases, at the same time exhibiting a change in the shape of the load-deflection curve. The load-deflection curve which exhibits a 'strengthening' effect as the load increases, also shows a 'weakening' effect of the roof as the roof height increases. This effect is also seen with the tension increments (Fig. 4-39). The tension increment which exhibits a 'strengthening' effect for roofs with height less than 12 feet has the opposite effect for roofs with height more than 12 feet. This height of 12 feet can be thought of as a dividing line between roofs of small curvatures and large curvatures which appear to be different in their nonlinear behaviour. It is also seen that the tension increments are greatest at this particular roof-height. This is clearly seen from graphs of tension increments plotted against roof-height, the latter expressed as a ratio of the roof width, (Fig. 4-40) at different load levels.

It is now appropriate to define a 'critical height' in relation to cable roofs as that height that produces the maximum tension in the cables at a particular load level. This will help to differentiate between small and large curvature roofs and determine their behaviour. The critical height changes as the applied load changes.

The orthogonal double roof analyzed here is also found

to exhibit a similar behaviour. The deflections and tension increments for roofs of different heights have been plotted against the applied load in figures (4-41) and (4-42) while the tension increment is plotted against roof height in figure(4-43). The critical height of the double roof is smaller than that of the single roof - 8 feet at a load of 2 kip/joint corresponding to 12 feet in the single roof.

4.2.9 Effect of Using a Sparser Net

A cable roof in practice will consist of a large number of joints and equations, three times this number will have to be written in analyzing the roof. When cable roofs covering large areas have to be analyzed, it becomes almost impossible even with the present day large computers. This necessitates the solution for a sparser net replacing the actual net for the purpose of computations, a scheme which is similar to the use of the finite difference mesh for continuous surfaces. It can also be said to be a similar approximation to using the method of continuity for cable roofs, only in the opposite sense.

In order to determine the loss of accuracy when a sparser net is used for the purpose of analysis, an actual single roof net with 113 joints was replaced by fictitious nets of equivalent stiffness but with smaller number of joints. The total steel area in each direction was assumed to remain the same so that when the number of cables is reduced, the steel area is proportionately increased. The pretension in

the cables is also correspondingly increased with the result that the total force in each direction remains constant. The resulting change in tensions are reduced in the same ratio by which the initial tensions were increased in other words, the stresses in the cables, rather than the actual tensions were considered. The results are shown in tables (4-3a) and (4-3b).

Table (4-3a) contains the data used in the calculations. The data in the first row of the table represent the actual net while the others represent equivalent nets. Table (4-3b) contains the calculated deflections and tension increments reduced in the original ratio and the percentage errors in the results. The errors in the centre deflections and tension increments are less than 10% in most cases.

4.3 Inelastic Analysis and Ultimate Load

The inelastic analysis for cable roofs was carried out using the theoretical model for the cable stress-strain curve developed in section (2-3). An incremental load method was used with the tangent modulii corresponding to the stress levels in the cables being updated at each step. Instead of using the modulus corresponding to the stress at the beginning of each step, a more accurate value of the modulus was used by first calculating the tension increments from the linear values of the displacements and basing the modulus on the average stress thus determined. The preliminary calculation of the tension increments also helps to determine whether

Table (4-3). Effect of Using a Sparser Net in Analysis

Type of Roof: Non-orthogonal Single

Applied Load = 50 psf of plan area

Dimensions of Roof: 120 ft x 240 ft x 12 ft high

E = 24,000 Ksi, Steel Area = 6.0 sq. in.

(a) Table of Data

No. of internodes	No. of joints	No. of cables	Steel area (sq. in)	Pretension (kips)	Load/jt. (kips)
8	113	15	6.00	500.0	5.63
6	61	11	8.18	681.7	10.00
5	41	9	10.00	833.3	14.40
4	25	7	12.86	1071.4	22.50
3	13	5	18.00	1500.0	40.00

(b) Table of Results

No. of internodes	Deflection at centre	Max. tension inc. (kips)		Reduced max. tension inc. (kips)		Error (%)	
		Negative	Positive	Negative	Positive	Deflection	Tension
8	1.31	-66.8	88.6	-66.8	88.6	0.0	0.0
6	1.29	-88.0	118.2	-64.5	87.0	-1.5	-1.8
5	1.25	-102.4	137.1	-62.0	82.2	-4.6	-7.2
4	1.23	-130.1	167.1	-60.8	78.0	-6.1	-12.0
3	1.20	-178.3	221.8	-59.7	74.0	-8.4	-16.4

unloading is taking place in the inelastic range so that the elastic modulus instead of the tangent modulus is used. This applies for reloading too until the previously attained inelastic stress is reached again. Thus simulation is made of the actual inelastic behaviour of the material in following different paths on the stress-strain curve while loading and unloading. The permanent deformation in the cable is also taken into account when a cable previously loaded into the inelastic range and now slack, is brought back into play.

When the ultimate load is calculated, the external load which is applied in any desired increment size, is increased repeatedly until the ultimate load is reached. If desired, a different increment size could be used after the first yielding starts. A smaller increment may be used to arrive at an accurate value for the ultimate load but it has been found that a larger increment will reduce the computer time without affecting the accuracy very much since the change in the modulus after the yield point is slow and the roof as a whole stiffens under increased tension and becomes less nonlinear.

The criterion for failure of the roof is the reaching of the ultimate stress in the most highly stressed segment of the cables. The cable segment is assumed to break at this point and the roof is considered to have reached its ultimate capacity. At smaller loads one or more segments might lose their pretension and become slack. This is not considered failure of the roof. The slack portions of the cables are theoretically removed from the system and are considered

non-existent as long as they remain slack. If the displacements of the joints at the end of such slack cables warrant it, these cables are automatically brought back into the system. It has been found in calculating the ultimate loads, that cables that become slack during the loading, become active again as the load increases and contribute to the load-carrying capacity of the roof.

In the numerical calculations of the ultimate load, values of 24,000 ksi for the elastic modulus, 155 ksi for the yield stress, 250 ksi for the ultimate stress and 4.5% for the ultimate strain were used. The proportional limit of the theoretical stress-strain curve fitted to these values is 124.9 ksi. The stress-strain curve is shown in figure (4-44) and the values of the tangent modulus at various stress-levels in the inelastic range are tabulated in table (4-4) together with the corresponding strains.

The value of the ultimate load for the single roof was calculated and found to be 49.1 kips/joint. It was 65.2 kip/joint for the double roof. Temperature changes of $\pm 50^{\circ}F$ did not alter the ultimate load noticeably in either case. The ultimate load for the single roof calculated with the optimum pretensions of 120 kips and 50 ksi in the ξ and η directions respectively, was slightly higher - 49.6 kips/joint.

Figures (4-45) and (4-46) show the inelastic variation of the maximum tension for single and double roofs respectively with heights of 6 feet, 12 feet and 60 feet. The ultimate load is highest for the flat roof. For the critical slope

Table (4-4). Values of Tangent Modulus in the Inelastic Range

Stress (ksi)	Strain(%)	Modulus(%)	Stress (ksi)	Strain(%)	Modulus(%)
124.9	0.519	24000	190.0	1.728	3036
125.0	0.521	23799	195.0	1.898	2845
130.0	0.547	15595	200.0	2.079	2677
135.0	0.585	11597	205.0	2.272	2527
140.0	0.634	9231	210.0	2.475	2393
145.0	0.693	7666	215.0	2.690	2273
150.0	0.764	6556	220.0	2.915	2164
155.0	0.846	5726	225.0	3.152	2066
160.0	0.939	5083	230.0	3.399	1975
165.0	1.043	4569	235.0	3.658	1893
170.0	1.158	4150	240.0	3.927	1817
175.0	1.284	3801	245.0	4.208	1747
180.0	1.421	3507	250.0	4.500	1682
185.0	1.569	3254			

Table (4-5). Ultimate Loads and Deflections

Roof Height (feet)	Single Roof			Double Roof		
	Ultimate Load		Deflection at ultimate load (feet)	Ultimate Load		Deflection at ultimate load (feet)
	kips/jt	psf		kips/jt	psf	
6	52.0	260	23.7	86.1	215	18.1
12	49.1	245	22.5	65.2	163	15.9
60	34.5	172	14.7	54.0	135	10.6

i.e. for height of 12 feet, the tension change is maximum initially but as the load increases, the stiffening of the roof counteracts the reduction in modulus and the ultimate load is high. For a steep slope, though the initial tension change is small, the ultimate load is low due to the weakening effect under load. For a gentle slope, the small initial change and stiffening effect add up to a higher ultimate load. The ultimate loads and the corresponding deflections for the three-heights are shown in table (4-5) for both the single and the double roofs.

CHAPTER V

EXPERIMENTAL INVESTIGATION

5.1 General Comments

Any theory, in order to uphold the correctness of results obtained by its use, should be supported by experimental results. The idealized conditions assumed in the theoretical analysis is impossible to realize in practice but a comparison with the experimental results will help to determine whether the theory is capable of predicting the actual behaviour of a structure within reasonable limits. The prime concern in carrying out the experimental investigation was, therefore, to verify the validity of the theoretical results. It was not intended to be a model analysis to determine the behaviour of a prototype.

The size of the experimental model used was small - 6 ft x 3 ft in plan. This choice was influenced by considerations of space limitations, cost and the amount of labour that would be involved in the fabrication and testing of the model. A model of a larger size could be expected to represent the behaviour of an actual structure better but since the theory could be used to analyze the smaller model without recourse to model laws and since there are no severe limitations on the use of the theory on a small-scale model, its use is perfectly justified.

In a previous study (48), a model of a non-orthogonal single roof fabricated of 1/8 inch diameter, solid aluminum wires was used. The tensions in the wires were measured by mounting strain gages directly on the wires. Deflections were measured by dial indicators set at the joints. The deflections were small and the behaviour was nearly linear due to the relatively high stiffness of the solid wires used. The wires, being solid, also possessed some definite bending stiffness which was neglected in the theory.

In the present study, it was intended to use a more flexible model which will exhibit nonlinear behaviour and to make more accurate measurements of the tensions and deflections. In addition to testing the efficiency of the theory in its use for nonlinear cable roof problems, it was also the intention to examine its performance in regard to the behaviour under different conditions such as the discontinuity that occurs due to the slackening of one or more cables during the loading.

5.2 Preliminary Work

In order to come up with a suitable model and to determine the best methods of measuring tensions and deflections, preliminary investigations were carried out on a model built specifically for this purpose. This consisted of 1/16 inch diameter, stainless steel wire ropes of 7 x 7 construction bounded by an unyielding rectangular frame. It was decided to use wire rope, instead of solid wire for two reasons:

(i) wire rope had greater flexibility and less stiffness than a solid wire of the same diameter thereby contributing to the nonlinearity of the model, (ii) wire rope is used in practical roofs and hence the model would be a true representation of one. Tension measurements in the model was made with precalibrated aluminum rings connected at the ends of the cables. Strain gages were mounted on the rings which were then calibrated before being built into the model. The strain measurements and the consequent tension measurements were found to be stable and this provided a satisfactory method of measuring the tensions. The deflections were first measured by dial indicators placed at the joints. The measurements were then repeated with displacement transducers. The latter measurements were found to be more accurate. Another advantage in using the displacement transducers was that their cores, being of negligible weight, exerted no extra load at the joints unlike the spring-loaded plunger of a dial indicator. It was therefore decided to use displacement transducers for the deflection measurements in the final work. The model exhibited nonlinear behaviour but this was still too small to be measured with the accuracy of measurement used.

5.3 Fabrication of the Final Models

5.3.1 General

Two models were built for the final tests. One was a non-orthogonal single roof model while the other was an orthogonal double roof model. It was decided to use the same

plan area for both, so the single roof model was built first, tested and on completion of this, the double roof model was built using the same boundary frame and tested. The frame consisted of four channels 12 in x 3 in x $\frac{1}{4}$ in welded to form a 6 ft x 3 ft x 1 ft deep rectangular box. Appropriate holes were driven on the webs of channels for end connections. A framework with members so oriented as to take the place of the edgebeams of the roof could have been used but instead the rectangular box with excessive rigidity was used to justify negligible support movement and for ease of construction.

Both models consisted of five cables in each direction and the same aluminum load cells - twenty of them - were used in both cases. The cables were 3/64 inch diameter stainless steel wire rope of 7 x 7 construction manufactured by MacWhyte wire rope company. They were soldered to bolt-like terminals at the ends for connection to the frame. Screw-threads were provided on these terminals for tensioning and also to adjust for any minor variations in length. The load-cells were connected at four inches from the ends of the wire ropes. A length of the wire rope equal to the diameter of the load cell was cut off and ball-and-shank terminals were soldered at the ends. The wire rope was then threaded through holes on the load cells. The end connection and connection to the load cells are illustrated in photographs (1) and (2) where the former shows the connection at a corner while the latter shows an intermediate connection . Small clamps were used to clamp the cables together at the joints (photograph 3).

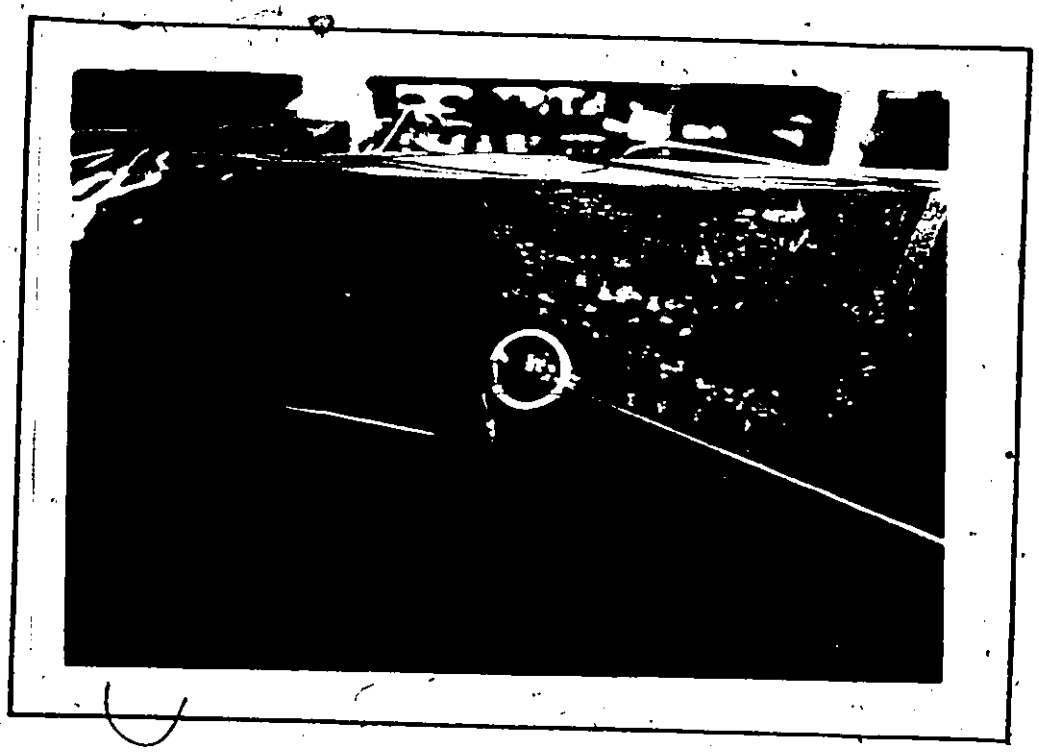

Photograph 1: Load Cell and End Connection at a Corner

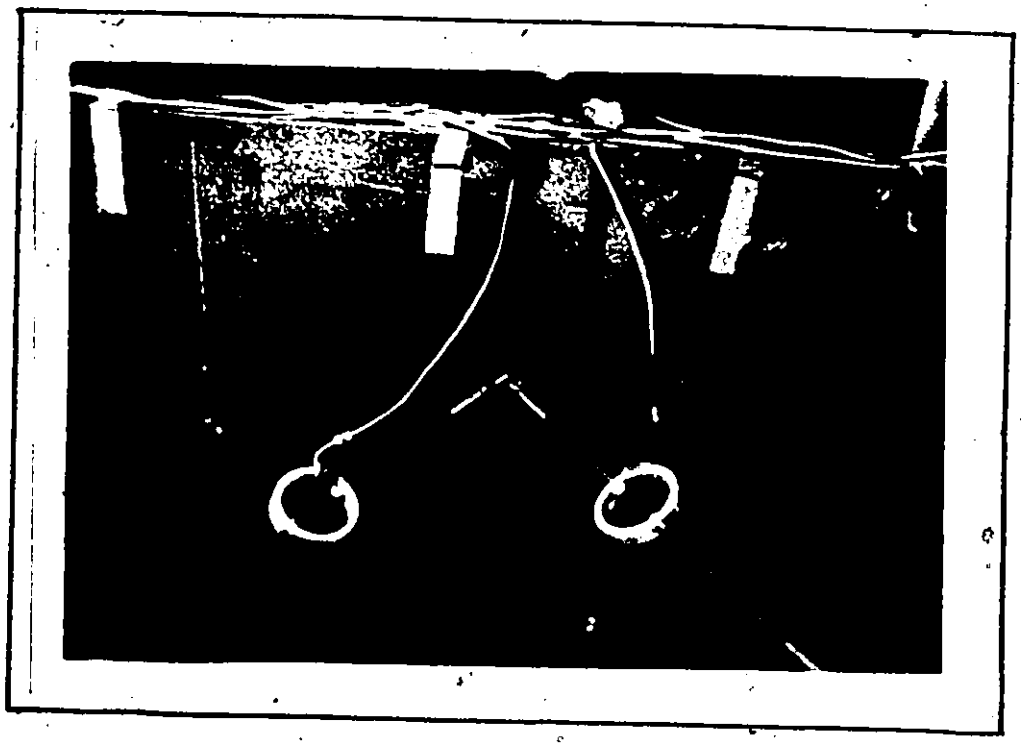

Photograph 2: An Intermediate End Connection and Load Cells

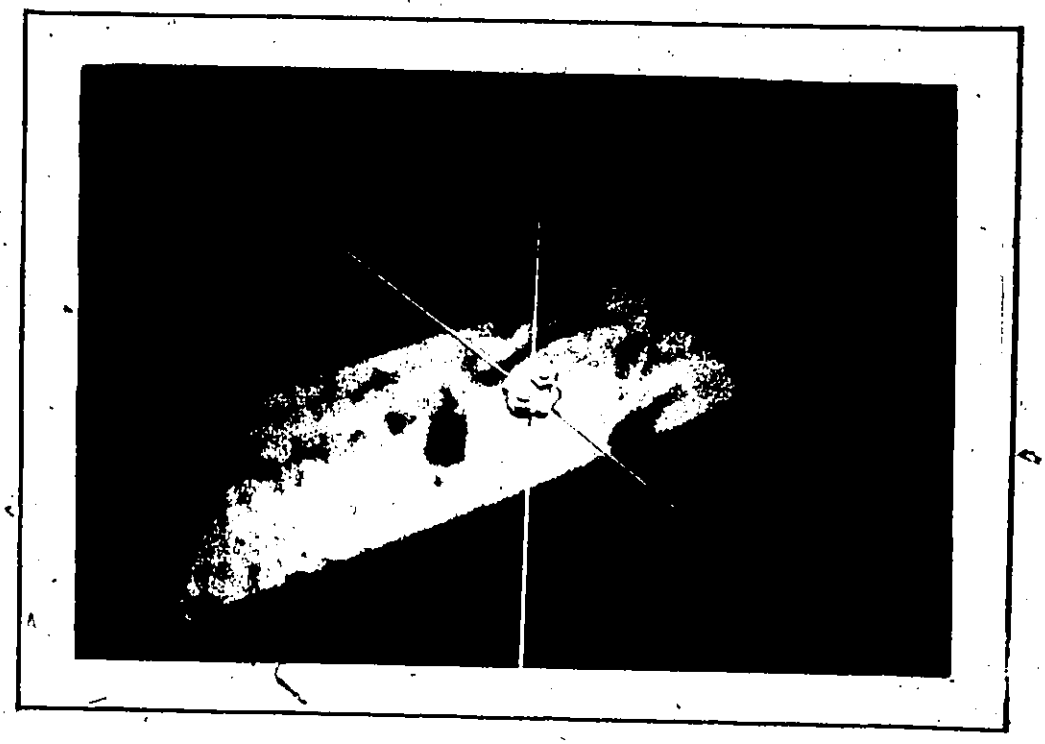

Photograph 3: Clamping of Cables at an Intersection

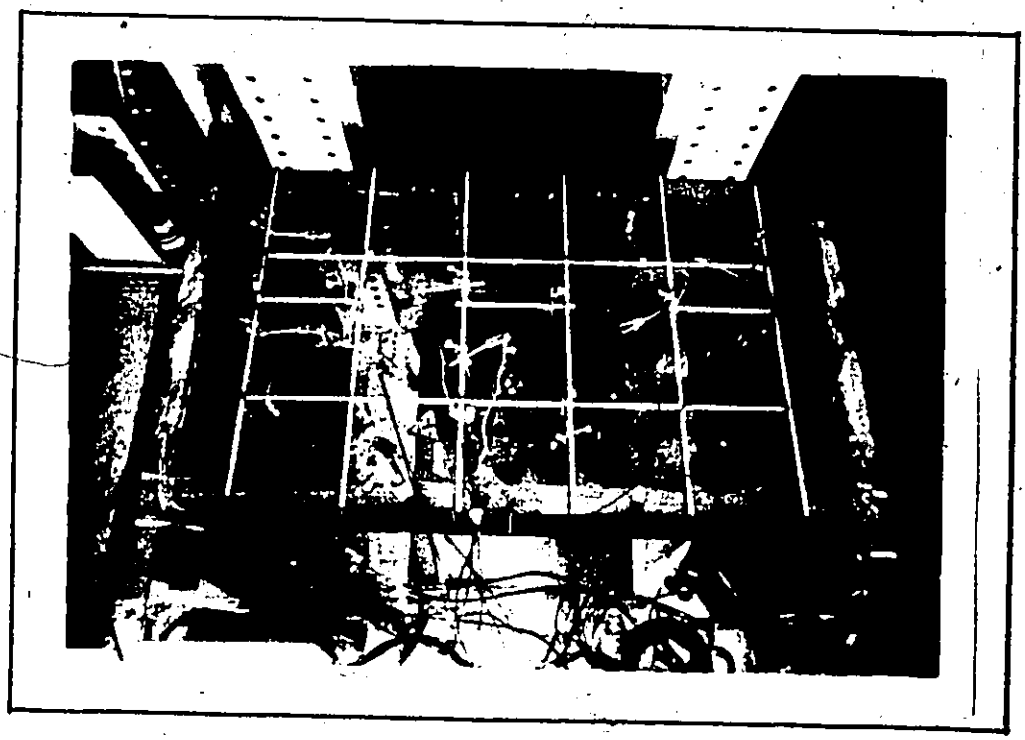

Photograph 4: Pipe Framework Used for Supporting the Displacement Transducers.

Small plates with holes to attach the displacement transducers were connected to the clamps. A suitable framework was built with 1 inch diameter pipes and was clamped on top of the rectangular box (photograph 4). The displacement transducers were held in place by nonmagnetic clamps connected to this pipe framework (photograph 5).

5.3.2 Non-orthogonal Single Roof Model

The non-orthogonal single roof is shown in isometric view in figure (5-1a) and in plan in figure (5-1b). Four holes on each side of the rectangular frame were drilled diagonally and along straight lines on the webs. The holes were drilled in the directions in which the cables met the frame. Washers with inclined faces of $\tan^{-1}\frac{1}{2}$ and $\tan^{-1} 2$ were used to tighten the cable end against the end frame on the longer and shorter sides of the rectangle respectively.

The model consisted of five cables in each direction approximately taking the shape of parabolas. It had thirteen joints and its dimensions were 36 inch x 72 inch in plan with a height of 9 inches. Photograph (6) shows a view of the model just after fabrication.

5.3.3 Orthogonal Double Roof Model

Isometric and plan views of the orthogonal double roof model are shown in figures (5-2a) and (5-2b) respectively. Holes inclined at 45° were drilled along lines ABCDEFA representing the edge beams of the model. Washers with 45° inclined

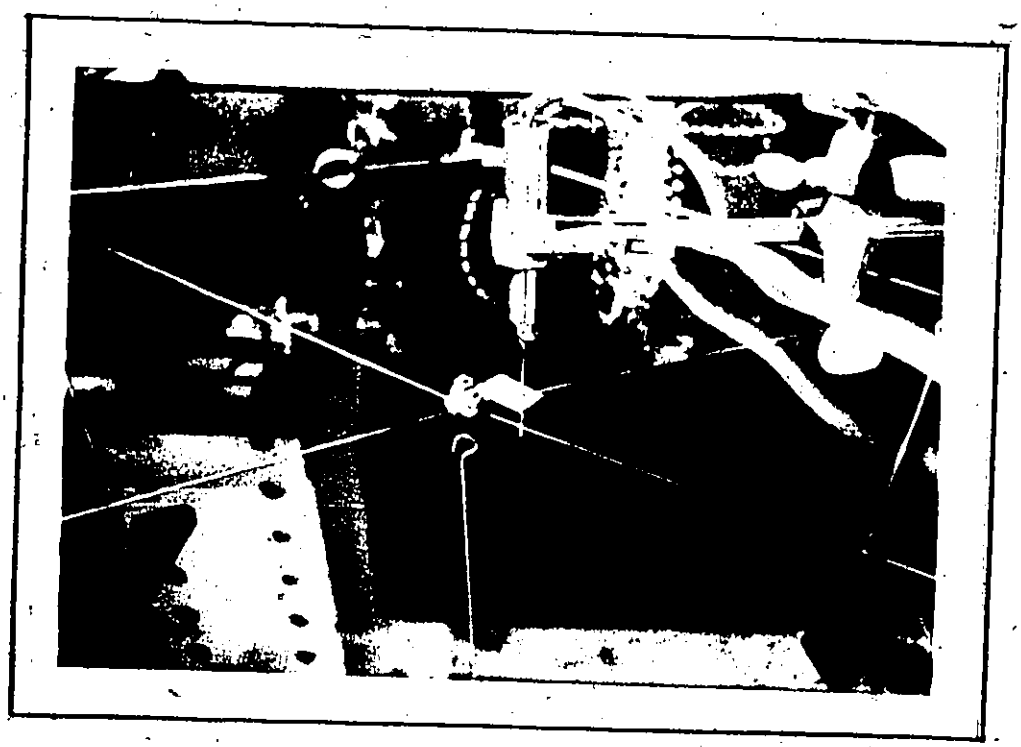

Photograph 5: Displacement Transducer Attached to a Joint of One of the Models.

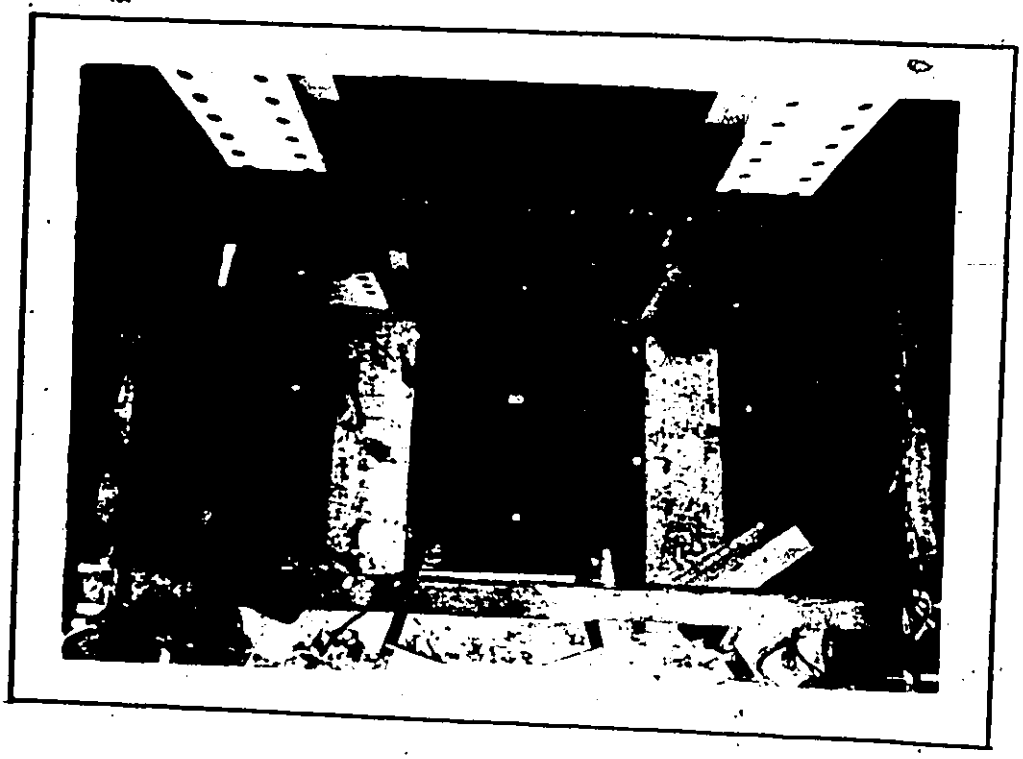

Photograph 6: A View of the Single Roof Model After Fabrication.

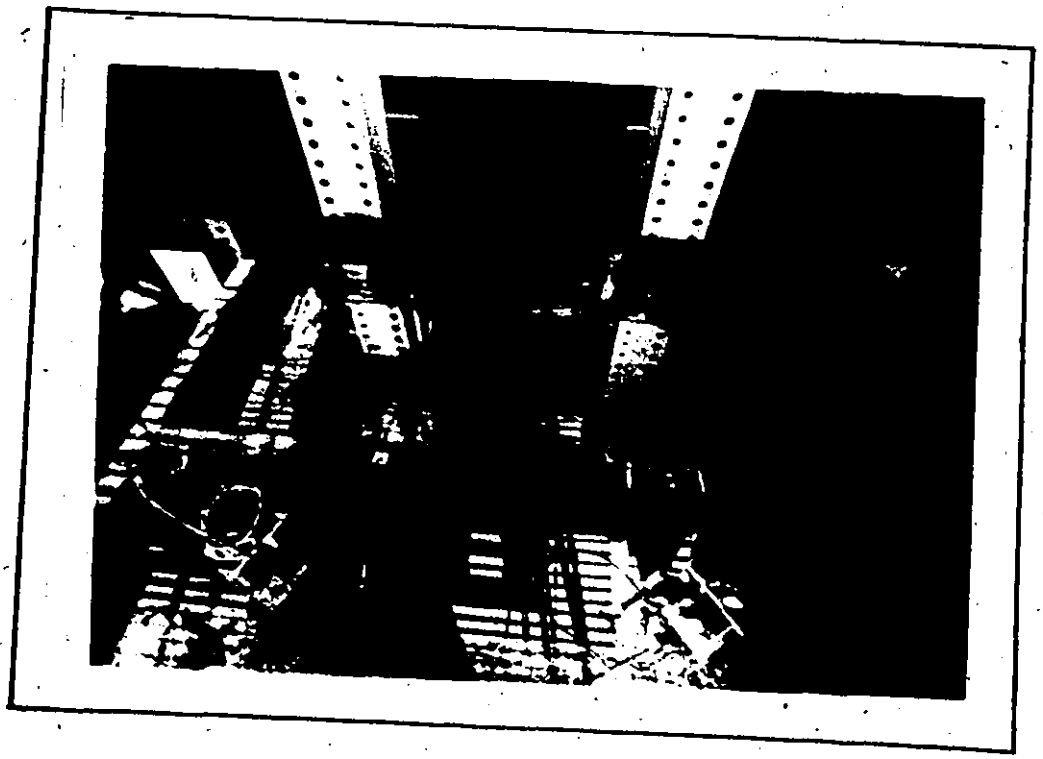

Photograph 7: A View of the Double Roof Model After Fabrication.

faces were used for the end connections. This model too had the same dimensions as the single roof model.- 36 inch x 72 inch x 9 inch. The number of cables in each direction was again five, all with the exception of the cables intersecting at the centre taking the shapes of parabolas. The two cables intersecting at the centre had points of inflection at this point. This model had eleven joints as against thirteen on the single roof model. The double roof model is shown in photograph (7).

5.4 Instrumentation

The load cells for the measurement of tensions in the cables were aluminum rings of $1\frac{1}{64}$ inch inner diameter, $1\frac{1}{4}$ inch outer diameter and $\frac{1}{4}$ inch width. They were so designed that the deflection in the ring is equal to the extension of the wire rope of length equal to the diameter of the ring. The calculations involved in this design are given in Appendix (B).

Two Bean metal foil strain gages (type BAE - 13 - 125BB - 120) were mounted on each ring, one on the inside and the other on the outside. The strain gages themselves were temperature-compensated for aluminum. They were connected in adjacent arms of a Wheatstone bridge so that any temperature strains still existent were cancelled out while the actual strains measured by the two gages added up. The gages were installed with Eastman 910 cement. Though doubts existed as

to the stability this cement will provide in transducer work, it was used owing to the simplicity of its application. It was also found that the stability it offered was ample for a short-term transducer of this type since gages mounted with the same adhesive on load cells used in the preliminary model gave stable results after several months.

The load cells were calibrated by suspending them with the same wire rope used in the construction of the model and applying dead weights. Hysterisis and any zero drift in the strain gages were minimized by subjecting the load cells to cycles of loading and unloading several times - at least ten - before calibration. The calibration constant of a load cell was obtained by taking several readings and determining the regression line through these points. The maximum load applied during calibration was 100 lbs which was not exceeded during the testing of the model. The calibration graph is perfectly linear for all practical purposes and a typical graph is given in figure (B-2) in Appendix (B). The calibration constants for the twenty load cells are tabulated in table (5-1). A Datran strain indicator coupled with a Switch and Balance Unit and a printer, was used to measure the strain gage output.

The displacement transducers used in the deflection measurements were manufactured by Hewlett Packard Ltd. Types 24DCDT100 and 24DCDT500 with ranges of ±.100 inch and ±.500 inch were used for the horizontal and vertical displacements respectively. The former had a calibration constant of approximately 100 volts/inch while the latter had a constant

Table (5-1). Calibration Constants of Load Cells

Load Cell No.	Calibration Constant ($\mu\epsilon$/lb)	Load Cell No.	Calibration Constant ($\mu\epsilon$/lb)
1	38.75	11	38.37
2	37.51	12	37.43
3	37.65	13	37.61
4	39.19	14	39.34
5	39.59	15	38.40
6	39.43	16	38.77
7	38.58	17	38.40
8	40.05	18	37.91
9	38.51	19	37.62
10	37.41	20	37.07

of approximately 25 volts/inch. D.C. power supplies by Hewlett packard were used to excite the transducers with 24 volts D.C. The output from the transducers was recorded by Honeywell Electronik 16 Multipoint Strip Chart Recorder with twenty-four channels. The voltage recorder, power supplies, strain indicator, switch and balance unit and printer are all seen in photograph (8) together with one of the models.

The extensional stiffness EA of the wire rope used in the models was determined by testing samples of it in an Instron testing machine which produced a load-elongation graph. The testing is illustrated in photograph (9) and a sample

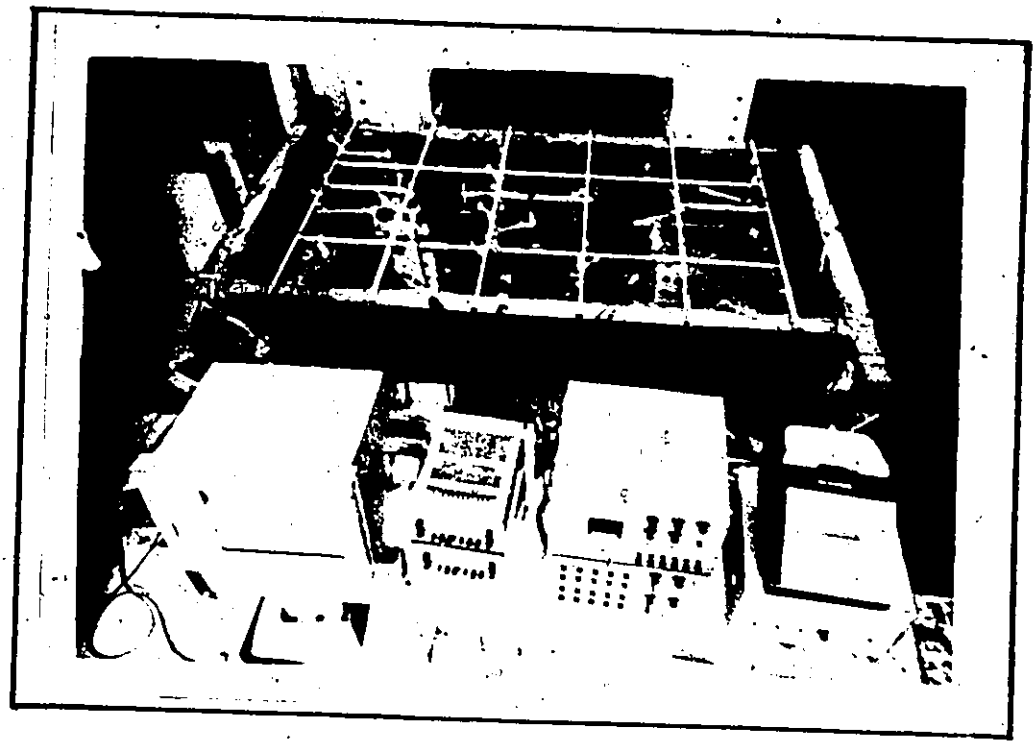

Photograph 8: Measuring Instruments and the Single Roof Model.

Photograph 9: Testing of Wire Rope to Determine its Stiffness

output from the Instron machine is shown in figure (5-3). To determine the change in modulus of the wire rope during testing of the model, samples of the wire rope before and after testing were tested to determine their stiffnesses; average values of 14850 ksi and 15200 ksi respectively, were obtained for the modulus from these tests. The average of the two modulii was used in the calculations to obtain the theoretical values for the models. The effective area of cross-section of the wire rope was determined as 0.00112 in^2 by measuring a 50 feet length of the wire rope and weighing it accurately. The catalogue breaking strength of the wire rope was 270 lbs. The load at which the wire rope broke while being tested to determine the stiffness, was less - about 200 lbs (Fig. 5-3). This was due to the fact that the wire rope broke at the grips due to crushing at these points. More elaborate tests to determine the actual breaking strength were not carried out since the testing of the models was confined to only the elastic range. Based on the effective area of cross-section and the catalogue breaking strength of the wire rope, the ultimate stress was found to be 242 ksi.

5.5 Experimental Procedure

The load cells were connected to the strain indicator with the strain-gages in half-bridges. Care was taken to see that the lead wires from the load cells hung loose and did not in any way contribute to the carrying capacity of the model.

The cables were first kept loose and the load cells were zeroed. These zero readings were recorded and the cables were tensioned in order to attain equal horizontal components of tensions in all the cables. The strain reading in each load cell corresponding to this horizontal component was precalculated and used while tensioning was done.

During tests on the preliminary model, the following procedure was adopted for the tensioning of the cables. All cables were tensioned to some degree initially. The five prestressing cables were then tensioned one by one to the required tension. This was followed by tensioning of the five load-carrying cables and the cycle was repeated. It took five to six cycles to get the tension in all the cables close to the required values. This procedure was changed in the final models and the prestressing and load-carrying cables were tensioned alternately. Convergence was faster now and the required tensions were reached in three or four cycles. It was also found that tensioning was faster with the double roof model than with the other, obviously due to the orthogonality of the net. In this case a close approximation to the required value was obtained even in two cycles.

Fine adjustments in the tensions were made after clamping the joints since the clamping changed the cable tensions slightly. When there was a difference between the readings of the load cells at the two ends of a cable - theoretically the two must be equal - the difference was adjusted equally between the two. The strain readings

corresponding to the pretension in the cables were recorded.

With the cables pretensioned and the joints clamped, the model was ready for testing. The displacement transducers were connected at the joints and the zero readings were recorded. The model was then loaded by means of dead weights placed on hangers suspended at each joint. The loading was increased in steps and at each step, the deflection and strain readings were recorded. The procedure was repeated while unloading after the maximum load was reached. A view of the loaded single roof model is shown in photograph (10) and that of the double roof model in photograph (11).

5.6 Experimental Results

5.6.1 General

During the tests the models were loaded uniformly up to a load of 5 lbs/joint in steps of 1 lb/joint. They were also loaded at specific joints with concentrated loads increasing from 1 lb to 7 lbs in addition to a uniform load of 1 lb/joint. These tests were carried out for values of the horizontal component of the initial tension of 20 lbs to 70 lbs increased in steps of 10 lbs. In no case did the absolute maximum tension in the models exceed 100 lbs which was the maximum load at which the load cells were calibrated. On unloading, the strain readings were found to be the same as the initial readings indicating that there was no hysterisis.

The horizontal displacements at the joints were measured by attaching the displacement transducers horizontally

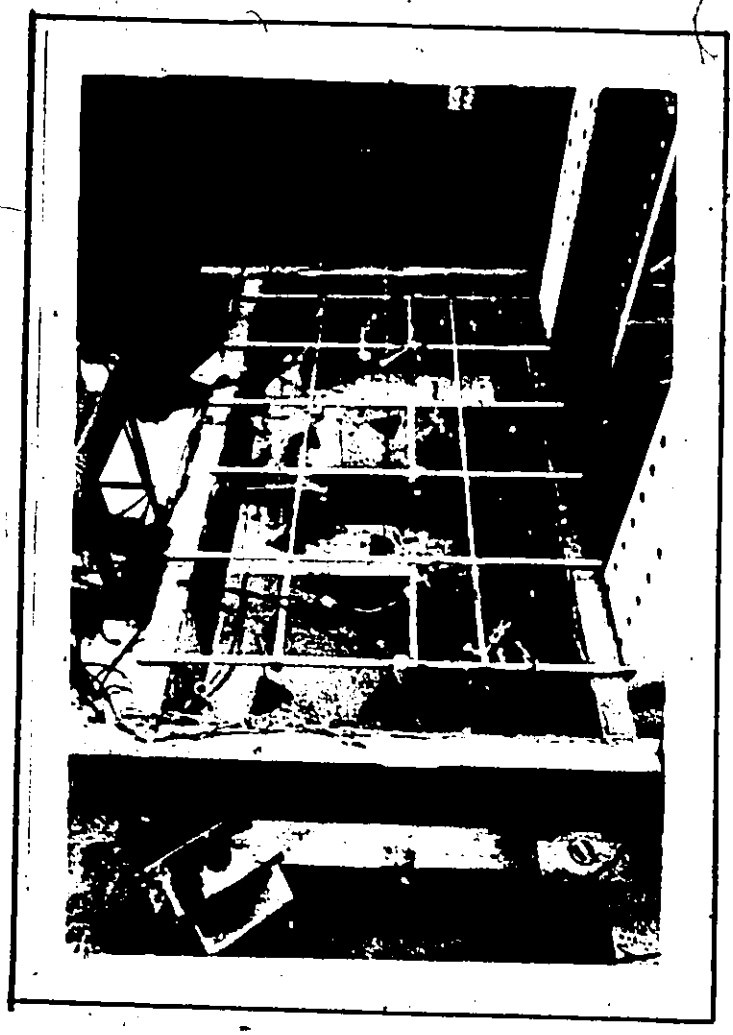

Photograph 10: A View of the Loaded Single Roof Model.

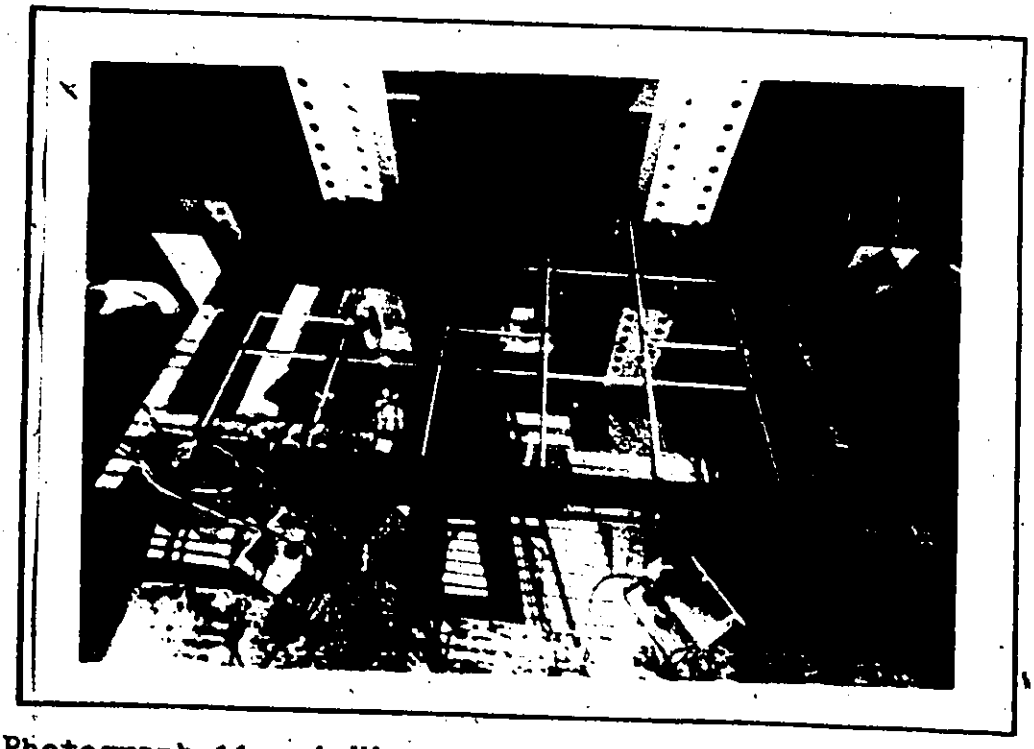

Photograph 11: A View of the Loaded Double Roof Model.

in two perpendicular directions. Accurate measurement was not possible since the horizontal displacements were too small and the simultaneous vertical movement of the joint could not be accommodated in the displacement transducers. The horizontal displacements measured at joint 1 of the single roof model are shown in figure (5-4).

5.6.2 Single Roof Model

Thirty-five tests in all were carried out on this model including three preliminary tests. The maximum deflection was at joint 7 (centre of model) on application of a uniform load and the maximum tension increment measured was in cable (1,1). This deflection and tension increment are plotted against the load for values of H from 20 lbs to 70 lbs in figures (5-5) and (5-6). Both theoretical and experimental values have been presented. There is a discontinuity in the deflection and the tension increment for H = 20 lb beyond a load of 3 lb/joint. This is due to some segments of the cables becoming slack beyond this load. This has been taken into account in the theoretical solution. The theoretical and experimental values of the twenty measured tensions are tabulated in table (5-2) for the maximum load of 5 lb/joint at H = 50 lb.

Concentrated loads increasing in steps of 1 lb to a total of 7 lbs, in addition to an initial uniform load of 1 lb/joint, were applied at joints 4, 6 and 7 in separate tests. These tests too, were carried out for the six values

Table (5-2). Theoretical and Experimental Values of Cable Tensions in Single Roof Model.

(Load = 5 lb/joint, H = 50 lb)

Load Cell No.	Cable	Cable Tensions (lb)		Tension Increments (lb)	
		Theory	Experiment	Theory	Experiment
1	(13,4)	41.0	40.0	-9.0	-9.2
2	(8,2)	76.1	75.5	25.7	25.4
3	(8,4)	28.6	27.7	-21.6	-22.0
4	(3,2)	62.8	61.2	12.7	12.1
5	(3,4)	25.4	25.8	-25.3	-24.5
6	(11,1)	62.8	62.0	12.7	12.6
7	(6,3)	28.6	30.1	-21.6	-20.2
8	(6,1)	76.1	75.3	25.7	24.9
9	(1,3)	41.0	41.7	-9.0	-8.8
10	(1,1)	81.2	77.8	30.2	29.1
11	(13,3)	41.3	41.6	-8.7	-8.9
12	(2,1)	75.9	74.5	25.4	24.1
13	(12,3)	29.0	29.3	-21.2	-20.5
14	(3,1)	62.6	62.4	12.5	12.4
15	(11,3)	25.4	26.0	-25.3	-23.2
16	(11,2)	62.6	61.9	12.5	12.1
17	(2,4)	29.0	28.9	-21.2	-20.5
18	(12,2)	75.9	74.0	25.4	24.0
19	(1,4)	41.3	41.9	-8.7	-8.9
20	(13,2)	81.2	80.2	30.2	29.2

of H from 20 lbs to 70 lbs. The maximum deflection and the maximum tension increment measured in each case are plotted in figures (5-7) to (5-12). The deflection was maximum at the joint at which the concentrated load was applied. For concentrated load at joint 4 or joint 7, the maximum tension increment was measured in cable (1,1), and for concentrated load at joint 6, the maximum tension increment was in cable (6,1).

Finally the single roof model was loaded uniformly with an unsymmetrical pretension of H_3 = 40 lbs and H_1 = 60 lbs. The maximum deflection and the tension increment are shown in figures (5-13) and (5-14).

5.6.3 Double Roof Model

Twenty-four tests were carried out on this model for values of H ranging from 20 lbs to 70 lbs. The results of the uniform loading are shown in figures (5-15), (5-16) and (5-17), the maximum deflection being plotted in figure (5-15) and the maximum tension increment in figure (5-17). The former is at joint 6 while the latter is in cable (10,3). The theoretical and experimental values of the twenty measured tensions are tabulated in table (5-3) for the maximum load of 5 lb/joint at H = 50 lbs.

Concentrated loads increasing in steps of 1 lb to a total of 7 lbs, in addition to an initial uniform load of 1 lb/joint, were applied at joints 2, 5 and 6 of this model in separate tests and at values of H from 20 lbs to 70 lbs. The maximum deflection and the maximum tension increment

Table (5-3). Theoretical and Experimental Values of Cable Tensions in Double Roof Model.

(Load = 5 lb/joint, H = 50 lb)

Load Cell No.	Cable	Cable Tensions (lb)		Tension Increments (lb)	
		Theory	Experiment	Theory	Experiment
1	(10,3)	72.4	71.6	20.6	21.2
2	(10,2)	53.9	55.1	3.7	4.9
3	(11,3)	57.0	57.4	6.8	6.9
4	(11,2)	33.7	35.3	-18.1	-17.8
5	(4,2)	44.6	46.3	-5.6	-4.4
6	(9,2)	72.4	72.8	20.6	21.2
7	(9,3)	53.9	55.5	3.7	5.0
8	(8,2)	57.0	56.9	6.7	6.4
9	(8,3)	33.7	34.3	-18.1	-17.8
10	(1,3)	44.6	43.1	-5.6	-5.9
11	(4,4)	71.5	75.8	19.8	21.4
12	(2,1)	54.9	57.6	4.7	5.8
13	(11,4)	57.0	55.0	6.8	8.0
14	(3,1)	32.9	34.4	-18.9	-18.2
15	(4,1)	44.7	44.5	-5.5	-4.8
16	(1,1)	71.5	75.1	19.8	21.2
17	(3,4)	54.9	55.2	4.7	5.5
18	(8,1)	57.0	56.2	6.8	6.5
19	(2,4)	32.9	33.9	-18.9	-18.6
20	(1,4)	44.7	44.4	-5.5	-5.7

measured in each case are given in figures (5-18) to (5-23). As in the single roof model, the deflection was maximum at the joint at which the concentrated load was applied. The maximum tension increment was measured in cables (2,1), (9,2) and (10,3) in the three cases of loading respectively.

CHAPTER VI

DISCUSSION OF RESULTS

6.1 Theoretical Results

6.1.1 Elastic Analysis

The deflections and tension changes due to a uniformly distributed load have been presented in figure (3-3) and figures (4-2) to (4-8). Both linear and nonlinear solutions of the deflections and tension changes have been presented. It is found that the deflections are more nonlinear than the tension increment. The linearized solution would overestimate the deflections by 40% and 50% in the single roof and double roof respectively. The maximum tension increment would be underestimated 15% by the linearized solution for the single roof while it is not very far removed from the nonlinear solution for the double roof. This suggests that the nonlinearity should not be neglected. The maximum applied load being the equivalent of 30 psf of plan area is not too large a load to assume even for a light weight roof-decking of a cable roof. It must also be remembered that the linearized solution can sometimes lead to grossly misleading results as shown in figures (4-11) and (4-12) where the cable tension decreases to a certain point and then starts increasing. This kind of reversal is likely to happen in the prestressing

cables, as the load is increased progressively. The linearized solution will predict a slack cable while the actual tension in the cable could even be greater than the pretension.

Maximum horizontal deflections have been plotted with the vertical deflections for the two roofs in figures (4-6) and (4-7). The horizontal deflections are of the order of 5-10% of the vertical deflections. It was shown earlier (48) that tension increments based on solutions neglecting horizontal displacements and those not neglecting them sometimes differ by more than 10%. The deflection contours drawn for the vertical deflections of the two roofs in figures (4-4) and (4-5) give a general idea of how the roofs deflect under a uniform load. The deflection is more or less uniform on all sides with the maximum deflection at the centre of the single roof while it is eccentric towards one of the longer sides of the double roof. This eccentricity being towards the lower-middle section of the roof, helps in properly draining the roof. Figure (6-2) shows the contours of the deformed double roof under the maximum load of 12 kip/joint. The contours are such that the entire roof can be drained at point E of the roof. There are no closed contours indicating areas of stagnation.

Contrary to this, the contours of the deformed single roof (Fig. 6-1) indicate that the entire area of the roof will drain to the centre of the roof. If proper drainage is not provided at the centre, which itself is not desirable, ponding will take place at the centre of the roof resulting in

increased loading at this point. But this is not a serious problem since it can be overcome. Use of a steeper slope will improve the situation in two ways by increasing the curvature of the roof and at the same time decreasing the deflections (Fig. 4-39). Figure (6-3) shows the contours of the deformed roof when the height is increased to 60 feet. The contours are now such that drainage will take place at the corners A and C. Using a high pretension also will decrease the deflections (Fig. 4-27). The use of a steep slope and a high initial tension have been found to be advantageous with respect to efficient performance of the roof. This will be discussed later in this section.

The combined vertical and horizontal loads simulate the effect of windload on cable roofs. For the single roof, it is found that equal loads in the η and z directions produce a greater tension increment than equal loads in the ξ and z directions or in all three directions (Fig. 4-9). This combined load increases the tension increment 35% over that produced by pure vertical loading. In the double roof, this combined load produces about 25% higher tension changes than pure vertical loading but the actual direction in which the horizontal load is applied makes only a negligible difference (Fig. 4-10). Even loading in all three directions does not produce a significantly higher tension change than the loading in the vertical and any one horizontal directions. Different combinations including partial loading should be considered to determine the worst combination in any particular case.

The results of the application of concentrated loads both symmetrical and unsymmetrical have been presented in figures (4-13) to (4-17) for the single roof and in figures (4-18) for the double roof. The difference between linear and nonlinear solutions when concentrated loads are applied are small for deflections (less than 10% in single roof and about 12.5% in double roof) but large for tension changes (25% to 30% in both roofs). The situation here is the opposite of what happens under a uniform load where the deflections were more nonlinear than the tension changes suggesting that even the same roof can behave differently with respect to nonlinearity under different conditions of loading. This confirms the contention that the nonlinear solution is the only safe solution to be used in cable roof design under all conditions.

It is also important to consider the effect of temperature changes on a cable roof structure. Temperature changes of $\pm 50^{o}F$ seem to have almost the same effect on tension changes in the single and double roofs (Figs. 4-23 and 4-24). Even though the temperature effect is small in these cases, it may become significant when larger spans are considered. Also, higher temperature changes than those considered here are not improbable. Positive temperature changes, as expected, reduce the tension changes. It would, therefore, be advantageous to erect a cable roof during the cold winter months when the temperatures are lowest.

Figures (4-25) and (4-26) show the effect of the

non-orthogonality of cables in the net. Although the deflections increase with the degree of non-orthogonality, there is practically no change in the tension increments as shown by tables (4-2a) and (4-2b). Even the change in deflections is not unduly large - less than 20% when an orthogonal net is changed into a non-orthogonal net with an angle of 53° ($\theta = 37°$) between the cables. Hence non-orthogonal roofs could be built according to necessity without fear of introducing additional stresses due to their non-orthogonality. When the non-orthogonality is slight, it could even be ignored for the purpose of analysis and design. The deflections and tension increments decrease with the increase of pretension as would be expected (Figs. 4-27 , 4-28, 4-30 and 4-31). The nonlinearity also decreases as the pretension is increased. But the maximum cable tensions with different pretensions to start with, converge to a narrow band at higher loads (Figs. 4-29 and 4-32). This suggests that by using a high initial tension the deflections can be kept to a minimum while the final cable tension is not appreciably increased making it necessary to use increased steel areas. Using a high initial tension also increases the stability of the roof and its capacity to resist flutter in winds.

In the case of the single roof, it is still more advantageous to use unsymmetrical pretensioning. For a given value of H in the load-carrying cables, an optimum value of H in the prestressing cables can be found at which the variation within all the final cable tensions is least (Fig. 4-34).

The maximum tension produced is also smallest with the result that the cables are used most efficiently with this combination of pretensions. Since the variation within the final tensions is small, the deformed shape is more even than with symmetrical prestressing. A further gain in advantage may be made by using unequal steel areas in the two directions. This may be combined with unsymmetrical pretensioning so that the cables are stressed to the maximum. Referring to figure (4-37), the minimum steel area in the 3 direction that can be used without exceeding the proportional limit is 1.10 in^2. This represents a saving of 7½% on the total steel used over an equal steel area of 1.25 in^2 in both directions. The use of unsymmetrical pretensioning or unequal steel areas does not improve the efficiency of the double roof owing to its symmetrical shape.

When the behaviour of the roof with change in height was examined, it was found that the deflections decrease with increase in the roof height (Fig. 4-38). The nonlinearity of the deflection is also initially high but it decreases with increasing roof height and changes sign i.e. the load-deflection curve has a convex shape for small heights and changes to a concave shape at larger heights. The tension increment is maximum at the critical height (defined in section 4.2.8) with the curve having a convex shape at heights below the critical height and a concave shape at heights above it (Fig. 4-39).

It was a generally accepted belief among authors of

previous studies on orthogonal roofs (8, 32, 67, 77) that increasing load has a stiffening effect on these roofs. But it is found that roofs with steep slopes can in fact weaken under load. Buchholdt noted such behaviour in the deflections of saddle-shaped orthogonal nets with circular arches on one pair of opposite boundaries (19), but did not relate this behaviour to the height of the roof.

The difference in the behaviour of small-sloped and steep-sloped roofs and the existence of the critical height can be physically explained as follows: when the roof is flat (or low-sloped), the hogging cables become sagging under load and aid the load-carrying cables in carrying the load. This is seen in the case of the single roof with height of 1 foot where, even under an initial load of 1 kip/joint, the tension changes are positive in all cables, both hogging and sagging. Table (6-1) illustrates this fact with the tension changes in cable segments in one quadrant of the single roof for roof-heights of 1 foot, 12 feet and 60 feet. When the slope is steep, the sagging or load-carrying cables are able to carry a larger load by virtue of their curvature i.e. their angle with the vertical is smaller. It follows that at some intermediate slope neither of the above advantages is present, resulting in maximum tensions being developed in the cables. The deflections are larger in a low-sloped roof since the cables have to deform more from near-horizontal positions to adjust themselves to the applied load.

The 'strengthening' of low-sloped and the 'weakening'

Table (6-1). Tension Increments in One Quadrant of Single Roof at 1 kip/joint. (H = 50 kips).

Joint No.	Tension Increment (kips)					
	Roof height = 1 ft		Roof height=12 ft		Roof height=60 ft	
	Dir'n 1 (Hogging)	Dir'n 4 (Sagging)	Dir'n 1 (Hogging)	Dir'n 4 (Sagging)	Dir'n 1 (Hogging)	Dir'n 4 (Sagging)
1	0.69	1.34	-13.69	3.13	-7.13	2.40
2	1.41	3.39	-13.81	9.05	-6.91	4.57
3	2.27	4.64	-11.60	14.20	-6.34	5.71
4	2.71	4.88	-8.07	17.80	-5.64	6.40
5	2.32	4.35	-4.02	19.34	-4.49	6.96
6	1.06	3.47	-0.67	18.07	-2.30	7.23
7	0.70	3.37	-13.66	9.04	-6.99	4.59
8	1.40	4.61	-13.78	14.15	-6.85	5.70
9	2.24	4.85	-11.61	17.73	-6.33	6.37
10	2.68	4.32	-8.11	19.25	-5.64	6.90
11	2.29	3.48	-4.07	18.04	-4.51	7.08
13	0.71	4.60	-13.63	14.15	-6.93	5.70
14	1.39	4.83	-13.76	17.69	-6.83	6.36
15	2.22	4.31	-11.62	19.18	-6.32	6.87
16	2.66	3.49	-8.14	18.01	-5.65	7.02
19	0.72	4.82	-13.62	17.68	-6.91	6.36
20	1.38	4.29	-13.74	19.15	-6.82	6.87
21	2.21	3.49	-11.64	17.98	-6.32	6.99
25	0.72	4.29	-13.61	19.13	-6.90	6.86
26	1.38	3.49	-13.74	17.95	-6.82	6.99
31	0.73	3.49	-13.60	17.94	-6.90	6.99

of steep-sloped roofs as the load increases are due to the fact that the prestressing cables of the latter keep losing their pretension while some of the former either do not lose or regain the lost pretension as the load is increased, thus contributing to an increase in stiffness. This is evident from table (6-2) where the tension changes in cable segments in one quadrant of the single roof under a load of 6 kip/joint have been tabulated for roof heights of 1 foot, 12 feet and 60 feet. It can be observed that at a height of 60 feet, there are large tension losses in the prestressing cables while at 12 feet height some cables have positive tension changes indicating that they have regained and even exceeded their pretension (compare with values in table (6-1)).

The critical height increases with the applied load (Figs. 4-40 and 4-43). It varies between 12 feet to 14 feet for loads between 1 kip/joint and 6 kip/joint on the single roof. For the equivalent load range of 2 kip/joint to 12 kip/joint on the double roof, the range of critical height is 8 feet - 12 feet. The smaller critical height for the double roof is understandable since for the same roof-height, the double roof is steeper than the single roof. It must also be noted that most of the numerical analysis presented in section (4.2) was done on single and double roofs with height 12 feet - critical height for both but at different load levels.

It was previously thought that the linear theory would overestimate the actual values but now it is seen that it can also underestimate the values in some cases and lead to unsafe

Table (6-2). Tension Increments in One Quadrant of Single Roof at 6 kip/joint. (H = 50 kips).

Joint No.	Tension Increment (kips)					
	Roof height = 1 ft		Roof height=12 ft		Roof height=60 ft	
	Dir'n 1 (Hogging)	Dir'n 4 (Sagging)	Dir'n 1 (Hogging)	Dir'n 4 (Sagging)	Dir'n 1 (Hogging)	Dir'n 4 (Sagging)
1	20.35	18.53	-31.98	26.51	-41.52	15.26
2	29.95	35.84	-23.45	59.95	-40.68	28.35
3	37.49	45.00	-6.70	86.33	-37.34	34.95
4	39.22	46.13	11.08	105.33	-32.89	39.04
5	33.15	40.29	23.52	112.71	-25.59	42.47
6	18.32	30.30	23.34	101.77	-12.05	44.86
7	20.47	35.49	-31.74	59.59	-40.78	28.40
8	29.65	44.54	-23.62	85.63	-40.39	34.83
9	37.05	45.67	-7.17	104.45	-37.29	38.82
10	38.76	39.93	10.43	111.79	-32.94	42.04
11	32.79	30.40	22.81	101.63	-25.78	43.94
13	20.63	44.31	-31.48	85.38	-40.46	34.84
14	29.44	45.36	-23.70	103.93	-40.27	38.74
15	36.76	39.68	-7.50	111.12	-37.28	41.86
16	38.52	30.54	9.98	101.50	-33.01	43.51
19	20.76	45.20	-31.23	103.73	-40.32	38.74
20	29.29	39.50	-23.75	110.69	-40.22	41.81
21	36.59	30.64	-7.77	101.28	-37.29	43.34
25	20.83	39.40	-31.04	110.50	-40.27	41.81
26	29.19	30.69	-23.83	101.05	-40.20	43.29
31	20.86	30.70	-30.93	100.90	-40.26	43.30

designs. For example, the maximum tension increment for the single roof with a 12 feet height is underestimated 15% by the linearized solution (Fig. 3-3). The tension increment-load curve decreases with increasing load at higher loads but initially the curvature is upwards and hence the higher nonlinear value. A point of inflection can be noticed around 1 lb/joint. Similar underestimations with the linear solution could be expected for the same roof with 18 feet or 24 feet height (Fig. 4-39).

One serious problem in the analysis of cable roofs, was the large amount of computer space needed to solve the large number of equations involved. This problem can be overcome by the use of an equivalent sparser net to replace the actual net in the analysis. There is no reason why this should not be done if the method of continuity can be used to approximate such discrete structure as the cable net. Even in the analysis of continuous structures like plates and shells using the finite difference method, a courser mesh is sometimes used to reduce the number of equations.

Table (4-3b) shows that the use of a sparser net does not involve an appreciable error in the deflections and tension increments. When a net with 61 joints is analyzed instead of the actual one with 113 joints (almost twice in number), the errors in the deflection and tension increment are less than 2% with a saving in computer time of 70% and only half of computer space needed. When replaced by a net of 41 joints, the error is still within limits - less than 5% in the

deflection and about 7% in the tension increment - with only about a fourth of the computer space needed. Even in the extreme case of 13 joints, the errors are only about 8% and 16% in the deflection and tension increment respectively. It should also be noted that in all cases considered here, the deflections and tension increments have been underestimated.

6.1.2 Inelastic Analysis and Ultimate Load

When cable roofs are loaded into the inelastic region, two distinct effects take place. The roof as a whole stiffens under increased tensions in the cables while the stiffnesses of the cables stressed into the inelastic region are reduced in magnitude. These two effects counteract each other and usually the former effect predominates with the result that the ultimate load is higher than that predicted by the linear elastic theory. This can be observed in figures (4-45) and (4-46) showing the load-maximum stress curves for the single and double roof respectively. Unlike in conventional structures where the reduction in modulus accelerates failure as the load is increased in the inelastic region, the stiffening of the cable roof brings out the 'hidden' or 'reserve' strength in the structure. In steep roofs, where the height is greater than the critical height, the 'weakening' effect under load may initially add to that caused by the reduction in modulus in the inelastic region. However, as the load is increased further even these roofs stiffen up and show some strengthening

until failure takes place. Another factor contributing to the increased strength at failure is that the prestressing cables at times behave as load-carrying cables and carry part of the load.

Figures (4-45) and (4-46) show load-maximum stress curves for the single and double roofs respectively with heights of 6 feet, 12 feet and 60 feet. The ultimate load decreases as the roof height increases. This dependence of the ultimate load on the roof height does not contradict the explanation of the roof behaviour in the elastic range, in relation to its height as discussed in section 6.1.1. In fact, the behaviour in the inelastic region could be explained on similar lines. When the roof height is smaller than the critical height, the tension increment is small initially. Increasing load has a strengthening effect on it and offsets the reduction in modulus giving it a high ultimate load capacity. At the critical height, the tension increment produced is maximum at working loads and the ultimate load is less. When the height is greater than the critical height, the tension increment is initially small but the weakening effect under increasing load supported by the reduction in modulus produces a low ultimate load capacity even though some stiffening takes place near failure.

Table (6-3) explains the difference in the ultimate loads by the distribution of the cable tensions at failure (listed for one quadrant of the single roof) for heights of 6 feet, 12 feet and 60 feet. The prestressing cables have

Table (6-3). Cable Tensions in One Quadrant of Single Roof at Ultimate Load, (H = 50 kips).

Joint No.	Cable Tensions (kips)					
	Roof height = 1 ft		Roof height=12 ft		Roof height=60 ft	
	Dir'n 1 (Hogging)	Dir'n 4 (Sagging)	Dir'n 1 (Hogging)	Dir'n 4 (Sagging)	Dir'n 1 (Hogging)	Dir'n 4 (Sagging)
1	219.2	228.0	190.4	220.4	0.0	169.3
2	271.9	278.7	243.3	270.9	0.0	220.8
3	281.7	289.1	266.8	301.5	0.0	253.9
4	274.8	312.0	271.5	309.9	14.4	282.5
5	256.8	285.1	256.0	304.2	35.6	305.3
6	225.3	257.6	217.1	263.5	144.9	308.4
7	209.1	263.4	195.5	256.9	0.0	217.8
8	262.2	287.0	234.5	284.2	0.0	248.6
9	276.8	295.9	253.4	293.9	0.0	275.4
10	275.5	290.1	256.4	292.6	2.9	292.7
11	256.1	262.0	242.7	267.9	20.0	310.7
13	233.4	276.7	200.6	274.7	0.0	245.8
14	257.3	283.2	228.4	282.3	0.0	270.5
15	265.8	279.3	244.0	282.9	0.0	286.0
16	264.3	264.7	247.1	269.6	0.0	299.2
19	265.6	277.2	204.2	276.3	0.0	268.0
20	250.1	273.1	224.5	276.0	0.0	281.2
21	260.1	264.7	238.9	268.3	0.0	292.4
25	235.8	269.1	206.4	272.6	0.0	278.8
26	247.6	263.0	222.7	265.9	0.0	287.7
31	236.4	262.2	207.3	264.2	0.0	285.2

been stressed well into the inelastic region at roof heights 6 feet and 12 feet, though to a smaller magnitude in the latter, while most of the prestressing cables are slack and therefore ineffective at height 60 feet. At moderate heights, cables that become slack at intermediate loads might become active again and share the load before failure takes place.

The deflections of cable roof structures at failure are excessively large compared to conventional structures. The maximum deflections at failure of the 6 feet, 12 feet and 60 feet high roofs have been calculated to be 23.7 feet, 22.5 feet and 14.7 feet respectively (Table 4-5). Such large deflections, though intolerable in building design, serve as a warning before collapse. The high-tensile strength of the steel used in cable roofs is attained at the expense of its ductility. Even with reduced ductility, cable roofs, due to their very nature of deforming geometrically under load, undergo large deflections thus giving sufficient warning at failure.

6.1.3 Comparison between Single and Double Roofs

Almost all the analyses were carried out for the single and double roofs described in section 4.1. The two roofs used in the analysis are 120 feet x 240 feet in plan and 12 feet high. The single roof is non-orthogonal with $\sin\theta = .60$ while the double roof is orthogonal. The former is anti-symmetrical about a diagonal and has 61 joints while the latter is symmetrical about the median joining the longer

sides and has only 28 joints. A total length of 3230 feet of cable is needed for the single roof while 2040 feet would suffice for the double roof. A uniformly distributed load of 5 psf is equivalent to 1 lb/joint of the former and 2 lb/joint of the latter.

The general behaviour of the two roofs were similar in many respects. The behaviour with respect to deflections and tension increments was similar under uniform and concentrated loads and under combined loads in the vertical and horizontal directions. Deviation of the cables from orthogonality increased the deflections in both roofs but did not significantly affect the tension changes. Likewise, high pretension in the cables reduced the deflections in the two roofs without overly increasing the final tensions in the cables. Use of unsymmetrical prestressing with a higher pretension in the prestressing cables was found to be advantageous in the single roof but not in the double roof due to the prestressing cables not being confined to one direction in the latter.

The behaviour of both roofs were affected in a similar fashion by the slope of the roof, each roof having a critical height of its own. The inelastic behaviour and the ultimate capacities of the roofs were also similarly affected by the slope of the roof.

Direct comparisons of the two roofs wherever possible have been given in table (6-4). Joints 20 and 42 of the single roof correspond to joints 9 and 20 respectively of the double

Table (6-4). Comparison between Single and Double Roofs

Roof Dimensions: 120 ft x 240 ft x 12 ft high

E = 24,000 ksi Steel area = 1.25 sq. in.

H = 50 kips

	Single Roof	Double Roof
Total length of cable	3230	2040
Deflection due to 30 psf load (feet)	5.11 (at Jt. 20)	4.09 (at Jt. 9)
	5.11 (at Jt. 42)	5.01 (at Jt. 20)
Load causing stress of 125 ksi (prop. limit)	30 psf	22.5 psf
$\frac{\text{Load}}{\text{1000 ft of Cable}}$	9.3	11.0
Ultimate load (psf)	245	163.0
$\frac{\text{Ultimate load}}{\text{1000 ft of cable}}$	76	80

roof (Figs. 4-1a and b). They correspond in plan although their vertical ordinates are different. The deflections at joints 20 and 42 of the single roof under a load of 30 psf are both 5.11 feet while they are 4.09 feet and 5.01 feet at joints 9 and 20 respectively of the double roof under the same load. The maximum deflection (5.82 feet) in the single roof is at the centre while it is at joint 20 in the double roof (Figs. 4-4 and 4-5). The single roof, therefore, deflects more than the double roof.

The load causing a maximum stress of 125 ksi which is the proportional limit is 30 psf for the single roof and 22.5 psf for the double roof; however, when this load is expressed as a ratio of the length of cable used it is 9.3 psf and 11.0 psf per 1000 feet of cable respectively. The ultimate capacities developed by the two roofs when expressed as a ratio of the cable length are 76 psf and 80 psf respectively per 1000 feet of cable used. Although the difference here is only about 7%, it becomes appreciable as the height diverges from the critical height. It is about 25 to 30% higher in the case of the double roof for heights of 1 foot and 60 feet.

Thus the double roof appears to possess an advantage over the single roof for the configuration considered here. The smaller deflections could be attributed to the orthogonality of the double roof and its greater curvature at the same height as the single roof. These qualities have been shown to reduce the deflections (Figs. 4-26 and 4-41). The contours of the deflected double roof is also advantageous

in proper draining of the roof (Fig. 6-2). In addition to these benefits, the double roof considered here requires much less computer space for the theoretical analysis and only 40% of the computer time needed for the analysis of the single roof.

6.2 Experimental Results

6.2.1 Accuracy of Measurements

The experimental study was conducted in order to verify the results obtained by the theory. The theory assumes idealized conditions and makes simplifying assumptions to facilitate numerical solution. It is therefore necessary to find out how well or within what limits the theory can predict what actually happens in practice. In the experimental study, therefore, conditions were controlled as far as practically possible to minimize the discrepancy between theory and practice. Proper consideration was given to accurately establishing the required pretensions in the cables since the accuracy of the entire experiment depended on this. The load-cells used to measure the tensions were calibrated initially under the same conditions using the same strain indicator. The hysterisis in the strain gages were minimized by several cycles of loading and unloading but some still remained giving a maximum difference in readings between loading and unloading of about 60 μin/in. Taking the average of the two readings ensured a maximum difference of $\pm$30 μin/in. The accuracy of the strain indicator readings could be taken as

± 10 μin/in. Hence the tensions were measured accurate to within 1 lb. The pretensions were adjusted to within 1 lb in most of the cables and the maximum error was less than 2 lbs. Based on an initial tension of 50 lb it could be said that the cables were pretensioned to within 5% of the correct value and the tension changes were measured to within 2%.

The displacement transducers used in the deflection measurement had an accuracy of 0.1% of full scale reading. However, the output from the transducers are monitored on a voltage recorder where the voltage can be read to 0.05 volts. Allowing for the accuracy of the recorder and taking that the accuracy of recording is 0.10 volts, the deflections were measured to .004 in. This represents an accuracy of 1-2% in most of the deflections measured.

The stiffness of the wire rope used in the model was determined experimentally. The samples of virgin rope showed a variation of 3% in their stiffnesses while the samples of used rope from the model showed an average increase in stiffness of 2% over that of the virgin rope with a variation of as much as 8% among them.

6.2.2 Errors and Their Possible Causes

Table (6-5) gives a summary of the errors in the experimental results based on the theoretical values for both models. The tension increments show excellant agreement between theory and experiment. The discrepancy is less than 5% in most cases, the percentages being based on the changes rather

Table (6-5). Errors in Experimental Results

(a) Single Roof Model

Figure No.	Loading	Size of Error	
		Maximum Deflection	Tension Increment
5-5 and 5-6	U.D.L.	Mostly less than 10%. Maximum 12% when H=70 lb.	Less than 4%
5-7 and 5-8	Concentrated load at Jt 4	Mostly between 10-20%. Maximum 25% when H=70 lb.	Mostly less than 5%. Maximum 9% when H=50 lb.
5-9 and 5-10	Concentrated load at Jt 6	Mostly between 10-15%. Maximum 17% when H=20 lb.	Less than 5%
5-11 and 5-12	Concentrated load at Jt 7	Less than 10%	Mostly less than 5%. Maximum 10% when H=50 lb.

(b) Double Roof Model

Figure No.	Loading	Size of Error	
		Maximum Deflection	Tension Increment
5-15 and 5-17	U.D.L.	Mostly 5-10%. Maximum 13% when H=20lb	Less than 4%
5-18 and 5-19	Concentrated load at Jt 2	About 15-20%	Mostly less than 5%. Maximum 9% when H=50lb
5-20 and 5-21	Concentrated load at Jt 5	Mostly about 10%. Maximum 14% when H=50 lb.	Less than 4%
5-22 and 5-23	Concentrated load at Jt 6	Mostly about 5%. Maximum 11% when H=20 lb.	Mostly less than 5%. Maximum 8% when H=50 lb.

than the actual tensions measured. When comparisons are made in terms of the final cable tensions, which would normally be used for purposes of design, the difference is even less than 2%.

The deflections measured are less accurate. The differences are about 10 to 15% on an average and the experimental values are consistantly lower than the theoretical results. This discrepancy could have been caused by one or more of the following:

(i) The cable possessing some bending stiffness which was neglected in the theory;

(ii) imperfections in the model;

(iii) rigidity of end connections, added stiffness caused by the introduction of the load cells and their connections to the cables and the rigidity of the joints;

(iv) effect of any temperature variation;

(v) creep in the cables;

(vi) the accuracy of the values of EA and T used in obtaining the theoretical results;

(vii) inaccuracy of the theory.

Considering the small diameter of the wire rope and its flexibility, the bending stiffness would be of negligible magnitude and hence could not have caused appreciable error in the results. However, whatever stiffness is present will tend to reduce the magnitude of the deflections. Any imperfections in the model also would have affected the results. The imperfections could have been due to errors in the dimensions of

the model, improper allignment of cables, the boundaries not being perfectly straight, the joints, especially the end connections, having finite dimensions instead of being dimensionless points etc. It is not possible to estimate the error introduced by these imperfections, but it can be assumed that it will not be significantly High.

The effect of frame deformations was neglected in the theoretical solution. The excessive rigidity of the frame used justifies this assumption. As for any direct effect on the measurement of deflections, only those deflections relative to the frame would have been measured since the displacement transducers were supported on the frame itself. The effect of temperature variation would have been twofold: (i) affecting the tension measurements by causing the strain gages to measure apparent strain that the load cell is not subjected to (ii) introducing temperature stresses in the model itself. The former effect was eliminated by doubly compensating for temperature changes. The latter could not have introduced significant error considering the short duration of the test and the small size of the model. Creep effects were also negligible since the duration of the tests were short. The tensions in the cables returned to their original values on unloading indicating that there was no loss due to creep.

It cannot be said that the theory is inaccurate since it was derived from first principles considering the equilibrium of the system. The equations of equilibrium were based

on the displaced geometry of the structure and nonlinear terms were not neglected. Figures (6-4) and (6-5) show the accuracy with which the nonlinear theory used here predicts the actual behaviour of the two models. The experimental values are within 5% of the nonlinear solution - almost as accurate as the measurements themselves - while the linear solution overestimates it by as much as 90%. In the theoretical calculations the load was incremented in steps of 1 lb to correspond to the method of actual loading in the experiment.

The theory also takes into account the discontinuity caused by individual cable segments becoming slack. Fig. (6-6) compares the theoretical and experimental tensions in cable (3,4) of the single roof model as it becomes slack under increased load. Figure (6-7) shows how closely the theory predicts the actual behaviour in a load-carrying cable the tension increment of which is affected by the slackening of the prestressing cables. In the theoretical calculations, the tension increments are computed from the displacements themselves and since there is excellent agreement between the theoretical and experimental tension increments, the discrepancy in the deflections could not have been caused by any inaccuracy or inadequacy of the theory.

The added stiffness caused by the load cells, their connections, the rigidity of the joints and the end connections is, therefore, the principal cause of the error in the experimental deflections. The consistently lower experimental

values bear testimony to this. The load cells were, of course, designed to have the same deflection as the piece of cable it replaced but nothing could be done about its increasing the lateral stiffness of the roof. The end connections consisted of rigid bolts soldered at the ends of the cables (Photographs 1 and 2). These bolts projected about an inch and a half inside the model thereby stiffening it or in effect reducing its dimensions. The joints which were assumed to be smooth in the theory were made rigid by the clamping. There could also have been some slip at the joints. The fact that the deflections were affected by the stiffening effect of the load cells and end connections is clearly seen in figure (6-8). The deflection at joint 3 of the single roof model is adjacent to three load cells and cable ends and has the maximum discripancy (24%) between theory and experiment. Next, joint 6 is adjacent to two and the accuracy is a little improved (22.5%). At an interior joint (joint 4), the accuracy is much better (10%) and at the centre (joint 7), it is best (only 8%). It is also seen from tables (6-5a and b) that the deflections at the centre of both models under uniformly applied or concentrated loads are less than 10% in all cases. Since the model itself is very flexible, any external stiffening considerably increases the stiffness of the roof as a whole and is responsible for the smaller deflections especially at the joints closer to these stiffening.

As for the inaccuracy in the values of T and EA used, it was shown that the former was established to within 5%.

The value of EA was obtained experimentally with a 3% variation within samples of the virgin rope. This value, as was expected of a wire rope, increased during the tests. This increase is only 2% based on the averages of values obtained from samples but the actual increase in each cable varied depending on how much load it was subjected to. This is shown by the 8% variation within the samples taken from the model. In other words, the value of EA did not remain constant at the average used but varied throughout the tests and from segment to segment of the cables by as much as 8%. The change in EA - caused by the tightening of the strands - during the tests would have been positive thus contributing to increased stiffness and decreased deflections.

6.2.3 General Comments

Examination of graphs (5-5) to (5-23) inclusive suggests that the deflection and tension increment are only slightly nonlinear in single roof model. They are noticeably more nonlinear in the double roof model especially at low pretensions. The nonlinearity is larger when concentrated loads are applied with the deflections decreasing with increasing load and the maximum tension increments increasing with increasing load in both cases. The curvature of the tension increment-load curves suggests that both models behave as steep roofs i.e. they have heights greater than the critical height. The critical height obtained for the roofs used in the theoretical analysis when reduced to the scale of the models is about 3½ inches and

hence the behaviour as steep roofs is justified.

Joint 5 of the double roof model exhibits a peculier behaviour under uniform load. The deflection is negative i.e. upwards at low pretensions (H = 20 and 30 lbs). At higher pretensions the deflection is downwards but increases in magnitude as the pretension increases (Fig. 5-17). The experimental results agree with the theoretical values although accurate measurement was not possible owing to the very small magnitude of the deflections. It is also apparent from figure (5-17) that the upward deflections at low pretensions will decrease in magnitude with the increase of load and will eventually become downward. This kind of behaviour presents a problem in the theoretical analysis since the Newton-Raphson method will not converge in a case like this where a reversal of curvature takes place. Greenberg contends that the physical behaviour of a cable network is such that divergence of a second order method is not possible (32). But it is seen from the behaviour encountered here that it is not necessarily so. Hence an incremental load method will have to be used to obtain convergence in such cases.

6.3 Design Recommendations

Based on the analytical results obtained in this study and their experimental verification, the following design recommendations are made for the types of roofs considered here.

It is advantageous to use a high initial tension in

the cables. This decreases considerably the deformation of the roof under load while there is only a slight increase in the final cable tensions. In single roofs, the efficiency can be improved by using a higher pretension in the prestressing cables than in the load-carrying cables.

Non-orthogonality of the cables does not affect the cable tensions. Only the deflections are slightly increased with some deviation from orthogonality. Therefore, whenever situations demand it, non-orthogonal roofs could be built without fear of introducing additional stresses due to the non-orthogonality.

The following considerations should be given to the selection of the roof slope. A gentle slope has the advantage of small tension changes at working loads and a high ultimate load capacity but has the disadvantage of large deflections. Steep slopes have small tension changes and deflections under working load but have low ultimate load capacity. Slopes near the critical slope have large tension changes under working loads. The intensity of the load should also be considered when deciding on a slope since the critical slope is dependent on it.

Considering the fact that the factor of safety against failure based on a working load corresponding to the proportional limit is excessively high in all cases of slopes, it would seem advantageous to use a steep slope with an increased working load and smaller deflections in exchange for a lower factor of safety. As a comparison, the factors of safety

corresponding to heights of 12 feet and 60 feet are 8.0 and 3.0 respectively and the working load for the height of 60 feet is about 80% higher than that for the height of 12 feet (Figure 4-45). A steep slope is also advantageous when it comes to proper draining of the roof.

The high factor of safety also suggests that a design stress level higher than that used in conventional structures could be used in cable roofs. Even when the working load is so high as to produce the yield stress (based on 0.2% permanent set) the factor of safety is high - 4.8 and 2.3 for heights of 12 feet and 60 feet respectively of the roof considered here.

It must be noted, however, that the inelastic behaviour has not been experimentally verified. Since good agreement was found between theory and experiment in the elastic region, it could be assumed that the theory holds in the inelastic region too. The only limitation is the accuracy of the assumed material stress-strain curve but the curve used is quite a close simulation of the actual behaviour of the high-tensile steel commonly used in cable roof structures.

CHAPTER VII

CONCLUSIONS

The equations to determine the displacements and tensions of a general non-orthogonal cable network have been derived with respect to a set of oblique axes. The derivation is based on the displaced geometry of the structure and second-order displacement terms have been included. The Newton-Raphson method has been suitably adapted for the solution of these nonlinear equations.

A theoretical model for the material stress-strain curve has been used to simulate the material behaviour in the elastic and inelastic regions and up to the ultimate load. Hence the effects of both geometric and material nonlinearities in the behaviour of cable roofs have been included in this study.

Using the nonlinear equations derived, the general behaviour of single and double roofs having hyperbolic paraboloid shapes were studied in the elastic and inelastic regions and their ultimate capacities were determined. The influence of varying certain parameters on these roofs were also studied.

Based on the results of the theoretical analysis presented, the following conclusions can be reached:

(1) Linearized equations are inadequate to predict actual cable-roof behaviour. Not only the linear solution is different from the nonlinear solution, it sometimes leads to grossly misleading results. It does not always give a conservative estimate of the true values as generally believed. It can also underestimate the deflections and tension changes in some cases.

(2) The use of a high pretension in these hyperbolic paraboloid roofs decreases the roof-deformations considerably without significantly increasing the final cable tensions from a static point of view. However, research into the aerodynamic stability of the roof is needed to determine the proper magnitude of pretension to be used.

(3) The use of a higher pretension in the prestressing cables than in the load-carrying cables has also been shown to result in efficient use of the cables in the single roof.

(4) When hyperbolic paraboloid roofs are constructed with a non-orthogonal network of cables, the roof behaviour is not adversely affected by the non-orthogonality of the cables.

(5) In practical design, the choice of roof-slope should not be based purely on aesthetic considerations. Importance should be given to considerations of strength and performance since the curvature considerably influences the behaviour of the roof. It has been shown

that there exists a critical roof height at which the tension changes are maximum. On the basis of this definition roofs can be classified into flat roofs and steep roofs.

(6) The steep slopes are advantageous to use in practice since the deflections and tension changes are small and drainage is easy.

(7) The inelastic behaviour and the ultimate capacity is also considerably influenced by the roof slope. Steep roofs have the minimum ultimate capacity but since the factor of safety against failure is quite high in comparison to a conventional structure, the use of steep roofs is justified.

(8) By a comparison of a non-orthogonal single roof and an orthogonal double roof covering the same area in plan, it is found that the latter has a higher ratio of load intensity to amount of steel used in the net.

(9) Theoretical solutions of practical roofs with very large number of joints may be obtained by analyzing an equivalent sparser net without much loss of accuracy.

The theoretical solutions have been supported by experimental results obtained by testing models of single and double roofs. Good agreement between theory and experiment indicate that the procedure developed here could be used successfully when the nonlinearity is high or when a discontinuity occurs in the structure. The behaviour in the inelastic region, however, has not been experimentally verified.

APPENDIX A

DETERMINATION OF THE INITIAL SHAPE OF A NON-ORTHOGONAL NET

Considering the equilibrium of a typical joint (m, n), the forces acting at the joint are the pretensions in the cables as shown in figure (A-1a). Resolving forces in the direction of the ξ axis,

$$(H_{m,n,n+1}-H_{m,n,n-1})+(H_{n,m,n+1}-H_{n,m,n-1})\sin\theta = 0 \quad \ldots \text{A-1}$$

Similarly in the η direction,

$$(H_{n,m,m+1}-H_{n,m,n-1})+(H_{m,n,n+1}-H_{m,n,n-1})\sin\theta = 0 \quad \ldots \text{A-2}$$

Solving equations (A-1) and (A-2),

$$(H_{m,n,n+1}-H_{m,n,n-1})-(H_{m,n,n+1}-H_{m,n,n-1})\sin^2\theta = 0$$

where $H_{m,n,n+1}$, $H_{m,n,n-1}$ etc. are horizontal components of the tensions in the cable segments considered.

i.e. $H_{m,n,n+1} = H_{m,n,n-1} = H_{\xi}$

Similarly,

$$H_{n,m,m+1} = H_{n,m,m-1} = H_\eta$$

i.e. The horizontal components of the tensions are constant throughout the cable.

Resolving in the direction of the z-axis,

$$V_{m,n,n+1}+V_{m,n,n-1}+V_{n,m,m+1}+V_{n,m,m-1} = 0 \qquad \ldots \text{A-3}$$

where $V_{m,n,n+1}$ etc. are vertical components of the tensions in the cable segments considered.

From figure (A-1c),

$$V_{m,n,n+1} = H \cot\gamma_{m,n,n+1}$$

where γ is the angle made by the cable segment with the vertical.

i.e. $$V_{m,n,n+1} = \frac{H_\eta(z_{m,n+1}-z_{m,n})}{a} \qquad \ldots \text{A-4}$$

where a is the length in plan of a cable segment and z's are the vertical ordinates.

Substituting for $V_{m,n,n+1}$ etc. into equation (A-3) we have,

$$H_\xi (z_{m,n+1}-2z_{m,n}+z_{m,n-1})+H_\eta (z_{m+1,n}-2z_{m,n}+z_{m-1,n}) = 0 \quad \ldots \text{A-5}$$

Equation (A-5) can be written in finite difference form as,

$$H_\xi \left(\frac{\partial^2 z}{\partial \xi^2}\right)+H_\eta \left(\frac{\partial^2 z}{\partial \eta^2}\right) = 0 \quad \ldots \text{A-6}$$

Assuming that $H_\xi = H_\eta$ and that the surface is continuous, equation (A-6) becomes,

$$\frac{\partial^2 z}{\partial \xi^2} + \frac{\partial^2 z}{\partial \eta^2} = 0 \quad \ldots \text{A-7}$$

$z = a(\xi^2-\eta^2)$ is a solution of equation (A-7). Taking a section with ξ = constant, the equation becomes,

$$z = K_1 - a\eta^2 \quad \ldots \text{A-8}$$

Similarly when η = constant

$$z = a\xi^2 - K_2 \quad \ldots \text{A-9}$$

where K_1, K_2 are constants.

Equations (A-8) and (A-9) represent parabolas of opposite curvature.

When z = constant, the solution to equation (A-7) becomes,

$$(\xi^2-\eta^2) = K \qquad \ldots A\text{-}10$$

It can be shown that equation (A-10) represents a set of rectangular hyperbolas irrespective of the non-orthogonality of the cables.

Using the relations in equations (2-2a) and (2-2b) equation (A-10) can be expressed in (x,y) coordinates as,

$$x^2-2xy\tan\theta-y^2 = K \qquad \ldots A\text{-}11$$

Using a rotation of axes through an angle of $(45-\theta/2)$ to a new set of axes (X,Y) (Fig. A-1b), which bisects the angle between the ξ and η axes, the (x,y) and (X,Y) coordinates can be related by,

$$x = X\cos(45-\theta/2)-Y\sin(45-\theta/2) \qquad \ldots A\text{-}12a$$

$$y = X\sin(45-\theta/2)+Y\sin(45-\theta/2) \qquad \ldots A\text{-}12b$$

Substituting equations (A-12) into equation (A-11) and simplifying, we have,

$$XY\sec\theta = K$$

or $$XY = \text{constant} \qquad \ldots A\text{-}13$$

Equation (A-13) represents a set of rectangular

hyperbolas with the X,Y axes as asymptotes. This means that sections of the initial surface by horizontal planes are rectangular hyperbolas irrespective of the non-orthogonality of the cable-net.

APPENDIX B

DESIGN OF THE LOAD CELL

Referring to figure (B-1), the stresses at point A in the outer and inner fibres of the ring can be expressed by,

$$\sigma_{A_i} = \frac{P}{2a} + K_i \frac{M_A c}{I} \quad \ldots \text{B-1}$$

$$\sigma_{A_o} = \frac{P}{2a} - K_o \frac{M_A c}{I} \quad \ldots \text{B-2}$$

where P is the applied load,

a is the area of cross-section,

c is $\frac{1}{2}$ the thickness of ring

and $M_A = \frac{1}{2} \times .364\ PR$. (page 180. Reference (63)).

The outer and inner diameter of the ring used are $1\frac{1}{4}$" and $1\frac{1}{64}$" and the width of the ring is $\frac{1}{4}$". The values of K_i and K_o are obtained from table (5) page 149 of Reference (63) and are approximately 1.08 and 0.93 respectively.

Hence for the ring used,

$$\sigma_{A_i} = 227\ P$$

and $$\sigma_{A_o} = -164\ P$$

The strain gages are connected in a Wheatstone bridge so that the strains add up numerically. Using a value of $E = 10 \times 10^6$ lb/in^2 for aluminum.

$$\epsilon_{A_i} - \epsilon_{A_o} = \frac{227 + 164}{10 \times 10^6} P$$

$$= 39.1 \; P \; \mu \text{in/in}$$

The sensitivity of the load cell is 39.1 $\mu\epsilon$/lb. This is close to the calibration constants obtained experimentally (Table 5-1).

The deflection in the ring in the direction of the load is expressed by,

$$\delta = \frac{P}{2}\left[\frac{R\pi}{2Ea} + \frac{R\pi}{2Ga} + \frac{.3R^3}{EI}\right] \qquad \text{(Reference (63))}$$

where $G = \frac{E}{2(1+\nu)} = \frac{10 \times 10^6}{2.6}$ lb/in^2

Hence $\delta = 88.0 \times 10^{-6} \; P$ in.

Extension in 1.25 in of cable $= \frac{P \times 1.25}{17500}$ in.

$$= 71.5 \times 10^{-6} \; P \text{ in.}$$

Hence the two deflections are approximately equal.

```
      C     NON-ORTHOGONAL CABLE ROOF
      C     NONLINEAR ANALYSIS OF THE COMPLETE NET
      C
      C  0. DIMENSION AND DECLARATION STATEMENTS.
      C
0001        DOUBLE PRECISION AX,CMX,AMX,RM,RT,B,RES,DIS,Z,COSG,T,EAT,COSA,COSB
0002        DOUBLE PRECISION HXI,HETA,EA,RS,HT,WDTH,E,TEM,F,FL,DELT,A,SINT
0003        DOUBLE PRECISION EM,AR,TM,SIGP,SIGY,SIGU,G,EF,C,C1,C2,C3,EPSY,EPSU
0004        DOUBLE PRECISION  BI,BJ,U,BE,SIDE,DT,H ,BI,TEM1,TEM2,BU
      C
      C     CAUTION: WHEN CHANGING DIMENSIONS CHECK THOSE IN SUBROUTINE ANMX.
      C
0005        DIMENSION AMX(8650),CMX(865),RM(183),RT(3,183),H(4),BU(183)
0006        DIMENSION BI(183),Z(61),RES(183),DIS(183),DELT(61,4),DT(61,4)
0007        DIMENSION EL(61,4),DL(61,4),DDL(61,4) ,EA(61,4),AR(4),HGT(4,10)
0008        COMMON EAT(61,4),T(61,4),COSG(61,4),COSA(4),COSB(4),F(20),FL(4)
0009        COMMON AX(4,3,3),B(183),BI(3,4),BJ(3),U(61,4),BE(183)
      C
      C  1. READ INPUT DATA
      C
0010        READ 110,NTYP,INDS,LDS,NDATA,KCRD,KPRNT
0011    110 FORMAT (2012)
0012        N=NTYP*INDS
0013        N1=N-1
0014        IND=INDS-1
0015        NJ=N*INDS+N1*IND
0016        NE=3*NJ
0017        IF (KORD.NE.1) GO TO 120
0018        READ 135,(Z(I),I=1,NJ)
0019        READ 135,(HGT(1,J),J=1,N)
0020        READ 135,(HGT(2,J),J=1,INDS)
0021        READ 135,(HGT(3,J),J=1,N)
0022        READ 135,(HGT(4,J),J=1,INDS)
0023    120 READ 130,HXI,HETA,RS,HT,WDTH,E
0024        READ 135,AXI,AETA,EM,SIGY,SIGU,EPSU
0025    130 FORMAT (4F5.0,F10.0,D10.4,F5.0)
0026    135 FORMAT (6F10.0)
0027    140 CONTINUE
0028        READ 110,NLDS
0029        DO 730 IEND=1,NLDS
0030        READ 150,(BJ(I),I=1,3),TEM
0031        DO 145 I=1,NJ
0032        B1(3*I-2)=BJ(1)
0033        B1(3*I-1)=BJ(2)
0034    145 B1(3*I)=BJ(3)
0035        READ 110,NCL
0036        IF (NCL.EQ.0) GO TO 148
0037        READ 147,((NC,B1(NC)),I=1,NCL)
0038    147 FORMAT (8(I5,F5.0))
0039    148 READ 110,KI,KY,KDIF
0040    150 FORMAT (15F5.0)
0041        KU=KI
0042        IF (KDIF.NE.0) KY=KI
0043        KULT=KY
0044        IF (IEND.GT.1) PRINT 152,TEM,(B1(I),I=1,NE)
0045        IF (IEND.GT.1) PRINT 185,KI,KULT
0046    152 FORMAT (1H1,////////50HOSUBSEQUENTLY ADDED LOAD (SUBSEQUENT TEMP. CH
     1ANGE= ,F5.1,1H)/(1H0,18F6.1))
```

```
0047            DO 155 I=1,NE
0048            B1(I)=B1(I)/KI
0049        155 CONTINUE
0050            TEM1=TEM
0051            TEM2=0.0
0052            TEM=TEM/KI
0053            IF (IEND.GT.1) GO TO 303
0054            PRINT 160
0055            PRINT 162,NTYP
0056            NSLK=0
0057        160 FORMAT (11H1INPUT DATA)
0058        162 FORMAT ( /16H TYPE OF ROOF:- ,I1)
0059            SIDE=WDTH/INDS
0060            RL=RS*WDTH
0061            A=SIDE*DSQRT(NTYP**2+RS**2)/2.0/NTYP
0062            SINT=(RS**2-NTYP**2)/(RS**2+NTYP**2)
0063            EPSY=SIGY/EM+.002
0064            C1=(SIGU-SIGY-EM*(EPSU-EPSY))**2
0065            C2=((SIGU-SIGY-EM*(EPSU-EPSY))*
               1    (SIGU*SIGY**2-SIGY*SIGU**2-EM*(EPSU*SIGY**2-EPSY*SIGU**2))
               2    -2.0*EM**2*(EPSU*SIGY-EPSY*SIGU)**2)
0066            C3=(SIGU*SIGY**2-SIGY*SIGU**2-EM*(EPSU*SIGY**2-EPSY*SIGU**2))**2
0067            C=(-C2-DSQRT(C2**2-C1*C3))/C1
0068            SIGP=DSQRT(C)
0069            G=-250.0*(SIGY-SIGP)**2
0070            EF=-G/EM-SIGP
0071            PRINT 165,HXI,HETA,AXI,AETA
0072            PRINT 170,HT,WDTH,RL,SINT,EM,E
0073            PRINT 172,SIGP,SIGY,EPSY,SIGU,EPSU
0074        165 FORMAT (6H0HXI= ,F6.1,5X,6HHETA= ,F6.1,10X,16HSTEEL AREA(XI)= ,
               1    F8.5,5X,17HSTEEL AREA(ETA)= ,F8.5)
0075        170 FORMAT (8H0RF HT.=,F6.1,5X,8HRF WDTH=,F6.1,5X,7HRF LTH=,F6.1,5X,
               1  11HSIN(THETA)=,F7.5,5X,11HELAS. MOD.=,F10.1,5X,13HTHERM COEFF.=,
               1    D10.3)
0076        172 FORMAT (13H0PROP. LIMIT= ,F10.2,5X,13HYIELD STRESS=,F10.2,5X,
               1    13HYIELD STRAIN=,F7.5,5X,12HULT. STRESS=,F10.2,5X,12HULT. STRAI
               2N=,F7.5)
0077            NLS=NLDS-1
0078            DO 173 I=1,NE
0079        173 BU(I)=KI*B1(I)
0080            PRINT 175,NCL,NLS,TEM1,(BU(I),I=1,NE)
0081        175 FORMAT (37H0LOAD (NO. OF ADDITIONAL CONC. LOADS=,I2,5X,
               1    38HNO. OF LOADS TO BE ADDED SUBSEQUENTLY=,I2,1H)
               2    10X,13HTEMP. CHANGE= ,F5.1/(1H0,18F7.2))
0082            DO 180 I=1,NE
0083            BU(I)=0.0
0084        180 DIS(I)=0.0
0085            PRINT 185,KI,KULT
0086        185 FORMAT ( 23H0INCREMENT SIZES= LOAD/,I2,10H AND LOAD/   ,I2)
0087            PRINT 190
0088        190 FORMAT (/22H0INITIAL CONFIGURATION                    )
0089            DO 195 I=1,NJ
0090            DO 195 J=1,4
0091        195 DELT(I,J)=0.0
0092            H(1)=HXI
0093            H(2)=HXI
0094            H(3)=HETA
0095            H(4)=HETA
```

```
0096            AR(1)=AXI
0097            AR(2)=AXI
0098            AR(3)=AETA
0099            AR(4)=AETA
0100            EPS=1.0E-15
0101            IF (KORD.EQ.1) GO TO 293
                C
                C  2. DETERMINE INITIAL ORDINATES OF THE JOINTS
                C
0102            JT=1
0103            IE=0
0104          205 DO 270 IC=1,N
0105            DO 210 I=1,NJ
0106          210 RM(I)=0.0
0107            RM(JT) = -2.0*HXI-2.0*HETA
0108            IF (JT.LE.N) GO TO 220
0109            IF (IC.EQ.1) GO TO 215
0110            RM(JT-N) = HXI
0111          215 IF (JT.GT.(NJ-N)) GO TO 227
0112          220 IF (IC.EQ.N)  GO TO 225
0113            RM(JT+N) = HXI
0114            IF (IC.EQ.1) GO TO 230
0115          225 RM(JT+N1) = HETA
0116          227 IF (IC.EQ.N) GO TO 238
0117          230 IF (JT.LE.N) GO TO 238
0118          235 RM(JT-N1) = HETA
0119          238 JT1=JT-N
0120            JT2=JT+N
0121          240 IF (JT.LE.N) GO TO 250
0122            IF (JT.GT.(NJ-N)) GO TO 260
0123            DO 245 II=JT1,JT2
0124            IE=IE+1
0125          245 CMX(IE)=RM(II)
0126            GO TO 266
0127          250 DO 255 II=1,JT2
0128            IE=IE+1
0129          255 CMX(IE)=RM(II)
0130            GO TO 266
0131          260 DO 265 II=JT1,NJ
0132            IE=IE+1
0133          265 CMX(IE)=RM(II)
0134          266 CONTINUE
0135          268 FORMAT (1H0,14F9.1)
0136            JT=JT+1
0137          270 CONTINUE
0138            IF (JT.GT.NJ) GO TO 288
0139            DO 285 IC=1,N1
0140            DO 275 I=1,NJ
0141          275 RM(I)=0.0
0142            RM(JT) = -2.0*HXI-2.0*HETA
0143            RM(JT-N) = HXI
0144            RM(JT+N) = HXI
0145            RM(JT+N1) = HETA
0146            RM(JT-N1) = HETA
0147            JT1=JT-N
0148            JT2=JT+N
0149            DO 280 I=JT1,JT2
0150            IE=IE+1
```

```
0151          280 CMX(IE)=RM(I)
0152              JT=JT+1
0153          285 CONTINUE
0154              GO TO 205
0155          288 DO 289 I=1,NJ
0156          289 Z(I)=0.0
0157              DO 290, I=1,INDS
0158              HGT(1,N-I+1)=I*HT/INDS
0159              HGT(2,I)=(2-NTYP)*(N+1-I)*HT/INDS+(NTYP-1)*(I-1)*HT/INDS
0160              HGT(3,INDS-I+1)=I*HT/INDS
0161              HGT(4,I)=(INDS+1-I)*HT/INDS
0162              Z(N-I+1)=-I*HT/INDS*HXI-(I-1)*HT/INDS*HETA
0163          290 Z(NJ-INDS+I)=Z(N-I+1)
0164              DO 291 I=1,INDS
0165              HGT(1,I)=(I-1)*HT/INDS
0166              HGT(3,N-INDS+I)=HGT(1,I)
0167              Z(I)=-(I-1)*HT/INDS*HXI-I*HT/INDS*HETA
0168          291 Z(NJ-N+INDS-I+1)=Z(I)
0169              DO 292 I=1,IND
0170              M1=(I-1)*(N+N1)+1
0171              M2=(2-NTYP)*(NJ-(I-1)*(N+N1))+(NTYP-1)*(N+(I-1)*(N+N1))
0172              Z(M1)=Z(I)
0173          292 Z(M2)= Z(I)
0174              Z(1)=-2.0*HT/INDS*HETA
0175              Z(N)=(NTYP-2)*(2.0*IND*HT/INDS*HXI+HT*HETA)+(1-NTYP)*(2.0*HT/INDS
                 1    *HXI)
0176              Z(NJ-N+1)=-2.0*IND*HT/INDS*HXI-HT*HETA
0177              Z(NJ)=(NTYP-2)*2.0*HT/INDS*HETA+(1-NTYP)*(HT*HXI+2.0*IND*HT/INDS*
                 1    HETA)
0178              CALL DGELB (Z,CMX,NJ,1,N,N,EPS,IER)
0179          293 PRINT 299,(Z(I),I=1,NJ)
0180              HGT(1,N+1)=HGT(2,1)
0181              HGT(2,INDS+1)=HGT(3,1)
0182              HGT(3,N+1)=HGT(4,1)
0183              HGT(4,INDS+1)=HGT(1,1)
0184              DO 294 I=1,INDS
0185              M=(I-1)*N+1
0186              F(I)=A*(1.0+8.0/3.0*(HGT(1,I+1)-Z(M))**2/((2*A*I)**2))
0187          294 F(N+INDS-I)=F(I)
0188              IF (NTYP.EQ.1) GO TO 296
0189              DO 295 I=INDS,N
0190              F(I)=A*(1.0+8.0/3.0*(HGT(1,I+1)-Z(M))**2/((A*N)**2))
0191          295 M=M+1
0192          296 NF=N+INDS-1
0193              PRINT 298,A,(F(I),I=1,NF)
0194          298 FORMAT (3HOA=,F16.8/20HOSECTION LENGTHS...  /(1HO,8F16.8))
0195          299 FORMAT (10HOORDINATES /(1HO,8D16.8))
              C
              C   3. CALCULATE COS(GAMA),SIN(GAMA)
              C
0196              IELAS=0
0197              IY=0
0198              INC=1
0199          303 CONTINUE
0200              K1= N
0201              K3= 0
0202              JT= 1
0203          305 K1= K1+1
```

```
0204            DO 340 IC=1,N
0205            IF (JT-N) 306,306,308
0206        306 CONTINUE
0207            COSG(JT,1)=( HGT(1,IC)-Z(JT))/F(K1-IC)
0208            COSG(JT,4)=(HGT(1,IC+1)-Z(JT))/F(K3+IC)
0209            GO TO 320
0210        308 IF (IC-1) 312,310,312
0211        310 COSG(JT,1)=(HGT(4,N+INDS+2-K1)-Z(JT))/F(K1-IC)
0212            COSG(JT,3)=(HGT(4,N+INDS+1-K1)-Z(JT))/F(K3+IC)
0213            GO TO 315
0214        312 COSG(JT,1) = (Z(JT-N)-Z(JT))/F(K1-IC)
0215        315 IF (JT-(NJ-N)) 320,320,318
0216        318 CONTINUE
0217            COSG(JT,2)=(HGT(3,N+1-IC)-Z(JT))/F(K1-IC)
0218            COSG(JT,3)=(HGT(3,N+2-IC)-Z(JT))/F(K3+IC)
0219            GO TO 327
0220        320 IF (IC-N) 323,321,323
0221        321 CONTINUE
0222            COSG(JT,2)=(HGT(2,K3+2)-Z(JT))/F(K1-IC)
0223            COSG(JT,4)=(HGT(2,K3+1)-Z(JT))/F(K3+IC)
0224            GO TO 325
0225        323 COSG(JT,2) = (Z(JT+N)-Z(JT))/F(K1-IC)
0226            IF(IC-1) 325,324,325
0227        324 COSG(JT,1)=(HGT(4,N+INDS+2-K1)-Z(JT))/F(K1-IC)
0228            COSG(JT,3)=(HGT(4,N+INDS+1-K1)-Z(JT))/F(K3+IC)
0229            GO TO 330
0230        325 COSG(JT,3) = (Z(JT+N1)-Z(JT))/F(K3+IC)
0231        327 IF (IC-N) 330,328,330
0232        328 CONTINUE
0233            COSG(JT,2)=(HGT(2,K3+2)-Z(JT))/F(K1-IC)
0234            COSG(JT,4)=(HGT(2,K3+1)-Z(JT))/F(K3+IC)
0235            GO TO 338
0236        330 IF (JT.LE.N) GO TO 338
0237            COSG(JT,4) =  (Z(JT-N1)-Z(JT))/F(K3+IC)
0238        338 JT=JT+1
0239        340 CONTINUE
0240            K3=K3+1
0241            IF (JT.GT.NJ) GO TO 348
0242            DO 345 IC=1,N1
0243            COSG(JT,1) = (Z(JT-N)-Z(JT))/F(K1-IC)
0244            COSG(JT,2) = (Z(JT+N)-Z(JT))/F(K1-IC)
0245            COSG(JT,3) = (Z(JT+N1)-Z(JT))/F(K3+IC)
0246            COSG(JT,4) = (Z(JT-N1)-Z(JT))/F(K3+IC)
0247            JT=JT+1
0248        345 CONTINUE
0249            GO TO 305
0250        348 KH=-1
0251        350 CONTINUE
0252            DO 360 I=1,NJ
0253            DO 360 J=1,4
0254            IF (INC.GT.1) GO TO 352
0255            T(I,J)=H(J)/DSQRT(1.0-COSG(I,J)**2)
0256            DL(I,J)=T(I,J)/AR(J)/EM
0257            EL(I,J)=0.0
0258            GO TO 355
0259        352 CONTINUE
0260            IF (T(I,J).LE.C.C) GC TO 360
0261        355 SIGMA=T(I,J)/AR(J)
```

```
0262                IF (SIGMA.GT.SIGP) GO TO 356
0263                EA(I,J)=EM*AR(J)
0264                GO TO 359
0265            356 IELAS = IELAS+1
0266                IF (IELAS.EQ.1) PRINT 366
0267                IF (KH.GE.0) GO TO 357
0268                TM=-G/(SIGMA+EF)
0269                GO TO 358
0270            357 TM=-G/((T(I,J)+DT(I,J)/2.0)/AR(J)+EF)
0271                DEL=-(SIGMA**2+2.0*EF*SIGMA+C)/2.0/G
0272                IF(INC.EQ.1) DL(I,J)=DEL
0273                IF (( DEL-SIGMA/EM).GT.EL(I,J)) EL(I,J)=DEL-SIGMA/EM
0274                IF (DT(I,J).LT.0.0.OR.DEL.LT.DL(I,J)) TM=EM
0275            358 EA(I,J)=TM*AR(J)
0276                IF (SIGMA.GE.SIGY) IY=IY+1
0277                IF (IY.EQ.1) PRINT 367
0278                IF (IY.EQ.1.AND.KDIF.EQ.0) GO TO 362
0279                IF (IY.EQ.1) IY=2
0280                IF (SIGMA.GE.SIGU) GO TO 375
0281            359 CONTINUE
0282                EAT(I,J)=EA(I,J)*(1.0+E*TEM)-T(I,J)
0283                U(I,J)=EA(I,J)*(1.0+E*TEM/2.0)-T(I,J)/2.0
0284            360 CONTINUE
0285                GO TO 390
0286            362 TEM=TEM*KI/KULT
0287                DO 364 I=1,NE
0288            364 B1(I)=B1(I)*KI/KULT
0289                IY=2
0290            366 FORMAT (//36HOPROPORTIONAL LIMIT HAS BEEN REACHED)
0291            367 FORMAT(//21HOYIELDING HAS STARTED   )
0292                GO TO 350
0293            370 FORMAT (1H0,4F16.6)
0294            375 CONTINUE
0295                DO 380 I=1,NE
0296            380 BU(I)=BU(I)-B1(I)*AR(J)*(SIGMA-SIGU)/DT(I,J)
0297                PRINT 385,(BU(I),I=1,NE)
0298            385 FORMAT (60H1ULTIMATE LOAD OF THE FOLLOWING MAGNITUDE HAS BEEN REAC
                   1HED          /(1H0,18F7.2))
0299                GO TO 730
0300            390 CONTINUE
                C
                C  4. GENERATE MATRIX OF LINEAR TERMS, CALCULATE INITIAL VALUES FOR
                C     DISPLACEMENTS AND ADD NONLINEAR TERMS TO MATRIX TO FORM FINAL
                C     STIFFNESS MATRIX.
                C
0301                MUD=3*(N+1)-1
0302                MA= NE*(2*MUD+1)-MUD*(MUD+1)/2
0303            401 LON=1
0304            402 DO 403 I=1,MA
0305            403 AMX(I)=0.0
0306                DO 404 I=1,NE
0307            404 RES(I)=0.0
0308            406 K1=N
0309                K3 = 0
0310                JT = 1
0311                IE = 0
0312            405 K1 = K1+1
0313                DO 470 IC=1,N
```

```
0314            DO 410 I =1,3
0315            DO 410 J =1,NE
0316        410 RT(I,J) = 0.0
0317            JM0 = (JT-1)*3
0318            JM1 = (JT-N-1)*3
0319            JM2 = (JT+N-1)*3
0320            JM3 = (JT+N-2)*3
0321            JM4 = (JT-N)*3
0322            CALL ANMX(JT,IC,K1,K3,A,SINT,N,NJ,LON)
0323        411 DO 412 I=1,3
0324            DO 412 J=1,3
0325        412 RT(I,JM0+J)=-AX(1,I,J)-AX(2,I,J)-AX(3,I,J)-AX(4,I,J)
0326            IF (JT.LE.N) GO TO 420
0327            IF (IC.EQ.1) GO TO 415
0328            DO 413 I=1,3
0329            DO 413 J=1,3
0330        413 RT(I,JM1+J)= AX(1,I,J)
0331        415 IF (JT.GT.(NJ-N)) GO TO 427
0332        420 IF (IC.EQ.N) GO TO 425
0333            DO 422 I=1,3
0334            DO 422 J=1,3
0335        422 RT(I,JM2+J)= AX(2,I,J)
0336            IF(IC.EQ.1) GO TO 430
0337        425 DO 426 I=1,3
0338            DO 426 J=1,3
0339        426 RT(I,JM3+J)= AX(3,I,J)
0340        427 IF (IC.EQ.N) GO TO 438
0341        430 IF (JT.LE.N) GO TO 438
0342            DO 435 I=1,3
0343            DO 435 J=1,3
0344        435 RT(I,JM4+J)= AX(4,I,J)
0345        438 JT1=3*(JT-N-1)-2
0346            JT2=3*(JT+N)-1
0347            IF (JT.LE.(N+1)) GO TO 450
0348            IF (JT.GE.(NJ-N)) GO TO 460
0349            DO 440 I=1,3
0350            JT1=JT1+1
0351            JT2=JT2+1
0352            DO 440 J=JT1,JT2
0353            IE=IE+1
0354            IF (KH.LT.0) GO TO 440
0355            RES(3*(JT-1)+I) = RES(3*(JT-1)+I)+RT(I,J)*B(J)/LCN
0356        440 AMX(IE)=AMX(IE)+RT(I,J)
0357            GO TO 466
0358        450 DO 455 I=1,3
0359            JT2=JT2+1
0360            DO 455 J=1,JT2
0361            IE=IE+1
0362            IF (KH.LT.0) GO TO 455
0363            RES(3*(JT-1)+I) = RES(3*(JT-1)+I)+RT(I,J)*B(J)/LCN
0364        455 AMX(IE)=AMX(IE)+RT(I,J)
0365            GO TO 466
0366        460 DO 465 I=1,3
0367            JT1=JT1+1
0368            DO 465 J=JT1,NE
0369            IE=IE+1
0370            IF (KH.LT.0) GO TO 465
0371            RES(3*(JT-1)+I) = RES(3*(JT-1)+I)+RT(I,J)*B(J)/LCN
```

```
0372          465 AMX(IE) = AMX(IE)+RT(I,J)
0373          466 JT = JT+1
0374          470 CONTINUE
0375              K3 = K3+1
0376              IF (JT.GT.NJ) GO TO 482
0377              DO 481 IC=1,N1
0378              DO 472 I=1,3
0379              DO 472 J=1,NE
0380          472 RT(I,J) = 0.0
0381              JM0=(JT-1)*3
0382              JM1 = (JT-N-1)*3
0383              JM2 = (JT+N-1)*3
0384              JM3 = (JT+N-2)*3
0385              JM4 = (JT-N)*3
0386              CALL ANMX(JT,IC,K1,K3,A,SINT,N,NJ,LON)
0387          473 DO 474 I=1,3
0388              DO 474 J=1,3
0389              RT(I,JM0+J) = -AX(1,I,J)-AX(2,I,J)-AX(3,I,J)-AX(4,I,J)
0390              RT(I,JM1+J) =  AX(1,I,J)
0391              RT(I,JM2+J) =  AX(2,I,J)
0392              RT(I,JM3+J) =  AX(3,I,J)
0393          474 RT(I,JM4+J) =  AX(4,I,J)
0394              JT1=3*(JT-N-1)-2
0395              JT2=3*(JT+N)-1
0396              IF (JT.LE.(N+1)) GO TO 477
0397              IF (JT.GE.(NJ-N)) GO TO 479
0398              DO 476 I=1,3
0399              JT1=JT1+1
0400              JT2=JT2+1
0401              DO 476 J=JT1,JT2
0402              IE=IE+1
0403              IF (KH.LT.0) GO TO 476
0404              RES(3*(JT-1)+I) = RES(3*(JT-1)+I)+RT(I,J)*B(J)/LCN
0405          476 AMX(IE)=RT(I,J) +AMX(IE)
0406              GO TO 481
0407          477 DO 478 I=1,3
0408              JT2=JT2+1
0409              DO 478 J=1,JT2
0410              IE=IE+1
0411              IF (KH.LT.0) GO TO 478
0412              RES(3*(JT-1)+I) = RES(3*(JT-1)+I)+RT(I,J)*B(J)/LCN
0413          478 AMX(IE)=RT(I,J) +AMX(IE)
0414              GO TO 481
0415          479 DO 480 I=1,3
0416              JT1=JT1+1
0417              DO 480 J=JT1,NE
0418              IE=IE+1
0419              IF (KH.LT.0) GO TO 480
0420              RES(3*(JT-1)+I) = RES(3*(JT-1)+I)+RT(I,J)*B(J)/LCN
0421          480 AMX(IE) = RT(I,J)+AMX(IE)
0422          481 JT=JT+1
0423              GO TO 405
0424          482 IF (KH) 483,496,496
0425          483 DO 484 I=1,NE
0426          484 B(I)=B1(I)+BE(I)
0427              CALL DGELB(B,AMX,NE,1,MUD,MUD,EPS,IER)
0428              IF (KPRNT.NE.1) GO TO 493
0429              PRINT 490,INC
```

```
0430          490 FORMAT (13H1INCREMENT NO,I2)
0431              PRINT 491
0432          491 FORMAT (16HOINITIAL VALUES /59HOJOINT NO        XI DISPL        ETA D
                 1ISPL        Z DISPL        )
0433              DO 492 I=1,NJ
0434          492 PRINT 495,I,(B(3*(I-1)+J),J=1,3)
0435          493 CONTINUE
0436          495 FORMAT (1HO,I5,5X,3D16.8)
0437              KH=0
0438              LON=3
0439              IF (NSLK.GE.1) GO TO 402
0440              GO TO 602
0441          496 LON=LON+1
0442              IF (LON.EQ.2) GO TO 406
              C
              C  5. CALCULATE RESIDUES, CHECK FOR CONVERGENCE AND GO BACK TO RECALCULA
              C     WITH NEW DISPLACEMENTS IF NECESSARY.
              C
0443              DO 505 I=1,NE
0444          505 RES(I)=RES(I)-(B1(I)+BE(I))
0445              DO 510 I=1,NE
0446              IF (DABS(RES(I))-1.0D-05) 510,535,535
0447          510 CONTINUE
0448              IF (KH.EQ.0) KH=1
0449              DO 515 I=1,NE
0450          515 DIS(I) = DIS(I)+B(I)
0451              PRINT 520,INC
0452          520 FORMAT (22H1DISPLACEMENTS IN STEP,I3/59HOJOINT NO        XI DISPL
                 1    ETA DISPL        Z DISPL        )
0453              DO 530 I=1,NJ
0454              PRINT 525,I,(DIS(3*(I-1)+J),J=1,3)
0455          525 FORMAT (1HO,I5,3D16.8)
0456          530 Z(I) = Z(I)+B(3*I)
0457              IF (KPRNT.NE.1) PRINT 570,KH
0458              GO TO 602
0459          535 CONTINUE
0460              IF (KPRNT.EQ.1) PRINT 540,(RES(I),I=1,NE)
0461          540 FORMAT (9HORESIDUES/(1HO,6D20.8))
0462              CALL DGELB(RES,AMX,NE,1,MUD,MUD,EPS,IER)
0463              DO 545 I=1,NE
0464          545 B(I) = B(I)-RES(I)
0465              KH = KH+1
0466              IF (KPRNT.NE.1) GO TO 558
0467              PRINT 550,KH
0468          550 FORMAT (13H1ITERATION NO,I3/59HOJOINT NO        XI DISPL        ETA D
                 1ISPL        Z DISPL        )
0469              DO 555 I=1,NJ
0470          555 PRINT 525,I,(B(3*(I-1)+J),J=1,3)
0471          558 IF (KH-10) 401,560,560
0472          560 PRINT 565,KH
0473          565 FORMAT (  ///21HONO CONVERGENCE AFTER,I2,12H ITERATIONS.     )
0474          570 FORMAT (///27HOCONVERGENCE OBTAINED AFTER,I2,12H ITERATIONS.     )
0475              GO TO 732
              C
              C  6. CALCULATE TENSION INCREMENTS AND NEW TENSIONS.
              C
0476          602 K1 = N
0477              K3 = 0
```

```
0478            JT =1
0479        610 K1=K1+1
0480            DO 630 IC=1,N
0481            CALL ANMX(JT,IC,K1,K3,A,SINT,N,NJ,LON)
0482            DO 620 I=1,4
0483            IF (T(JT,I).GT.0.0) DT(JT,I)=(AX(I,1,1)-E*TEM)*EA(JT,I)
0484            IF (KH.EQ.0) GO TO 618
0485            DDL(JT,I)=AX(I,1,1)-E*TEM
0486            DL(JT,I)=DL(JT,I)+AX(I,1,1)-E*TEM
0487            IF (T(JT,I).GT.0.0) GO TO 620
0488            IF (DL(JT,I).LT.EL(JT,I)) GO TO 615
0489            IF (EAT(JT,I).LE.0.0) DL(JT,I)=EL(JT,I)
0490            EA(JT,I)=EM*AR(I)
0491            EAT(JT,I)=EA(JT,I)*(1.0+E*TEM)
0492            U(JT,I)=EA(JT,I)*(1.0+E*TEM/2.0)
0493            DT(JT,I)=(DL(JT,I)-EL(JT,I))*EA(JT,I)
0494            GO TO 620
0495        615 EAT(JT,I)=0.0
0496            U(JT,I)=0.0
0497            DT(JT,I)=0.0
0498            GO TO 620
0499        618 IF (T(JT,I).GT.0.0 .OR. (DL(JT,I)+AX(I,1,1)-E*TEM).LE.EL(JT,I))
              1   GO TO 620
0500            EA(JT,I)=EM*AR(I)
0501            EAT(JT,I)=EA(JT,I)*(1.0+E*TEM)
0502            U(JT,I)=EA(JT,I)*(1.0+E*TEM/2.0)
0503        620 CONTINUE
0504            JT = JT+1
0505        630 CONTINUE
0506            K3 =K3+1
0507            IF (JT.GT.NJ) GO TO 650
0508            DO 645 IC=1,N1
0509            CALL ANMX(JT,IC,K1,K3,A,SINT,N,NJ,LON)
0510            DO 640 I=1,4
0511            IF (T(JT,I).GT.0.0) DT(JT,I)=(AX(I,1,1)-E*TEM)*EA(JT,I)
0512            IF (KH.EQ.0) GO TO 638
0513            DDL(JT,I)=AX(I,1,1)-E*TEM
0514            DL(JT,I)=DL(JT,I)+AX(I,1,1)-E*TEM
0515            IF (T(JT,I).GT.0.0) GO TO 640
0516            IF (DL(JT,I).LT.EL(JT,I)) GO TO 635
0517            EA(JT,I)=EM*AR(I)
0518            IF (EAT(JT,I).LE.0.0) DL(JT,I)=EL(JT,I)
0519            EAT(JT,I)=EA(JT,I)*(1.0+E*TEM)
0520            U(JT,I)=EA(JT,I)*(1.0+E*TEM/2.0)
0521            DT(JT,I)=(DL(JT,I)-EL(JT,I))*EA(JT,I)
0522            GO TO 640
0523        635 EAT(JT,I)=0.0
0524            U(JT,I)=0.0
0525            DT(JT,I)=0.0
0526            GO TO 640
0527        638 IF (T(JT,I).GT.0.0 .OR. (DL(JT,I)+AX(I,1,1)-E*TEM).LE.EL(JT,I))
              1   GO TO 640
0528            EA(JT,I)=EM*AR(I)
0529            EAT(JT,I)=EA(JT,I)*(1.0+E*TEM)
0530            U(JT,I)=EA(JT,I)*(1.0+E*TEM/2.0)
0531        640 CONTINUE
0532        645 JT = JT+1
0533            GO TO 610
```

```
0534          650 IF (KH.EQ.0) GO TO 350
0535              PRINT 655
0536          655 FORMAT (62H1JOINT NO.
                 1CREMENT /56H                                          TENSION IN
                 2N       )
0537              PRINT 660
0538          660 FORMAT (94H
                 1    DIRECTION 3          DIRECTION 1          DIRECTION 2
                                    DIRECTION 4       )
0539              DO 665 I=1,NJ
0540              DO 662 J=1,4
0541              T(I,J)=T(I,J)+DT(I,J)
0542          662 DELT(I,J)=DELT(I,J)+DT(I,J)
0543          665 PRINT 670,I,(DELT(I,J),J=1,4)
0544          670 FORMAT (1H0,I5,5X,4(5X,D16.8))
0545              PRINT 675,INC
0546              PRINT 660
0547          675 FORMAT (63H1JOINT NO.                                 FINAL TENSIONS
                 1 IN STEP,I3)
0548              DO 680 I=1,NJ
0549          680 PRINT 670,I,(T(I,J),J=1,4)
0550          685 FORMAT (1H0,8F16.5)
              C
              C  7. CHECK FOR SLACK CABLE SECTIONS AND RECALCULATE IF NECESSARY.
              C     GO TO NEXT LOAD INCREMENT IF NOT FINAL.
              C
0551          710 KX = 1
0552              DO 720 I=1,NJ
0553              DO 720 J=1,4
0554              IF (T(I,J).GE.0.0) GO TO 720
0555              DELT(I,J)=DELT(I,J)-T(I,J)
0556              T(I,J)=0.0
0557              DT(I,J)=0.0
0558              KX = 2
0559          720 CONTINUE
0560              GO TO (726,722),KX
0561          721 PRINT 760
0562          722 DO 723 I=1,NE
0563          723 DIS(I)=DIS(I)-B(I)
0564              DO 724 I=1,NJ
0565              Z(I)=Z(I)-B(3*I)
0566              DO 724 J=1,4
0567              T(I,J)=T(I,J)-DT(I,J)
0568              DL(I,J)=DL(I,J)-DDL(I,J)
0569          724 DELT(I,J)=DELT(I,J)-DT(I,J)
0570              KH=-1
0571          725 NSLK=NSLK+1
0572              PRINT 735
0573              IF (NSLK-5) 390,390,728
0574          726 KU=KU-KDIF
0575              INC=INC+1
0576              NSLK=0
0577              DO 727 I=1,NE
0578          727 BU(I)=BU(I)+BI(I)
0579              TEM2=TEM2+TEM
0580              IF (DABS(TEM2+TEM/2.0).GT.DABS(TEM1)) TEM=0.0
0581              IF (KU) 303,730,303
0582          728 PRINT 755
0583              GO TO 732
```

```
0584          730 CONTINUE
0585          732 LDS=LDS-1
0586          735 FORMAT (//50HOCABLES SLACK, RECALCULATING LAST STEP.
0587              IF (LDS) 740,740,140
0588          740 NDATA=NDATA-1
0589              IF (NDATA) 750,750,120
0590          750 CONTINUE
0591          755 FORMAT (/////49HOINSUFFICIENT PRETENSION, CALCULATIONS TERMINATED
0592          760 FORMAT (//52HOSLACK CABLES BECOMING TAUT, RECALCULATING LAST STEP
0593              STOP
0594              END
```

```
0001          SUBROUTINE ANMX(JT,IC,K1,K3,A,SINT,N,NJ,LON)
              C
              C     CALCULATES MATRIX OF LINEAR TERMS, MATRIX OF NONLINEAR TERMS OR
              C     TENSION INCREMENTS  DEPENDING ON THE VALUE OF LON.
              C
0002          DOUBLE PRECISION F,FL,A,SINT
0003          DOUBLE PRECISION EAT,T,COSG,COSA,COSB,AX,B,BI,BJ,U,BE,EAU
0004          COMMON EAT(61,4),T(61,4),COSG(61,4),COSA(4),COSB(4),F(20),FL(4)
0005          COMMON AX(4,3,3),B(183),BI(3,4),BJ(3),U(61,4),BE(183)
0006          N1 = N-1
0007          IF (LON.NE.2) GO TO 4
0008          FL(1) = F(K1-IC)**2
0009          FL(3) = F(K3+IC)**2
0010          GO TO 5
0011        4 FL(1) = F(K1-IC)
0012          FL(3) = F(K3+IC)
0013          BE(3*JT-2)=0.0
0014          BE(3*JT-1)=0.0
0015          BE(3*JT)=0.0
0016        5 CONTINUE
0017          FL(2) = FL(1)
0018          FL(4) = FL(3)
0019          COSA(1) = -A/F(K1-IC)
0020          COSA(2) =  A/F(K1-IC)
0021          COSA(3) = -A/F(K3+IC)*SINT
0022          COSA(4) =  A/F(K3+IC)*SINT
0023          COSB(1) = -A/F(K1-IC)*SINT
0024          COSB(2) =  A/F(K1-IC)*SINT
0025          COSB(3) = -A/F(K3+IC)
0026          COSB(4) =  A/F(K3+IC)
0027          IF (LON.LT.2) GO TO 38
0028          BJ(1) = B(3*JT-2)
0029          BJ(2) = B(3*JT-1)
0030          BJ(3) = B(3*JT)
0031          IF (JT-N) 6,6,8
0032        6 BI(1,1) = 0.0
0033          BI(2,1) = 0.0
0034          BI(3,1) = 0.0
0035          BI(1,4) = 0.0
0036          BI(2,4) = 0.0
0037          BI(3,4) = 0.0
0038          GO TO 20
0039        8 IF (JT-(K3*(N+N1)+1)) 12,10,12
0040       10 BI(1,1) = 0.0
0041          BI(2,1) = 0.0
0042          BI(3,1) = 0.0
0043          BI(1,3) = 0.0
0044          BI(2,3) = 0.0
0045          BI(3,3) = 0.0
0046          GO TO 15
0047       12 BI(1,1) = B(3*(JT-N)-2)
0048          BI(2,1) = B(3*(JT-N)-1)
0049          BI(3,1) = B(3*(JT-N))
0050       15 IF (JT-(NJ-N)) 20,20,18
0051       18 BI(1,2) =0.0
0052          BI(2,2) =0.0
0053          BI(3,2) =0.0
0054          BI(1,3) = 0.0
```

```
0055                BI(2,3) = 0.0
0056                BI(3,3) = 0.0
0057                GO TO 27
0058             20 IF (IC-N) 23,22,23
0059             22 BI(1,2) = 0.0
0060                BI(2,2) = 0.0
0061                BI(3,2) = 0.0
0062                BI(1,4) = 0.0
0063                BI(2,4) = 0.0
0064                BI(3,4) = 0.0
0065                GO TO 25
0066             23 BI(1,2) = B(3*(JT+N)-2)
0067                BI(2,2) = B(3*(JT+N)-1)
0068                BI(3,2) = B(3*(JT+N))
0069                IF (JT-(K3*(N+N1)+1)) 25,24,25
0070             24 BI(1,1) = 0.0
0071                BI(2,1) = 0.0
0072                BI(3,1) = 0.0
0073                BI(1,3) = 0.0
0074                BI(2,3) = 0.0
0075                BI(3,3) = 0.0
0076                GO TO 30
0077             25 BI(1,3) = B(3*(JT+N1)-2)
0078                BI(2,3) = B(3*(JT+N1)-1)
0079                BI(3,3) = B(3*(JT+N1))
0080             27 IF (IC-N) 30,28,30
0081             28 BI(1,2) = 0.0
0082                BI(2,2) = 0.0
0083                BI(3,2) = 0.0
0084                BI(1,4) = 0.0
0085                BI(2,4) = 0.0
0086                BI(3,4) = 0.0
0087                GO TO 38
0088             30 IF (JT.LE.N) GO TO 38
0089                BI(1,4) = B(3*(JT-N1)-2)
0090                BI(2,4) = B(3*(JT-N1)-1)
0091                BI(3,4) = B(3*(JT-N1))
0092             38 DO 50 I=1,4
0093                IF (LON-2) 40,42,45
0094             40 CONTINUE
0095                EAU=2.0*(EAT(JT,I)-U(JT,I))
0096                AX(I,1,1) = (EAT(JT,I)*COSA(I)**2-EAU     )/FL(I)
0097                AX(I,1,2) = (EAT(JT,I)*COSA(I)*COSB(I)-EAU     *SINT)/FL(I)
0098                AX(I,1,3) =  EAT(JT,I)*COSA(I)*COSG(JT,I)/FL(I)
0099                AX(I,2,1) = (EAT(JT,I)*COSA(I)*COSB(I)-EAU     *SINT)/FL(I)
0100                AX(I,2,2) = (EAT(JT,I)*COSB(I)**2-EAU     )/FL(I)
0101                AX(I,2,3) =  EAT(JT,I)*COSB(I)*COSG(JT,I)/FL(I)
0102                AX(I,3,1) = (EAT(JT,I)*COSA(I)*COSG(JT,I)/FL(I))
0103                AX(I,3,2) =  EAT(JT,I)*COSB(I)*COSG(JT,I)/FL(I)
0104                AX(I,3,3) = (EAT(JT,I)*COSG(JT,I)**2-EAU     )/FL(I)
0105                BE(3*JT-2)=BE(3*JT-2)+(EAU+T(JT,I))*COSA(I)
0106                BE(3*JT-1)=BE(3*JT-1)+(EAU+T(JT,I))*COSB(I)
0107                BE(3*JT)  =BE(3*JT)  +(EAU+T(JT,I))*COSG(JT,I)
0108                GO TO 50
0109             42 CONTINUE
0110                AX(I,1,1) = (BI(1,I)-BJ(1))*(EAT(JT,I)*3.0*COSA(I)
                  1                -2.0*U(JT,I) *COSA(I)**3)/FL(I)
                  2           + (BI(2,I)-BJ(2))*(EAT(JT,I)*(2.0*SINT*COSA(I)+COSB(I))
```

```
     3                -2.0*U(JT,I) *COSA(I)**2*COSB(I))/FL(I)
     4          + (BI(3,I)-BJ(3))*(EAT(JT,I)*COSG(JT,I)
     5                -2.0*U(JT,I)*COSA(I)**2*COSG(JT,I))/FL(I)
0111  AX(I,1,2) = (BI(1,I)-BJ(1))*(EAT(JT,I)*(2.0*SINT*COSA(I)+COSB(I))
     1                -2.0*U(JT,I)*COSA(I)**2*COSB(I))/FL(I)
     2          + (BI(2,I)-BJ(2))*(EAT(JT,I)*(COSA(I)+2.0*COSB(I)*SINT)
     3                -2.0*U(JT,I)*COSA(I)*COSB(I)**2)/FL(I)
     4          + (BI(3,I)-BJ(3))*(EAT(JT,I)*SINT*COSG(JT,I)
     5                -2.0*U(JT,I)*COSA(I)*COSB(I)*COSG(JT,I))/FL(I)
0112  AX(I,1,3) = (BI(1,I)-BJ(1))*(EAT(JT,I)*COSG(JT,I)
     1                -2.0*U(JT,I)*COSA(I)**2*COSG(JT,I))/FL(I)
     2          + (BI(2,I)-BJ(2))*(EAT(JT,I)*SINT*COSG(JT,I)
     3                -2.0*U(JT,I)*COSA(I)*COSB(I)*COSG(JT,I))/FL(I)
     4          + (BI(3,I)-BJ(3))*(EAT(JT,I)*COSA(I)
     5                -2.0*U(JT,I)*COSA(I)*COSG(JT,I)**2)/FL(I)
0113  AX(I,2,1) = (BI(1,I)-BJ(1))*(EAT(JT,I)*(2.0*SINT*COSA(I)+COSB(I))
     1                -2.0*U(JT,I)*COSA(I)**2*COSB(I))/FL(I)
     2          + (BI(2,I)-BJ(2))*(EAT(JT,I)*(COSA(I)+2.0*SINT*COSB(I))
     3                -2.0*U(JT,I)*COSA(I)*COSB(I)**2)/FL(I)
     4          + (BI(3,I)-BJ(3))*(EAT(JT,I)*SINT*COSG(JT,I)
     5                -2.0*U(JT,I)*COSA(I)*COSB(I)*COSG(JT,I))/FL(I)
0114  AX(I,2,2) = (BI(1,I)-BJ(1))*(EAT(JT,I)*(COSA(I)+2.0*SINT*COSB(I))
     1                -2.0*U(JT,I)*COSA(I)*COSB(I)**2)/FL(I)
     2          + (BI(2,I)-BJ(2))*(EAT(JT,I)*3.0*COSB(I)
     3                -2.0*U(JT,I)*COSB(I)**3)/FL(I)
     4          + (BI(3,I)-BJ(3))*(EAT(JT,I)*COSG(JT,I)
     5                -2.0*U(JT,I)*COSB(I)**2*COSG(JT,I))/FL(I)
0115  AX(I,2,3) = (BI(1,I)-BJ(1))*(EAT(JT,I)*SINT*COSG(JT,I)
     1                -2.0*U(JT,I)*COSA(I)*COSB(I)*COSG(JT,I))/FL(I)
     2          +(BI(2,I)-BJ(2))*(EAT(JT,I)*COSG(JT,I)
     3                -2.0*U(JT,I)*COSB(I)**2*COSG(JT,I))/FL(I)
     4          + (BI(3,I)-BJ(3))*(EAT(JT,I)*COSB(I)
     5                -2.0*U(JT,I)*COSB(I)*COSG(JT,I)**2)/FL(I)
0116  AX(I,3,1) = (BI(1,I)-BJ(1))*(EAT(JT,I)*COSG(JT,I)
     1                -2.0*U(JT,I)*COSA(I)**2*COSG(JT,I))/FL(I)
     2          + (BI(2,I)-BJ(2))*(EAT(JT,I)*SINT*COSG(JT,I)
     3                -2.0*U(JT,I)*COSA(I)*COSB(I)*COSG(JT,I))/FL(I)
     4          + (BI(3,I)-BJ(3))*(EAT(JT,I)*COSA(I)
     5                -2.0*U(JT,I)*COSA(I)*COSG(JT,I)**2)/FL(I)
0117  AX(I,3,2) = (BI(1,I)-BJ(1))*(EAT(JT,I)*SINT*COSG(JT,I)
     1                -2.0*U(JT,I)*COSA(I)*COSB(I)*COSG(JT,I))/FL(I)
     2          + (BI(2,I)-BJ(2))*(EAT(JT,I)*COSG(JT,I)
     3                -2.0*U(JT,I)*COSB(I)**2*COSG(JT,I))/FL(I)
     4          + (BI(3,I)-BJ(3))*(EAT(JT,I)*COSB(I)
     5                -2.0*U(JT,I)*COSB(I)*COSG(JT,I)**2)/FL(I)
0118  AX(I,3,3) = (BI(1,I)-BJ(1))*(EAT(JT,I)*COSA(I)
     1                -2.0*U(JT,I)*COSA(I)*COSG(JT,I)**2)/FL(I)
     2          + (BI(2,I)-BJ(2))*(EAT(JT,I)*COSB(I)
     3                -2.0*U(JT,I)*COSB(I)*COSG(JT,I)**2)/FL(I)
     4          + (BI(3,I)-BJ(3))*(EAT(JT,I)*3.0*COSG(JT,I)
     5                -2.0*U(JT,I)*COSG(JT,I)**3)/FL(I)
0119       GO TO 50
0120   45 AX(I,1,1)=((BI(1,I)-BJ(1))*COSA(I)
     1          +(BI(2,I)-BJ(2))*COSB(I)+(BI(3,I)-BJ(3))*COSG(JT,I)
     2         +((BI(1,I)-BJ(1))**2+2.0*(BI(1,I)-BJ(1))*(BI(2,I)-BJ(2))*
     3      SINT +(BI(2,I)-BJ(2))**2+(BI(3,I)-BJ(3))**2)/2.0/FL(I))/FL(I)
0121   50 CONTINUE
0122       RETURN
```

```
0123      END
```

```
C
C ..................................................................
C
C   SUBROUTINE DGELB
C
C   PURPOSE
C      TO SOLVE A SYSTEM OF SIMULTANEOUS LINEAR EQUATIONS WITH A
C      COEFFICIENT MATRIX OF BAND STRUCTURE.
C
C   USAGE
C      CALL DGELB(R,A,M,N,MUD,MLD,EPS,IER)
C
C   DESCRIPTION OF PARAMETERS
C      R      - DOUBLE PRECISION M BY N RIGHT HAND SIDE MATRIX
C               (DESTROYED). ON RETURN R CONTAINS THE SOLUTION
C               OF THE EQUATIONS.
C      A      - DOUBLE PRECISION M BY M COEFFICIENT MATRIX WITH
C               BAND STRUCTURE (DESTROYED).
C      M      - THE NUMBER OF EQUATIONS IN THE SYSTEM.
C      N      - THE NUMBER OF RIGHT HAND SIDE VECTORS.
C      MUD    - THE NUMBER OF UPPER CODIAGONALS (THAT MEANS
C               CODIAGONALS ABOVE MAIN DIAGONAL).
C      MLD    - THE NUMBER OF LOWER CODIAGONALS (THAT MEANS
C               CODIAGONALS BELOW MAIN DIAGONAL).
C      EPS    - SINGLE PRECISION INPUT CONSTANT WHICH IS USED AS
C               RELATIVE TOLERANCE FOR TEST ON LOSS OF
C               SIGNIFICANCE.
C      IER    - RESULTING ERROR PARAMETER CODED AS FOLLOWS
C               IER=0  - NO ERROR,
C               IER=-1 - NO RESULT BECAUSE OF WRONG INPUT PARAME-
C                        TERS M,MUD,MLD OR BECAUSE OF PIVOT ELEMENT
C                        AT ANY ELIMINATION STEP EQUAL TO 0,
C               IER=K  - WARNING DUE TO POSSIBLE LOSS OF SIGNIFI-
C                        CANCE INDICATED AT ELIMINATION STEP K+1,
C                        WHERE PIVOT ELEMENT WAS LESS THAN OR
C                        EQUAL TO THE INTERNAL TOLERANCE EPS TIMES
C                        ABSOLUTELY GREATEST ELEMENT OF MATRIX A.
C
C   REMARKS
C      BAND MATRIX A IS ASSUMED TO BE STORED ROWWISE IN THE FIRST
C      ME SUCCESSIVE STORAGE LOCATIONS OF TOTALLY NEEDED MA
C      STORAGE LOCATIONS, WHERE
C        MA=M*MC-ML*(ML+1)/2    AND    ME=MA-MU*(MU+1)/2    WITH
C        MC=MIN(M,1+MUD+MLD),  ML=MC-1-MLD,  MU=MC-1-MUD.
C      RIGHT HAND SIDE MATRIX R IS ASSUMED TO BE STORED COLUMNWISE
C      IN N*M SUCCESSIVE STORAGE LOCATIONS. ON RETURN SOLUTION
C      MATRIX R IS STORED COLUMNWISE TOO.
C      INPUT PARAMETERS M, MUD, MLD SHOULD SATISFY THE FOLLOWING
C      RESTRICTIONS      MUD NOT LESS THAN ZERO
C                        MLD NOT LESS THAN ZERO
C                        MUD+MLD NOT GREATER THAN 2*M-2.
C      NO ACTION BESIDES ERROR MESSAGE IER=-1 TAKES PLACE IF THESE
C      RESTRICTIONS ARE NOT SATISFIED.
C      THE PROCEDURE GIVES RESULTS IF THE RESTRICTIONS ON INPUT
C      PARAMETERS ARE SATISFIED AND IF PIVOT ELEMENTS AT ALL
C      ELIMINATION STEPS ARE DIFFERENT FROM 0. HOWEVER WARNING
C      IER=K - IF GIVEN - INDICATES POSSIBLE LOSS OF SIGNIFICANCE.
C      IN CASE OF A WELL SCALED MATRIX A AND APPROPRIATE TOLERANCE
```

```
C           EPS, IER=K MAY BE INTERPRETED THAT MATRIX A HAS THE RANK K.
C           NO WARNING IS GIVEN IF MATRIX A HAS NO LOWER CODIAGONAL.
C
C       SUBROUTINES AND FUNCTION SUBPROGRAMS REQUIRED
C           NONE
C
C       METHOD
C           SOLUTION IS DONE BY MEANS OF GAUSS ELIMINATION WITH
C           COLUMN PIVOTING ONLY, IN ORDER TO PRESERVE BAND STRUCTURE
C           IN REMAINING COEFFICIENT MATRICES.
C
C     ******************************************************************
0001        SUBROUTINE DGELB(R,A,M,N,MUD,MLD,EPS,IER)
C
0002        DIMENSION R(1),A(1)
0003        DOUBLE PRECISION R,A,PIV,TB,TOL
C
C       TEST ON WRONG INPUT PARAMETERS
0004        IF(MLD)47,1,1
0005      1 IF(MUD)47,2,2
0006      2 MC=1+MLD+MUD
0007        IF(MC+1-M-M)3,3,47
C
C       PREPARE INTEGER PARAMETERS
C           MC=NUMBER OF COLUMNS IN MATRIX A
C           MU=NUMBER OF ZEROS TO BE INSERTED IN FIRST ROW OF MATRIX A
C           ML=NUMBER OF MISSING ELEMENTS IN LAST ROW OF MATRIX A
C           MR=INDEX OF LAST ROW IN MATRIX A WITH MC ELEMENTS
C           MZ=TOTAL NUMBER OF ZEROS TO BE INSERTED IN MATRIX A
C           MA=TOTAL NUMBER OF STORAGE LOCATIONS NECESSARY FOR MATRIX A
C           NM=NUMBER OF ELEMENTS IN MATRIX R
0008      3 IF(MC-M)5,5,4
0009      4 MC=M
0010      5 MU=MC-MUD-1
0011        ML=MC-MLD-1
0012        MR=M-ML
0013        MZ=(MU*(MU+1))/2
0014        MA=M*MC-(ML*(ML+1))/2
0015        NM=N*M
C
C       MOVE ELEMENTS BACKWARD AND SEARCH FOR ABSOLUTELY GREATEST ELEMENT
C       (NOT NECESSARY IN CASE OF A MATRIX WITHOUT LOWER CODIAGONALS)
0016        IER=0
0017        PIV=0.D0
0018        IF(MLD)14,14,6
0019      6 JJ=MA
0020        J=MA-MZ
0021        KST=J
0022        DO 9 K=1,KST
0023        TB=A(J)
0024        A(JJ)=TB
0025        TB=DABS(TB)
0026        IF(TB-PIV)8,8,7
0027      7 PIV=TB
0028      8 J=J-1
0029      9 JJ=JJ-1
```

```
      C
      C     INSERT ZEROS IN FIRST MU ROWS (NOT NECESSARY IN CASE MZ=0)
0030          IF(MZ)14,14,10
0031       10 JJ=1
0032          J=1+MZ
0033          IC=1+MUD
0034          DO 13 I=1,MU
0035          DO 12 K=1,MC
0036          A(JJ)=0.D0
0037          IF(K-IC)11,11,12
0038       11 A(JJ)=A(J)
0039          J=J+1
0040       12 JJ=JJ+1
0041       13 IC=IC+1
      C
      C     GENERATE TEST VALUE FOR SINGULARITY
0042       14 TOL=EPS*PIV
      C
      C
      C     START DECOMPOSITION LOOP
0043          KST=1
0044          IDST=MC
0045          IC=MC-1
0046          DO 38 K=1,M
0047          IF(K-MR-1)16,16,15
0048       15 IDST=IDST-1
0049       16 ID=IDST
0050          ILR=K+MLD
0051          IF(ILR-M)18,18,17
0052       17 ILR=M
0053       18 II=KST
      C
      C     PIVOT SEARCH IN FIRST COLUMN (ROW INDEXES FROM I=K UP TO I=ILR)
0054          PIV=0.D0
0055          DO 22 I=K,ILR
0056          TB=DABS(A(II))
0057          IF(TB-PIV)20,20,19
0058       19 PIV=TB
0059          J=I
0060          JJ=II
0061       20 IF(I-MR)22,22,21
0062       21 ID=ID-1
0063       22 II=II+ID
      C
      C     TEST ON SINGULARITY
0064          IF(PIV)47,47,23
0065       23 IF(IER)26,24,26
0066       24 IF(PIV-TOL)25,25,26
0067       25 IER=K-1
0068       26 PIV=1.D0/A(JJ)
      C
      C     PIVOT ROW REDUCTION AND ROW INTERCHANGE IN RIGHT HAND SIDE R
0069          ID=J-K
0070          DO 27 I=K,NM,M
0071          II=I+ID
0072          TB=PIV*R(II)
0073          R(II)=R(I)
0074       27 R(I)=TB
```

```
      C
      C     PIVOT ROW REDUCTION AND ROW INTERCHANGE IN COEFFICIENT MATRIX A
0075        II=KST
0076        J=JJ+IC
0077        DO 28 I=JJ,J
0078        TB=PIV*A(I)
0079        A(I)=A(II)
0080        A(II)=TB
0081     28 II=II+1
      C
      C     ELEMENT REDUCTION
0082        IF(K-ILR)29,34,34
0083     29 ID=KST
0084        II=K+1
0085        MU=KST+1
0086        MZ=KST+IC
0087        DO 33 I=II,ILR
      C
      C     IN MATRIX A
0088        ID=ID+MC
0089        JJ=I-MR-1
0090        IF(JJ)31,31,30
0091     30 ID=ID-JJ
0092     31 PIV=-A(ID)
0093        J=ID+1
0094        DO 32 JJ=MU,MZ
0095        A(J-1)=A(J)+PIV*A(JJ)
0096     32 J=J+1
0097        A(J-1)=0.DO
      C
      C     IN MATRIX R
0098        J=K
0099        DO 33 JJ=I,NM,M
0100        R(JJ)=R(JJ)+PIV*R(J)
0101     33 J=J+M
0102     34 KST=KST+MC
0103        IF(ILR-MR)36,35,35
0104     35 IC=IC-1
0105     36 ID=K-MR
0106        IF(ID)38,38,37
0107     37 KST=KST-ID
0108     38 CONTINUE
      C     END OF DECOMPOSITION LOOP
      C
      C
      C     BACK SUBSTITUTION
0109        IF(MC-1)46,46,39
0110     39 IC=2
0111        KST=MA+ML-MC+2
0112        II=M
0113        DO 45 I=2,M
0114        KST=KST-MC
0115        II=II-1
0116        J=II-MR
0117        IF(J)41,41,40
0118     40 KST=KST+J
0119     41 DO 43 J=II,NM,M
0120        TB=R(J)
```

```
0121                MZ=KST+IC-2
0122                ID=J
0123                DO 42 JJ=KST,MZ
0124                ID=ID+1
0125             42 TB=TB-A(JJ)*R(ID)
0126             43 R(J)=TB
0127                IF(IC-MC)44,45,45
0128             44 IC=IC+1
0129             45 CONTINUE
0130             46 RETURN
                 C
                 C
                 C     ERROR RETURN
0131             47 IER=-1
0132                RETURN
0133                END
```

APPENDIX D. SAMPLE COMPUTER OUTPUT OF RESULTS

```
INPUT DATA

TYPE OF ROOF:- 2

HXI=   50.0     HETA=   50.0          STEEL AREA(XI)=  1.25000     STEEL AREA(ETA)=  1.25000

RF HT.=  12.0     RF WIDTH= 120.0     RF LTH= 240.0     SIN(THETA)=0.0          ELAS. MOD.=   24000.0     THERM COEFF.= 0.6960-05

PROP. LIMIT=    124.92     YIELD STRESS=    155.00     YIELD STRAIN=0.00846     ULT. STRESS=    250.00     ULT. STRAIN=0.0450

LOAD (NO. OF ADDITIONAL CONC. LOADS= 0     NO. OF LOADS TO BE ADDED SUBSEQUENTLY= 01          TEMP. CHANGE=   .0

  0.0   0.0   1.00   0.0   0.0   1.00   0.0   0.0   1.00   0.0   0.0   1.00   0.0   0.0   1.00   0.0   0.0   1.00
  0.0   0.0   1.00   0.0   0.0   1.00   0.0   0.0   1.00   0.0   0.0   1.00   0.0   0.0   1.00   0.0   0.0   1.00
  0.0   0.0   1.00   0.0   0.0   1.00   0.0   0.0   1.00   0.0   0.0   1.00   0.0   0.0   1.00   0.0   0.0   1.00
  0.0   0.0   1.00   0.0   0.0   1.00   0.0   0.0   1.00   0.0   0.0   1.00   0.0   0.0   1.00   0.0   0.0   1.00
  0.0   0.0   1.00   0.0   0.0   1.00   0.0   0.0   1.00   0.0   0.0   1.00

INCREMENT SIZES= LOAD/ 1 AND LOAD/ 1

INITIAL CONFIGURATION

ORDINATES

 0.333234640 01  0.598519620 01  0.846039970 01  0.846039970 01  0.598519620 01  0.333234640 01  0.532938560 01  0.661139900 01
 0.723619990 01  0.661139900 01  0.532938560 01  0.600000000 01  0.600000000 01  0.600000000 01  0.600000000 01  0.600000000 01
 0.600000000 01  0.667061440 01  0.538860100 01  0.476980010 01  0.538860100 01  0.667061440 01  0.866765360 01  0.601480380 01
 0.353960030 01  0.353960030 01  0.601480380 01  0.866765360 01

A=    28.28427125

SECTION LENGTHS...

 28.29477794     28.32629802     28.37855213     28.29474690     28.29474690     28.37855213     28.32629802     28.29477794
```

DISPLACEMENTS IN STEP 1

JOINT NO	XI DISPL	ETA DISPL	Z DISPL
1	0.49228141D-03	0.12216384D-05	-0.97224822D-01
2	0.11884278D-01	0.92832812D-02	-0.21893537D 00
3	0.83870352D-02	0.30961042D-01	-0.32601907D 00
4	-0.30961042D-01	-0.83870352D-02	-0.32601907D 00
5	-0.92832812D-02	-0.11884278D-01	-0.21893537D 00
6	-0.12216384D-05	-0.49228141D-03	-0.97224822D-01
7	-0.26507473D-02	0.19081422D-02	-0.20862161D 00
8	0.12930439D-01	0.25157242D-01	-0.41192247D 00
9	-0.83127964D-03	0.83127964D-03	-0.61819956D 00
10	-0.25157242D-01	-0.12930439D-01	-0.41192247D 00
11	-0.19081422D-02	0.26507473D-02	-0.20862161D 00
12	0.35178675D-02	-0.37852774D-02	-0.14959192D 00
13	-0.11313058D-01	0.11632435D-01	-0.30704492D 00
14	0.44036512D-02	-0.29923877D-02	-0.64578705D 00
15	0.29923877D-02	-0.44036512D-02	-0.64578705D 00
16	-0.11632435D-01	0.11313058D-01	-0.30704492D 00
17	0.37852774D-02	-0.35178675D-02	-0.14959192D 00
18	-0.16846069D-02	0.25902354D-02	-0.21296443D 00
19	-0.25209993D-01	-0.11851624D-01	-0.43282264D 00
20	0.14978543D-02	-0.14978543D-02	-0.65656965D 00
21	0.11851624D-01	0.25209993D-01	-0.43282264D 00
22	-0.25902354D-02	0.16846069D-02	-0.21296443D 00
23	-0.17304179D-05	-0.76457785D-03	-0.10190826D 00
24	-0.86303808D-02	-0.11661786D-01	-0.22693668D 00
25	-0.31405228D-01	-0.10479392D-01	-0.35810619D 00
26	0.10479392D-01	0.31405228D-01	-0.35810619D 00
27	0.11661786D-01	0.86303808D-02	-0.22693668D 00
28	0.76457785D-03	0.17304179D-05	-0.10190826D 00

JOINT NO.	TENSION INCREMENT IN DIRECTION 1	DIRECTION 2	DIRECTION 3	DIRECTION 4
1	-0.113741650 02	-0.113672410 02	0.261081650 01	0.260822700 01
2	-0.276836430 01	-0.271713490 01	0.755338310 01	0.757575910 01
3	0.527537070 01	0.531686800 01	0.121703010 02	0.120646330 02
4	0.120646330 02	0.121703010 02	0.531686800 01	0.527537070 01
5	0.757575910 01	0.755338310 01	-0.271713490 01	-0.276836430 01
6	0.260822700 01	0.261081650 01	-0.113672410 02	-0.113741650 02
7	-0.113672410 02	-0.114019670 02	0.756741480 01	0.755338310 01
8	-0.271713490 01	-0.263844030 01	0.120806630 02	0.121703010 02
9	0.531686800 01	0.533939370 01	0.533939370 01	0.531686800 01
10	0.121703010 02	0.120806630 02	-0.263844030 01	-0.271713490 01
11	0.755338310 01	0.756741480 01	-0.114019670 02	-0.113672410 02
12	-0.704709100 01	-0.701432050 01	0.760197660 01	0.756741480 01
13	-0.114019670 02	-0.114689870 02	0.120454340 02	0.120806630 02
14	-0.263844030 01	-0.258034310 01	0.537822070 01	0.533939370 01
15	0.533939370 01	0.537822070 01	-0.258034310 01	-0.263844030 01
16	0.120806630 02	0.120454340 02	-0.114689870 02	-0.114019670 02
17	0.756741480 01	0.760197660 01	-0.701432050 01	-0.704709100 01
18	-0.701432050 01	-0.699431350 01	0.120264060 02	0.120454340 02
19	-0.114689870 02	-0.115690090 02	0.542931190 01	0.537822070 01
20	-0.258034310 01	-0.254854700 01	-0.254854700 01	-0.258034310 01
21	0.537822070 01	0.542931190 01	-0.115690090 02	-0.114689870 02
22	0.120454340 02	0.120264060 02	-0.699431350 01	-0.701432050 01
23	-0.235682690 01	-0.235315890 01	0.120381510 02	0.120264060 02
24	-0.699431350 01	-0.700193280 01	0.549058470 01	0.542931190 01
25	-0.115690090 02	-0.117196410 02	-0.250546470 01	-0.254854700 01
26	-0.254854700 01	-0.250546470 01	-0.117196410 02	-0.115690090 02
27	0.542931190 01	0.549058470 01	-0.700193280 01	-0.699431350 01
28	0.120264060 02	0.120381510 02	-0.235315890 01	-0.235682690 01

JOINT NO. 1

FINAL TENSIONS IN STEP 1

	DIRECTION 1	DIRECTION 2	DIRECTION 3	DIRECTION 4
1	0.387741560 02	0.387570240 02	0.526247420 02	0.526221520 02
2	0.473351570 02	0.472951150 02	0.575667890 02	0.577027220 02
3	0.552819910 02	0.553641940 02	0.622767690 02	0.627581470 02
4	0.627581570 02	0.622767690 02	0.553641940 02	0.552819910 02
5	0.577027220 02	0.575667890 02	0.472951150 02	0.473351570 02
6	0.526221520 02	0.526247420 02	0.387570240 02	0.387741560 02
7	0.387570240 02	0.386119990 02	0.575814330 02	0.575667890 02
8	0.472951150 02	0.473732370 02	0.620922710 02	0.622767690 02
9	0.553641940 02	0.553867190 02	0.553867190 02	0.553641940 02
10	0.622767690 02	0.620922710 02	0.473732370 02	0.472951150 02
11	0.575667890 02	0.575814330 02	0.386119990 02	0.387570240 02
12	0.430780060 02	0.429996980 02	0.577270740 02	0.575814330 02
13	0.386119990 02	0.385426210 02	0.620594010 02	0.620922710 02
14	0.473732370 02	0.474669820 02	0.553898980 02	0.553867190 02
15	0.553867190 02	0.553898980 02	0.474669820 02	0.473732370 02
16	0.620922710 02	0.620594010 02	0.385426210 02	0.386119990 02
17	0.575814330 02	0.577270740 02	0.429996980 02	0.430780060 02
18	0.429996980 02	0.430190920 02	0.621506720 02	0.620594010 02
19	0.385426210 02	0.385374590 02	0.554415610 02	0.553898980 02
20	0.474669820 02	0.474987790 02	0.474987790 02	0.474669820 02
21	0.553898980 02	0.554415610 02	0.385374590 02	0.385426210 02
22	0.620594010 02	0.621506720 02	0.430190920 02	0.429996980 02
23	0.476570990 02	0.476607670 02	0.623864720 02	0.621506720 02
24	0.430190920 02	0.431250300 02	0.556141060 02	0.554415610 02
25	0.385374590 02	0.386738830 02	0.475011560 02	0.474987790 02
26	0.474987790 02	0.475011560 02	0.386738830 02	0.385374590 02
27	0.554415610 02	0.556141060 02	0.431250300 02	0.430190920 02
28	0.621506720 02	0.623864720 02	0.476607670 02	0.476570990 02

REFERENCES

1. AISI. Tentative Criteria for Structural Applications of Steel Cables for Buildings. New York. 1966.

2. AISI. Steel Cable in Building Design.Structural Metal - Cable. New York. 1967.

3. AISI. Design Imagination: Steel Cable. Structural Metal - Cable. New York. 1968.

4. AISI. Bibliography: Structural Applications of Steel Cable Systems. Structural Metal - Cable. New York. 1969.

5. AISI. Designer's Handbook: Steel Wire. New York. 1969.

6. AISI. "New Approach to Roofs in Tension," Architectural Record, Sept. 1956, 211-216.

7. Avent, R. R. "Nonlinear Field Analysis of Structural Nets," ASCE Proceedings, Journal of Structural Division, ST5, May 1969, 889-907.

8. Baron, F. and Venkatesan, M. S. "Nonlinear Analysis of Cable and Truss Structures," ASCE Proceedings, Journal of Structural Division, 97, ST2, Feb. 1971, 679-710.

9. Bathish, G. N. Membrane Analysis of Cable Roofs. Ph.D. Dissertation submitted to the Graduate School of Arts and Sciences of the University of Pennsylvania. 1966.

10. Bethlehem Steel. Excerpts from 'Hanging Roofs', Proceedings of the IASS Colloquium on Hanging Roofs, Continuous Metallic Shell Roofs and Superficial Lattice Roofs. Bethlehem, Pa. 1962.

11. Bethlehem Steel. Cable Roof Structures. Structural Metal - Roofs. Bethlehem, Pa. 1968.

12. Bethlehem Steel. Specifications and Standards - Bethlehem Wire Rope Booklet 1902-A. Bethlehem, Pa.

13. Birnstiel, C. et al. "Cable Suspended Roof Construction State-of-the-Art," ASCE Proceedings, Journal of Structural Division, 97, ST6, June 1971, 1715-1701.

14. Brebbia, C. and Connor, J. "Geometrically Nonlinear Finite-Element Analysis," ASCE Proceedings, Journal of Engineering Mechanics Division, EM2, April 1969, 463-483.

15. British Construction Steelwork Association Ltd. Suspended Structures. London: BCSA.

16. Buchanan, G. R. and Akin, J. E. The Deflection Analysis of Structural Nets Using the Reflection Method. International Conference on Space Structures, 1966. Paper N4, Dept. of Civil Engineering, University of Surrey, England, 9pp.

17. Buchanan, G. R. "Two-dimensional Cable Analysis," ASCE Proceedings, Journal of Structural Division, ST7, July 1970, 1581-1587.

18. Buchholdt, H. A. The Behaviour of Small Prestressed Cable Roofs Subjected to Uniformly Distributed Loading. International Conference on Space Structures, 1966. Paper N3, Dept. of Civil Engineering, University of Surrey, England, 9pp.

19. Buchholdt, H. A. Deformation of Prestressed Cable Nets. Acta Polytechnica Scandinavica, Civil Engineering and Building Construction Series No. 38, Trondheim, 1966, 16pp.

20. Buchholdt, H. A. "A Nonlinear Deformation Theory Applied to Two-Dimensional Pretensioned Cable Assemblies," Proceedings of the Institution of Civil Engineers, Paper 7153, v 42, Jan. 1969, 129-141.

21. Buchholdt, H. A. "Pretensioned Cable Girders," Proceedings of the Institution of Civil Engineers, Paper 453-469.

22. CISC. Case Histories No.12. Cable Supported Steel Cantilevers. CISC Publication No. 1517. April 1969.

23. Day, A. S. and Bunce, J. "Analysis of Cable Network by Dynamic Relaxation," Civil Engineering and Public Works Review, Apr. 1970, 383-386.

24. Dean, D. L. and Ugarte, C. P. "Analysis of Structural Nets," International Association for Bridge and Structural Engineering - Publications, 1963, 71-90.

25. Engineering News-Record. Ice Rink's Wood Roof Hangs on Cables. Oct. 26, 1967, 26-28.

26. Esquillan, N. and Saillard, Y. eds. Hanging Roofs, Proceedings of the IASS Colloquium on Hanging

Roofs, Continuous Metallic Shell Roofs and Superficial Lattice Roofs, Paris 9-11, July 1962. Amsterdam: North-Holland Publishing Company. 1963.

27. Fisher Jr., F. Design of Cable Roof for Madison Square Garden. Preprint. ASCE Environmental Engineering Conference, Dallas, Texas, Feb. 6-9, 1967. Conference Preprint 425, 18p.

28. Gero, J. S., Ding, G. D. and Cowan, H. J. Research in Space Structures. International Conference on Space Structures, 1966, Dept. of Civil Engineering, University of Surrey, England. 11p.

29. Gero, J. S. "The Analysis of Cable Networks Using an Iteration Technique," Architectural Science Review, Mar. 1967.

30. Goldberg, J. E. and Richard, R. M. "Analysis of Nonlinear Structures," ASCE Proceedings, Journal of Structural Division, ST4, Aug. 1963, 333-351.

31. Greenberg, D. P. "Inelastic Analysis of Suspension Roof Structures," ASCE Proceedings, Journal of Structural Division, ST5, May 1970, 905-931.

32. Greenberg, D. P. Suspension Roof Structures: Their Elastic and Inelastic Behaviour and Their Ultimate Load Capacities. Ph. D. Thesis Submitted to the Graduate School of Cornell University, Jan. 1968.

33. Grigorian, M. "Free Vibrations of Supported Cable Nets," Proceedings of the Institution of Civil Engineers Paper 7257, Synopsis p 279.

34. Hartree, D. R. Numerical Analysis. London: Oxford University Press, 1958.

35. Howard, S. "Prestressing Prevents Flutter of Cable Roofs," Architectural Record, Aug. 1959, 178-182.

36. Howard, S. "Suspension Structures," Architectural Record, Sept. 1960, v 128, 230-237.

37. Hunt, H. W. "Engineered Structures at Expo '67", Civil Engineering, Mar. 1967, 40-51.

38. Jawerth, O. D. and Schulz, H. "Ein Beitrag zur Frage der eigenschwingungen, windanfachenden Krafte und aerodynamischen stabilitat bei hangenden Dacheru," der Stahlbau, Jan. 1966, 1-8.

39. Jawerth, O. D. and Schulz, H. "Die Dachkonsfruction der Sporthalle 'Victor Hugo' in Bordeaux," der Stahlbau,

40. Jennings, A. "The Free Cable," Engineer, London, v 214, No. 5579, 1111-1112.

41. Jonatowski, J. J. and Birnstiel, C. "Inelatic Stiffened Suspension Space Structures," ASCE Proceedings, Journal of Structural Division, v 96, ST6, June 1970, 1143-1166.

42. Krishna, P. Analysis of Funicular Suspension Systems. Ph. D. Thesis submitted to the University of London, 1964.

43. Krishna, P. and Agarwal, T. P. "Study of Suspended Roof Model," ASCE Proceedings, Journal of Structural Division, v 97, ST6, June 1971, 1671-1684.

44. Krishna, P. and Kohli, A. K. "Design of a Doubly Curved Suspended Cable Roof with Prestressed Concrete Beams," Indian Concrete Journal , Nov. 1968, 461- 472.

45. Krishna, P. and Natarajan, P. R. "Analysis of Doubly Curved Suspended Cable Roof Networks," International Association for Shell Structures, Bul. No. 34, June 1968, 49-67.

46. Krishna, P. and Sparks, S. R. "Analysis of Pretensioned Cable Systems," (with discussion), Proceedings of Institution of Civil Engineers, Jan. 1968, 103-109.

47. Krishna, P. and Sparkes, S. R. "An Influence Coefficient Method for Pretensioned Cable Systems," Proceedings of the Institution of Civil Engineers, Nov. 1968, 543-548.

48. Kumanan, T. Analysis of Non-orthogonal Cable Roofs, M.A.Sc. Thesis presented to the Faculty of Graduate Studies, University of Windsor, 1969.

49. Langewiesche, W. " 'Bubbles'- Newest Thing in Building," Reader's Digest, v 99, No. 592, August 1971, 49-53.

50. Michalos, J. and Birnstiel, C. "Movements of a Cable due to Changes in Loading," ASCE Transactions, v 127, 1962, Part II, 267-303.

51. Middleton, G. W. and Fead, J. W. N. Fundamental Cable Analysis.

52. Mollman, H. "Analysis of Plane Prestresses Cable Structures," ASCE Proceedings, Journal of Structural Division, ST10, Oct. 1970, 2059-2083.

53. Normandin, M. "Quelques Notes Cocernant les Cables, les Arcs et les reseaux d'arcs," Transactions of

EIC , No. A-8, Nov. 1964, Paper No. EIC-G4-ER and STR8.

54. O'Brien, T. "General Solution of Suspended Cable Problems," ASCE Proceedings, Journal of Structural Division, No. ST1, Feb. 1967, 1-26.

55. O'Brien, T. "Behaviour of Loaded Cable Systems," ASCE Proceedings, Journal of Structural Division, ST10, Oct. 1968, 2281-2303.

56. O'Brien, T. and Francis, A. J. "Cable Movements under Two-Dimensional Loads," ASCE Proceedings, Journal of Structural Division, ST3, June 1964, 89-123.

57. Poskitt, T. J. "The Application of Elastic Catenary Functions to the Analysis of Suspended Cable Structures," The Structural Engineer, v 41, n 5, May 1963, 167-170.

58. Poskitt, T. J. "Numerical Solution of Nonlinear Structures," ASCE Proceedings, Journal of Structural Division, ST4, Aug. 1967, 69-94. Discussion, June 1968, 1613-1627, Jan. 1969, 89-91.

59 Saafan, A. S. "Theoretical Analysis of Suspension Roofs," ASCE Proceedings, Journal of Structural Division, ST2, Feb. 1970, 393-405.

60. Saini, I. C. Behaviour and Analysis of Doubly Curved Suspended Cable Networks, Paper presented to the Dept. of Civil Engineering, University of Roorkee, Roorkee, India, Oct. 1967.

61. Schmidt, V. R. and Kammenhuber, J. "Unsymmetrisches Hangedach in Biel, Gestutzt in nur vierrnoten," Schweizerische Banzeitung, June 1967, 410-412.

62. Scott, J. L., Omally, K. K. and Gulley, H. G. "Suspended Catenary Cable Roof of Oklahoma State Fair Arena," Journal of American Concrete Institute, 1st April, 1965, 385-402.

63. Seely, F. B. and Smith, J. O. Advanced Mechanics of Materials, 2nd Ed. New York, John Wiley. 1957.

64. Shaw, F. S. "Some Notes on Cable Suspension Roof Structures," Journal of the Institution of Engineers, Australia, Apr.-May, 1964, 105-113.

65. Siev, A. Stability of Prestressed Suspended Roofs, D.Sc. Thesis presented to the Technion Institute of Technology, Israel, May 1961. Abstract.

66. Siev, A. Analysis of Prestressed Suspended Roofs by Means of an Electronic Computer. Paper No. 23. 23.1-23.11.

67. Siev, A. "A General Analysis of Prestressed Nets," International Association for Bridge and Structural Engineering-Publications, 1963, 283-292.

68. Siev, A. "Geometry of Suspended Cloth Roofs," ASCE Proceedings, Journal of Structural Division, ST6, Dec. 1965, 251-263.

69. Siev, A. "Experimental Study of Flutter in Suspended Roofs," International Association for Shell Structures Bul. No. 23. 3-10, Sept. 1965.

70. Siev, A. "Prestressed Suspended Roofs Bounded by Main Cables," International Association for Bridge and Structural Engineering Publications, v 27, 1967, 171-185.

71. Siev, A. and Eidelman, J. Shapes of Suspended Roofs in Hanging Roofs, ed. Esquillan, N. and Saillard, Y. Amsterdam: North-Holland Publishing Company, 1963.

72. Siev, A. and Eidelman, J. "Stress Analysis of Prestressed Suspended Roofs," ASCE Proceedings, Journal of Structural Division, ST4, Aug. 1964. 103-121.

73. Soler, A. I. and Afshari, H. "On Analysis of Cable Network Vibrations using Galerkin's Method," ASME Transactions, Sept. 1970, 606-611.

74. Spunt, Leonard. "Optimization of Redundant Prestressed Structures," ASCE Proceedings, Journal of Structural Division, ST12, Dec. 1970, 2589-2606.

75. Sterner, J. A. "Madison Square Garden: Fabrication and Erection of Cable Supported Roof," Civil Engineering -ASCE, October 1967, 43-47.

76. Thornton, C. H. Analysis of Three-dimensional Suspension Structures. Ph.D. thesis submitted to the School of Engineering and Science, New York Univeristy, Feb. 1966.

77. Thornton, C. H. and Birnstiel, C. "Three-dimensional Suspension Structures," ASCE Proceedings, Journal of Structural Division, ST2, Apr. 1967, 247-270.

78. Tottenham, H. and Williams, P. G. "Cable Net: Continuous System Analysis," ASCE Proceedings, Journal of Engineering Mechanics Division, EM3, June 1970, 277-293.

79. Tsuboi, Y. and Kawamata, S. The Design and Construction of a Suspension Structure. International Conference on Space Structures, 1966, Dept. of Civil Engineering, University of Surrey, England, Paper P7, 9p.

80 Tsuboi, Y. and Kawaguchi, M. Design Problems of Suspension Roof Structure- Tokyo Olympic Swimming Pools. International Association for Shell Structures.

81. Tsuboi, Y. and Kawaguchi, M. Suspension Structure for the Tokyo Olympics. Proceedings of the Symposium on the High Rise and Long Span Structures. Japan Society for the Promotion of Science. Sept. 1964, 76-83.

82. Tung, D. H. H. and Kudder, R. J. "Analysis of Cables as Equivalent Two Force Members," AISC Engineering Journal, Jan. 1968, 12-19.

83. United States Steel. Suspended Structures - Concepts. Publication ADUSS 55-1898. Oct. 1966, Pittsburgh, Pa.

84. United States Steel. Tiger Brand Wire Rope Engineering Handbook. Publication ADUSS 55-1542-01, Oct. 1968, Pittsburgh, Pa.

85. United States Steel. Steel Design Manual. Publication ADUSS 27-3400-02, Nov. 1968, Pittsburgh, Pa.

86. White, R. N. "Optimum Solution Technique for Finite Difference Equations," ASCE Proceedings, Journal of Structural Division, v 89, ST8, Aug. 1963, 115-136.

87. Zerna, W. "On the Design of Prestressed Suspension Roofs," Architectural Science Review, July 1959, 97-100.

88. Zetlin, L. "Steel Cable Creates Novel Structural Space Systems," AISC Engineering Journal, Jan. 1964, 1-11.

89. Zetlin, L. Elimination of Flutter in Suspension Roofs, in Hanging Roofs, ed. Esquillan, N. and Saillard, Y. Amsterdam: North-Holland Publishing Company. 1963.

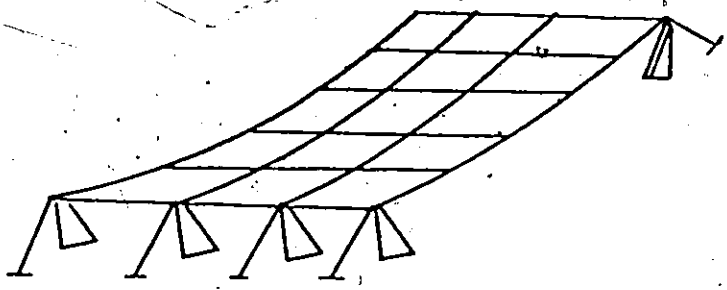

(a) SINGLE CURVATURE ROOF

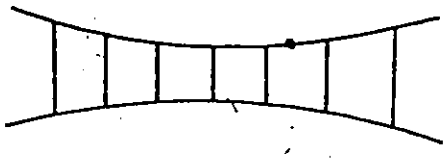

(b) CABLE TRUSS WITH TIES

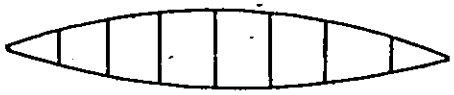

(c) CABLE TRUSS WITH STRUTS

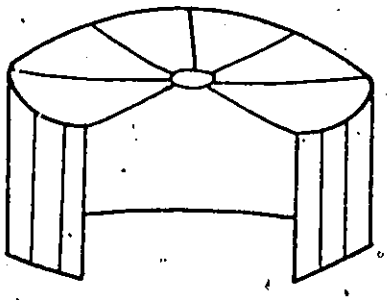

(d) CIRCULAR ROOF WITH SINGLE SET OF CABLES

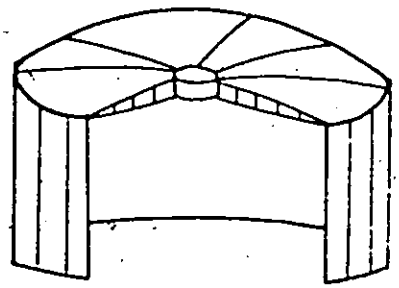

(e) CIRCULAR ROOF WITH CABLE TRUSSES

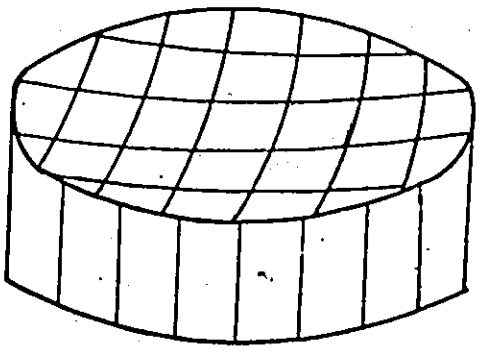

(f) POSITIVE CURVATURE NETWORK

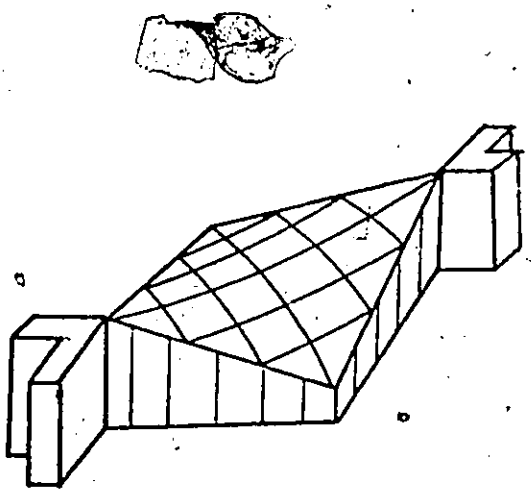

(g) NEGATIVE CURVATURE NETWORK

Fig. (1-1)

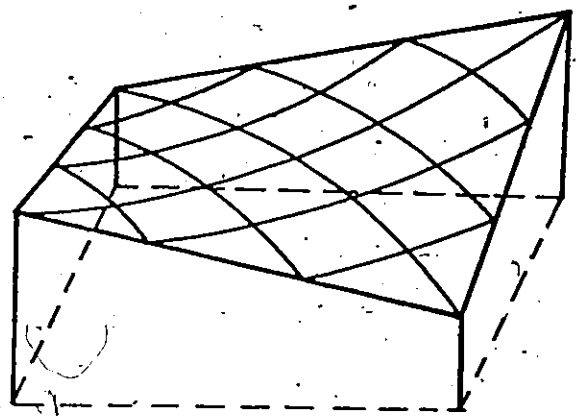

Fig. (1-2a) SINGLE ROOF

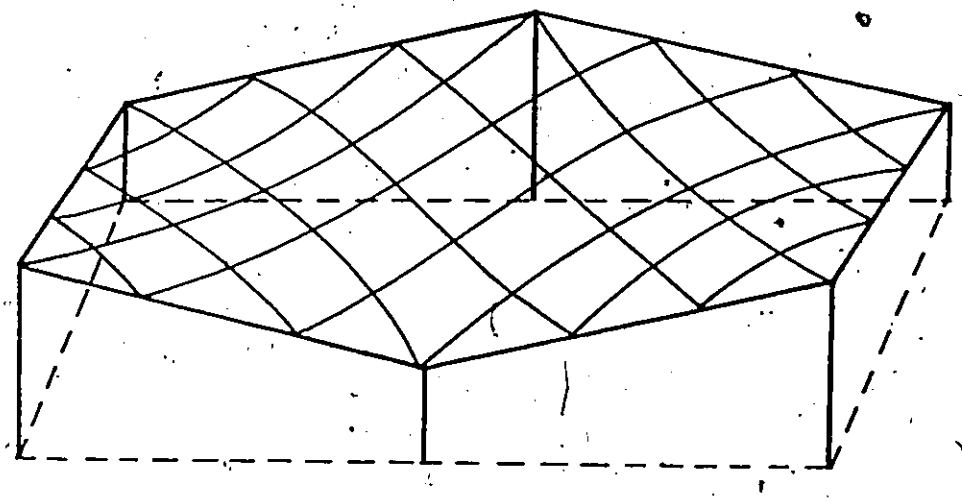

Fig. (1-2b) DOUBLE ROOF

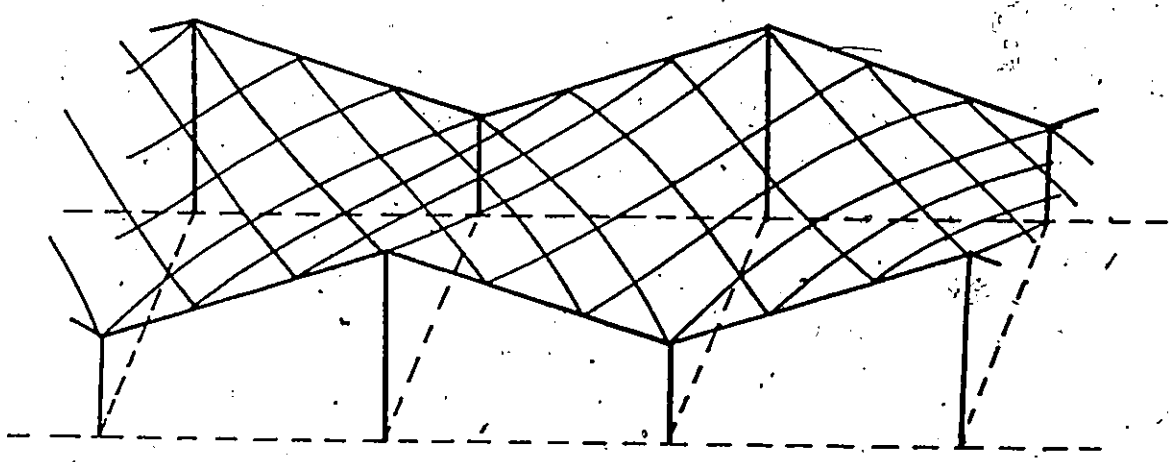

Fig. (1-2c) CONTINUOUS MULTIROOF

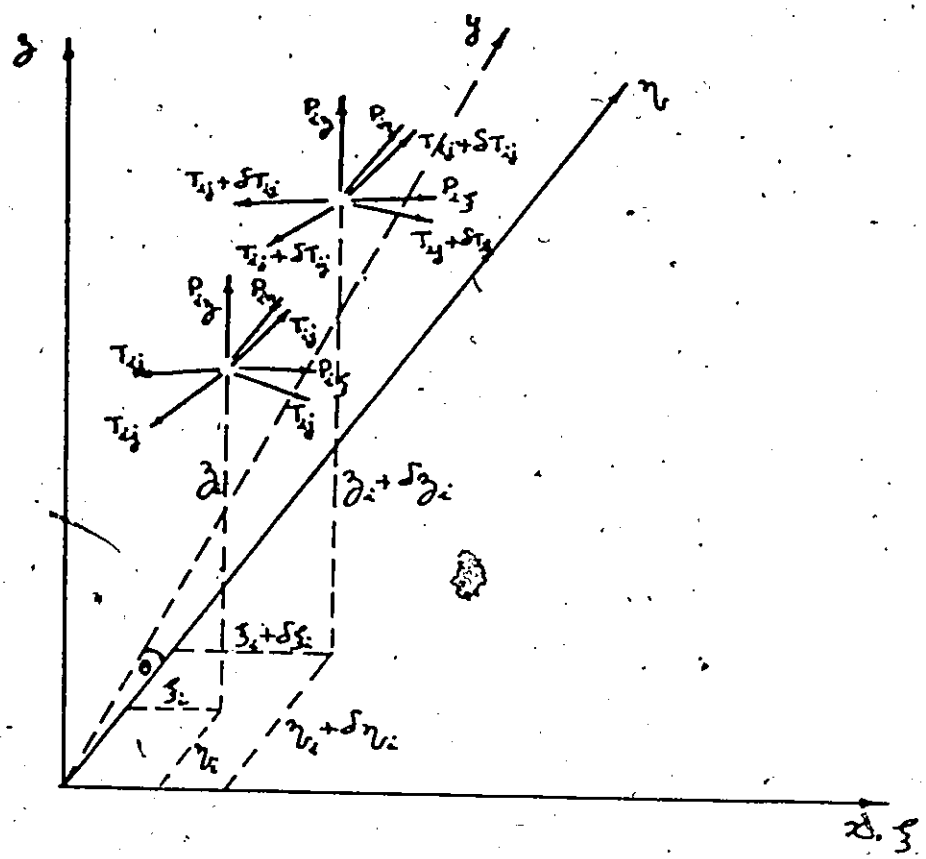

EQUILIBRIUM OF A JOINT IN THE INITIAL AND DISPLACED POSITIONS

Fig. (2-1)

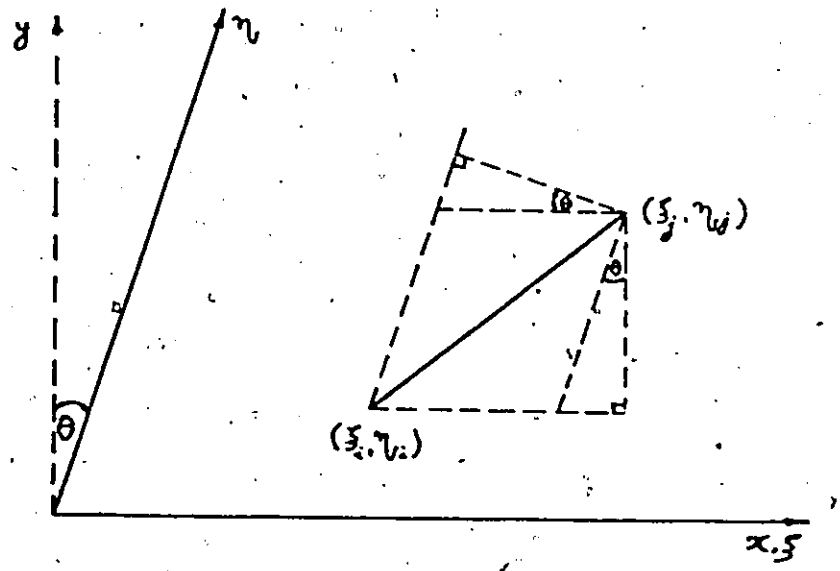

PLAN OF A CABLE SEGMENT BETWEEN JOINTS I AND J

Fig. (2-2)

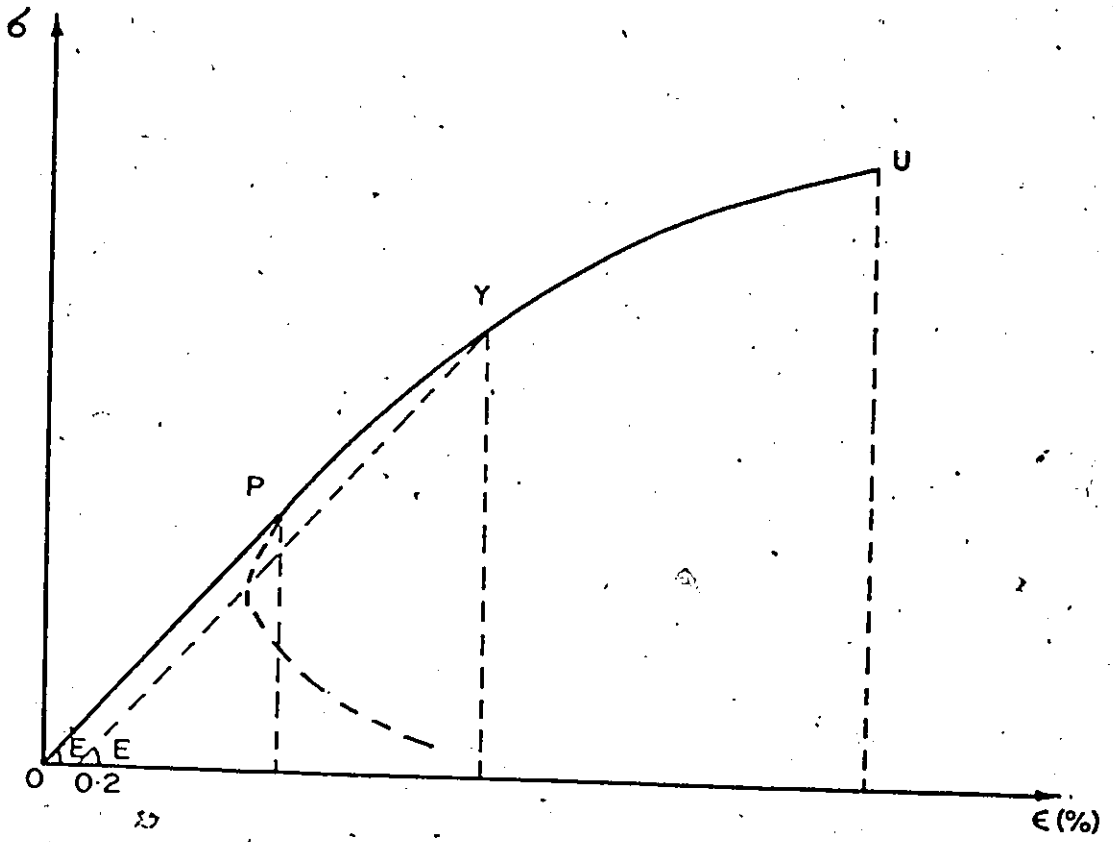

MATHEMATICAL MODEL OF CABLE STRESS-STRAIN CURVE

Fig. (2-3)

Fig. (3 - 1) FLOW DIAGRAM FOR MAIN COMPUTER PROGRAM

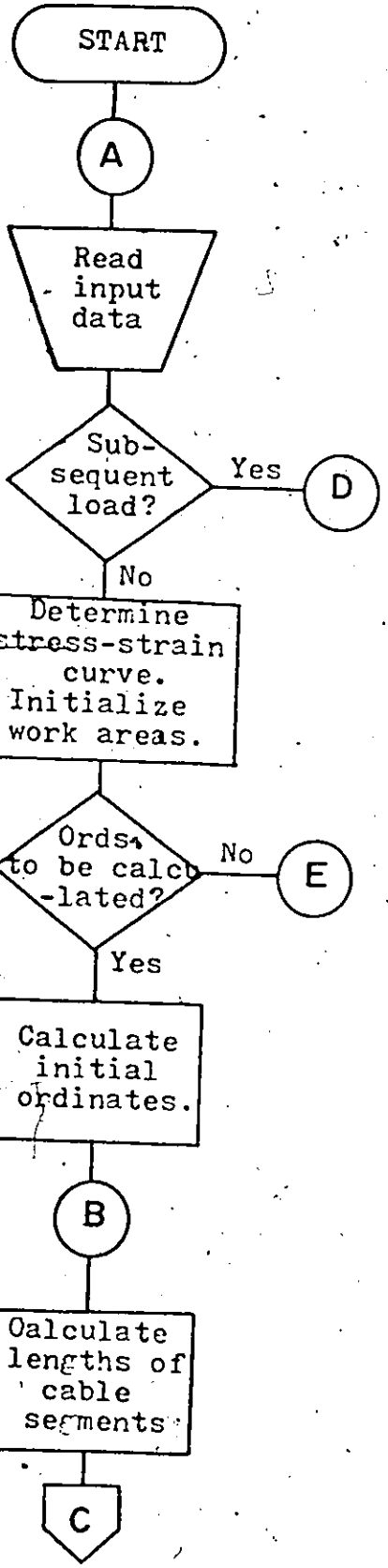

Fig. (3-1) (CONT'D)

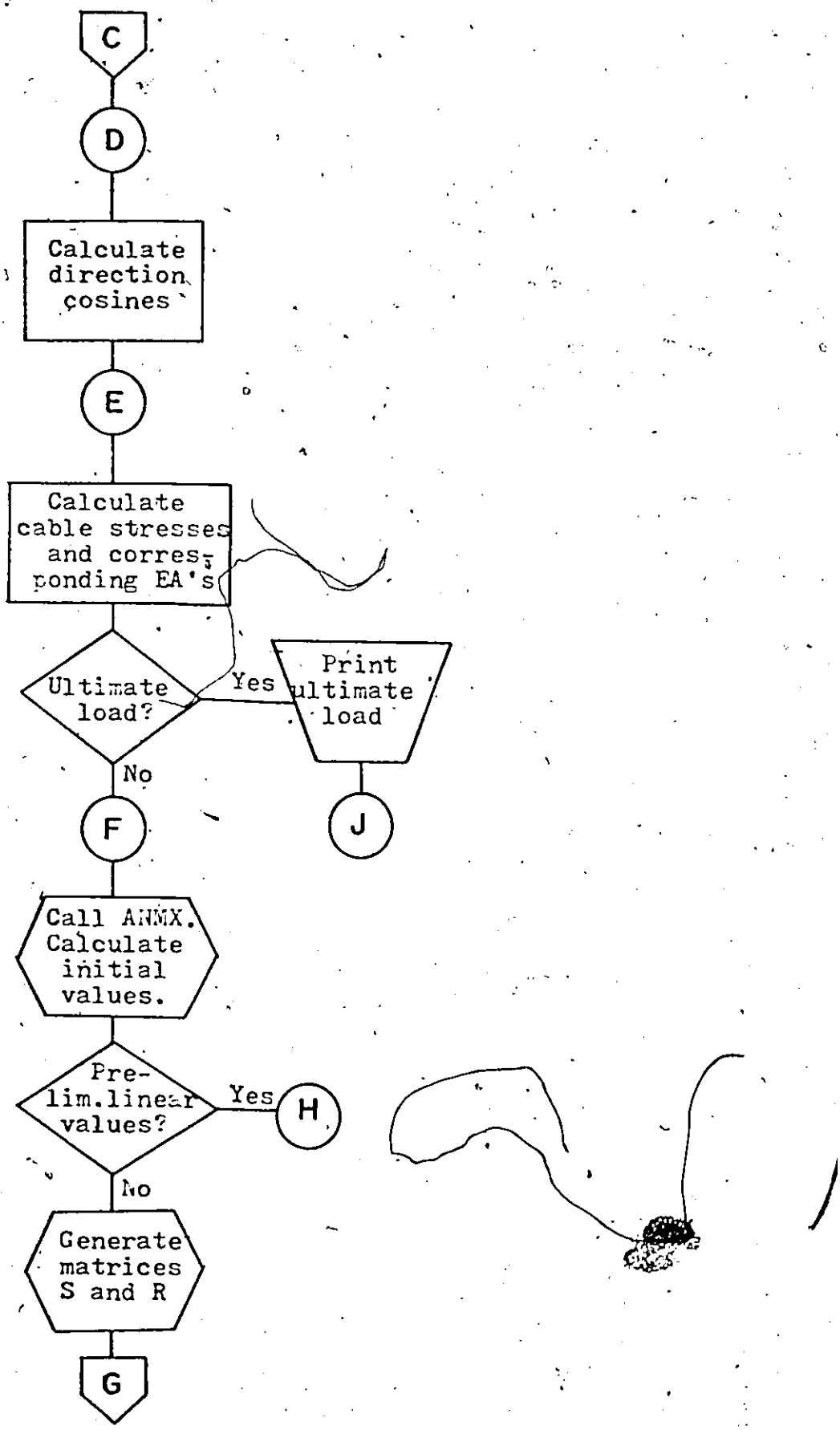
C
D
Calculate direction cosines
E
Calculate cable stresses and corresponding EA's
Ultimate load?
Yes
Print ultimate load
J
No
F
Call ANMX. Calculate initial values.
Pre-lim.linear values?
Yes
H
No
Generate matrices S and R
G

Fig. (3-1) (CONT'D)

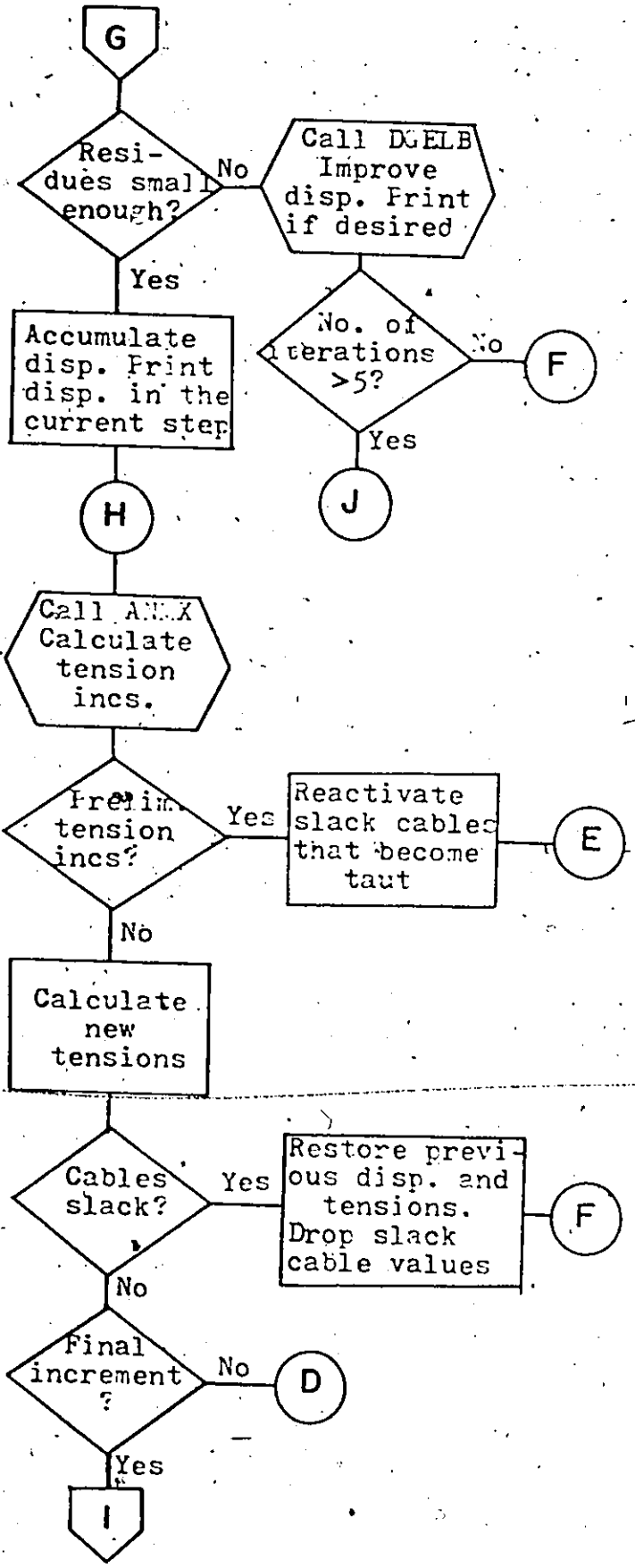
G
Resi-dues small enough?
No
Call DELB Improve disp. Print if desired
Yes
No. of iterations >5?
No
F
Yes
J
Accumulate disp. Print disp. in the current step
H
Call ANAX Calculate tension incs.
Prelim. tension incs?
Yes
Reactivate slack cables that become taut
E
No
Calculate new tensions
Cables slack?
Yes
Restore previous disp. and tensions. Drop slack cable values
F
No
Final increment ?
No
D
Yes
I

Fig. (3-1) (CONT'D)

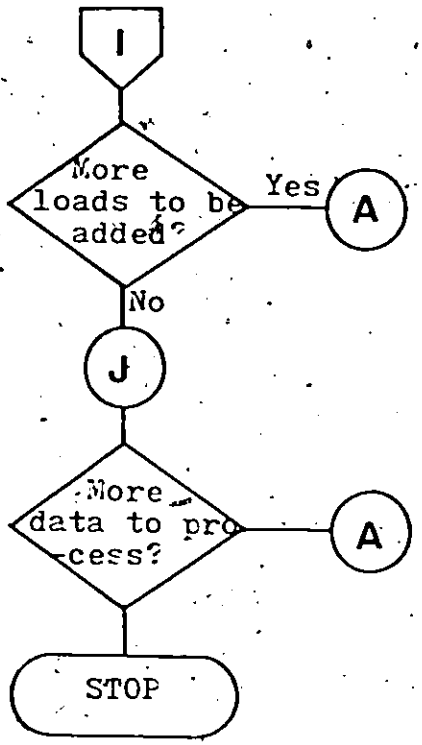

3641	3212	119	0	0	0	-1336	-802	-30	0	0	0	0	0	0
3212	3646	72	0	0	0	-802	-483	-18	0	0	0	0	0	0
119	72	17	0	0	0	-30	-18	-3	0	0	0	0	0	0
0	0	0	3646	3212	72	-483	-802	-18	0	0	0	0	0	0
0	0	0	3212	3641	119	-802	-1336	-30	0	0	0	0	0	0
0	0	0	72	119	17	-18	-30	-3	0	0	0	0	0	0
-1336	-802	-30	-483	-802	-18	3638	3207	0	-483	-802	18	-1336	-802	30
-802	-483	-18	-802	-1336	-30	3207	3638	0	-802	-1336	30	-802	-483	18
-30	-18	-3	-18	-30	-3	0	0	12	18	30	-3	30	18	-3
0	0	0	0	0	0	-483	-802	18	3646	3212	-72	0	0	0
0	0	0	0	0	0	-802	-1336	30	3212	3641	-119	0	0	0
0	0	0	0	0	0	18	30	-3	-72	-119	17	0	0	0
0	0	0	0	0	0	-1336	-802	30	0	0	0	3641	3212	-120
0	0	0	0	0	0	-802	-483	18	0	0	0	3212	3646	-72
0	0	0	0	0	0	30	18	-3	0	0	0	-119	-72	17

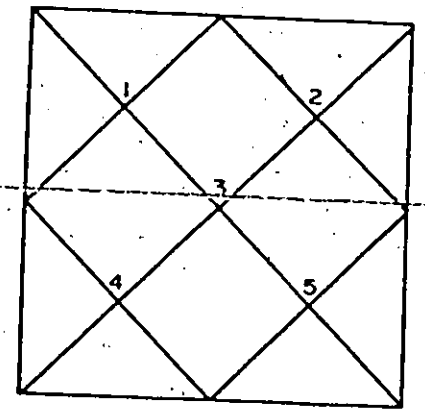

Fig. (3-2) STIFFNESS MATRIX FOR A 5-JOINT CABLE-NET

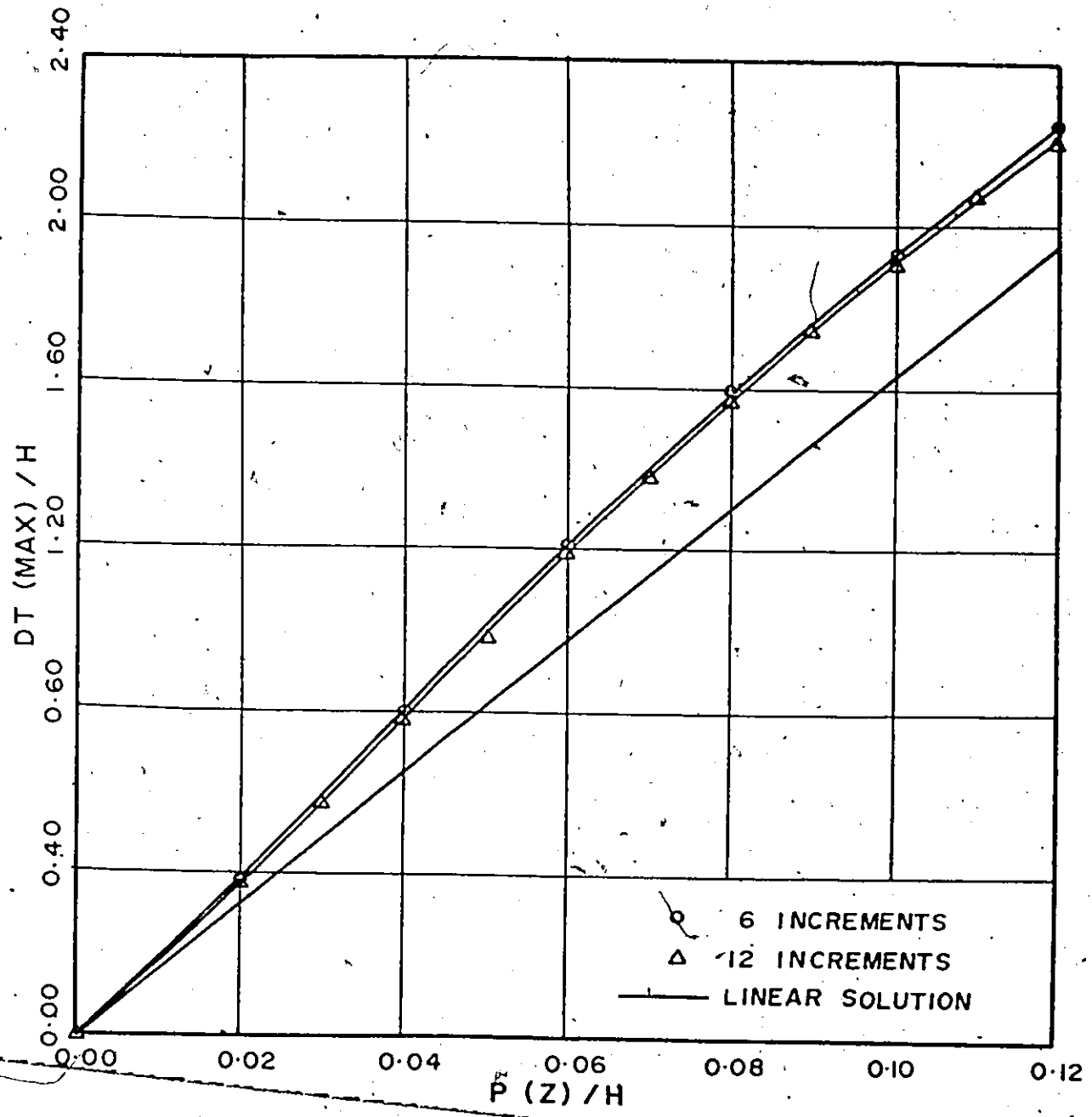

VARYING NO· OF INCREMENTS OF LOADING
(NONORTHOGONAL SINGLE· ROOF)

Fig· (3-3)

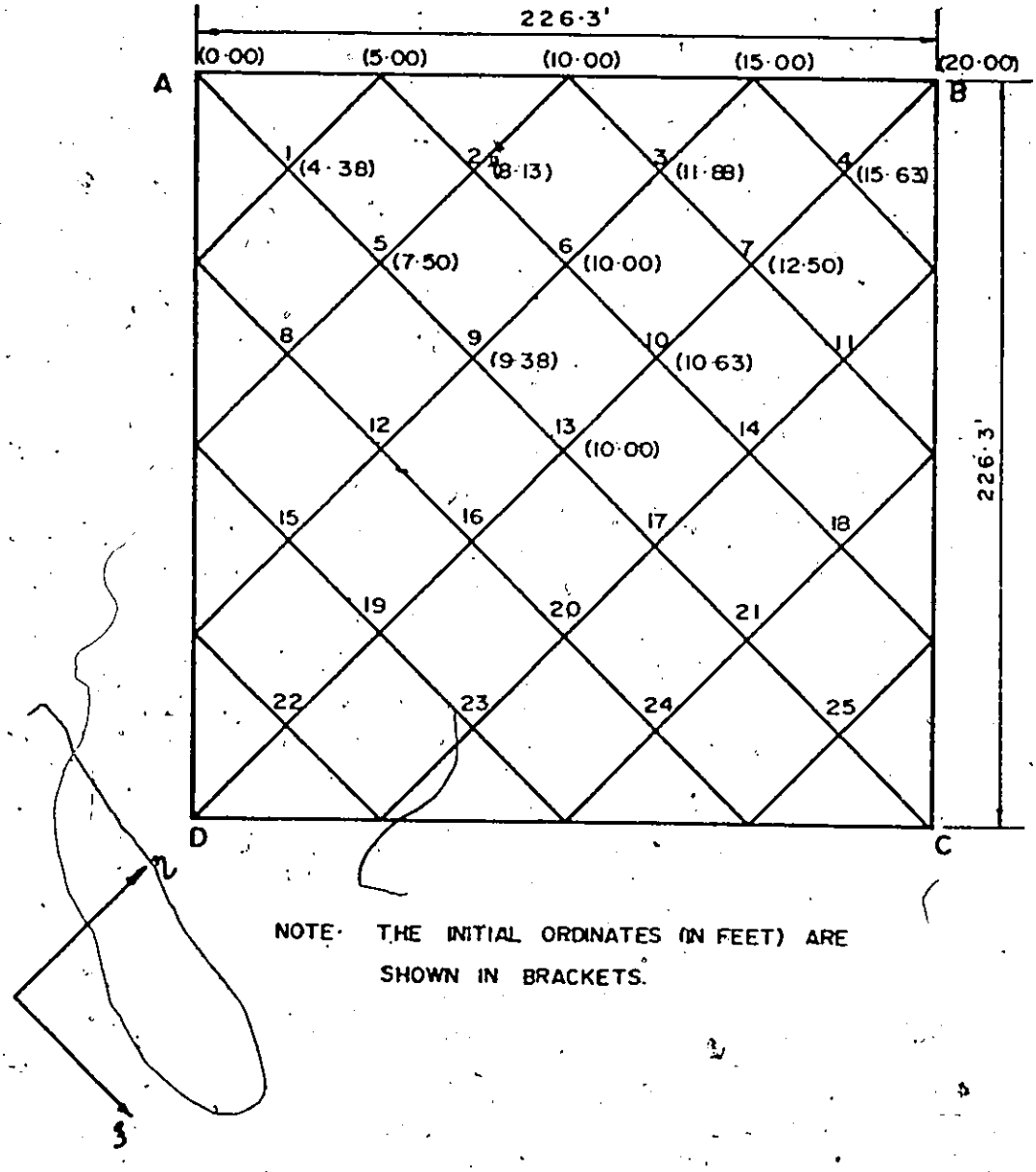

NOTE· THE INITIAL ORDINATES (IN FEET) ARE SHOWN IN BRACKETS.

ORTHOGONAL HYPERBOLIC PARABOLOID NET WITH 25 JOINTS

Fig· (3-4)

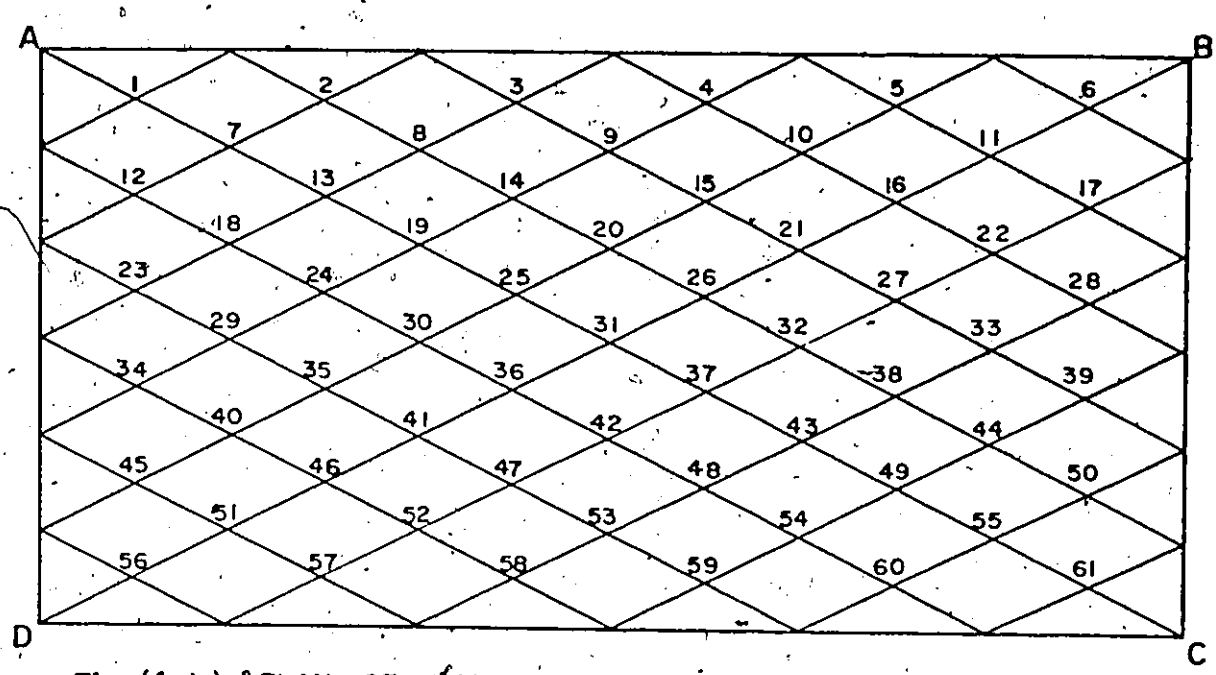

Fig. (4-1a) PLAN OF NON ORTHOGONAL SINGLE ROOF

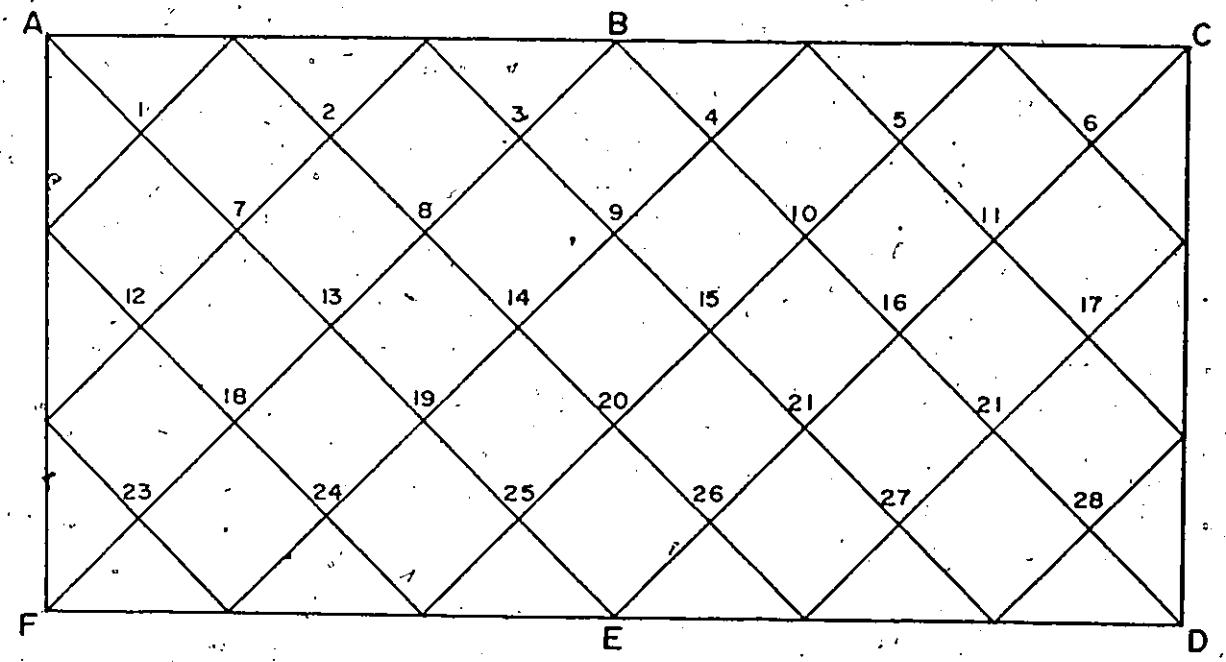

Fig. (4-1b) PLAN OF ORTHOGONAL DOUBLE ROOF

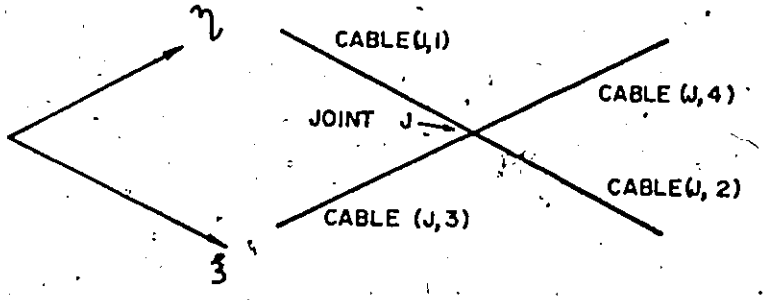

Fig. (4-1c) NUMBERING SYSTEM OF CABLE SEGMENTS

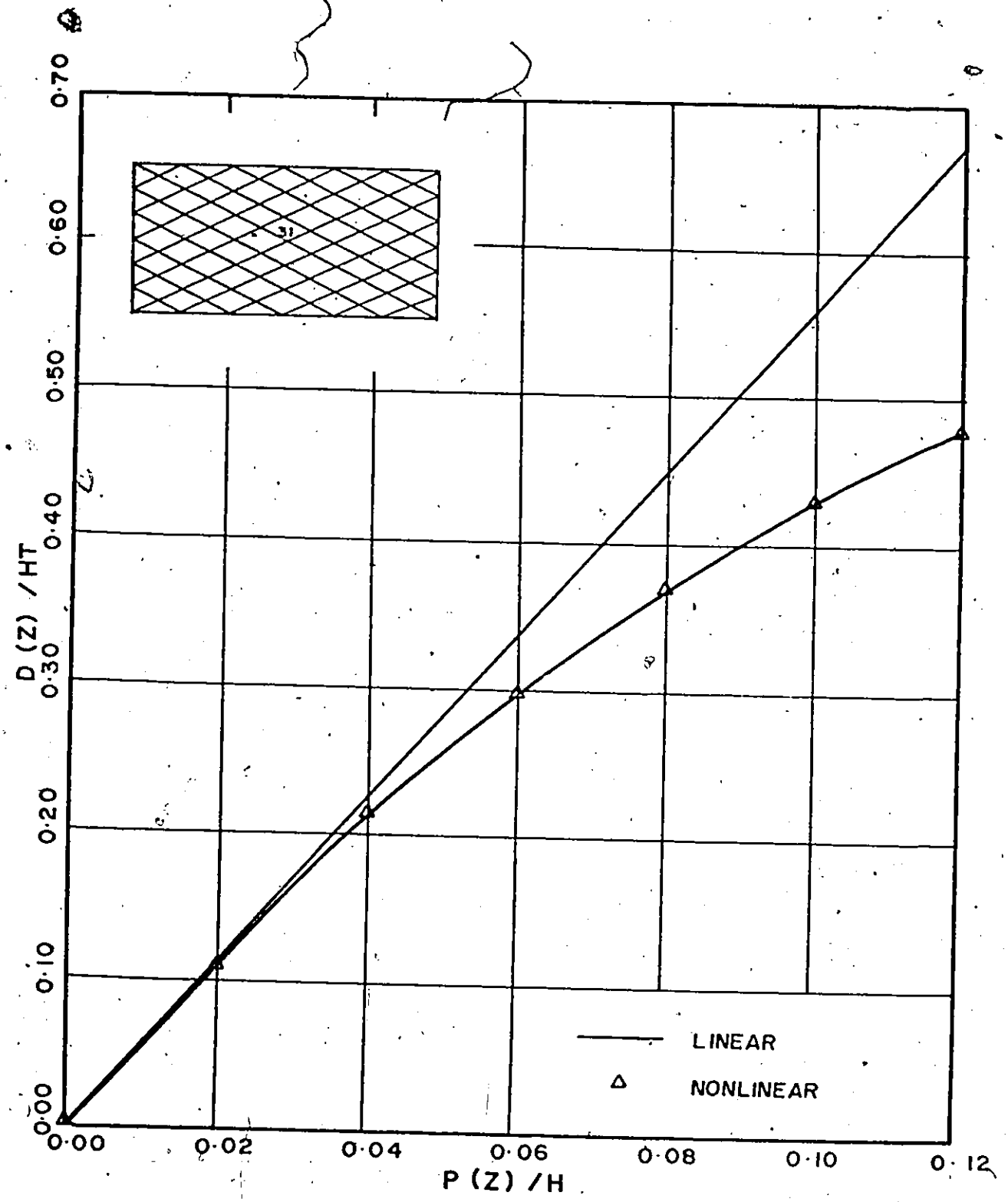

DEFLECTION AT JOINT 31 DUE TO A UNIFORM LOAD
(NONORTHOGONAL SINGLE ROOF)

Fig. (4-2)

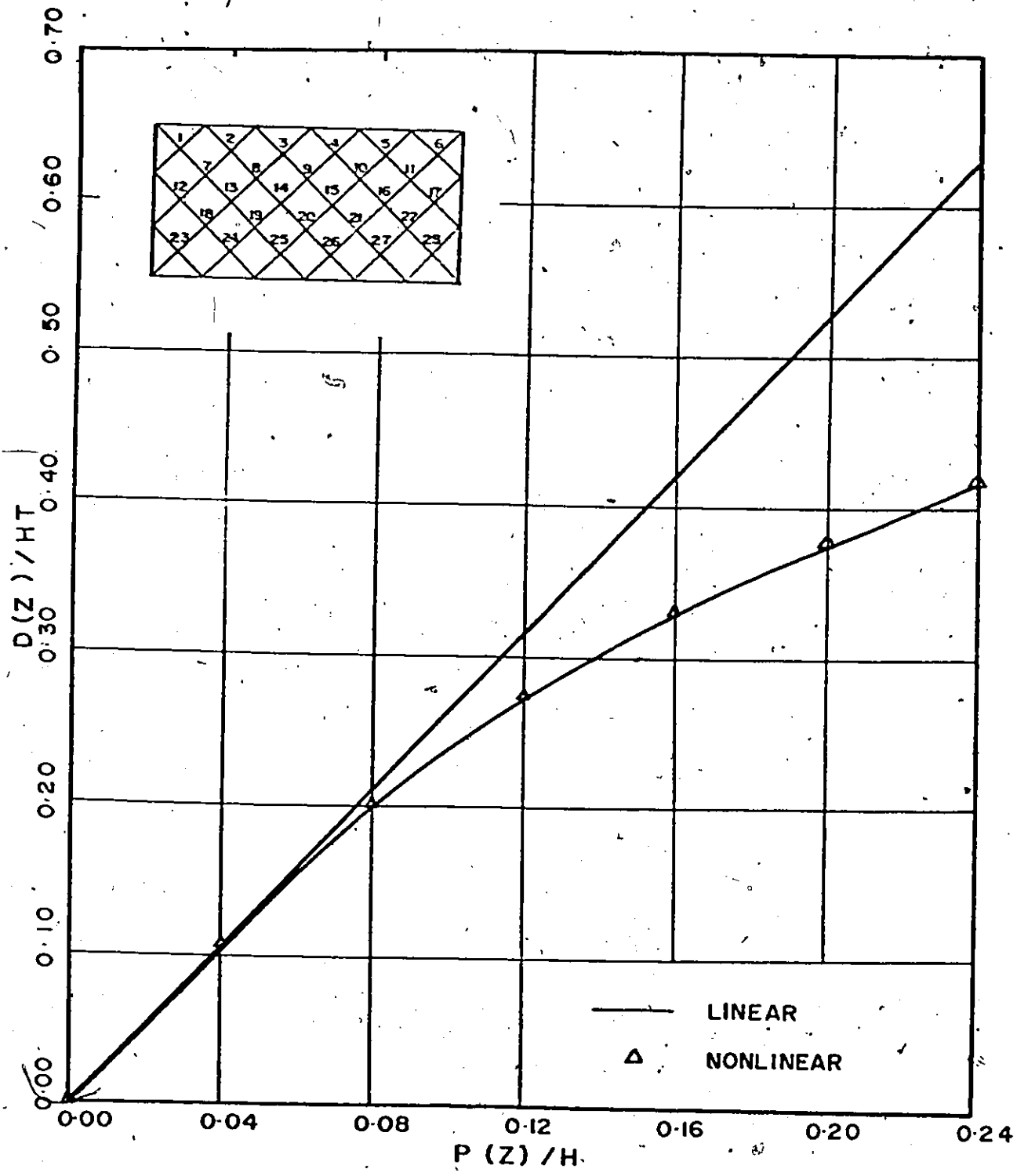

DEFLECTION AT JOINT 20 DUE TO A UNIFORM LOAD
(ORTHOGONAL DOUBLE ROOF)

Fig·(4-3)

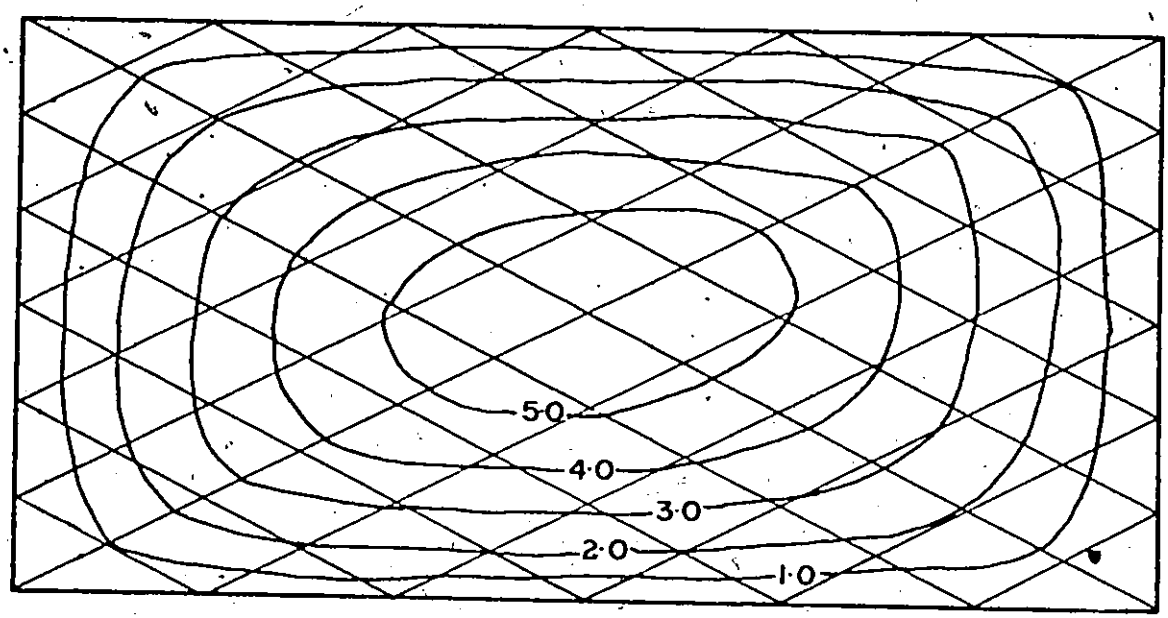

DEFLECTION CONTOURS FOR SINGLE ROOF

(LOAD = 6 K/J)

Fig (4-4)

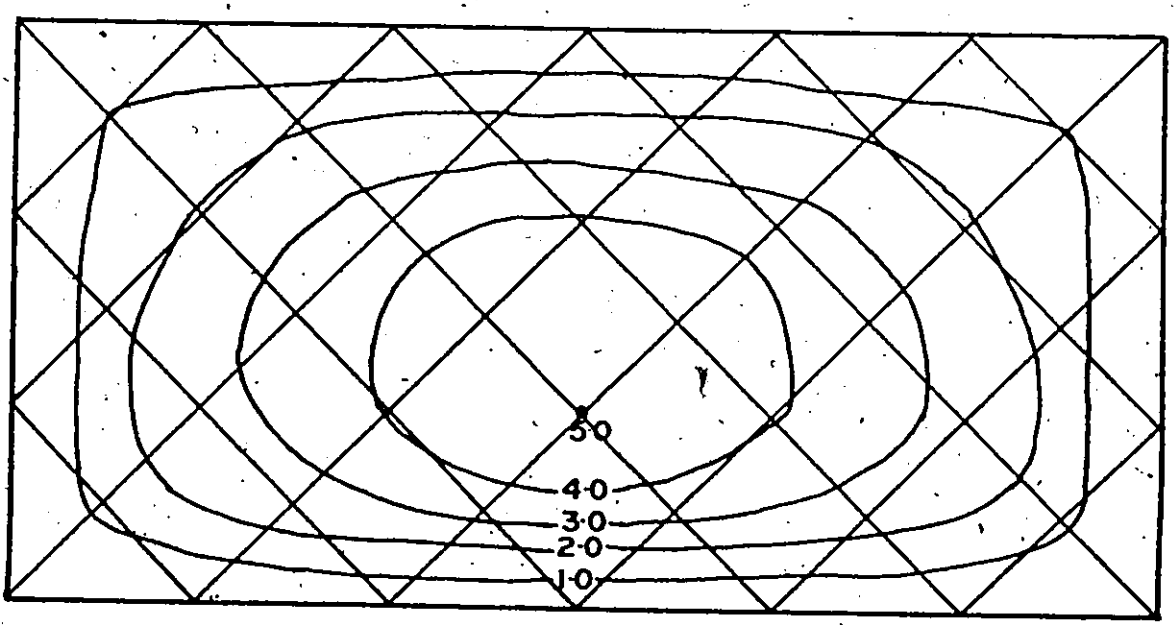

DEFLECTION CONTOURS FOR DOUBLE ROOF

(LOAD = 12 K/J)

Fig- (4-5)

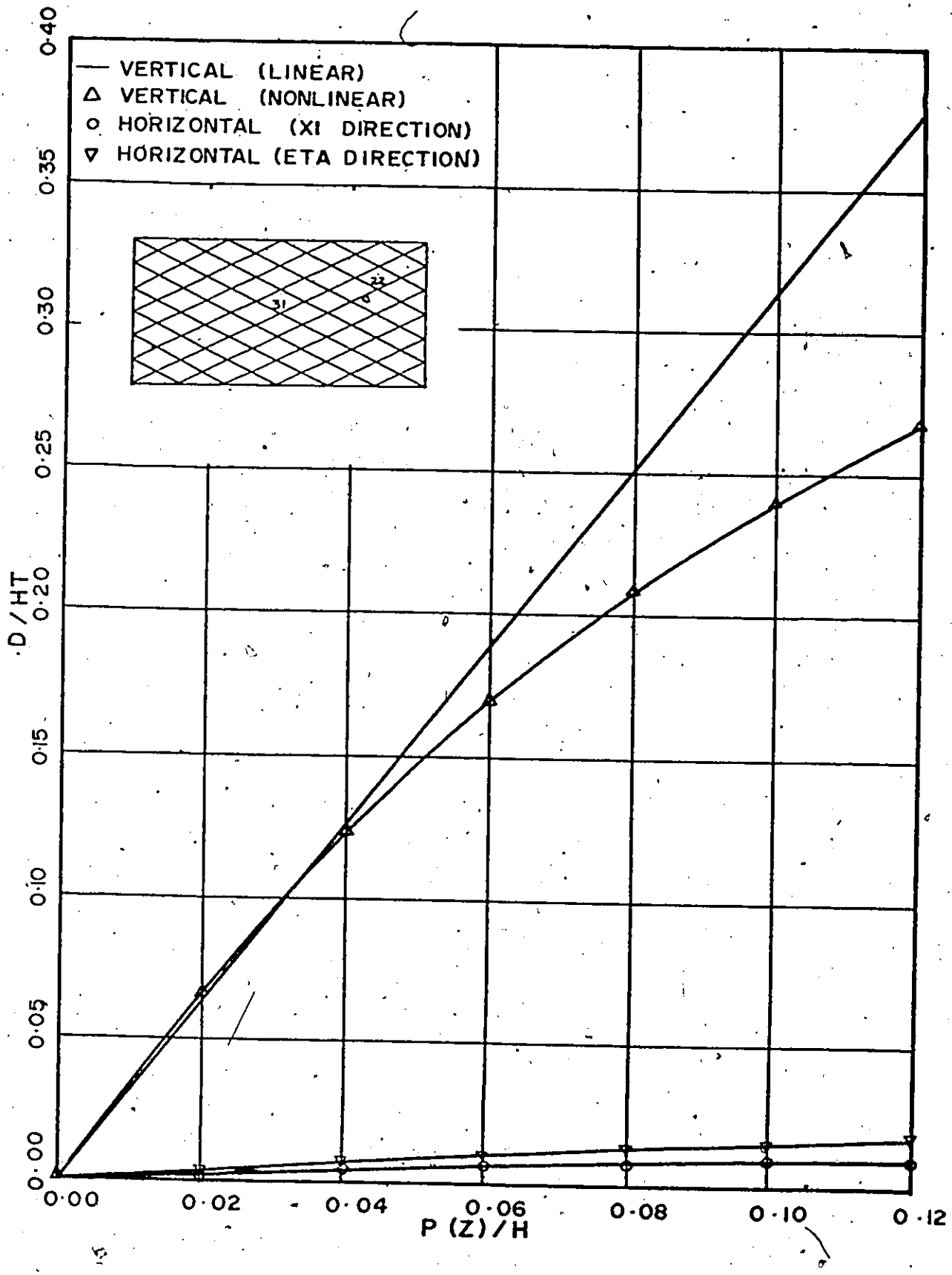

DEFLECTIONS AT JOINT 22 UNDER A UNIFORM LOAD
(NONORTHOGONAL SINGLE ROOF)

Fig. (4-6)

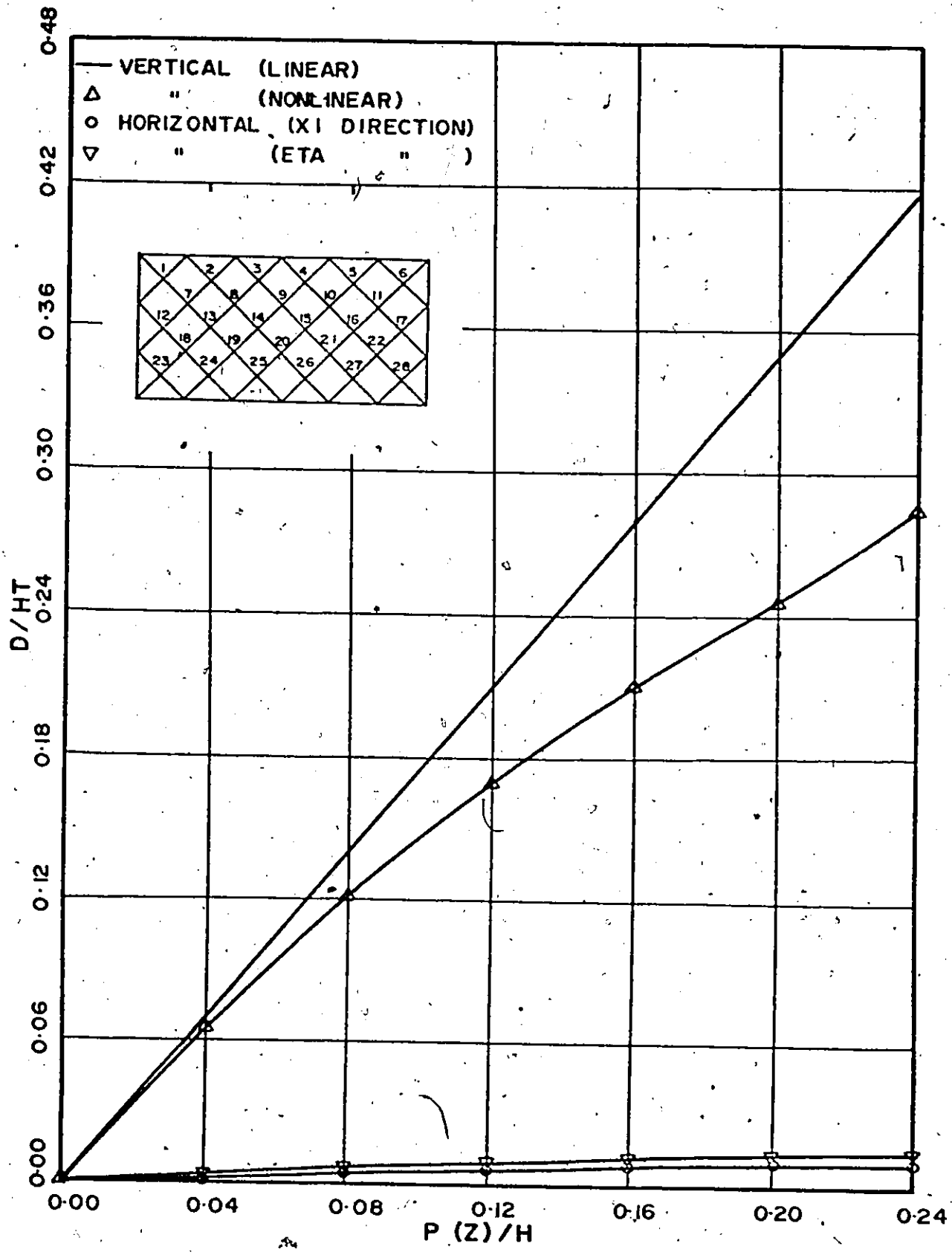

DEFLECTIONS AT JOINT 8 UNDER A UNIFORM LOAD
(ORTHOGONAL DOUBLE ROOF)

Fig. (4-7)

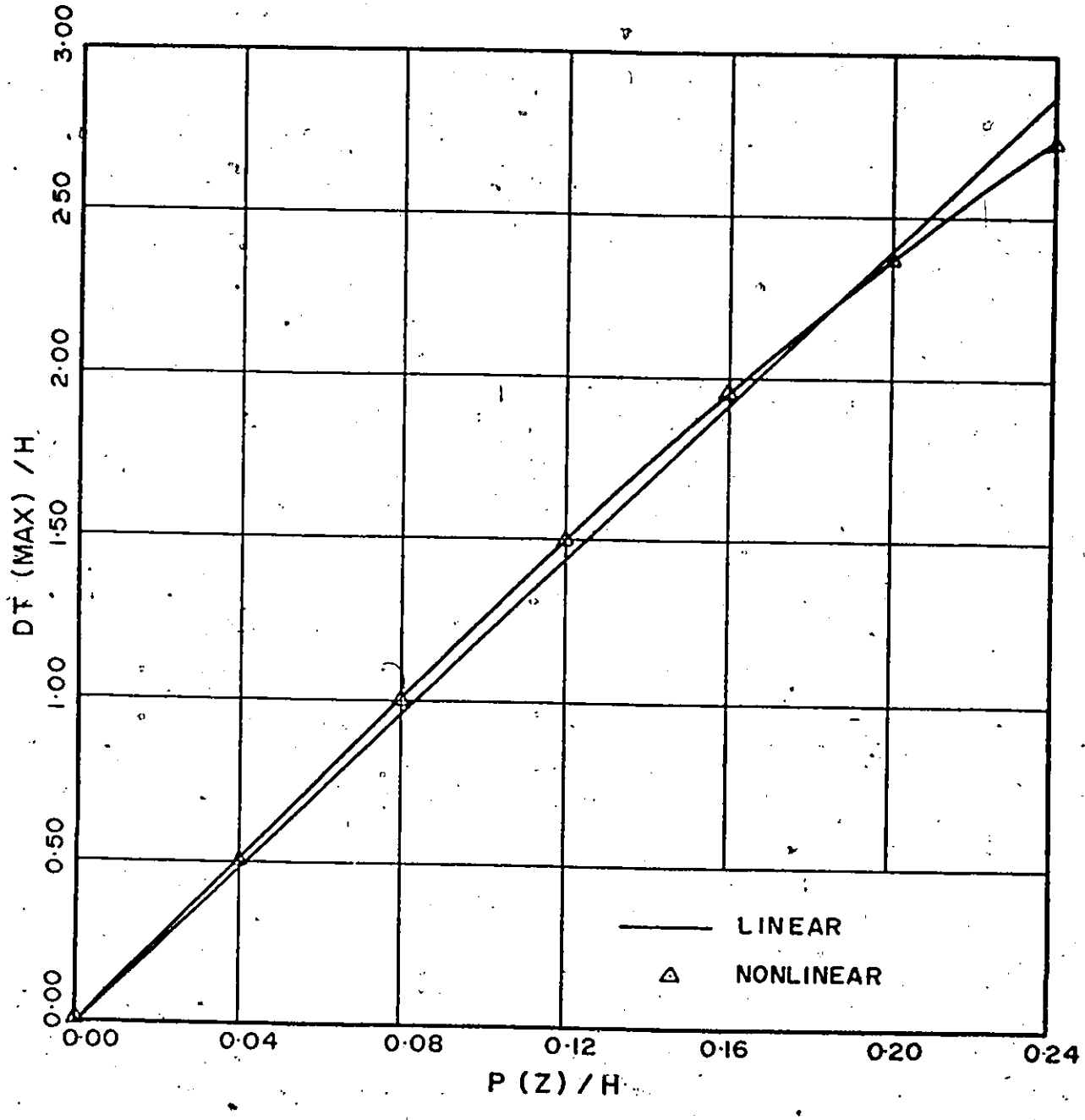

MAXIMUM TENSION INCREMENT UNDER A UNIFORM LOAD
(ORTHOGONAL DOUBLE ROOF)

Fig. (4-8)

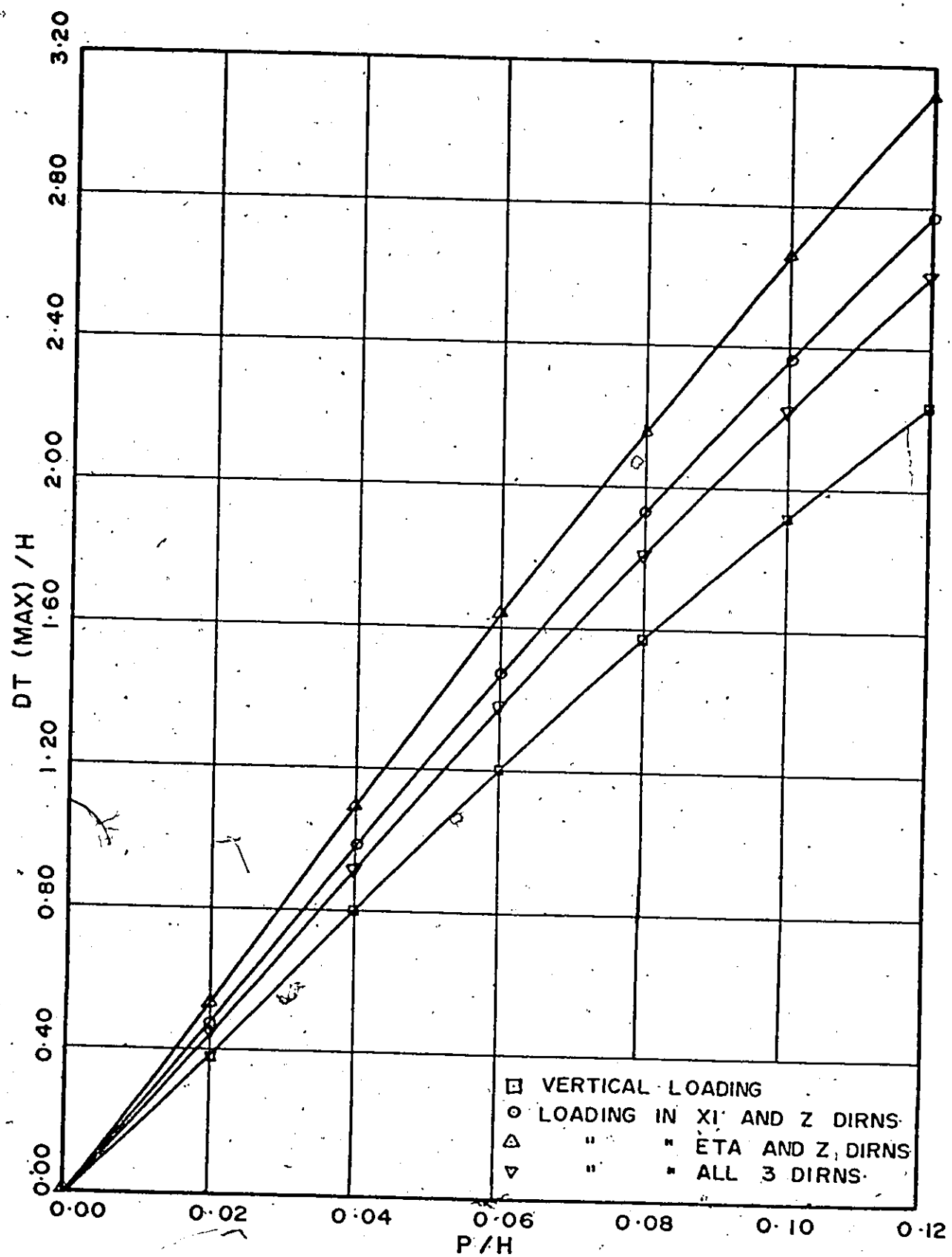

TENSION INCREMENT DUE TO COMBINED LOADINGS
(NONORTHOGONAL SINGLE ROOF)

Fig. (4-9)

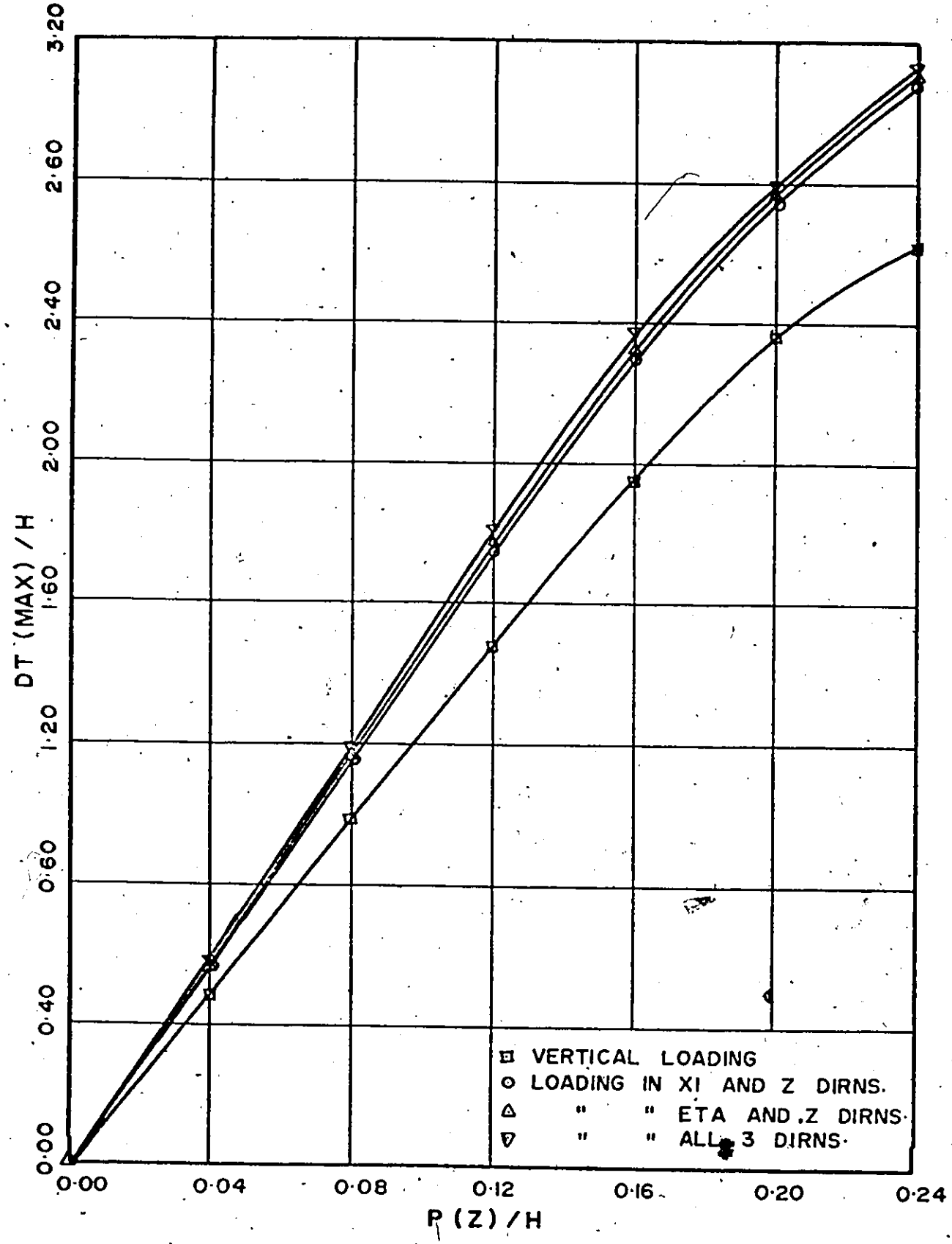

TENSION INCREMENT DUE TO COMBINED LOADINGS
(ORTHOGONAL DOUBLE ROOF)

Fig. (4-10)

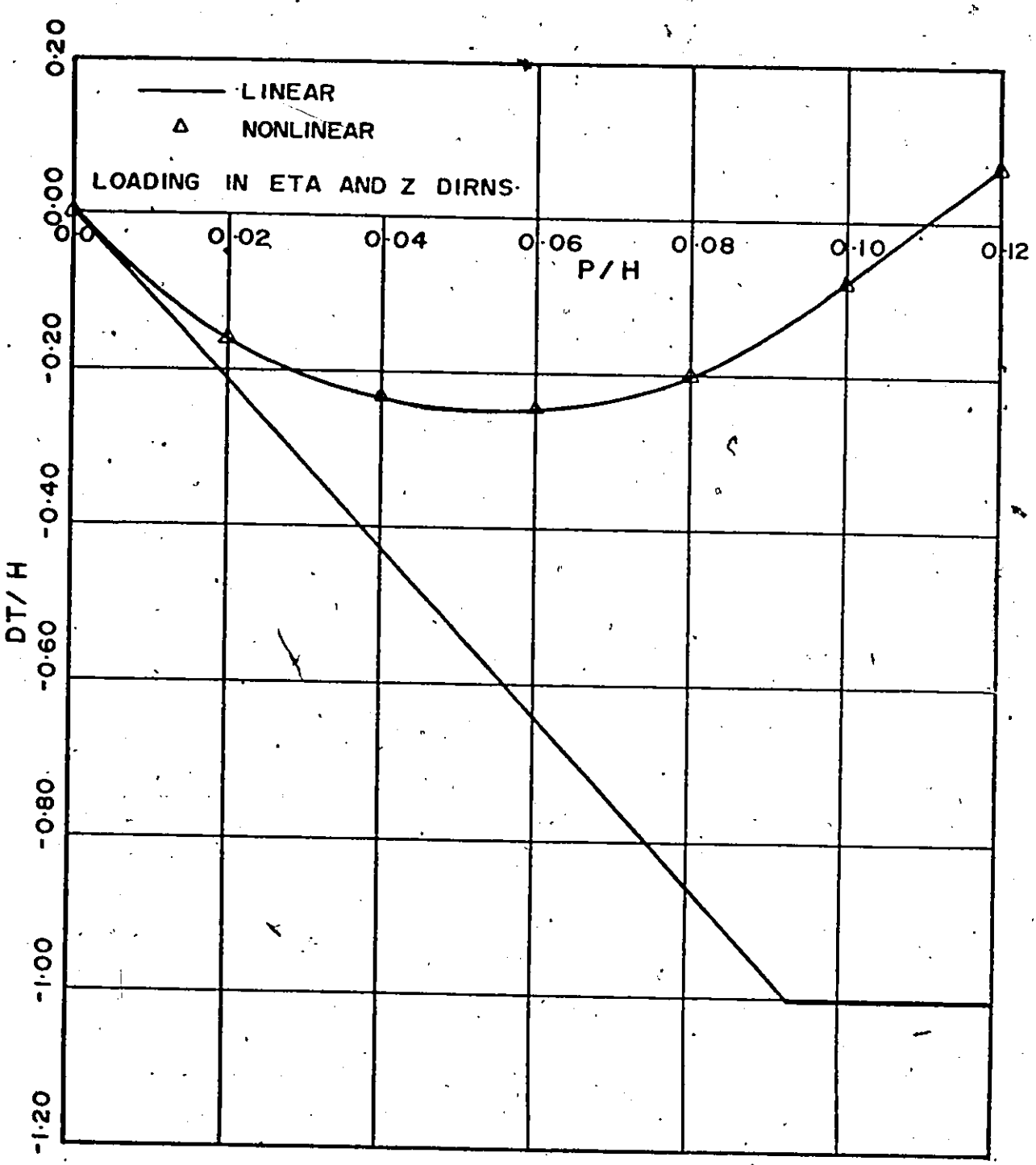

VARIATION OF TENSION INCREMENT IN CABLE (1,1)
(NONORTHOGONAL SINGLE ROOF)

Fig. (4-11)

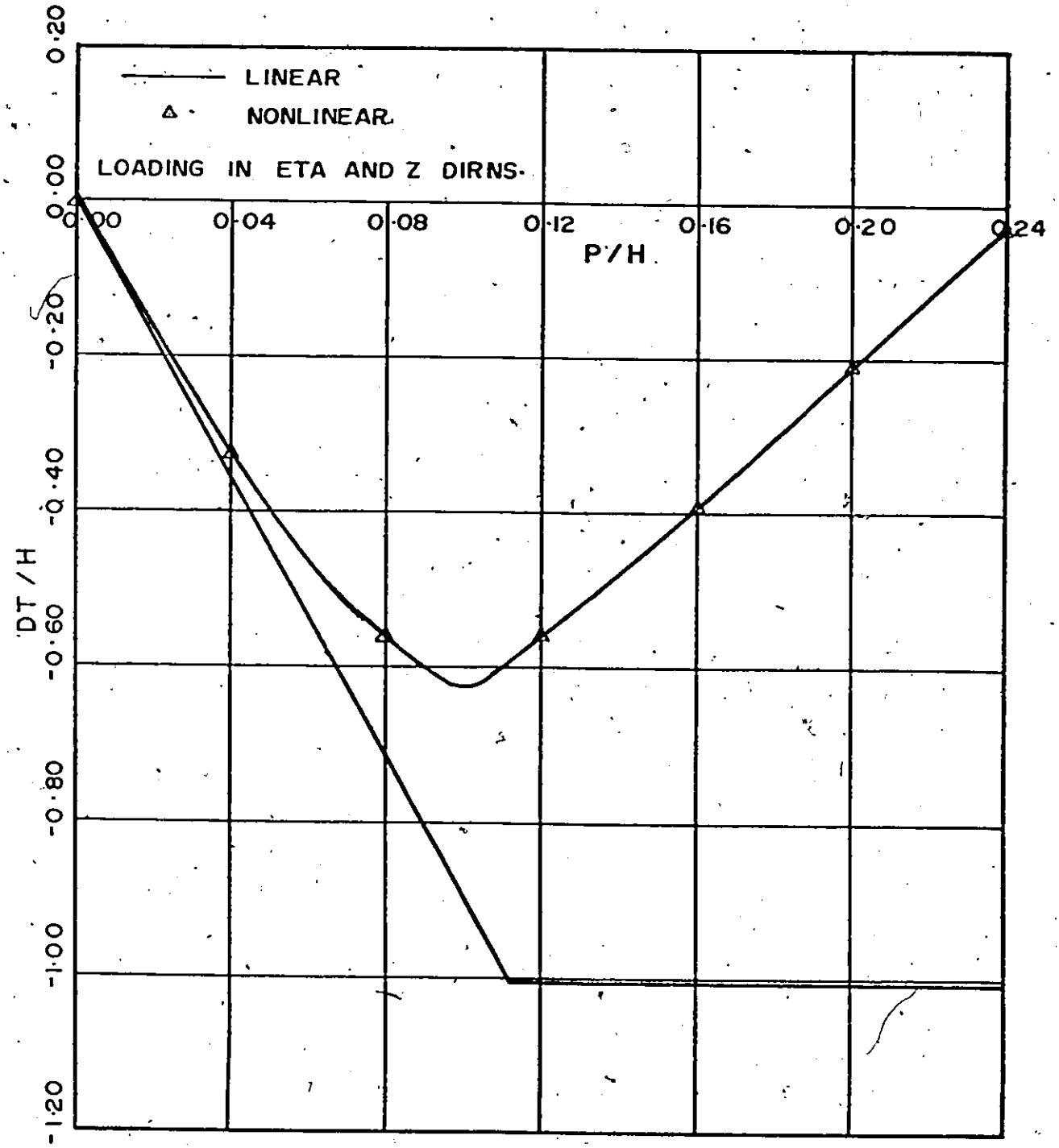

VARIATION OF TENSION INCREMENT IN CABLE (6, 4)
(ORTHOGONAL DOUBLE ROOF)

Fig. (4-12)

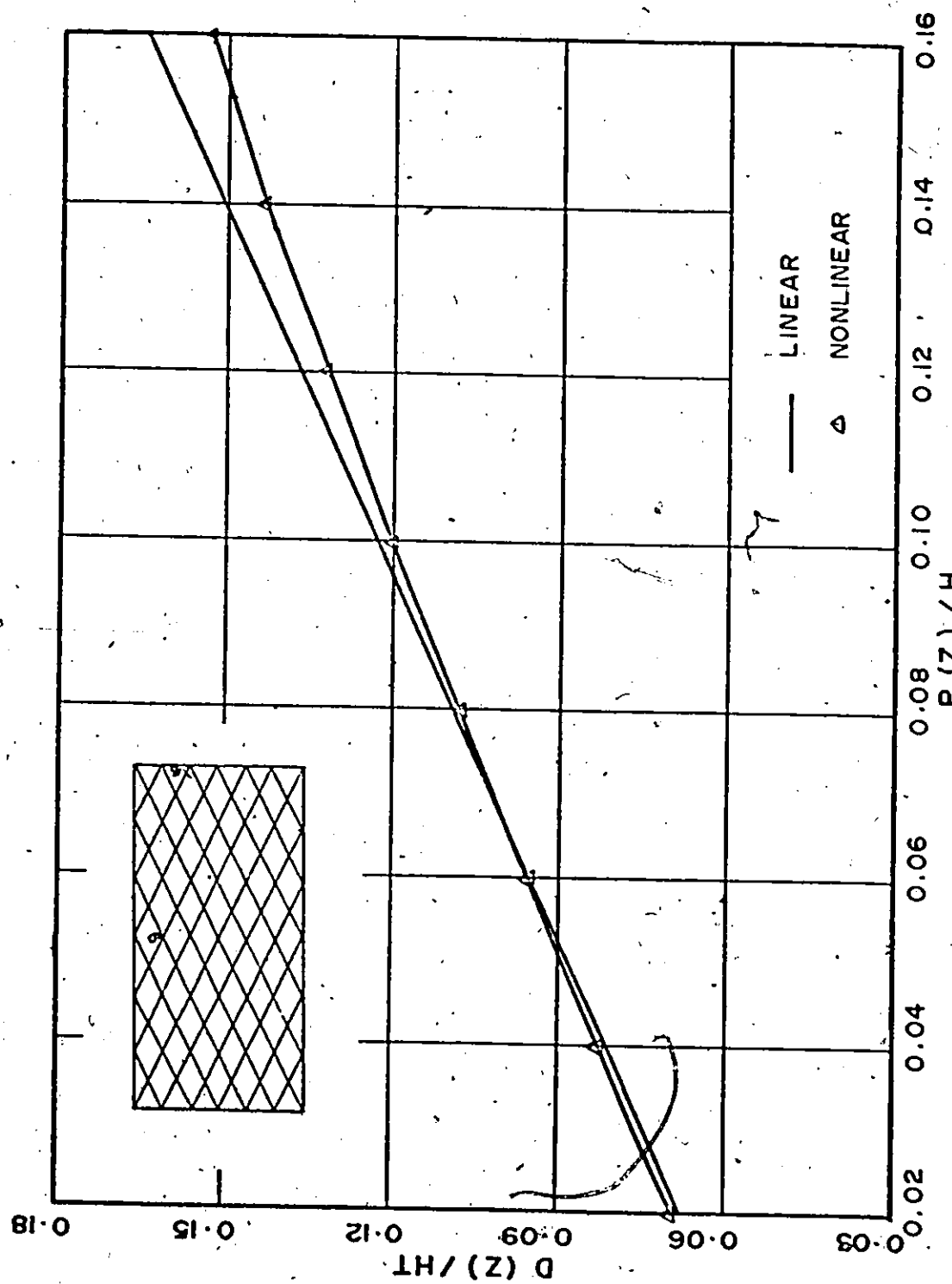

DEFLECTION AT JOINT 9 DUE TO A CONCENTRATED LOAD
(NONORTHOGONAL SINGLE ROOF. LOADING = 1 K/J+CONC. LOAD AT JT 9)

Fig. (4-13)

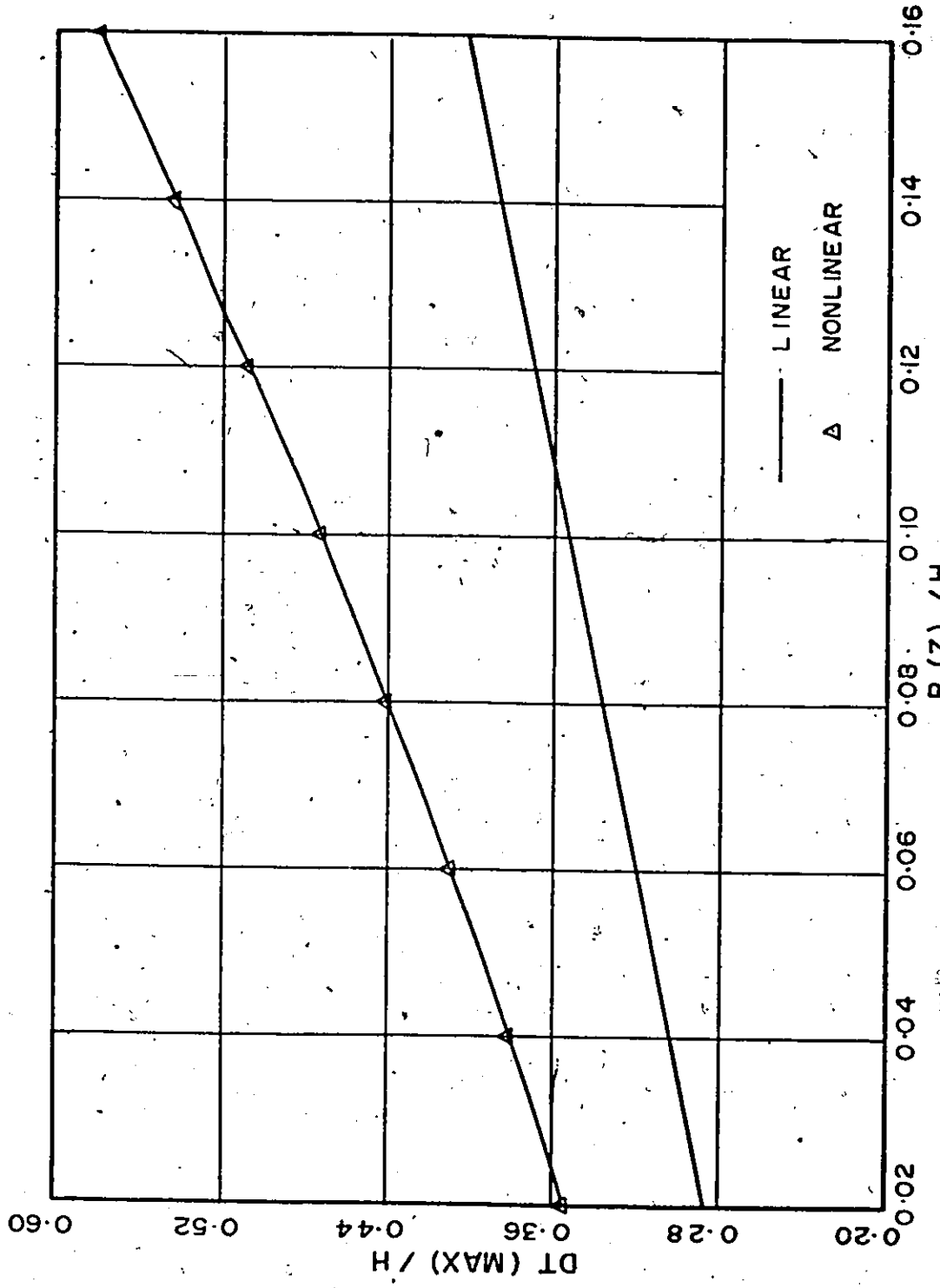

MAX. TENSION INC. DUE TO A CONCENTRATED LOAD
(NONORTHOGONAL SINGLE ROOF. LOADING = 1 K/J*CONC. LOAD AT JT. 9)

Fig. (4-14)

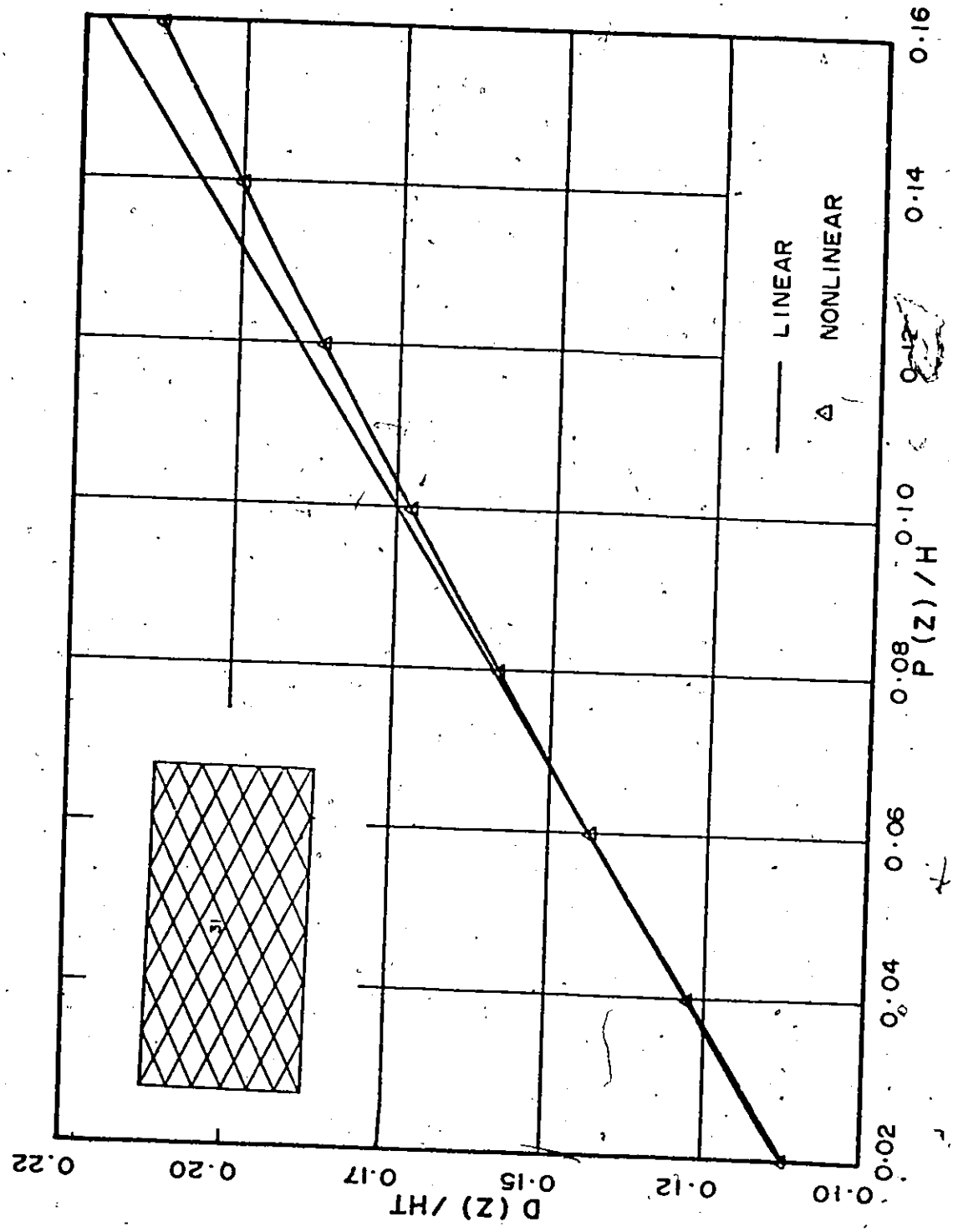

DEFLECTION AT JOINT 31 DUE TO A CONCENTRATED LOAD
(NONORTHOGONAL SINGLE ROOF, LOADING = 1 K/J+CONC. LOAD AT JT. 31)

Fig. (4-15)

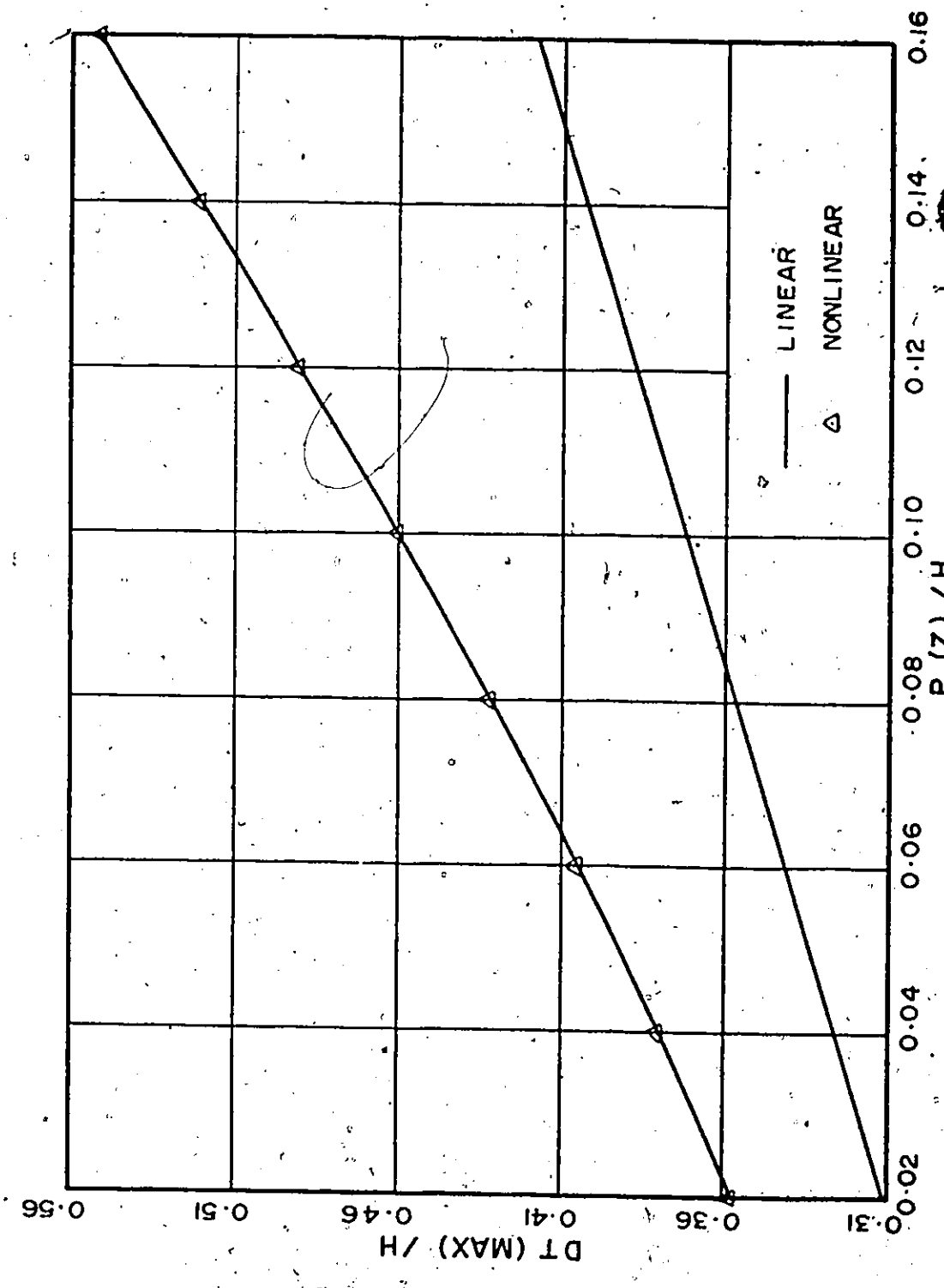

MAX TENSION INC DUE TO A CONCENTRATED LOAD
(NONORTHOGONAL SINGLE ROOF. LOADING = 1 K/J+CONC. LOAD AT JT. 31)

Fig. (4-16)

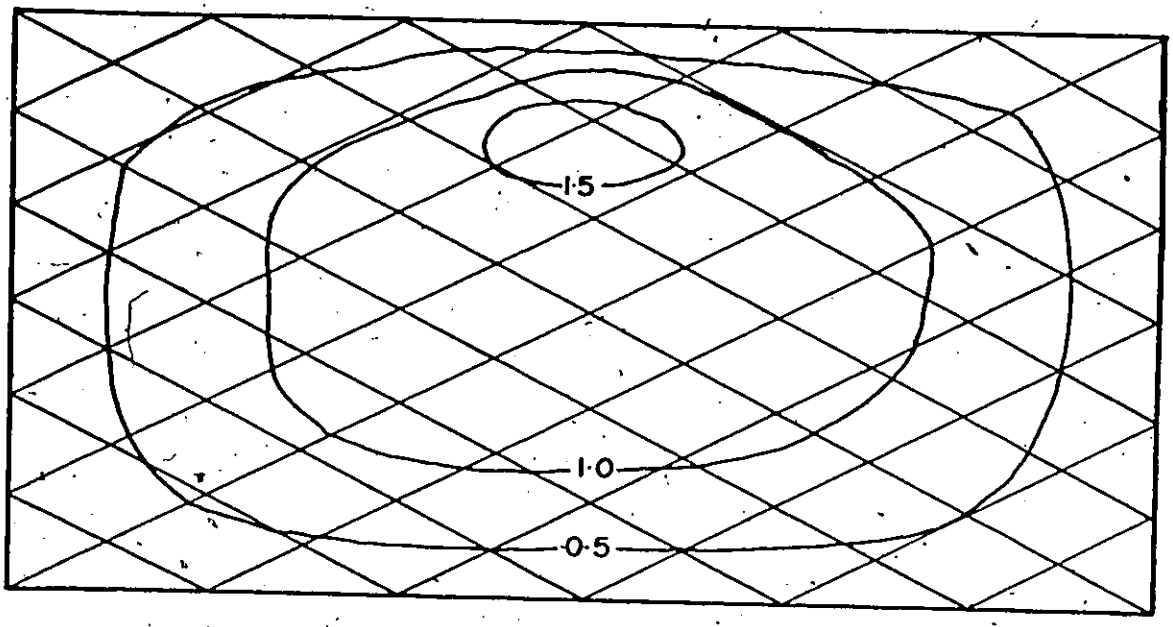

DEFLECTION CONTOURS FOR SINGLE ROOF
(LOAD = 1 K/J• CONC· LOAD AT JT· 9)

Fig· (4-17a)

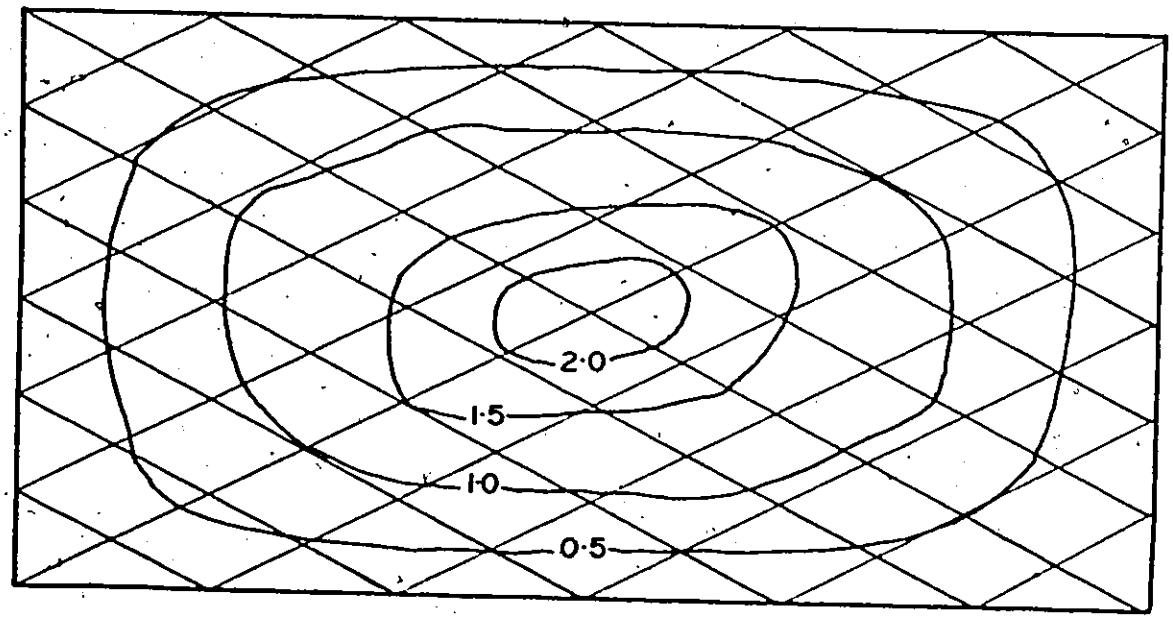

DEFLECTION CONTOURS FOR SINGLE ROOF
(LOAD = 1 K/J• CONC· LOAD AT JT· 31)

Fig· (4-17b)

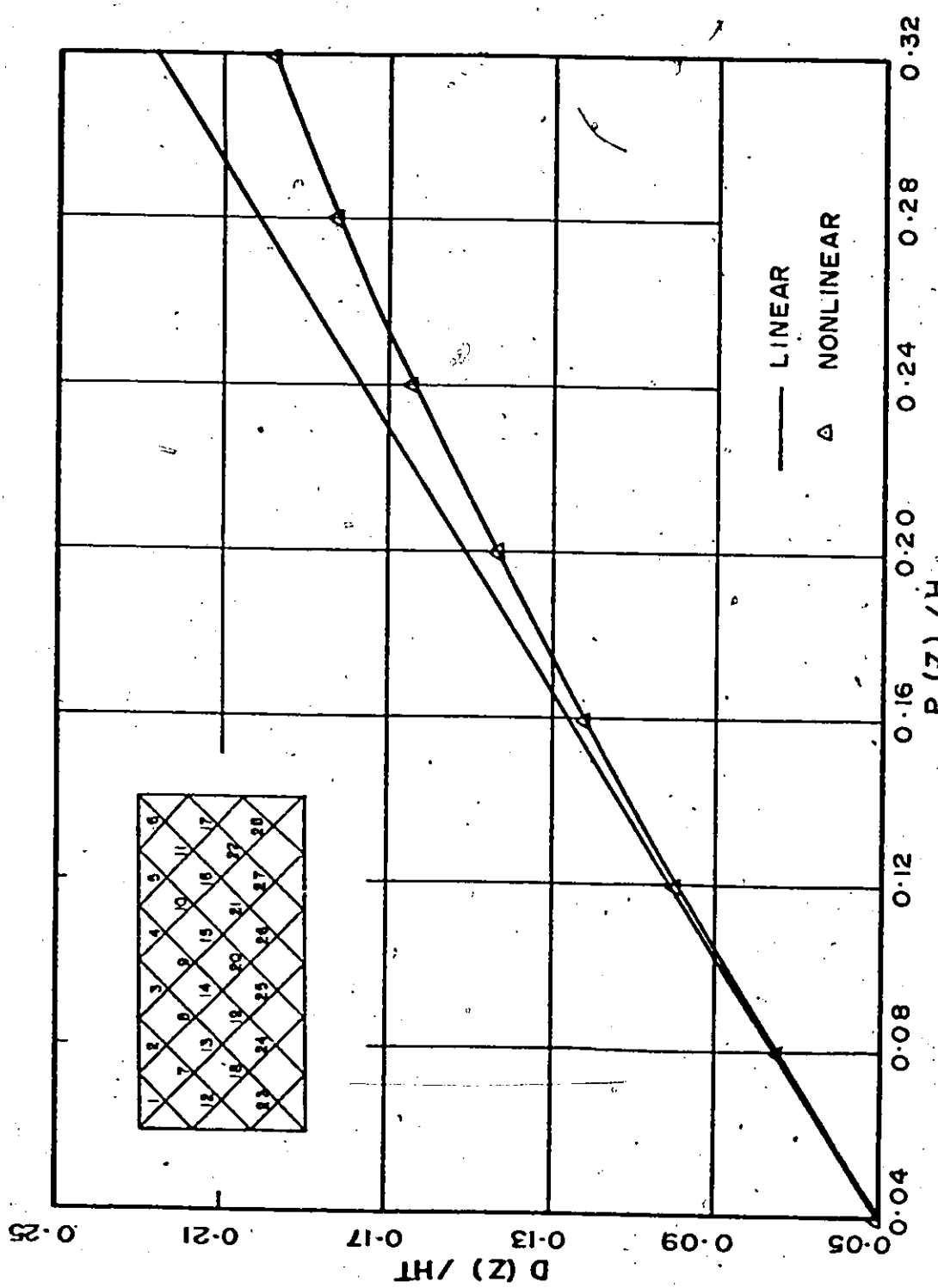

DEFLECTION AT JOINT 13 DUE TO A CONCENTRATED LOAD
(ORTHOGONAL DOUBLE ROOF, LOADING = 2 K/J+CONC. LOAD AT JOINT 13)

Fig. (4-18)

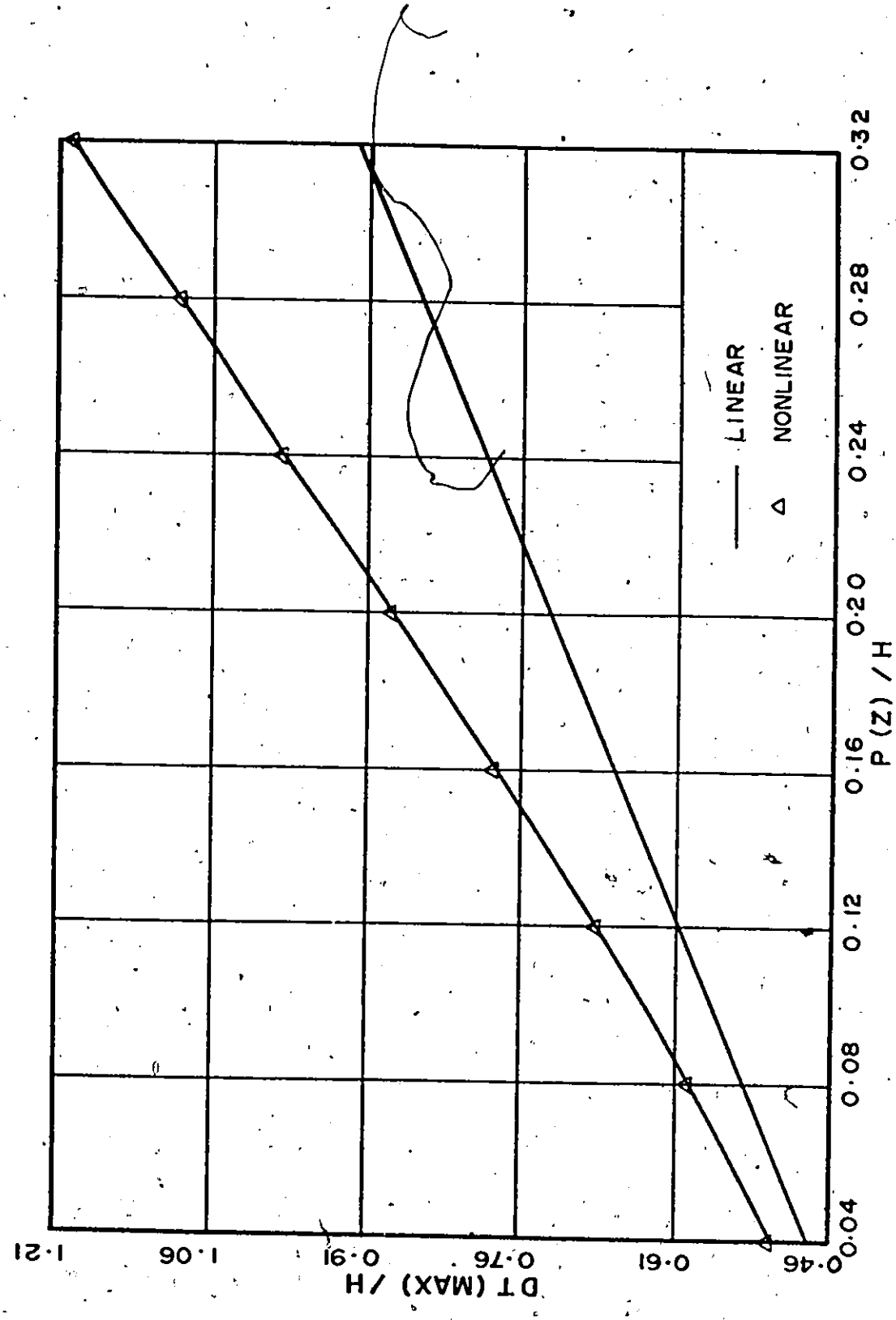

MAX TENSION INC DUE TO A CONCENTRATED LOAD
(ORTHOGONAL DOUBLE ROOF, LOADING = 2 K/J* CONC. LOAD AT JOINT 13)

Fig. (4-19)

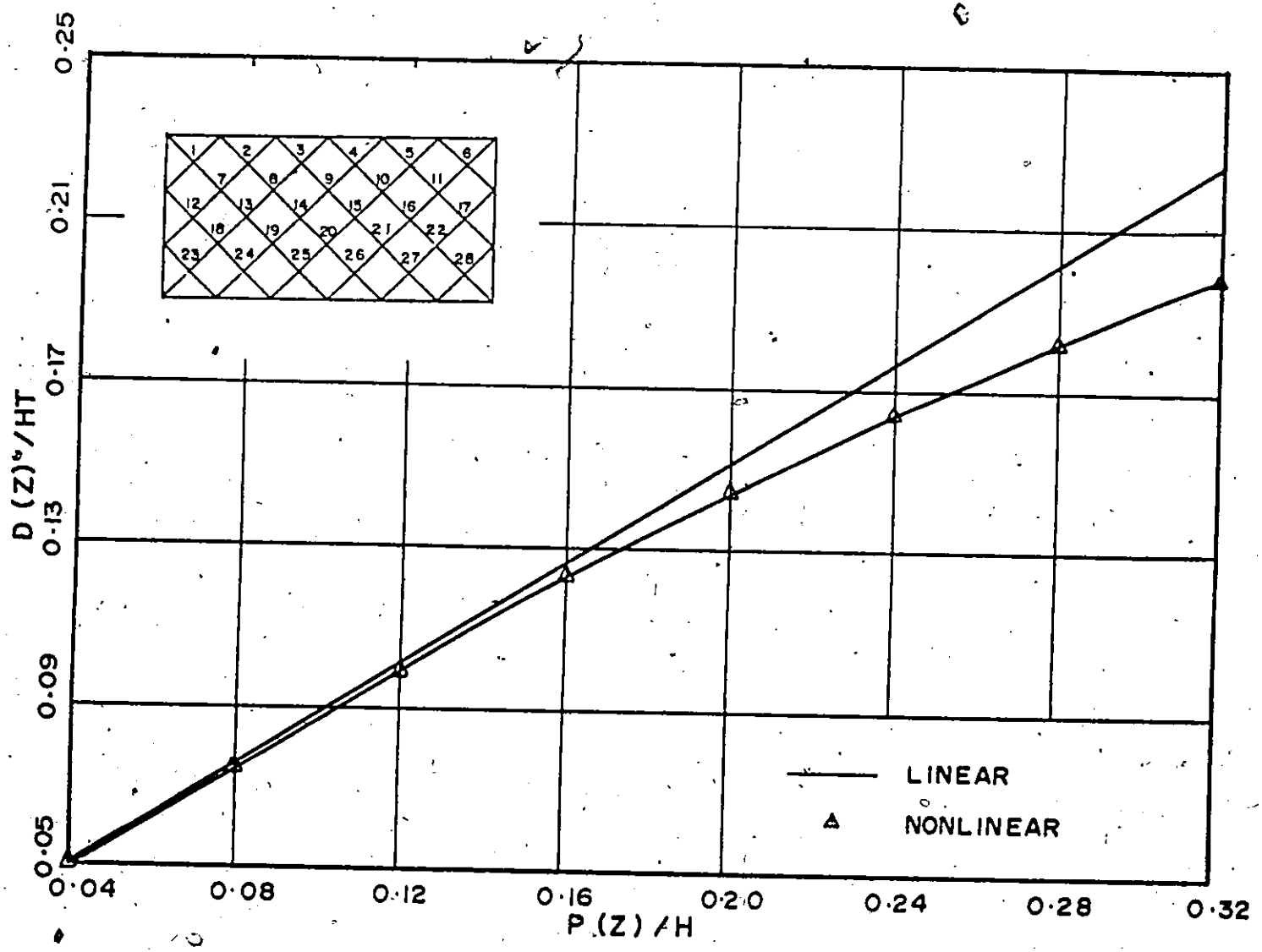

DEFLECTION AT JOINT 13 DUE TO A CONCENTRATED LOAD
(ORTHOGONAL DOUBLE ROOF. LOADING = 2 K/J+ CONC. LOAD AT JTS. 13 AND 16)
Fig. (4-20)

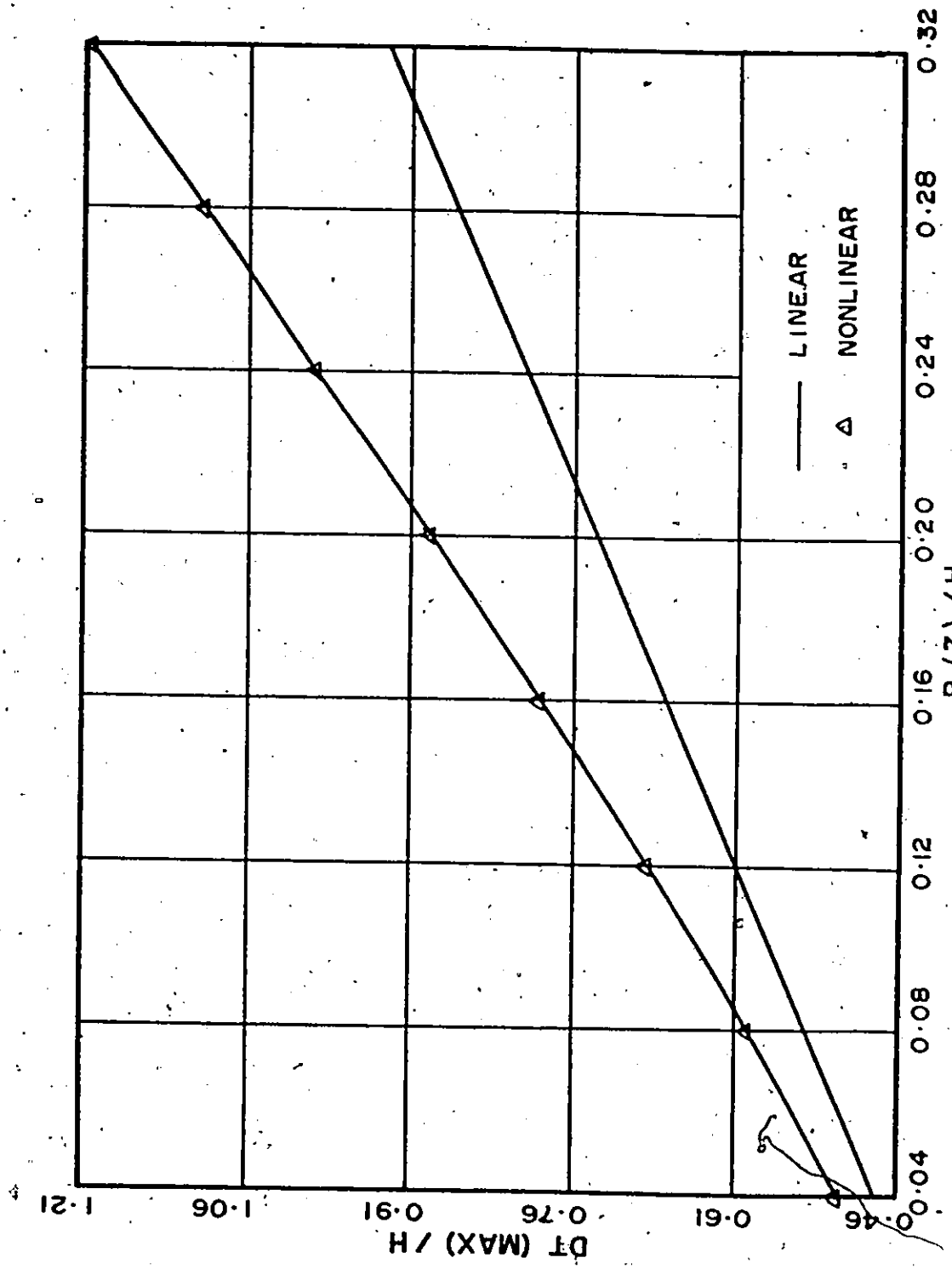

MAX TENSION INC. DUE TO A CONCENTRATED LOAD
(ORTHOGONAL DOUBLE ROOF, LOADING = 2 K/J+CONC. LOAD AT JTS. 13 AND 16)

Fig. (4-24)

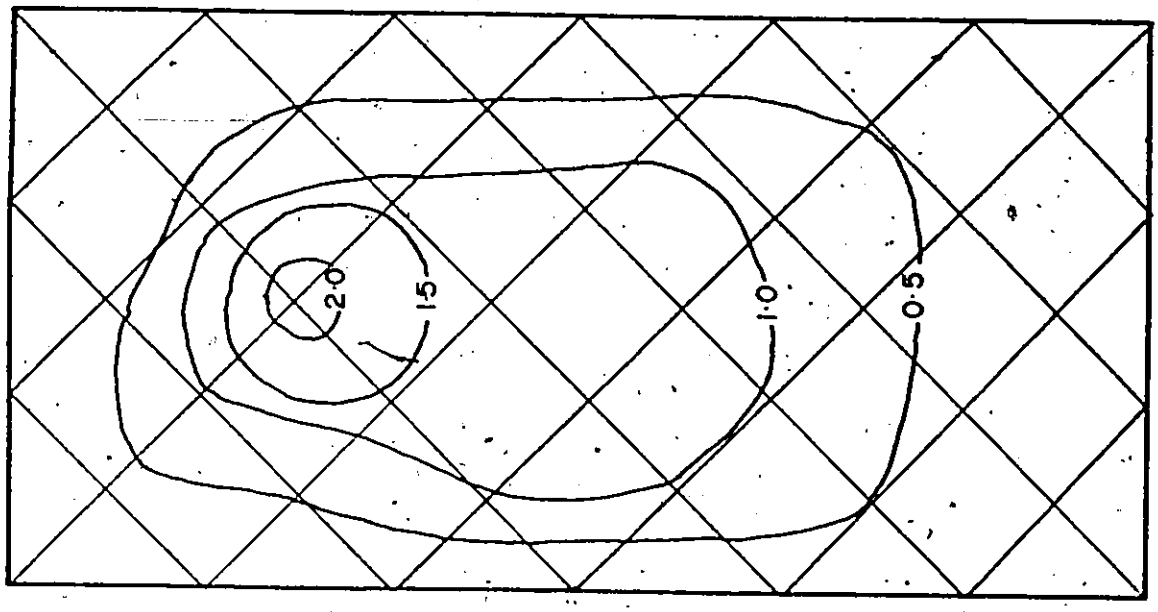

DEFLECTION CONTOURS FOR DOUBLE ROOF

(LOAD = 2 K/J+ CONC. LOAD AT JT. 13)

Fig. (4-22a)

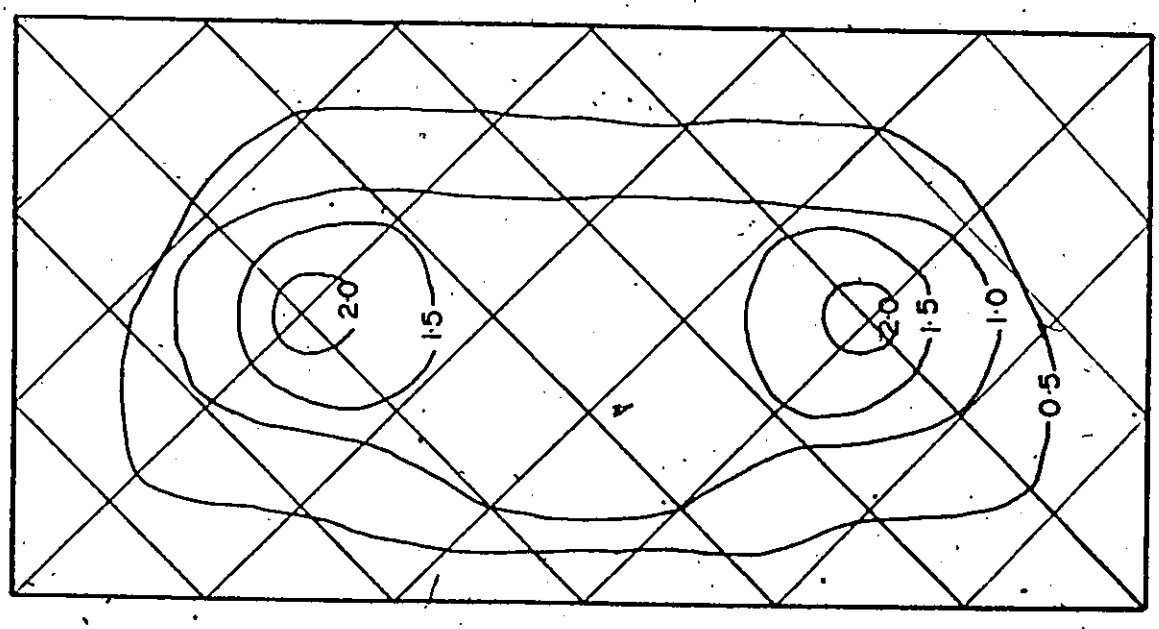

DEFLECTION CONTOURS FOR DOUBLE ROOF

(LOAD = 2 K/J+ CONC. LOAD AT JTS. 13 AND 16)

Fig. (4-22b)

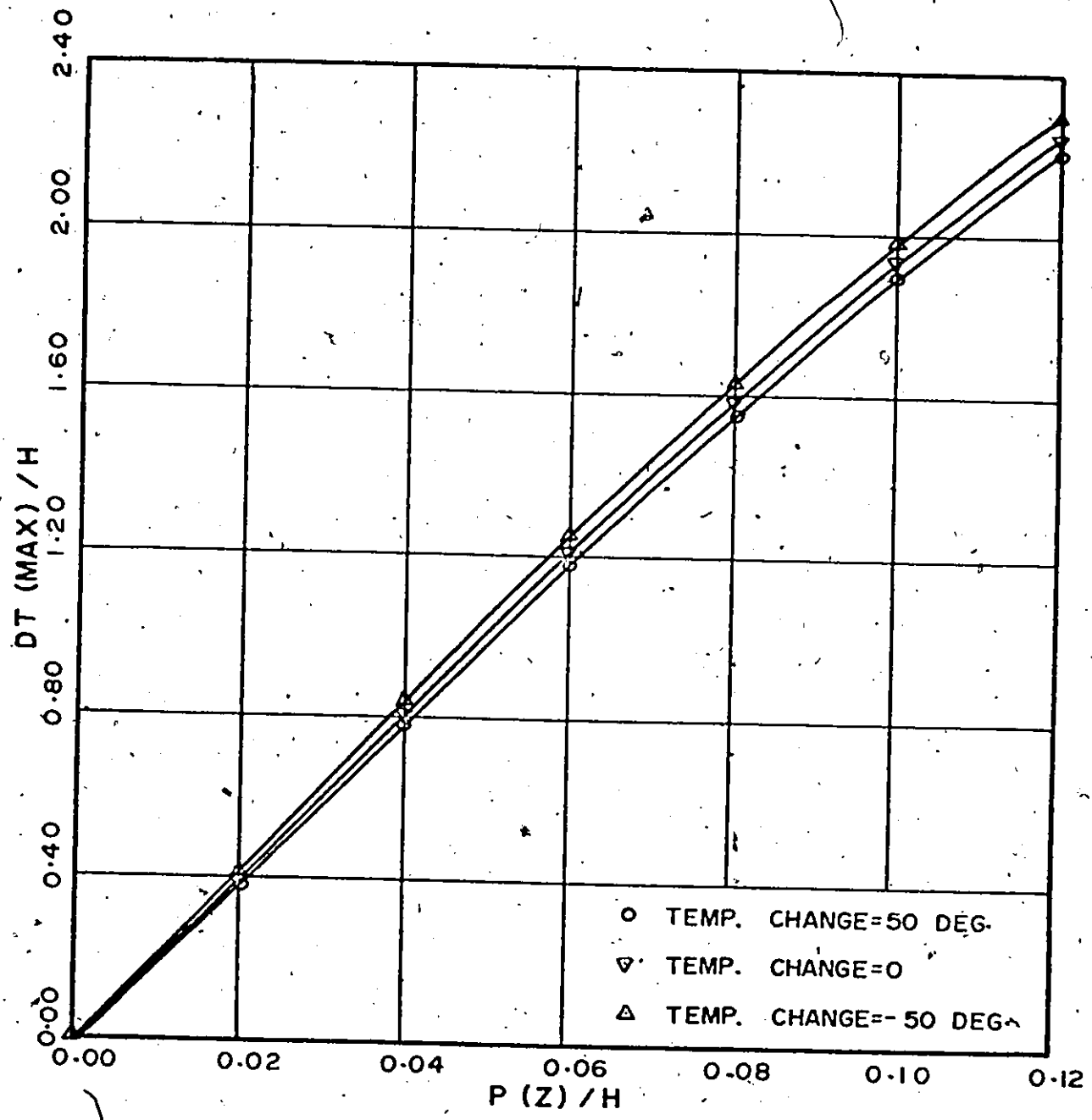

EFFECT OF TEMP. CHANGE ON TENSION INCREMENT
(NONORTHOGONAL SINGLE ROOF)

Fig. (4-23)

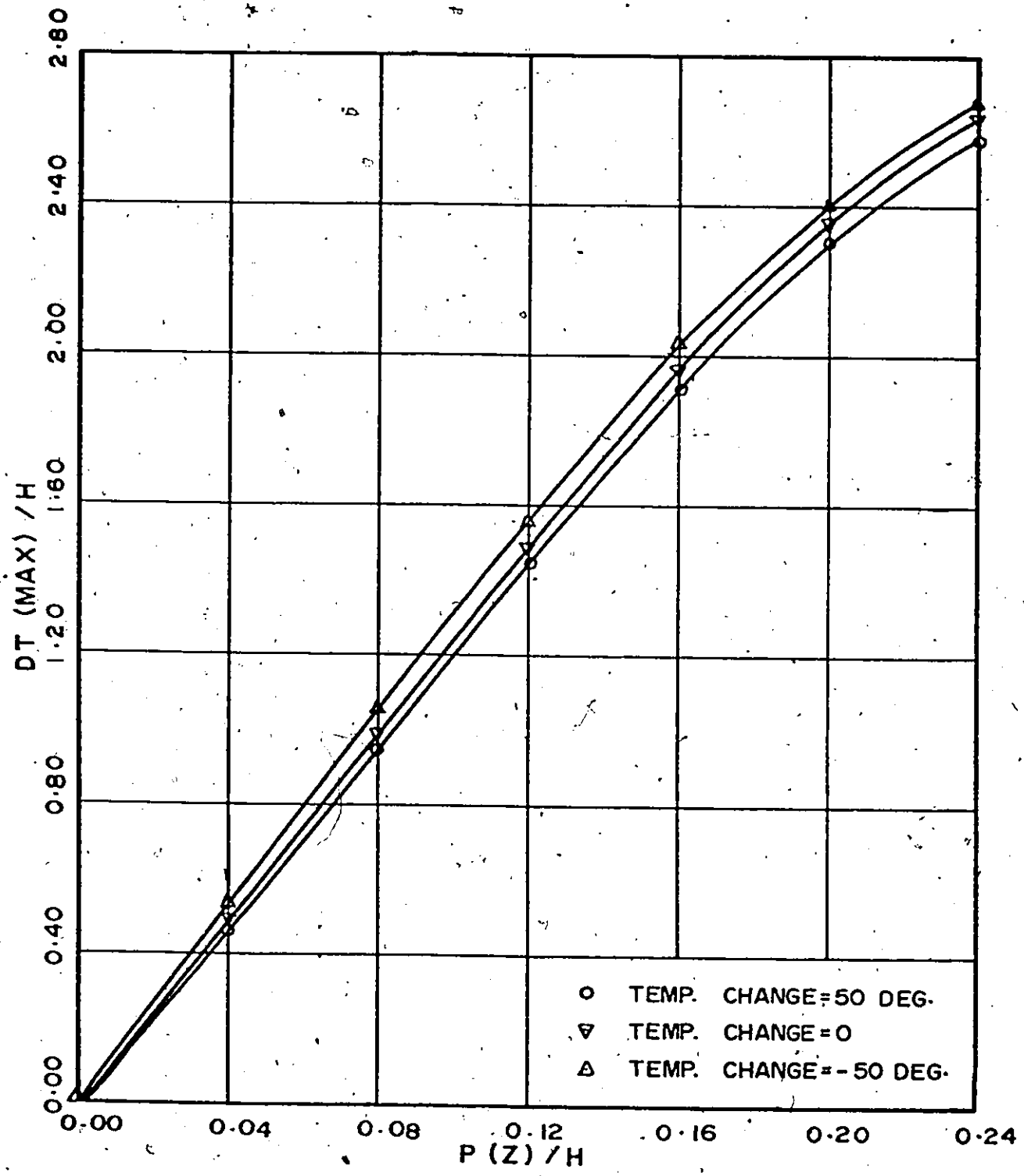

EFFECT OF TEMP. CHANGE ON TENSION INCREMENT
(ORTHOGONAL DOUBLE ROOF)

Fig. (4-24)

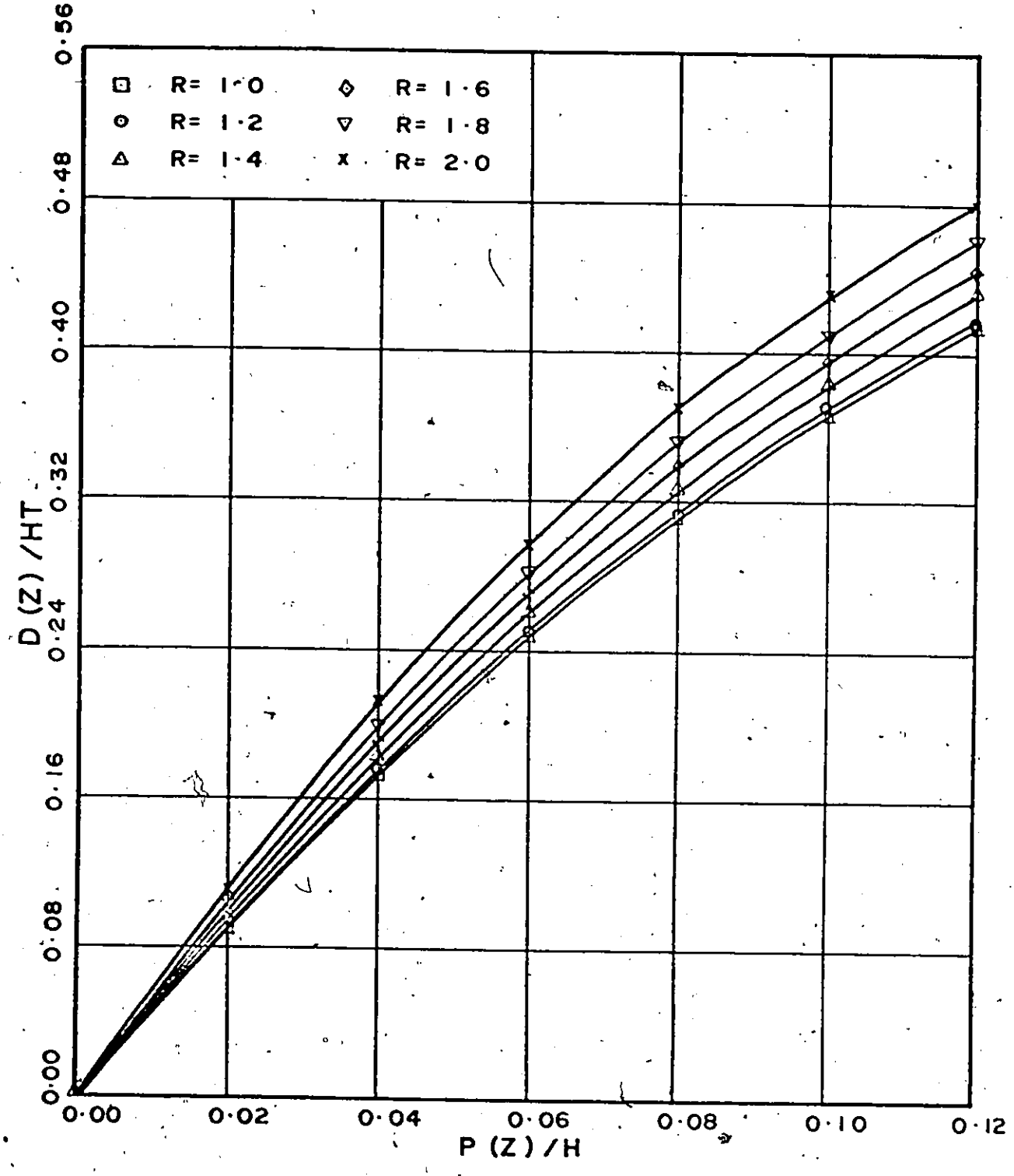

MAX. DEFLECTION VS LOAD-EFFECT OF CHANGING R
(NONORTHOGONAL SINGLE ROOF)

Fig. (4-25)

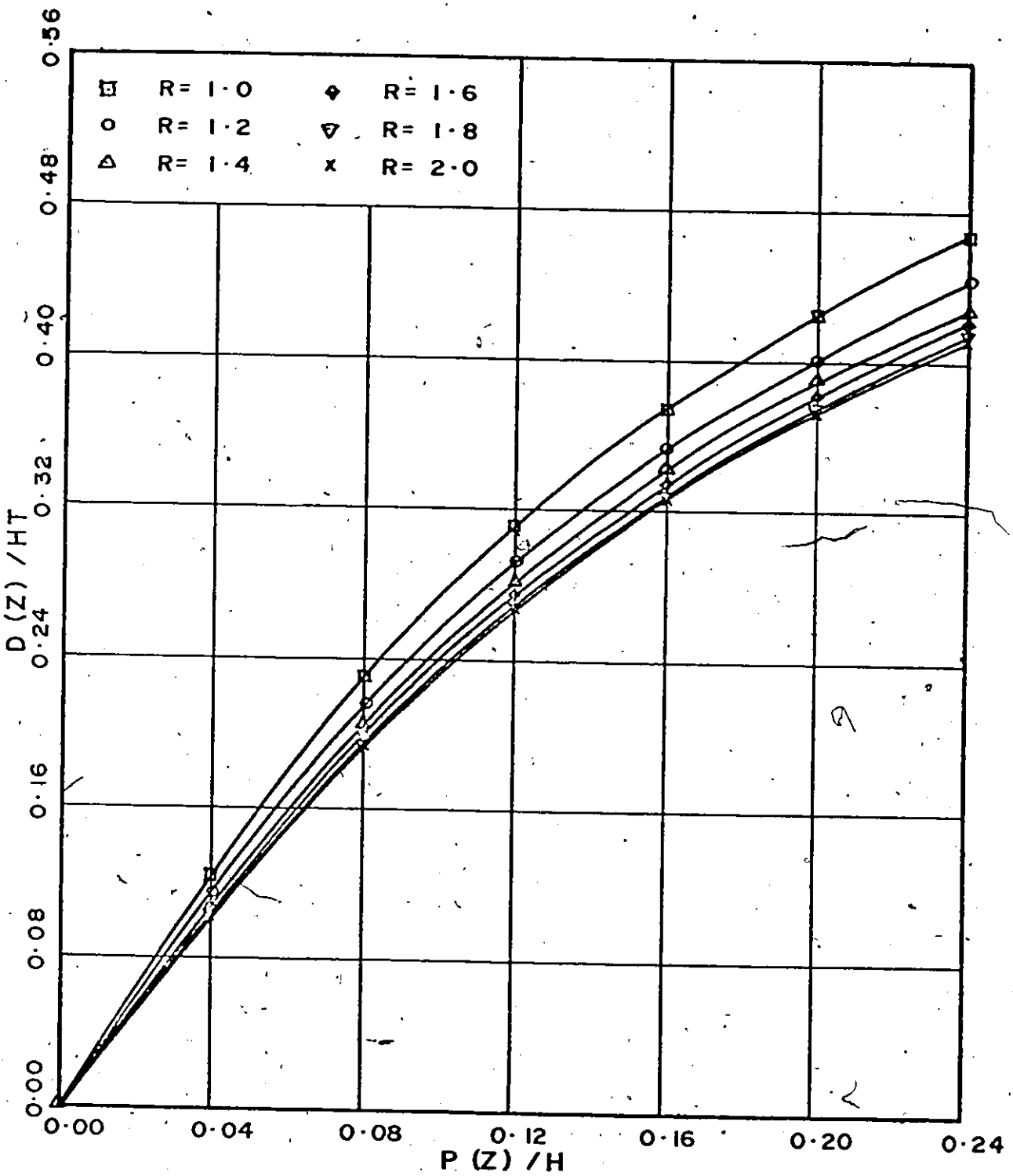

MAX· DEFLECTION VS LOAD-EFFECT OF CHANGING R
(ORTHOGONAL DOUBLE ROOF)

Fig· (4-26)

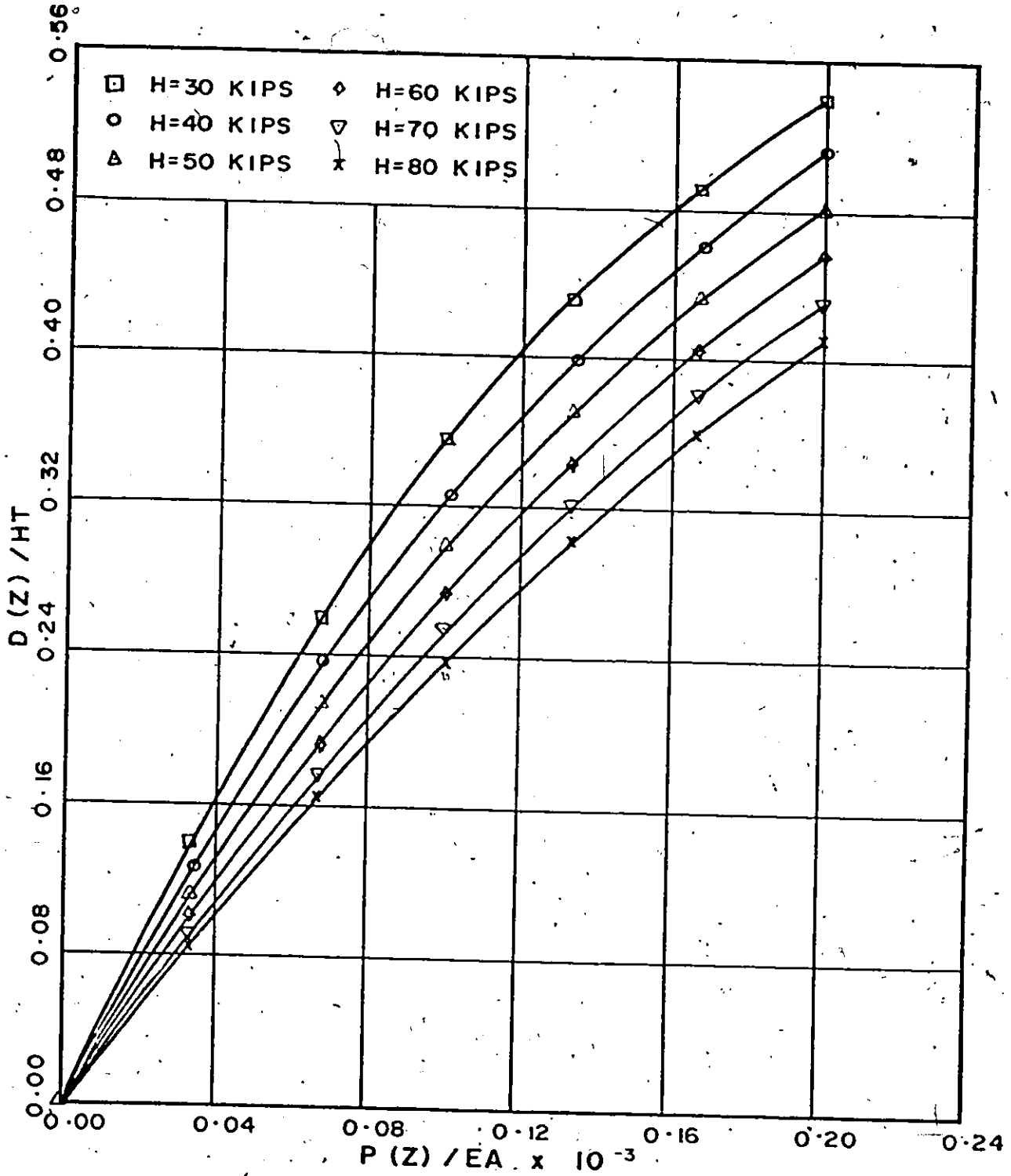

MAX. DEFLECTION VS LOAD-EFFECT OF CHANGING H
(NONORTHOGONAL SINGLE ROOF)

Fig. (4-27)

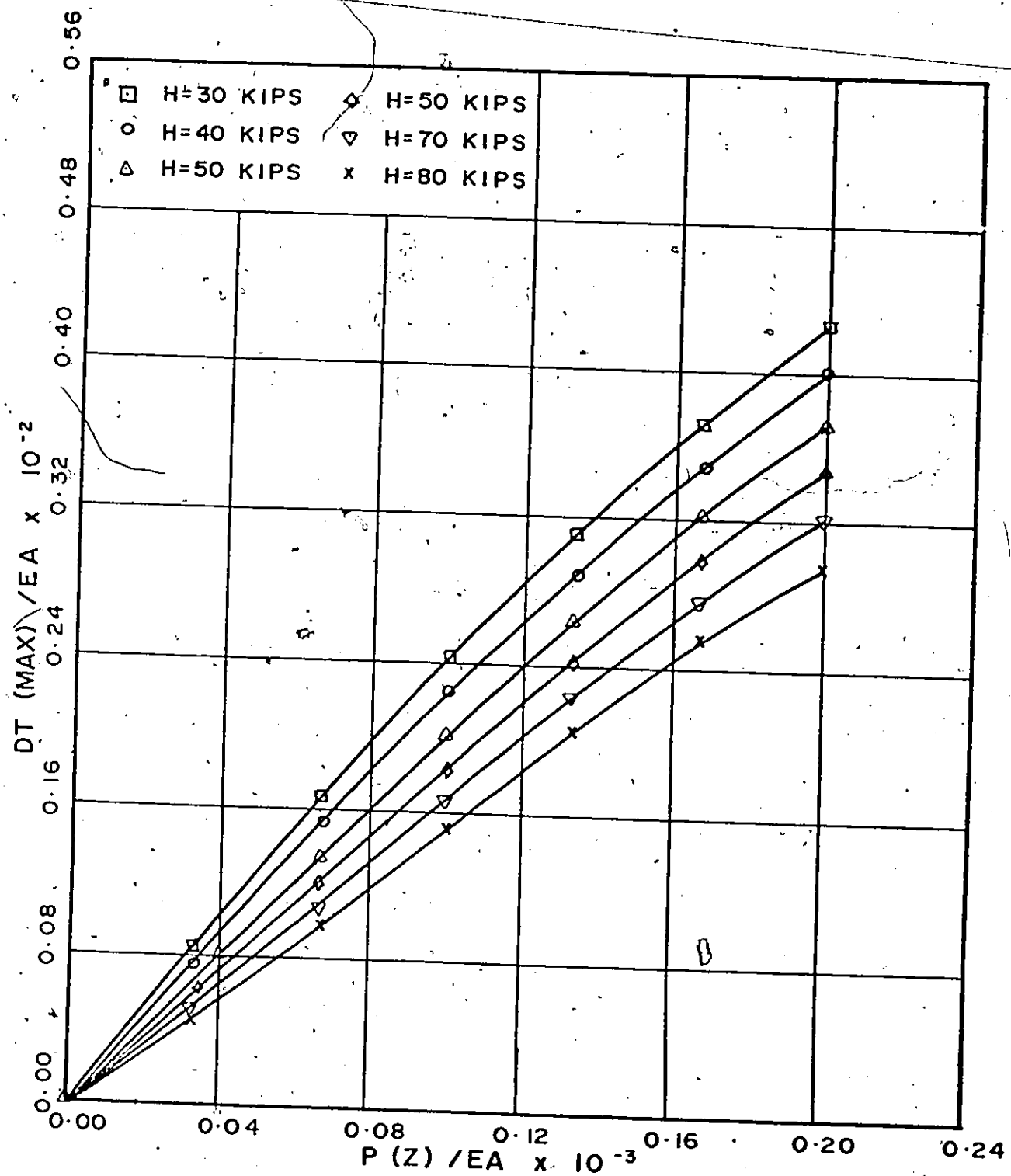

MAX. TENSION INC. VS LOAD-EFFECT OF CHANGING H
(NONORTHOGONAL SINGLE ROOF)

Fig. (4-28)

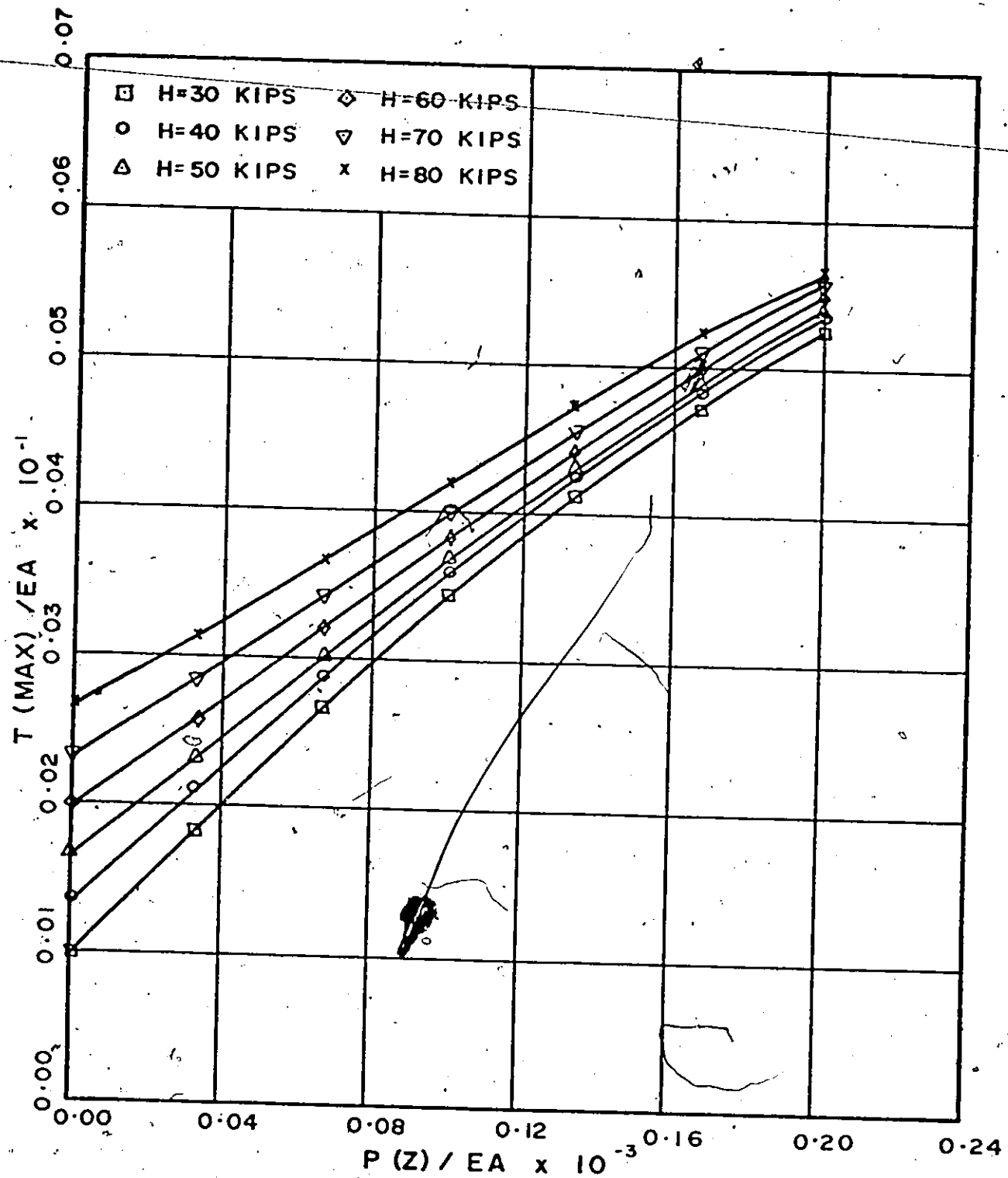

MAX. TENSION VS LOAD-EFFECT OF CHANGING H
(NONORTHOGONAL SINGLE ROOF)

Fig. (4-29)

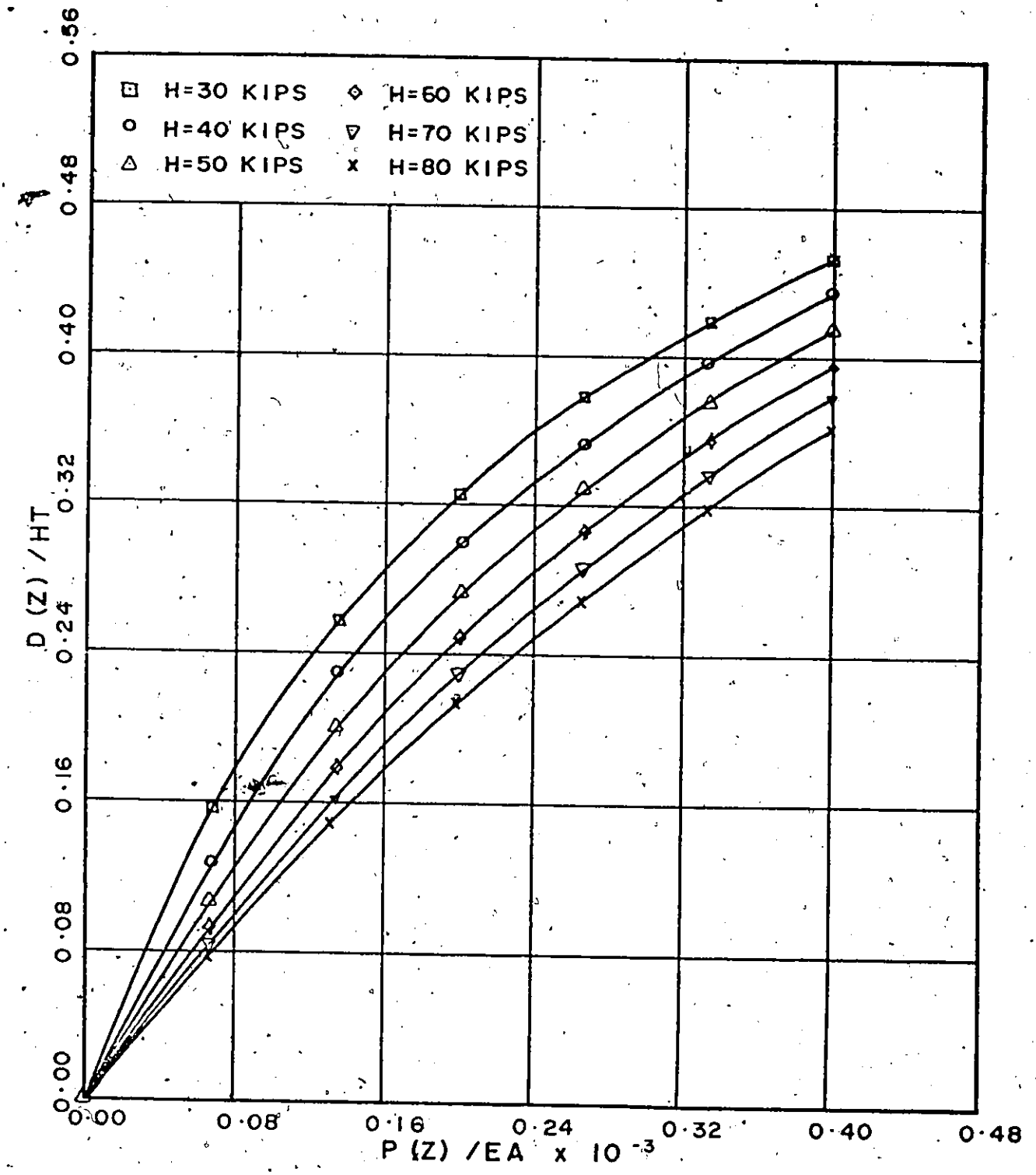

MAX. DEFLECTION VS LOAD-EFFECT OF CHANGING H
(ORTHOGONAL DOUBLE ROOF)

Fig. (4-30)

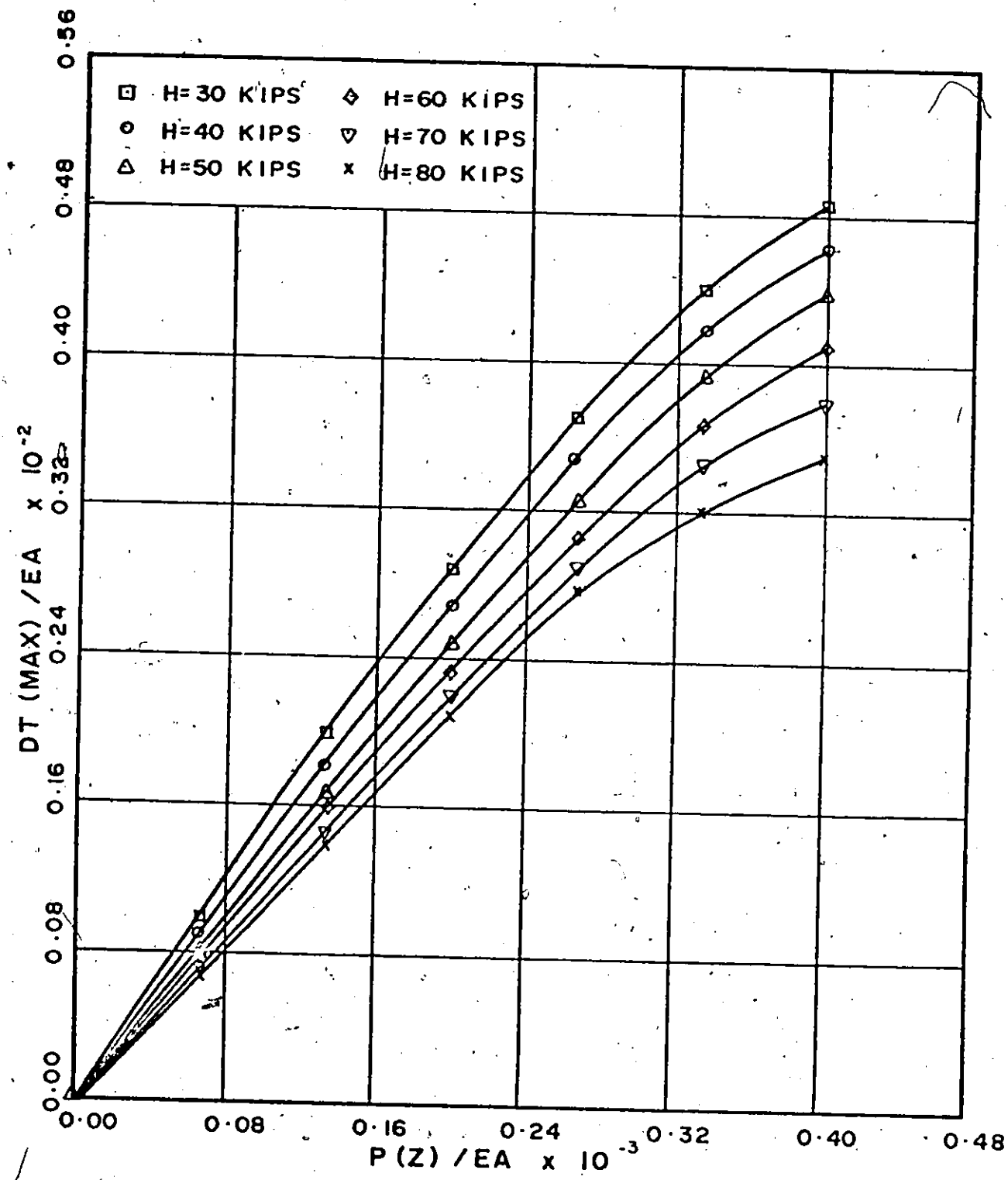

MAX. TENSION INC. VS LOAD-EFFECT OF CHANGING H
(ORTHOGONAL DOUBLE ROOF)

Fig. (4-31)

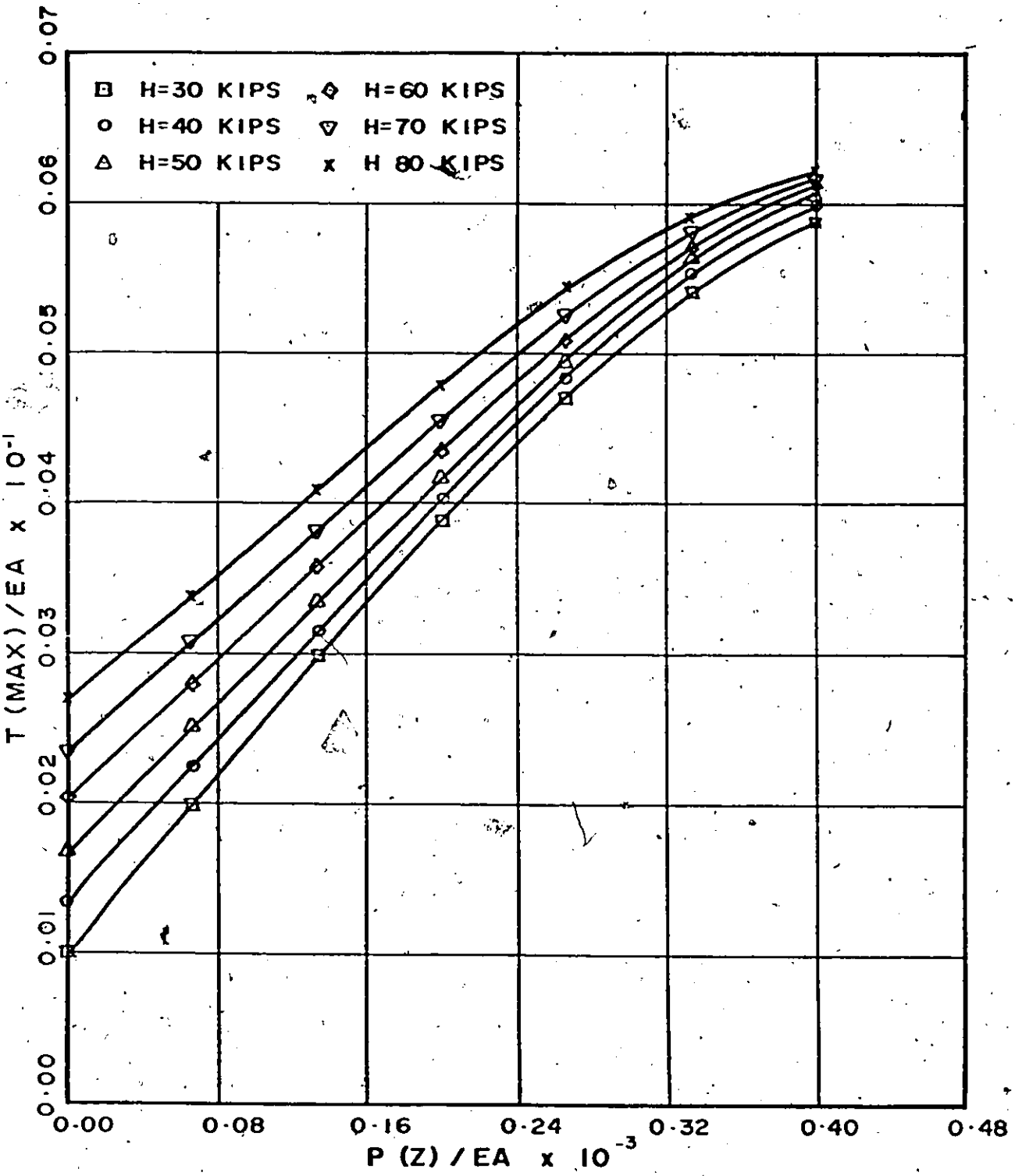

MAX. TENSION VS LOAD-EFFECT OF CHANGING H
(ORTHOGONAL DOUBLE ROOF)

Fig. (4-32)

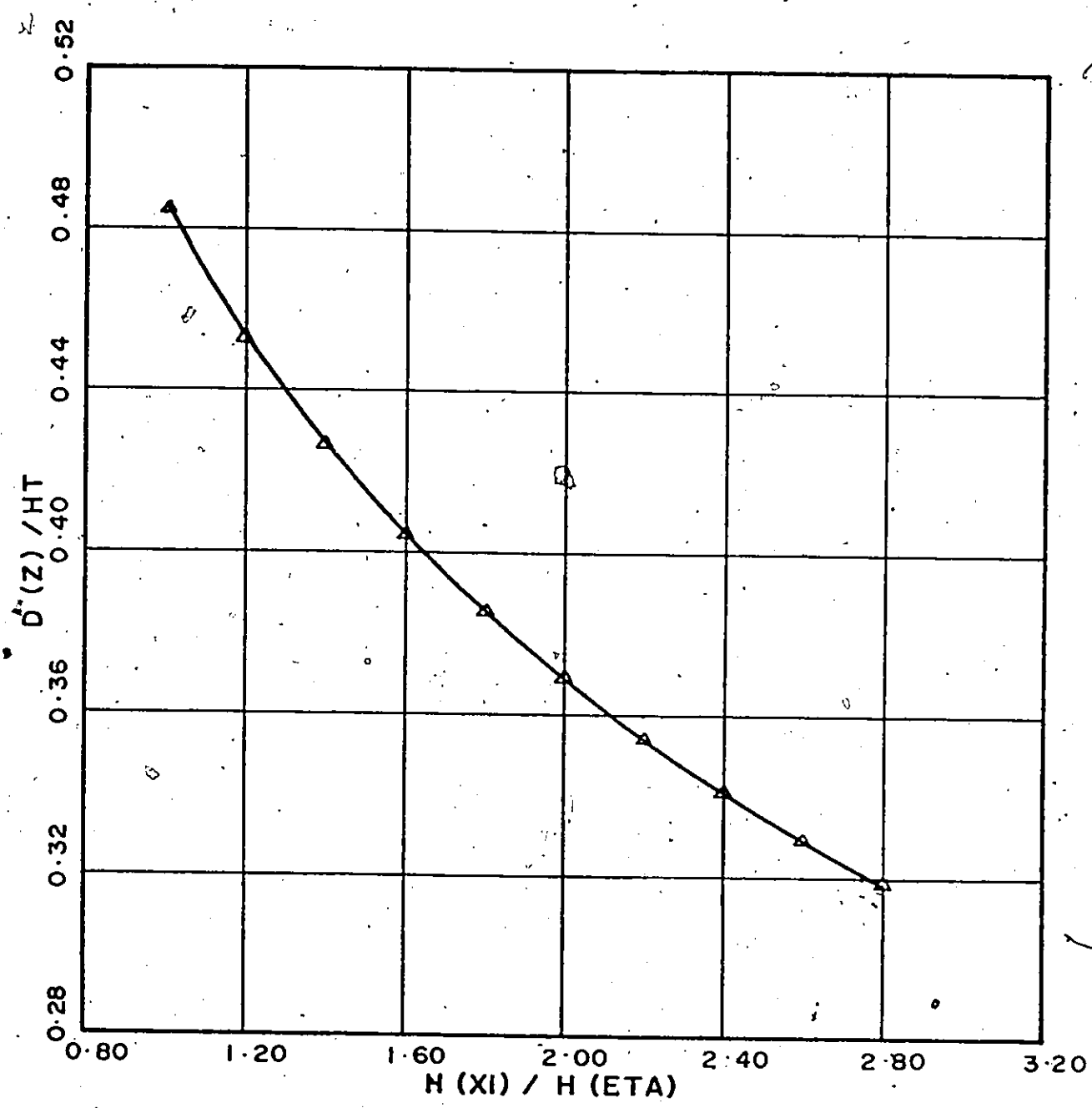

MAX. DEFLECTION VS PRETENSION IN XI DIRECTION
(NONORTHOGONAL SINGLE ROOF. H (ETA) = 50 KIPS.)

Fig. (4-33)

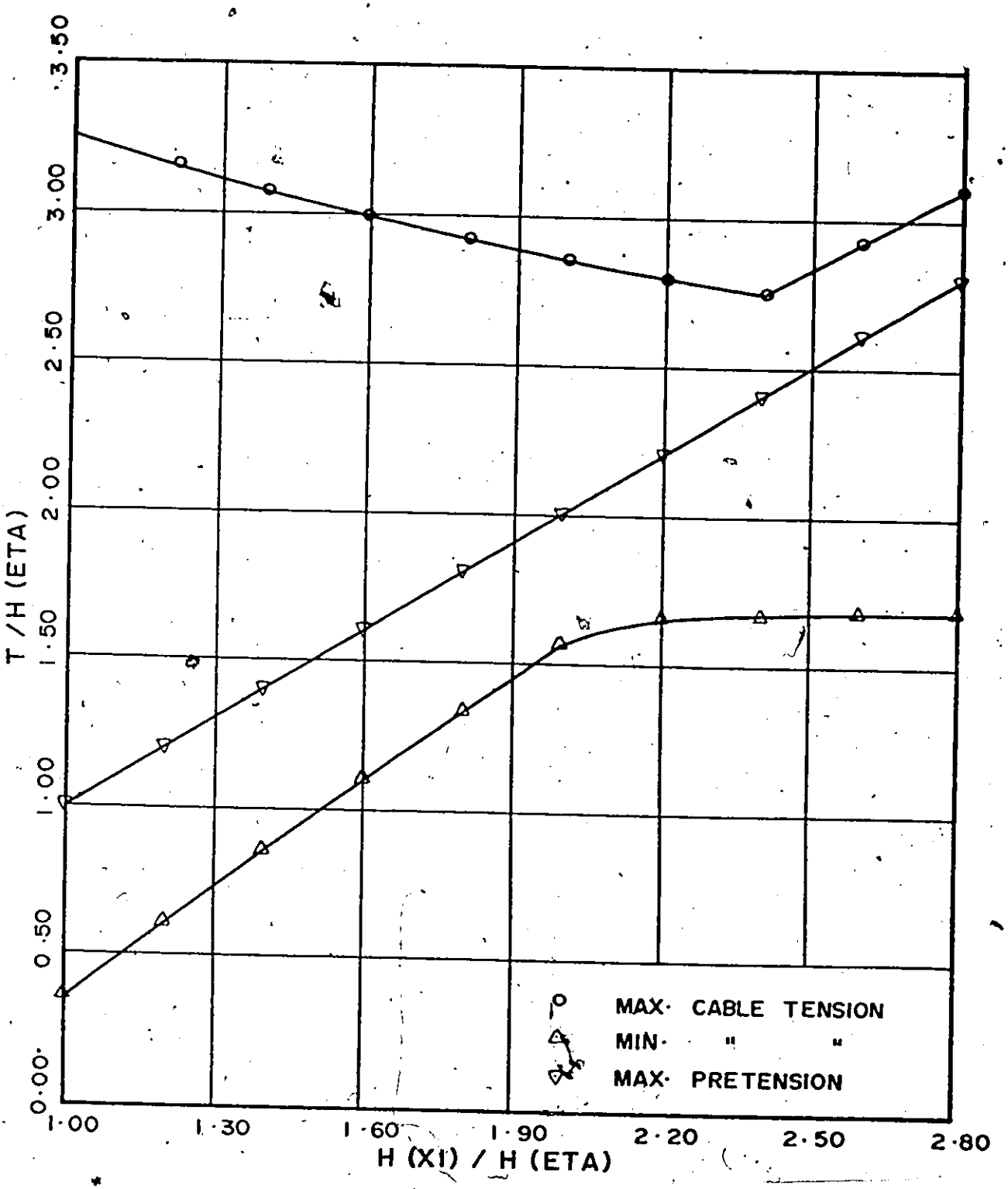

CABLE TENSION VS PRETENSION IN XI DIRECTION
(NONORTHOGONAL SINGLE ROOF. H (ETA) = 50 KIPS)

Fig. (4 - 34)

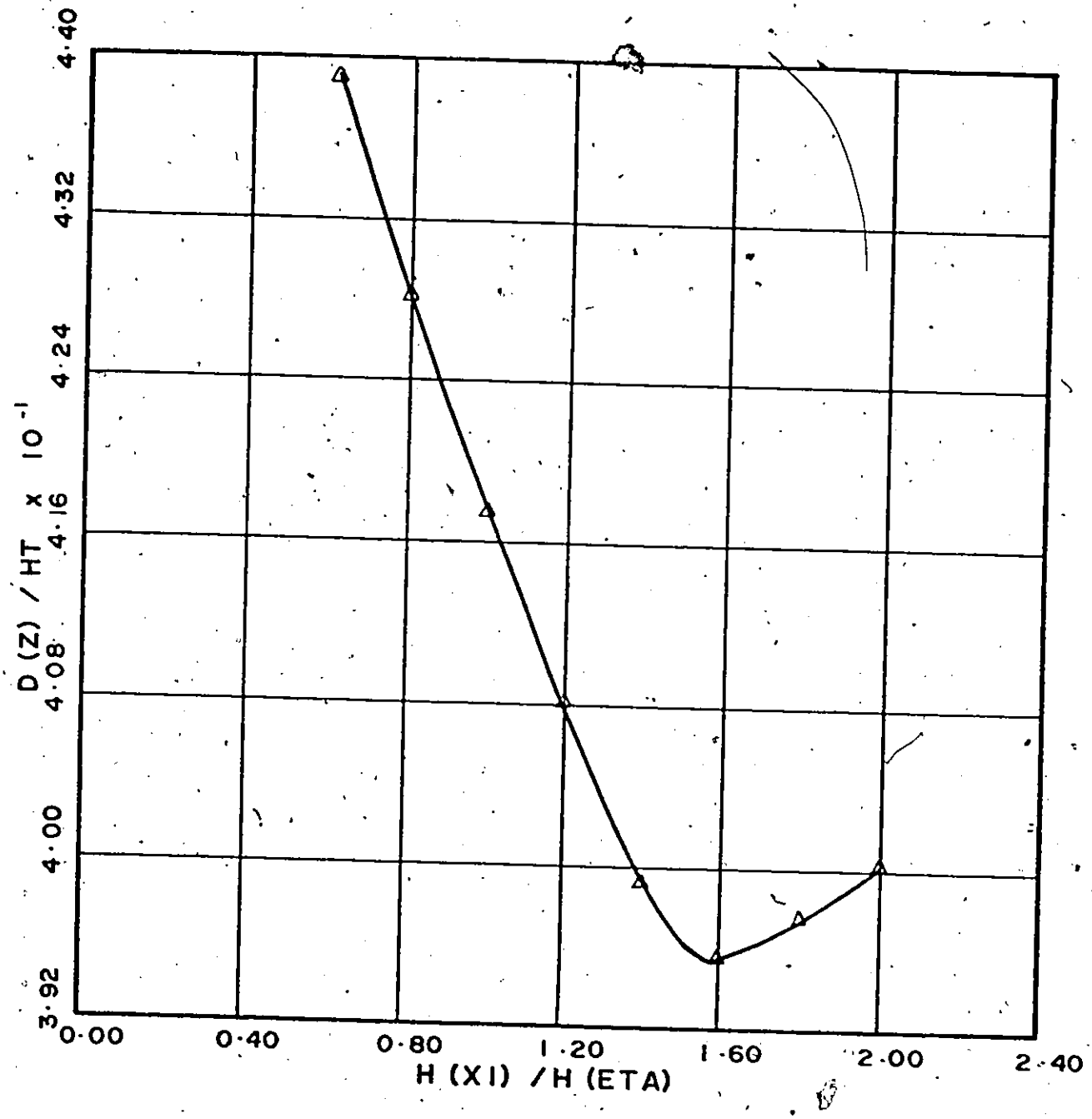

MAX. DEFLECTION VS PRETENSION IN XI DIRECTION
(ORTHOGONAL DOUBLE ROOF. H (ETA) = 50 KIPS)

Fig. (4-35)

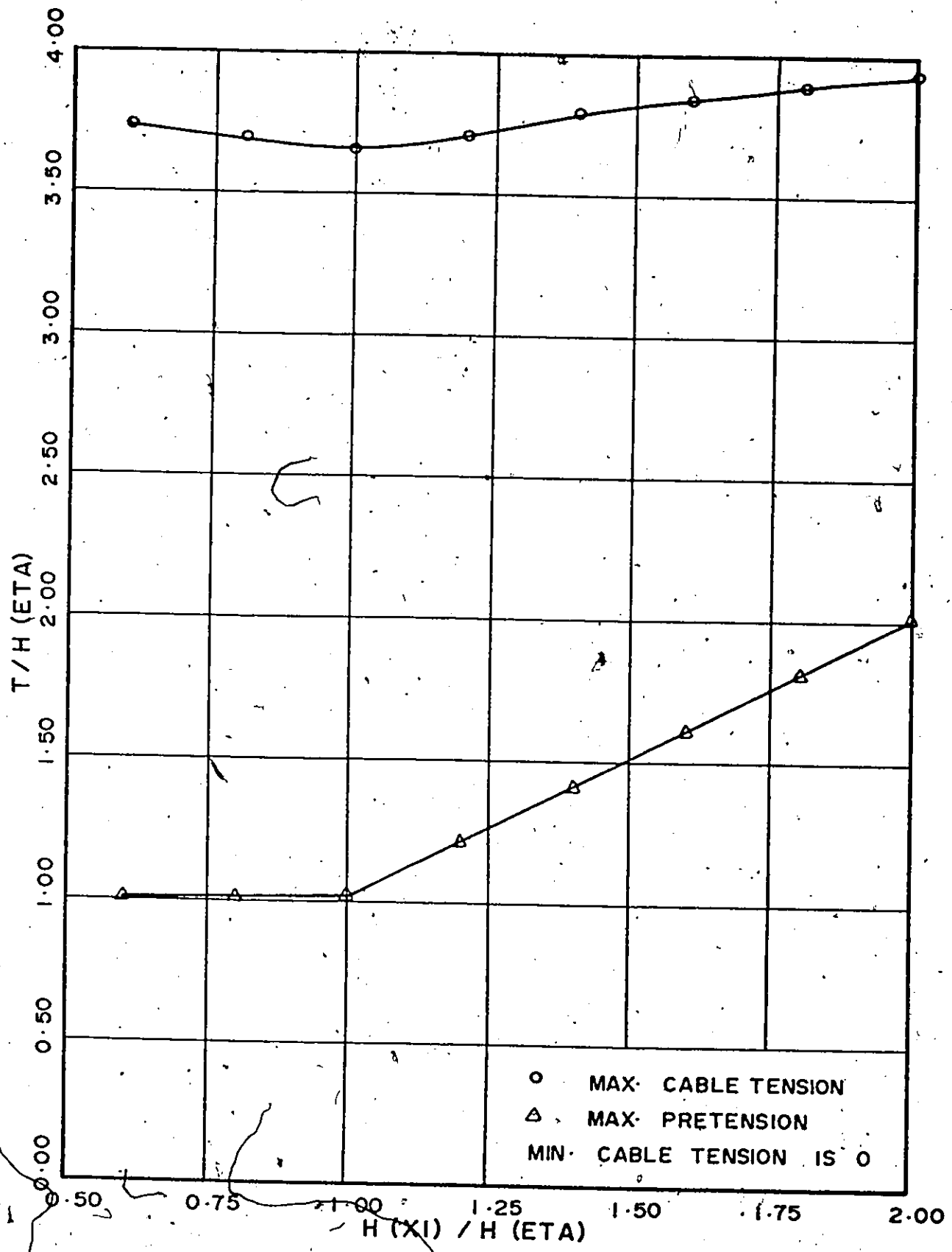

CABLE TENSION VS PRETENSION IN XI DIRECTION

(ORTHOGONAL DOUBLE ROOF· H(ETA)=50 KIPS)

Fig· (4-36)

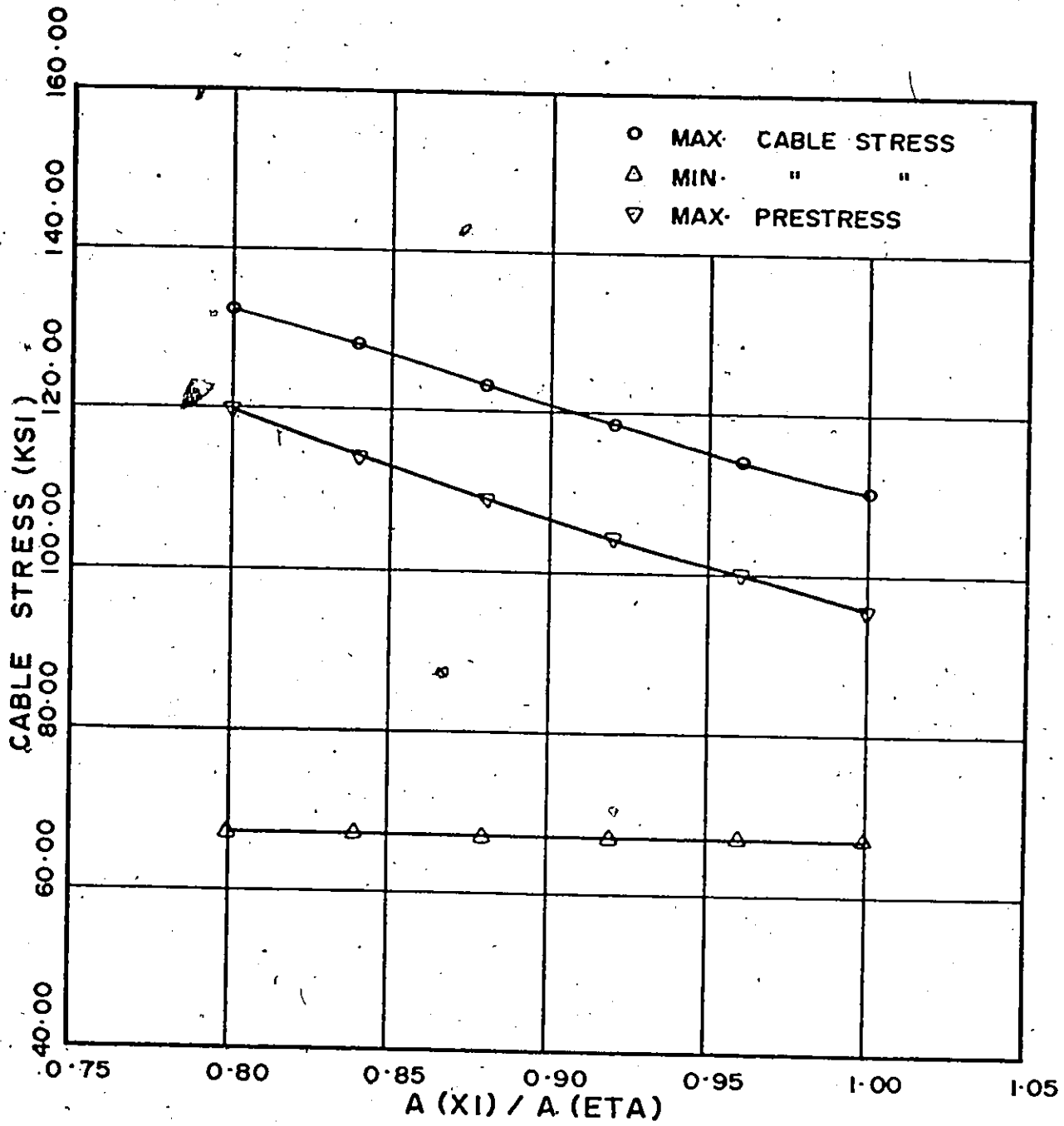

CABLE STRESS - VARIATION WITH A(XI)
(NONORTHOGONAL SINGLE ROOF)

(H (XI) = 120 K. H(ETA) = 50 K. A (ETA) = 1.25 SQ. IN)

Fig. (4-37)

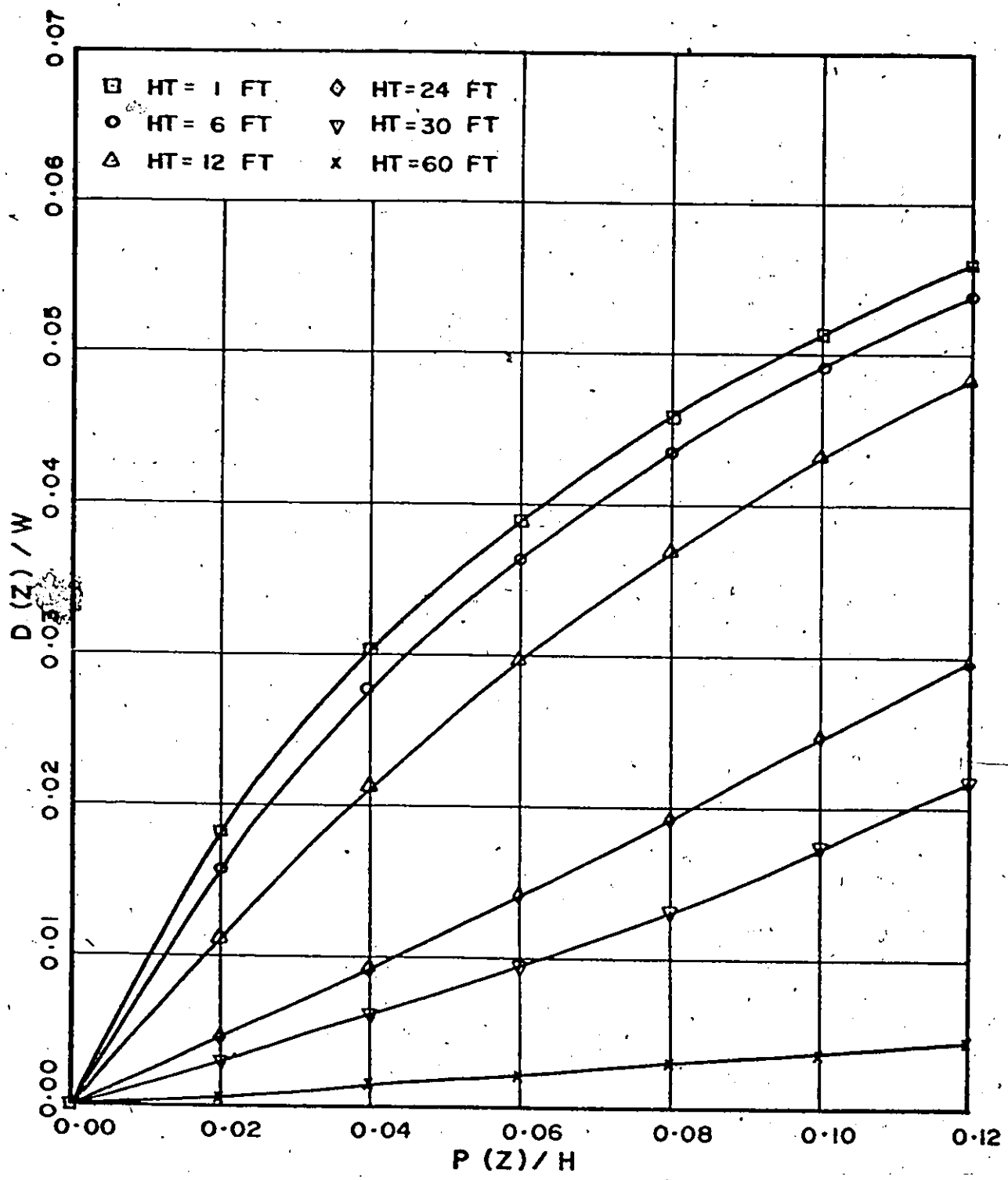

MAX. DEFLECTION VS LOAD - EFFECT OF CHANGING HT
(NONORTHOGONAL SINGLE ROOF)

Fig. (4 - 38)

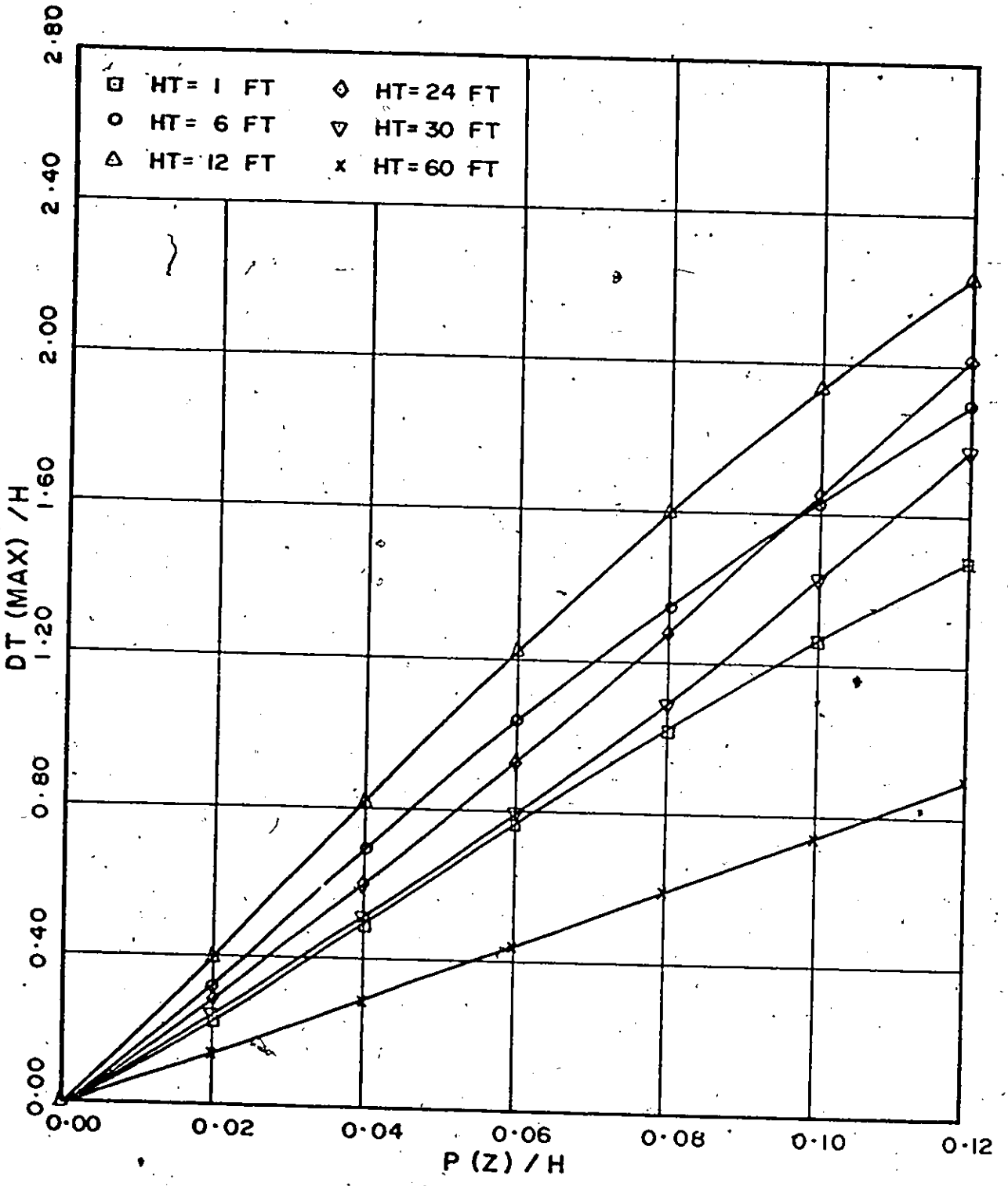

MAX. TENSION INC. VS LOAD-EFFECT OF CHANGING HT
(NONORTHOGONAL SINGLE ROOF)

Fig. (4-39)

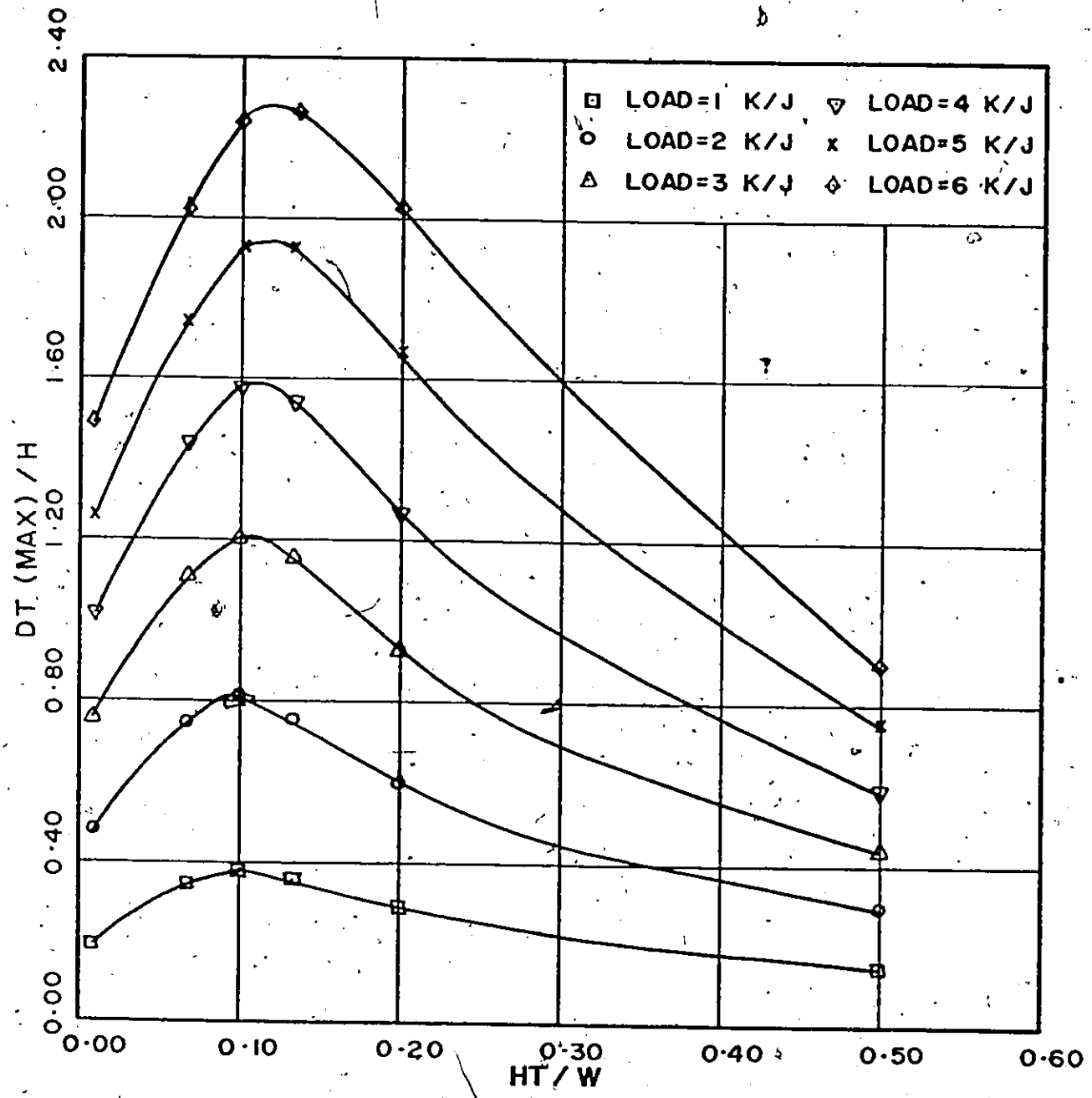

VARIATION OF MAX. TENSION INC. WITH ROOF HT.
(NONORTHOGONAL SINGLE ROOF)

Fig. (4-40)

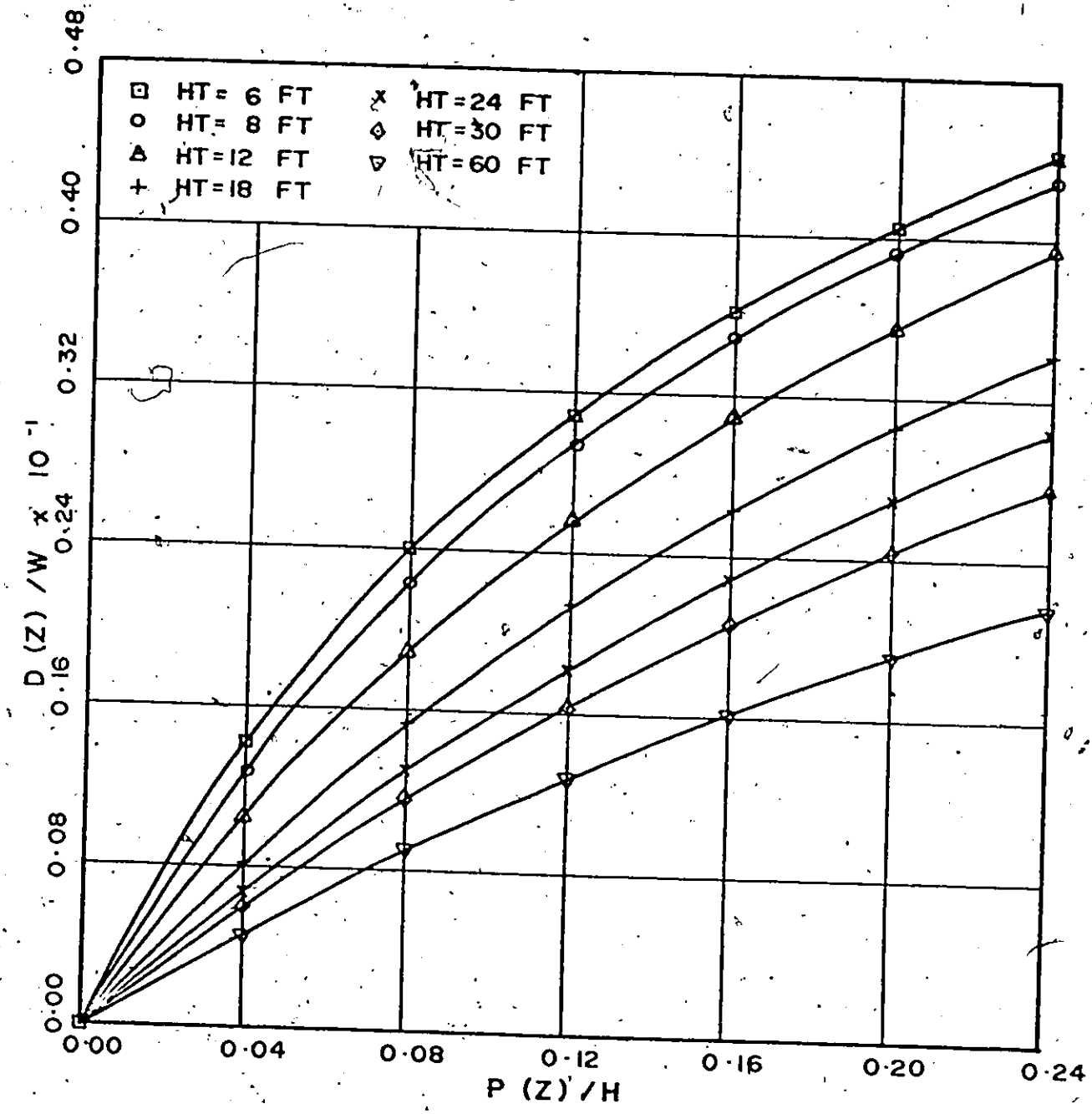

MAX. DEFLECTION VS LOAD - EFFECT OF CHANGING HT
(ORTHOGONAL DOUBLE ROOF)

Fig. (4-41)

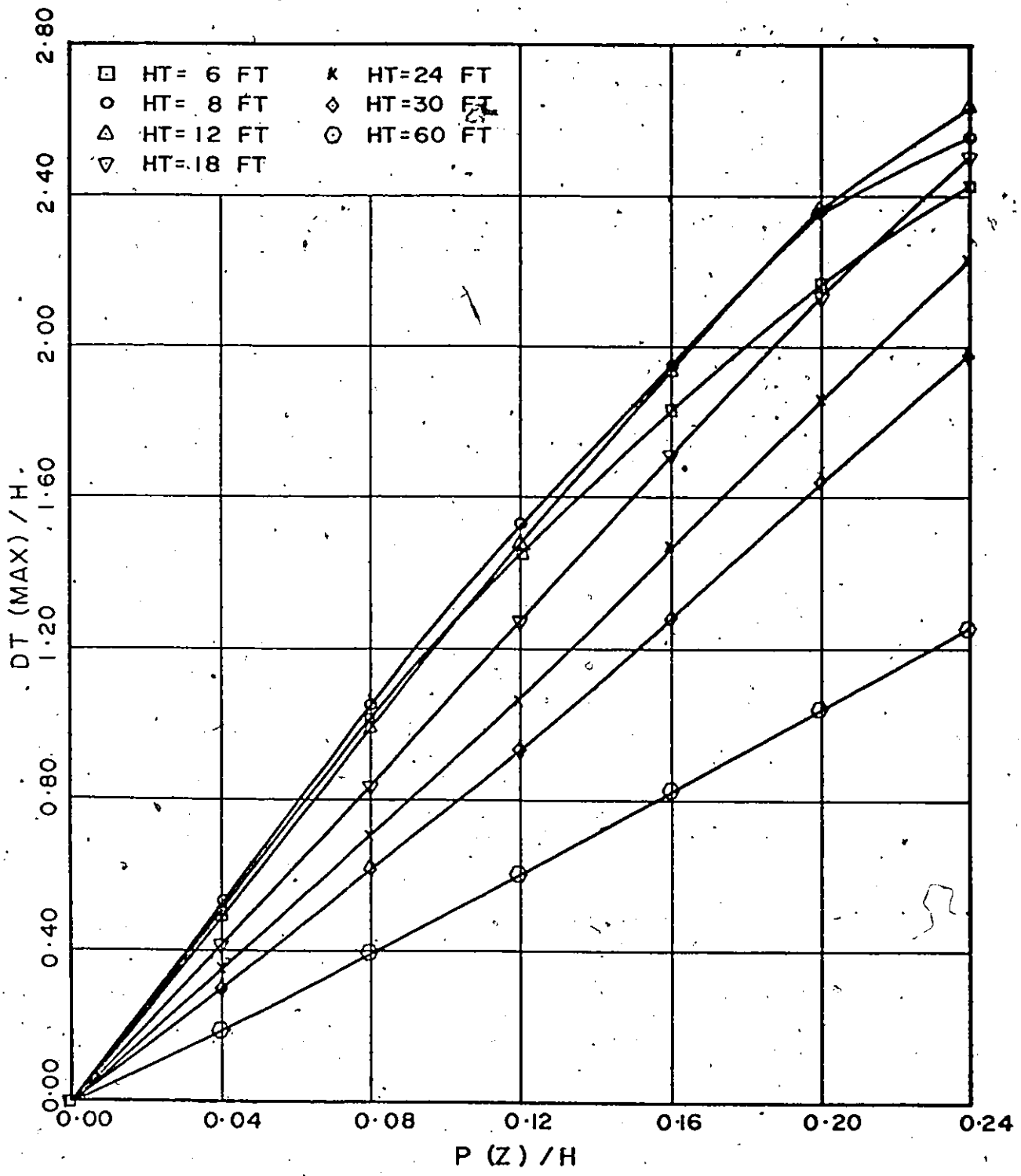

MAX· TENSION INC· VS LOAD-EFFECT OF CHANGING HT
(ORTHOGONAL DOUBLE ROOF)

Fig· (4-42)

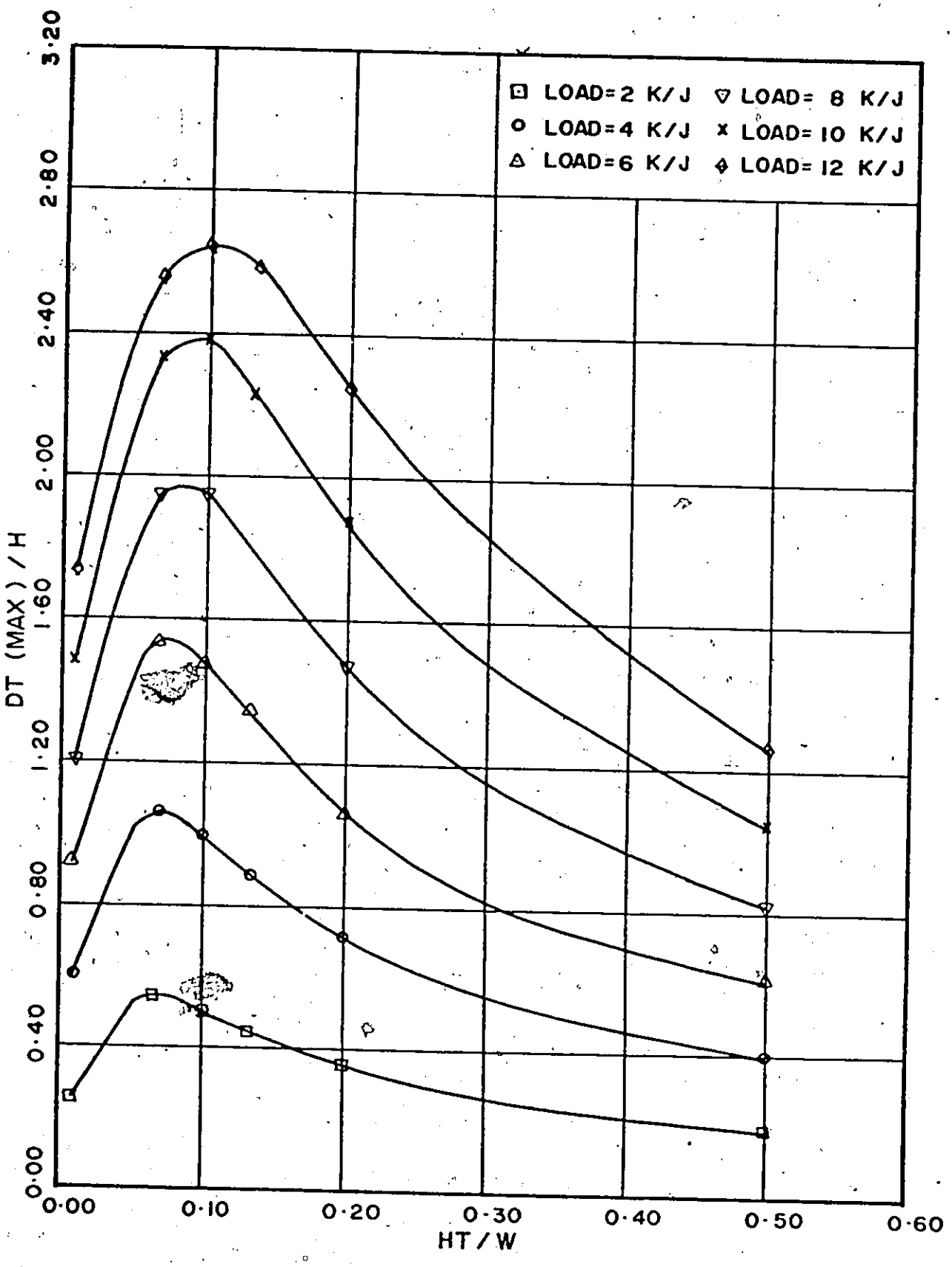

VARIATION OF MAX· TENSION INC· WITH ROOF HT·
(ORTHOGONAL DOUBLE ROOF)

Fig· (4 - 43)

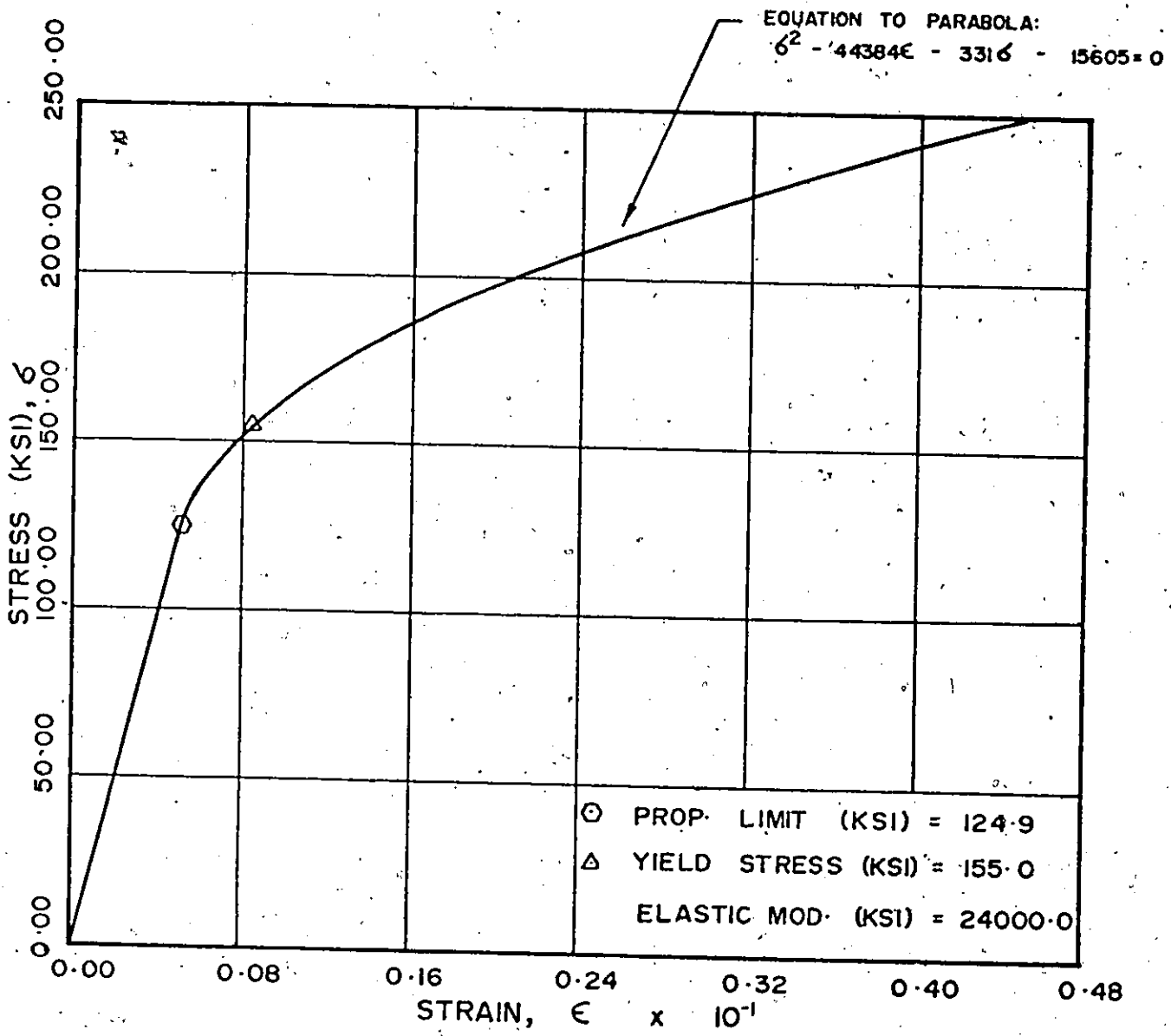

STRESS-STRAIN CURVE FOR CABLE

Fig· (4 - 44)

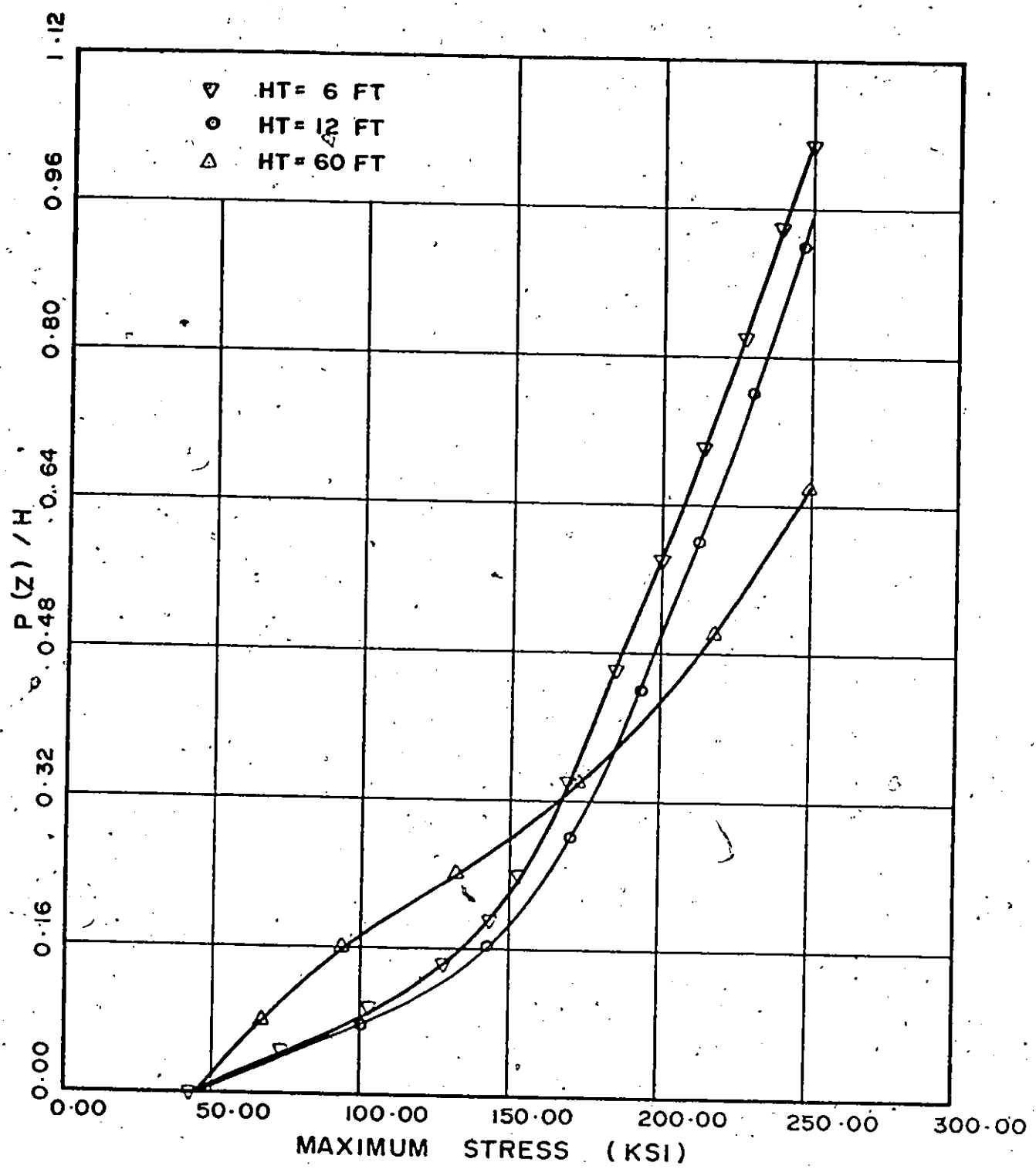

INELASTIC VARIATION OF MAXIMUM TENSION
(NONORTHOGONAL SINGLE ROOF)

Fig. (4-45)

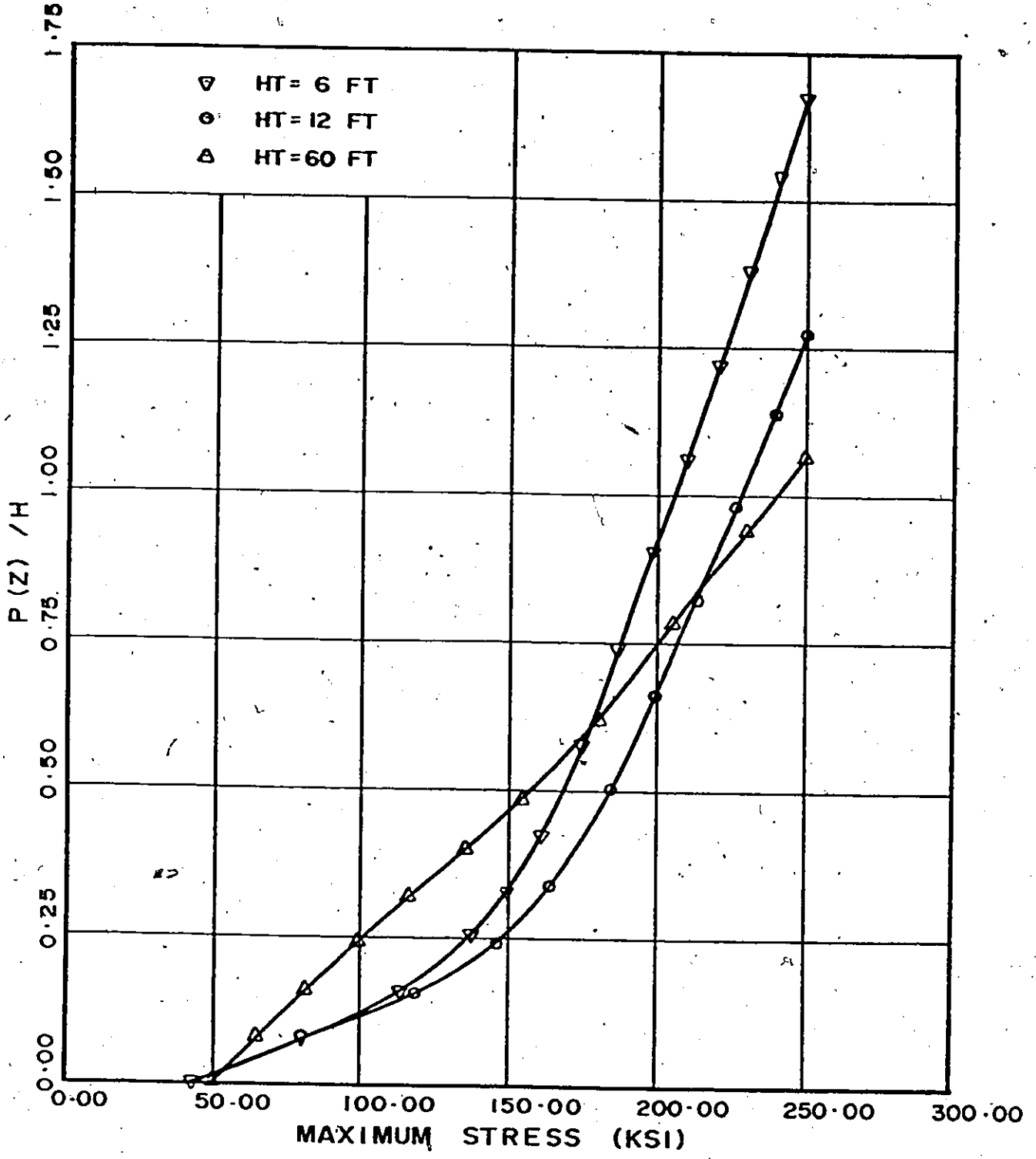

INELASTIC VARIATION OF MAXIMUM TENSION
(ORTHOGONAL DOUBLE ROOF)

Fig· (4 - 46)

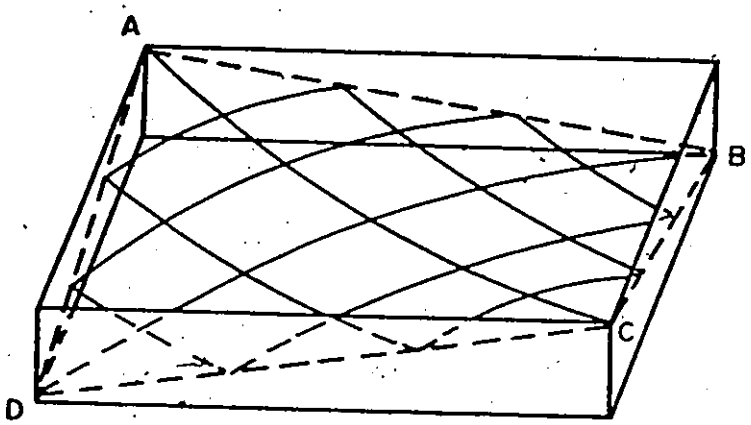

ISOMETRIC VIEW OF SINGLE ROOF MODEL

Fig. (5-1a)

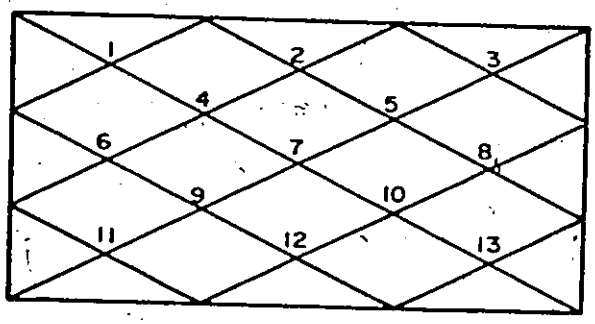

PLAN OF SINGLE ROOF MODEL

Fig. (5-1b)

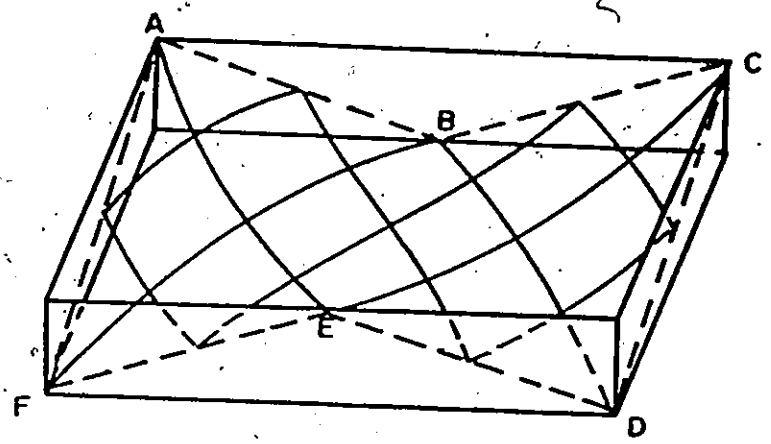

ISOMETRIC VIEW OF DOUBLE ROOF MODEL

Fig- (5-2a)

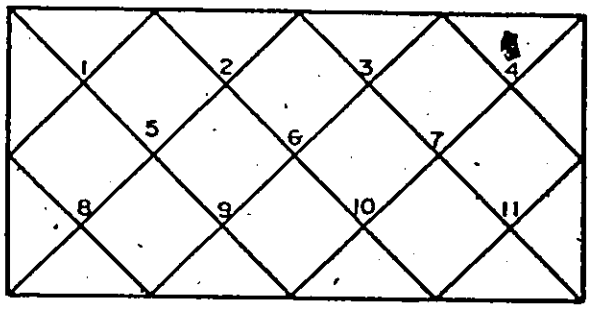

PLAN OF DOUBLE ROOF MODEL

Fig- (5-2b)

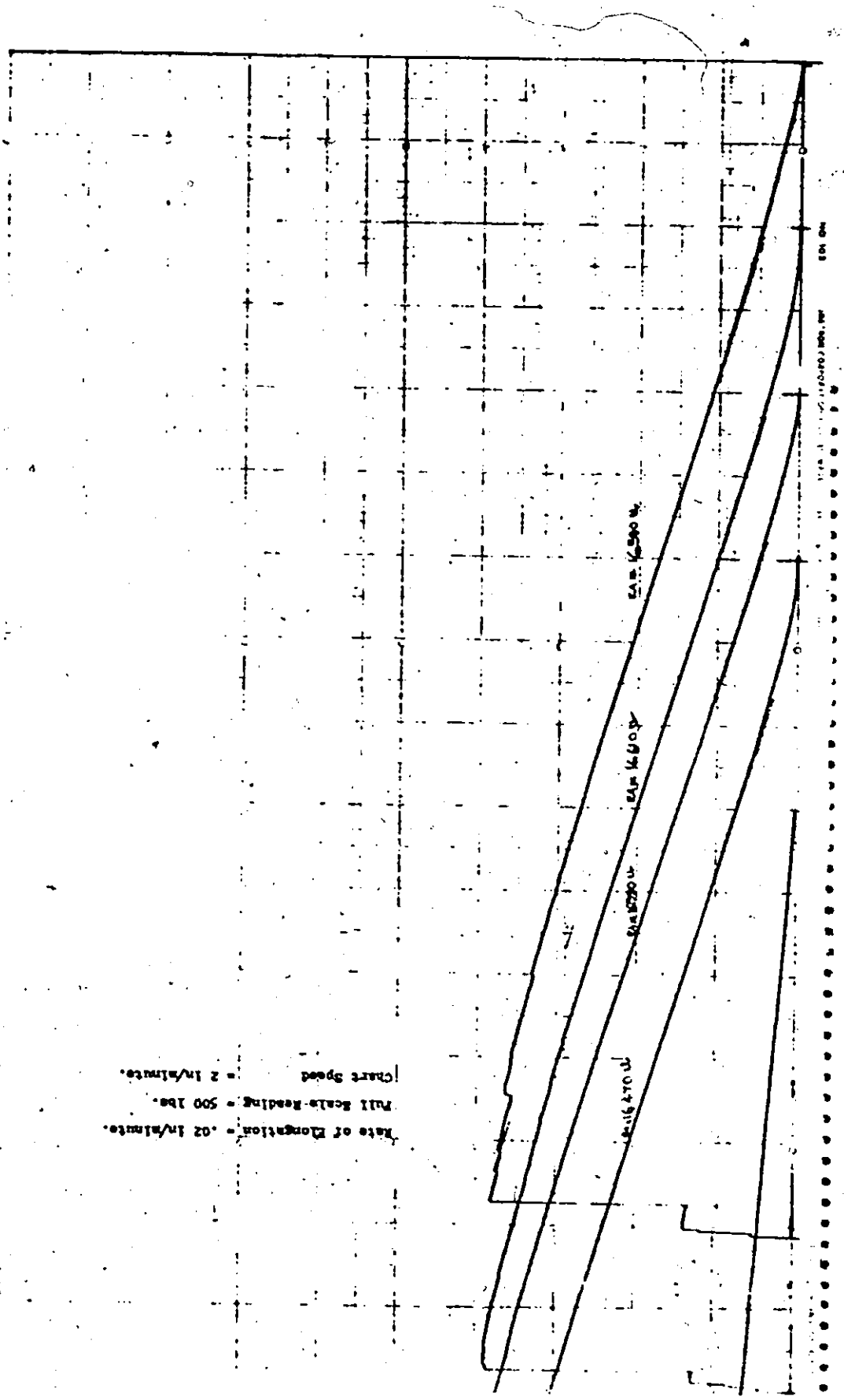

Fig. (5-3) SAMPLE OUTPUT FROM INSTRON TESTING MACHINE

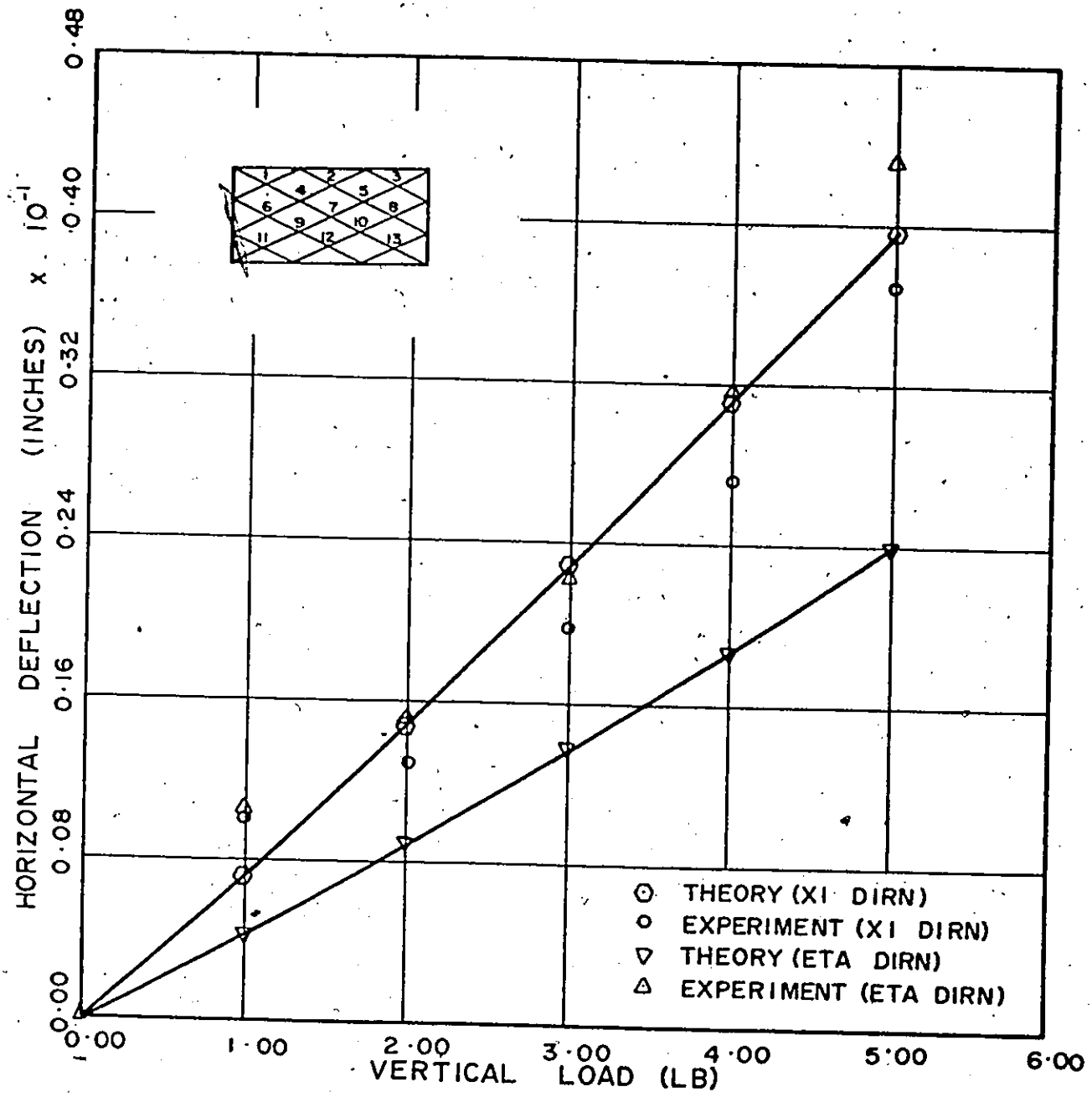

HOR· DEFLECTIONS AT JT· 1 OF SINGLE ROOF MODEL
(H= 50 LB· UNIFORM LOADING)

Fig· (5-4)

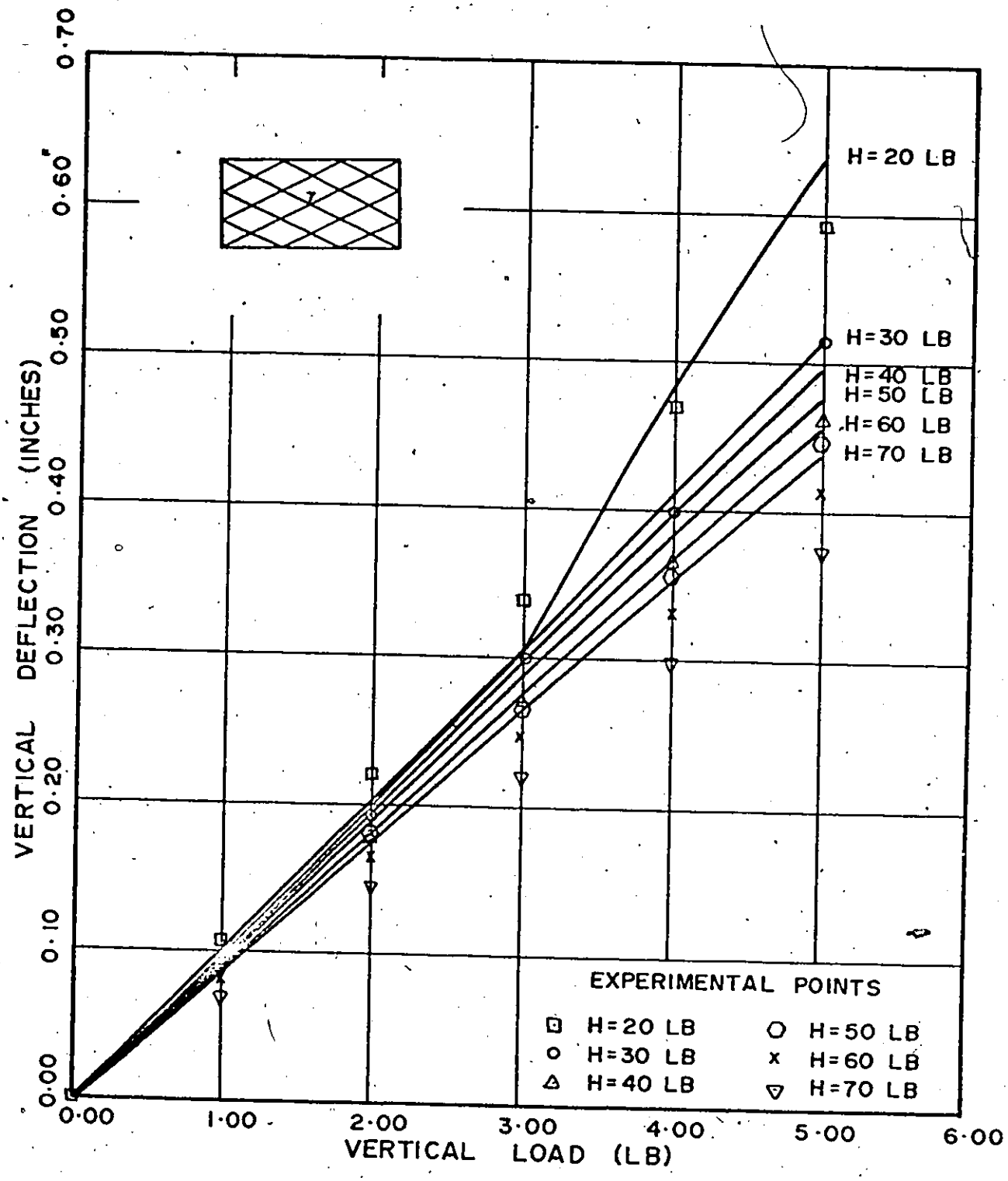

DEFLECTION AT JOINT 7 OF SINGLE ROOF MODEL
(UNIFORM LOADING)

Fig· (5-5)

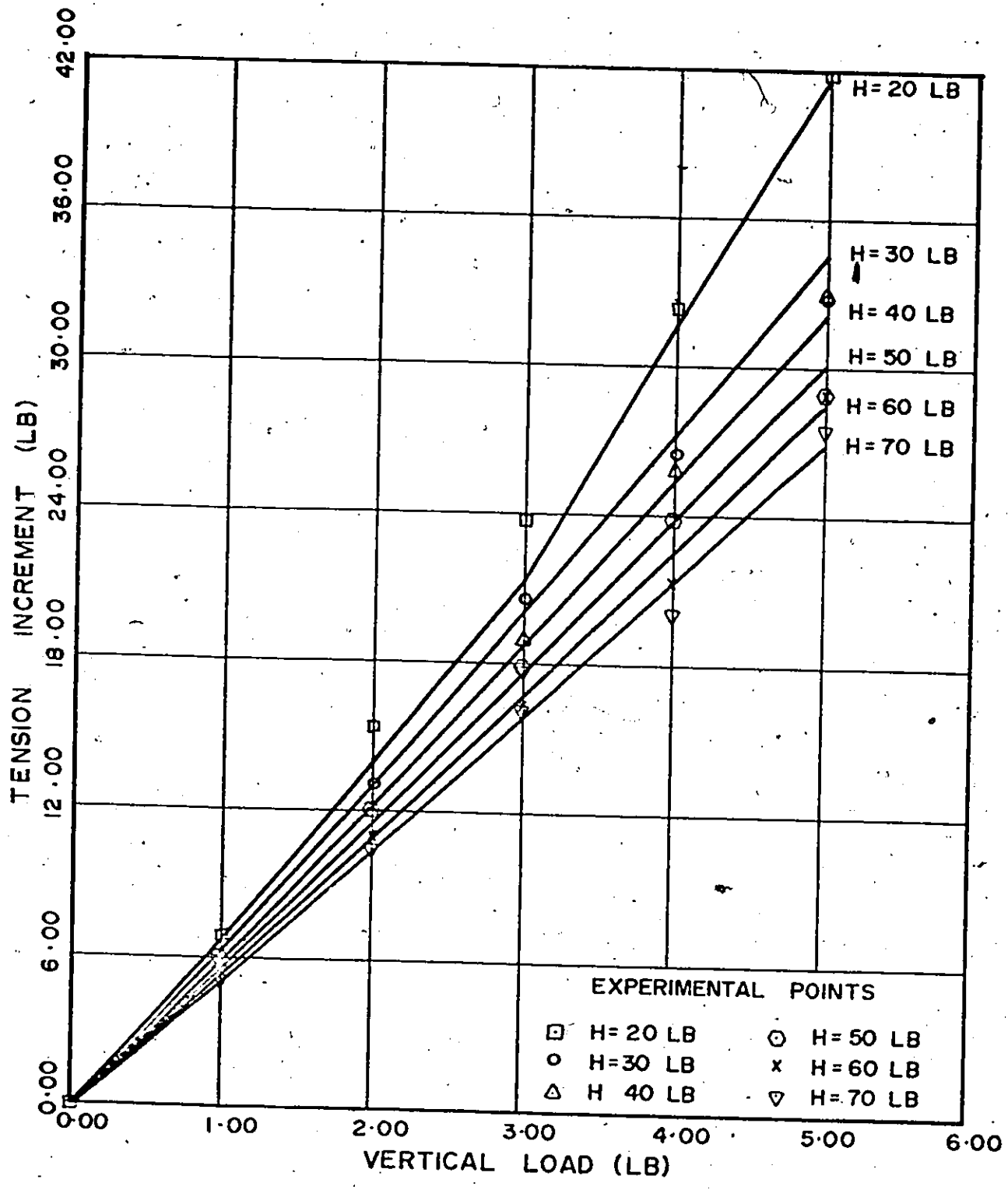

MAX. TENSION INCREMENT IN SINGLE ROOF MODEL
(UNIFORM LOADING)

Fig. (5-6)

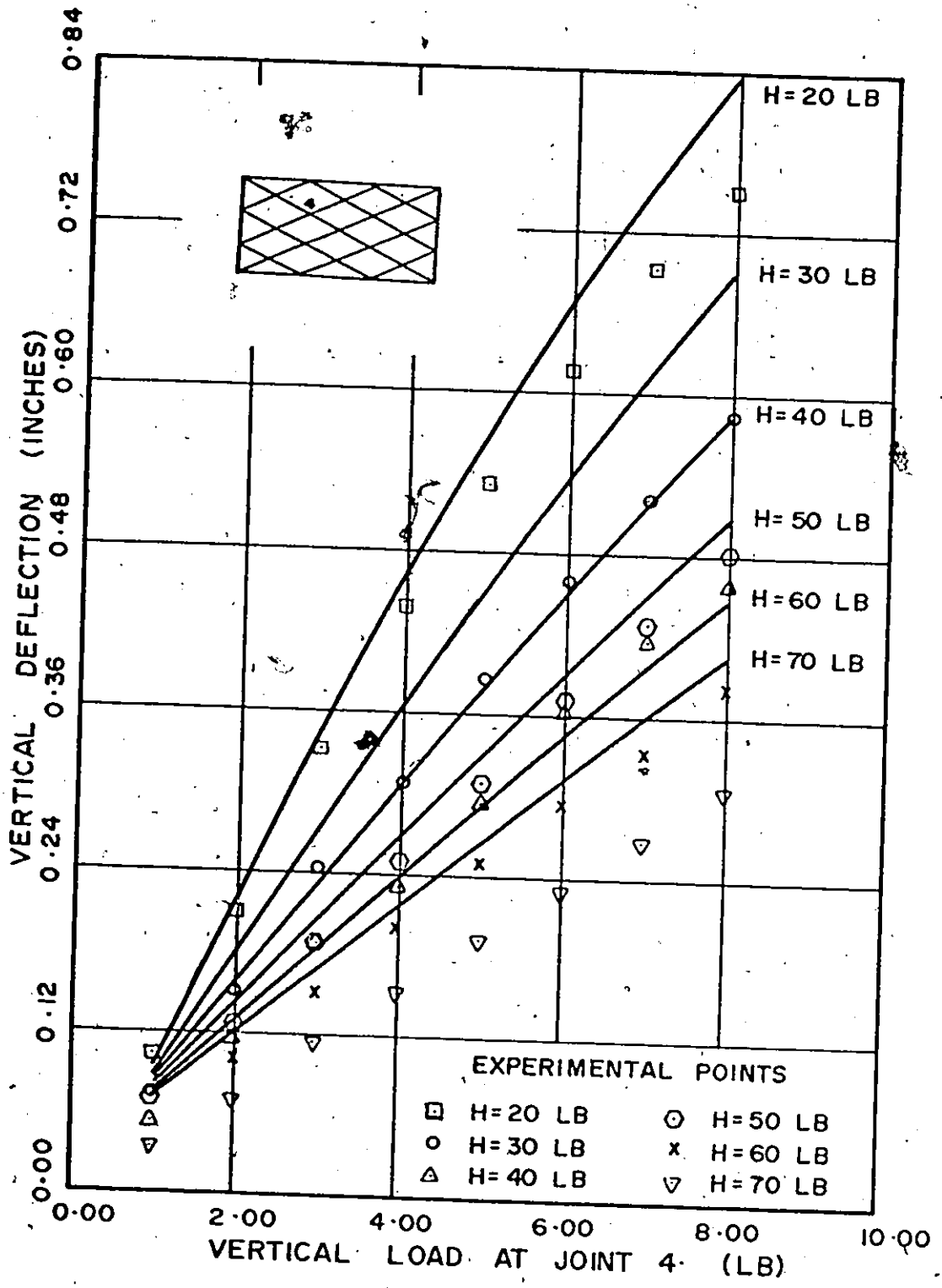

DEFLECTION AT JOINT 4 OF SINGLE ROOF MODEL
(UNIFORM LOAD OF 1 LB/JT + CONC. LOAD AT THE JT)

Fig. (5-7)

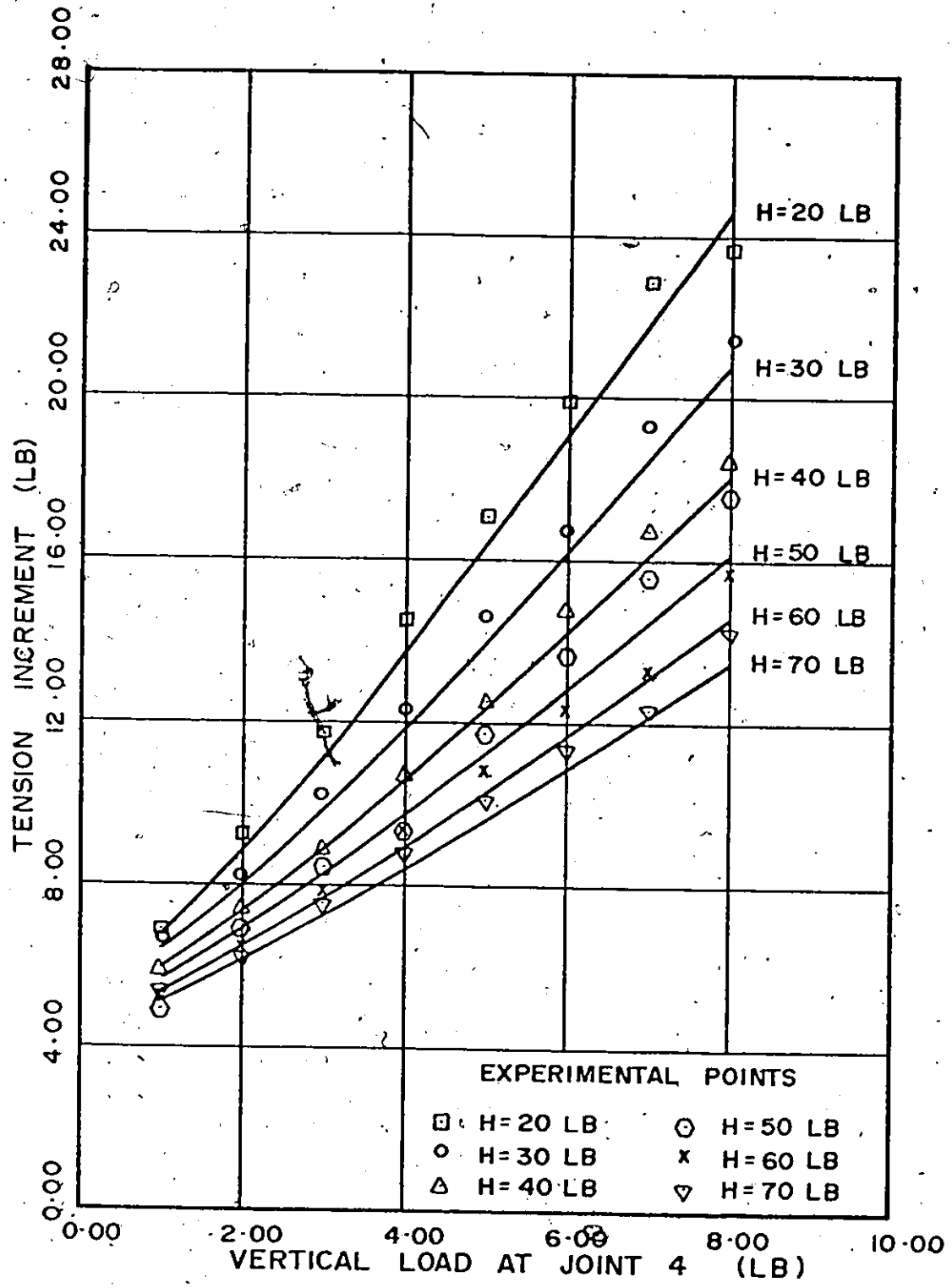

MAX. TENSION INCREMENT IN SINGLE ROOF MODEL
(UNIFORM LOAD OF 1 LB/JT + CONC. LOAD AT THE JT)

Fig. (5-8)

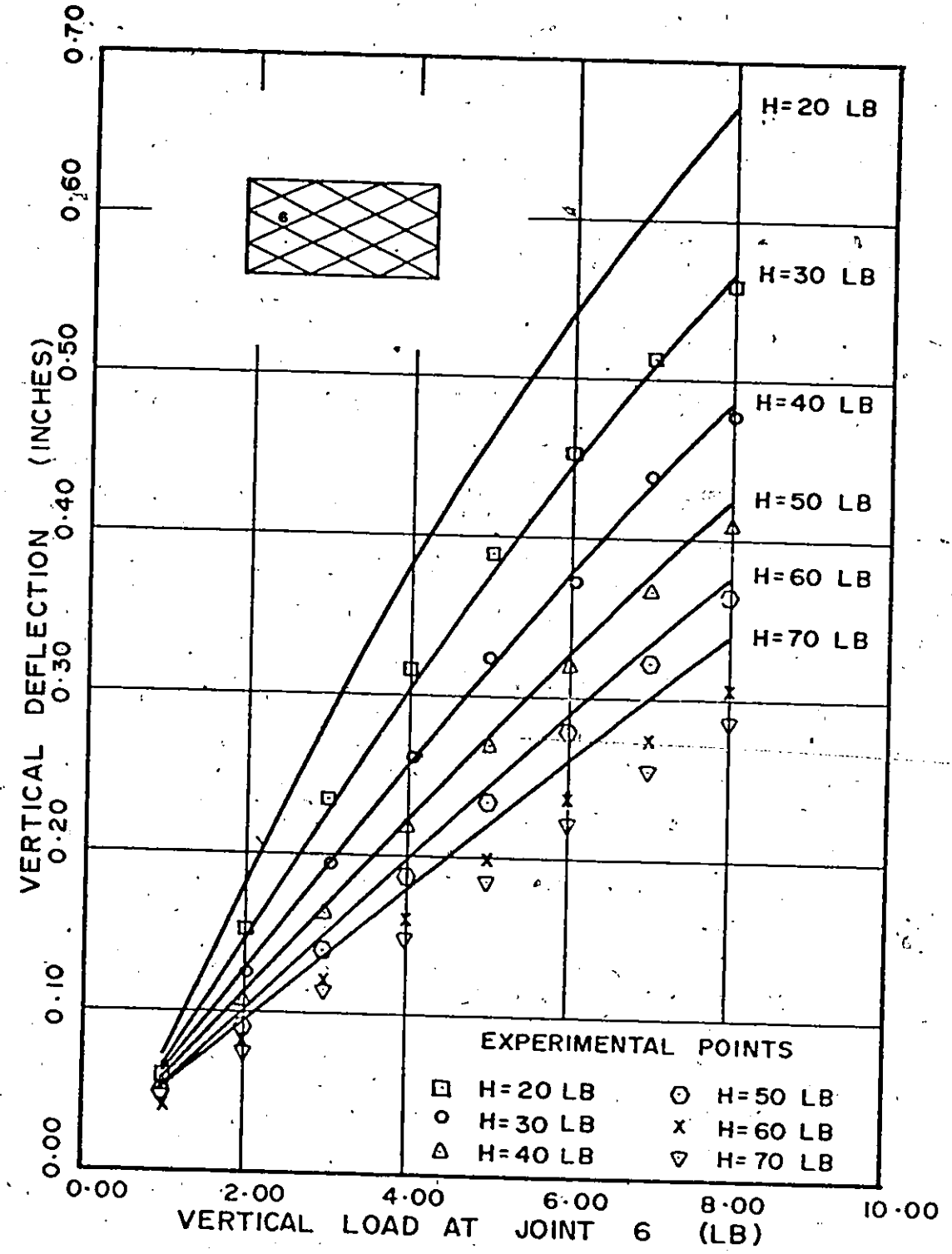

DEFLECTION AT JOINT 6 OF SINGLE ROOF MODEL
(UNIFORM LOAD OF 1 LB/JT + CONC. LOAD AT THE JT)

Fig (5-9)

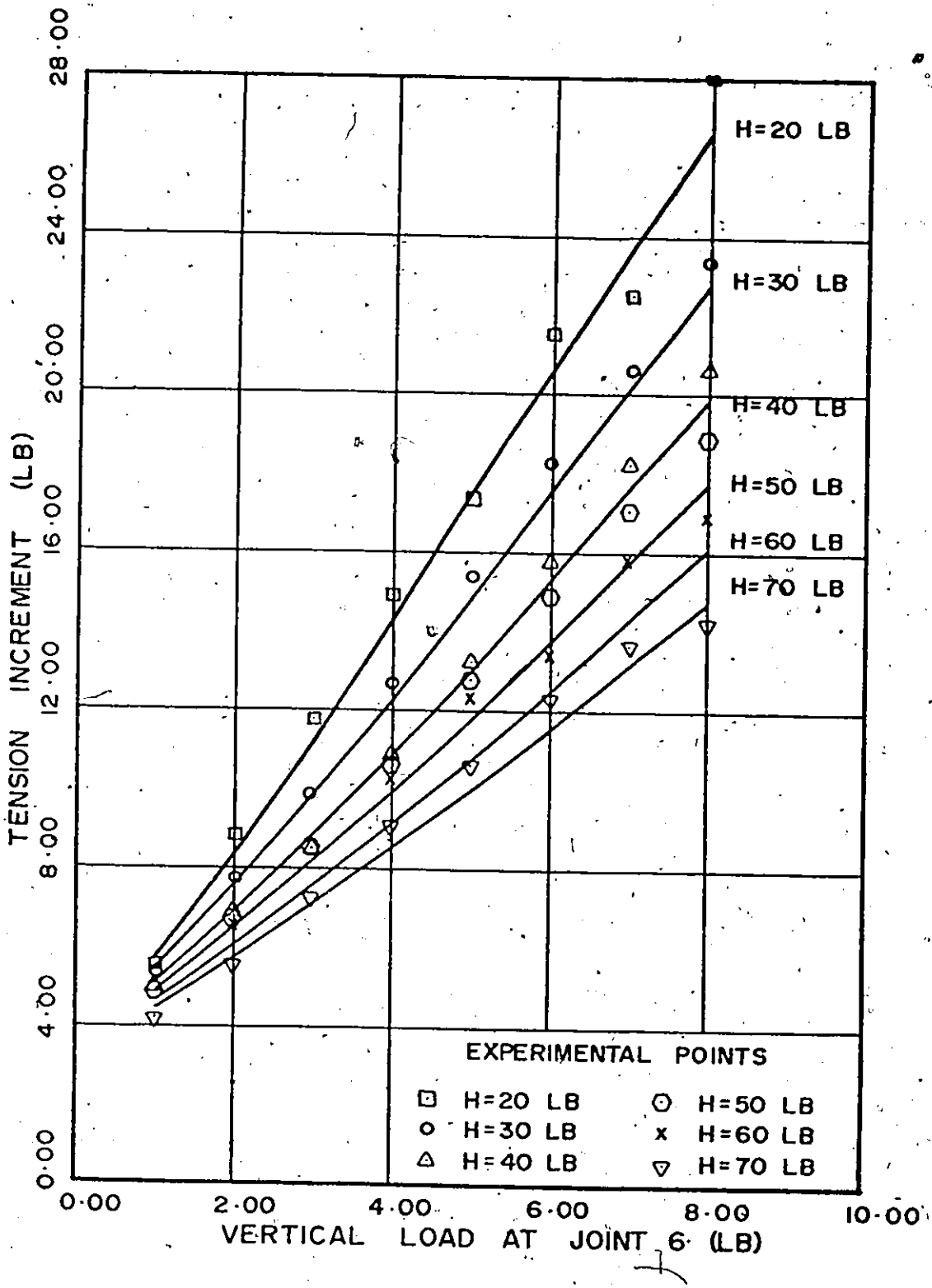

MAX. TENSION INCREMENT IN SINGLE ROOF MODEL
(UNIFORM LOAD OF 1 LB/JT + CONC. LOAD AT THE JT)

Fig (5 - 10)

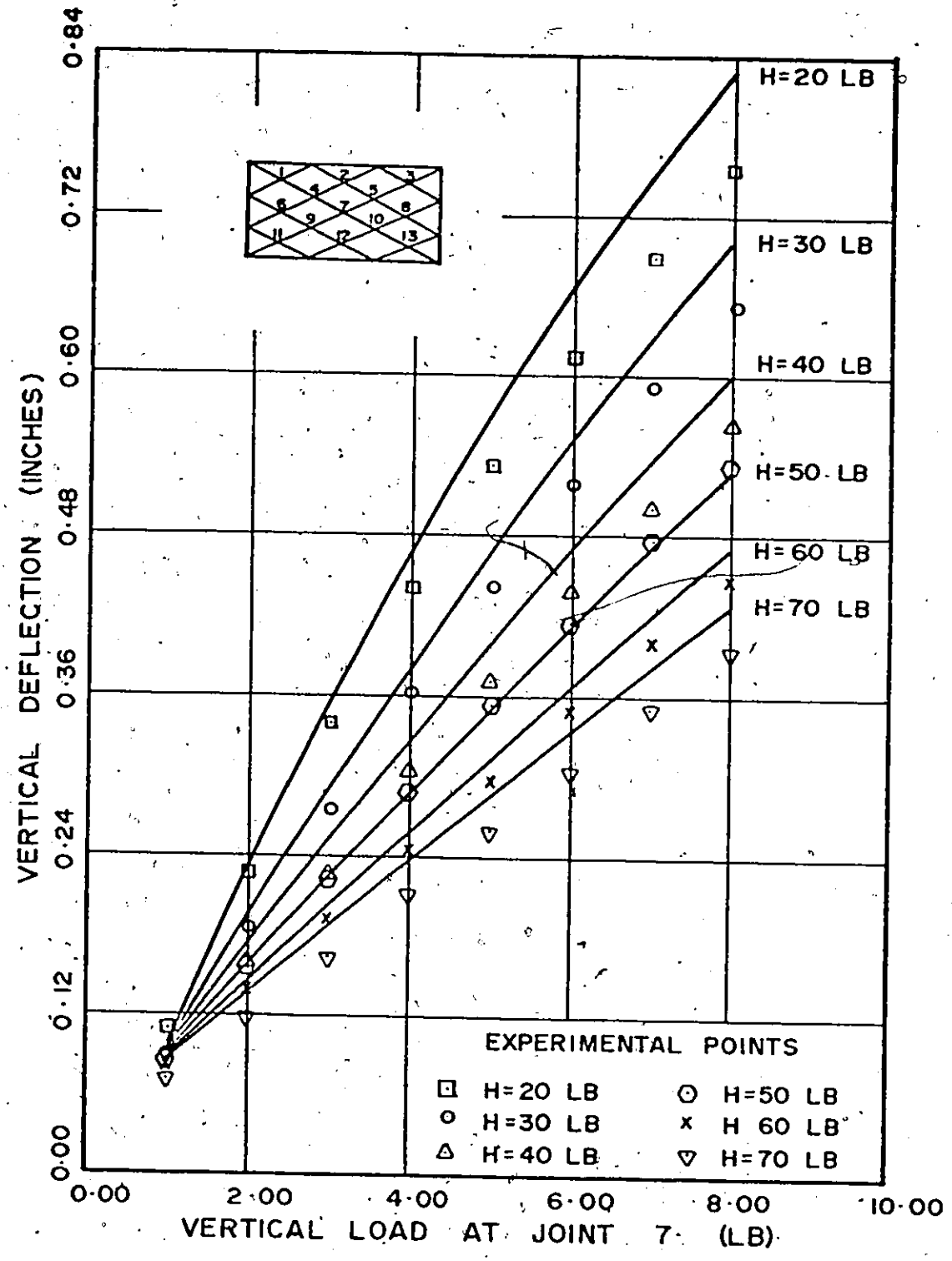

DEFLECTION AT JOINT 7 OF SINGLE ROOF MODEL
(UNIFORM LOAD OF 1 LB/JT + CONC LOAD AT THE JT)

Fig. (5-11)

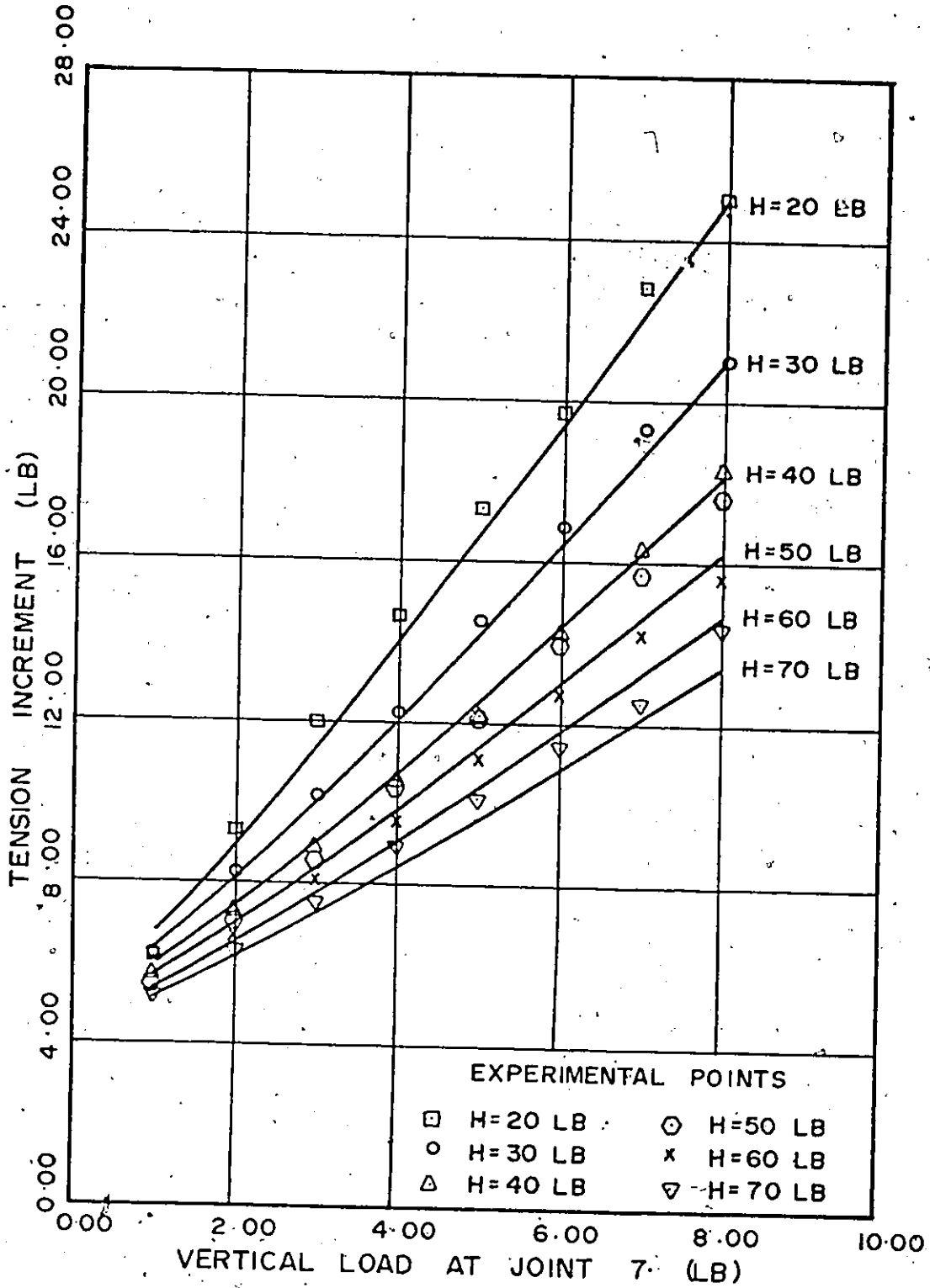

MAX. TENSION INCREMENT IN SINGLE ROOF MODEL
(UNIFORM LOAD = 1 LB/JT + CONC. LOAD AT THE JT)

Fig. (5-12)

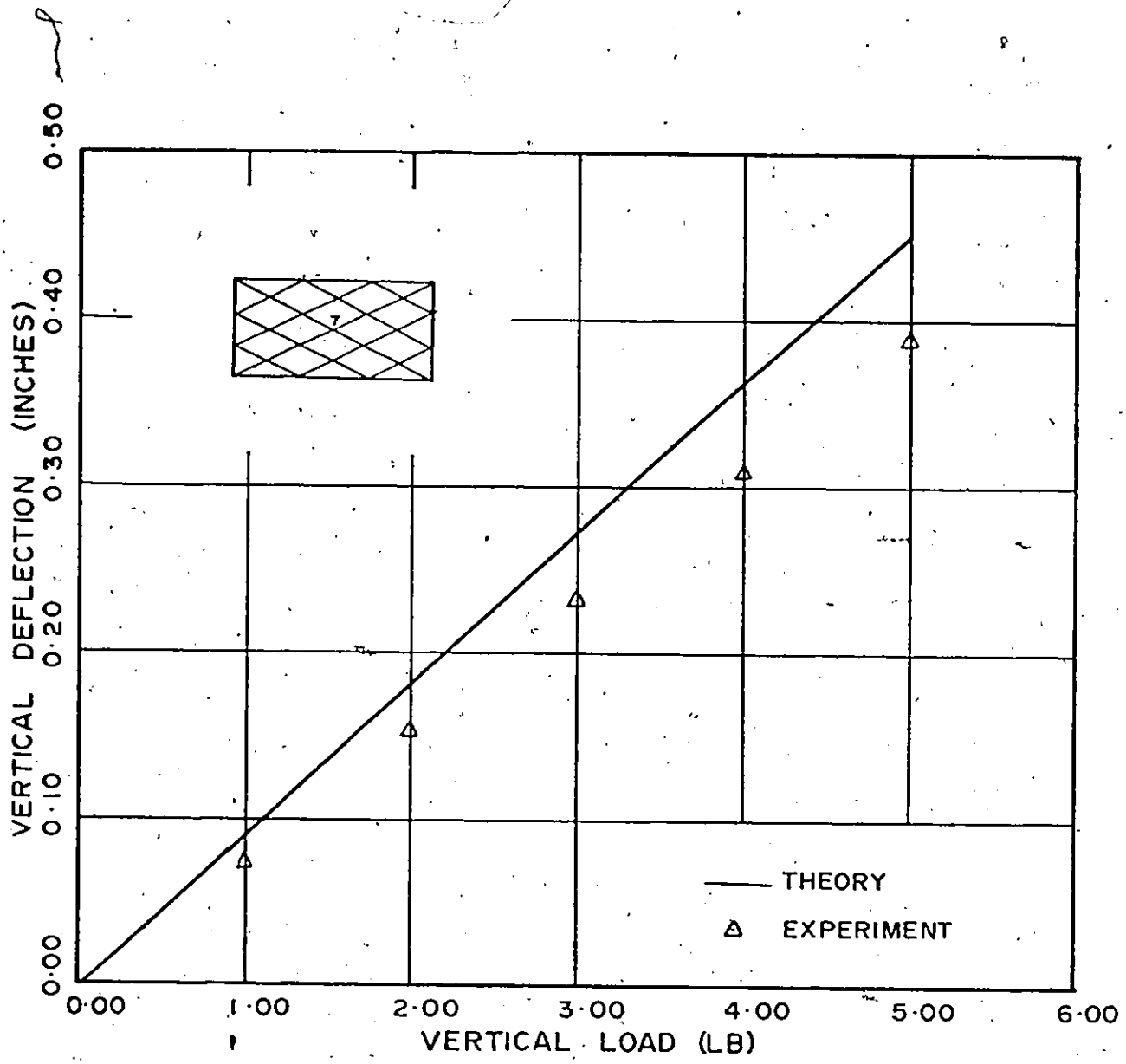

DEFLECTION AT JOINT 7 OF SINGLE ROOF MODEL
(H(X1) = 40 LB. H(ETA) = 60 LB. UNIFORM LOADING)

Fig. (5-13)

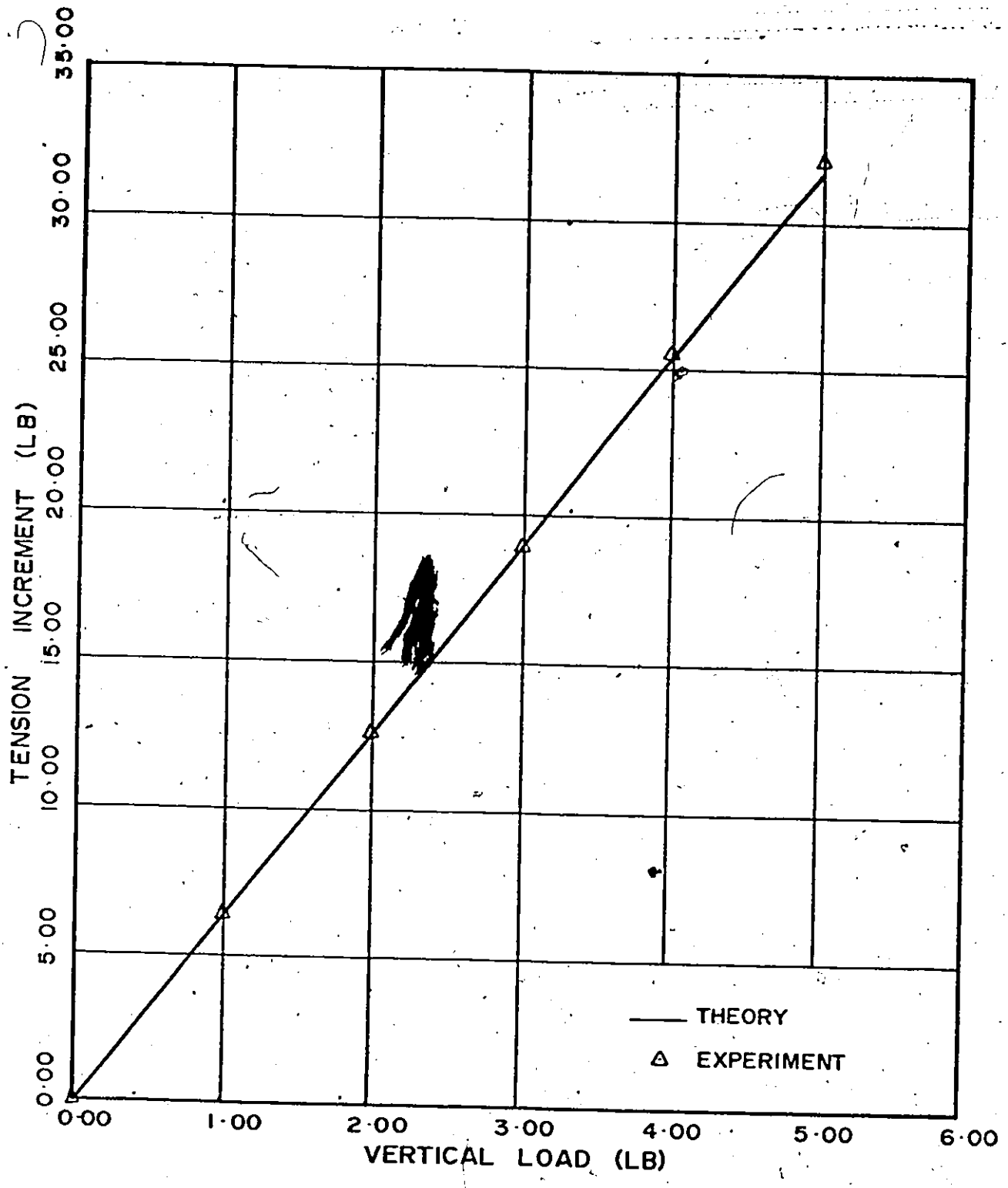

MAX. TENSION INCREMENT IN SINGLE ROOF MODEL
(H (XI) = 40 LB. H (ETA) = 60 LB. UNIFORM LOADING)

Fig. (5 - 14)

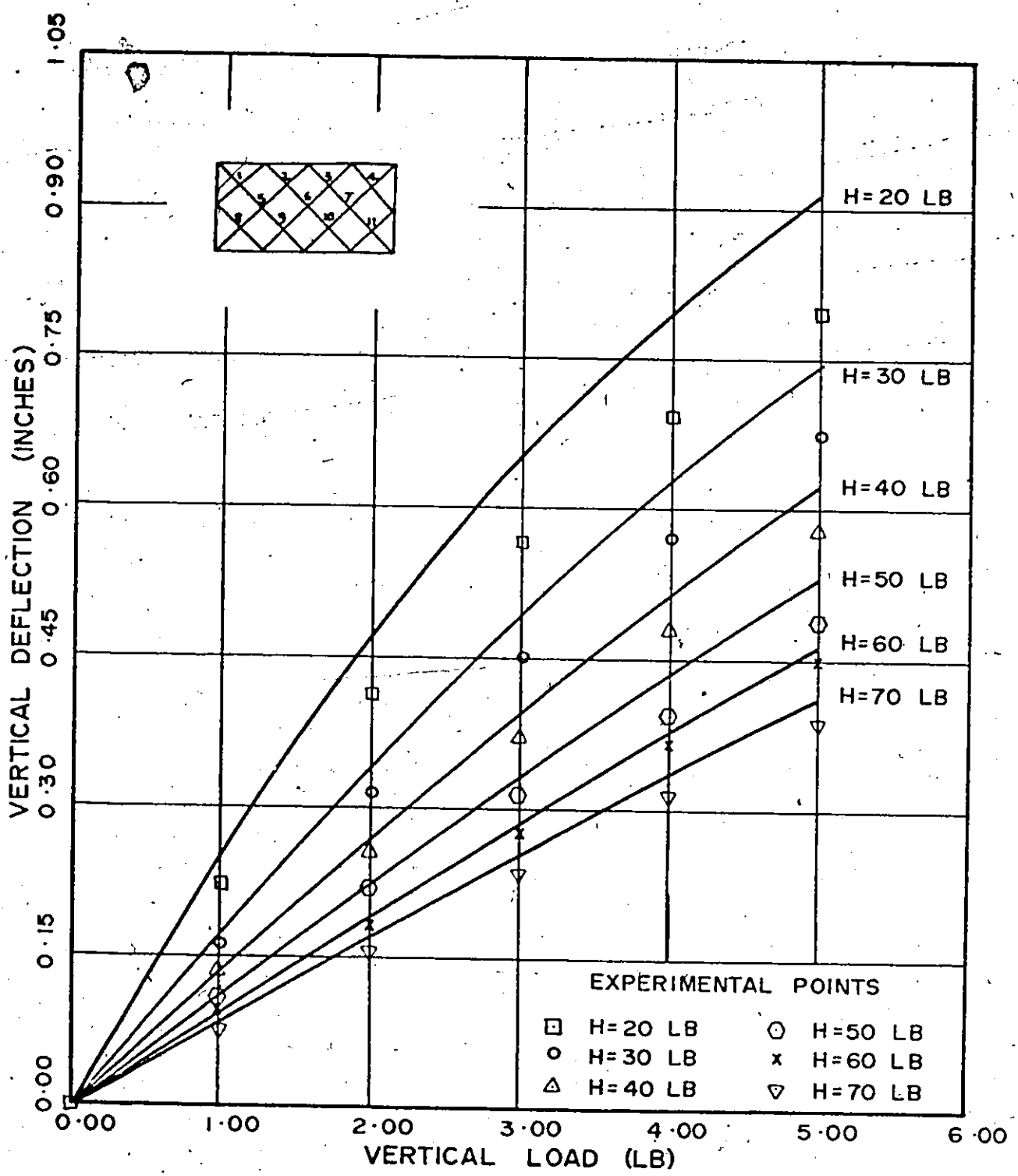

DEFLECTION AT JOINT 6 OF DOUBLE ROOF MODEL
(UNIFORM LOADING)

Fig· (5-15)

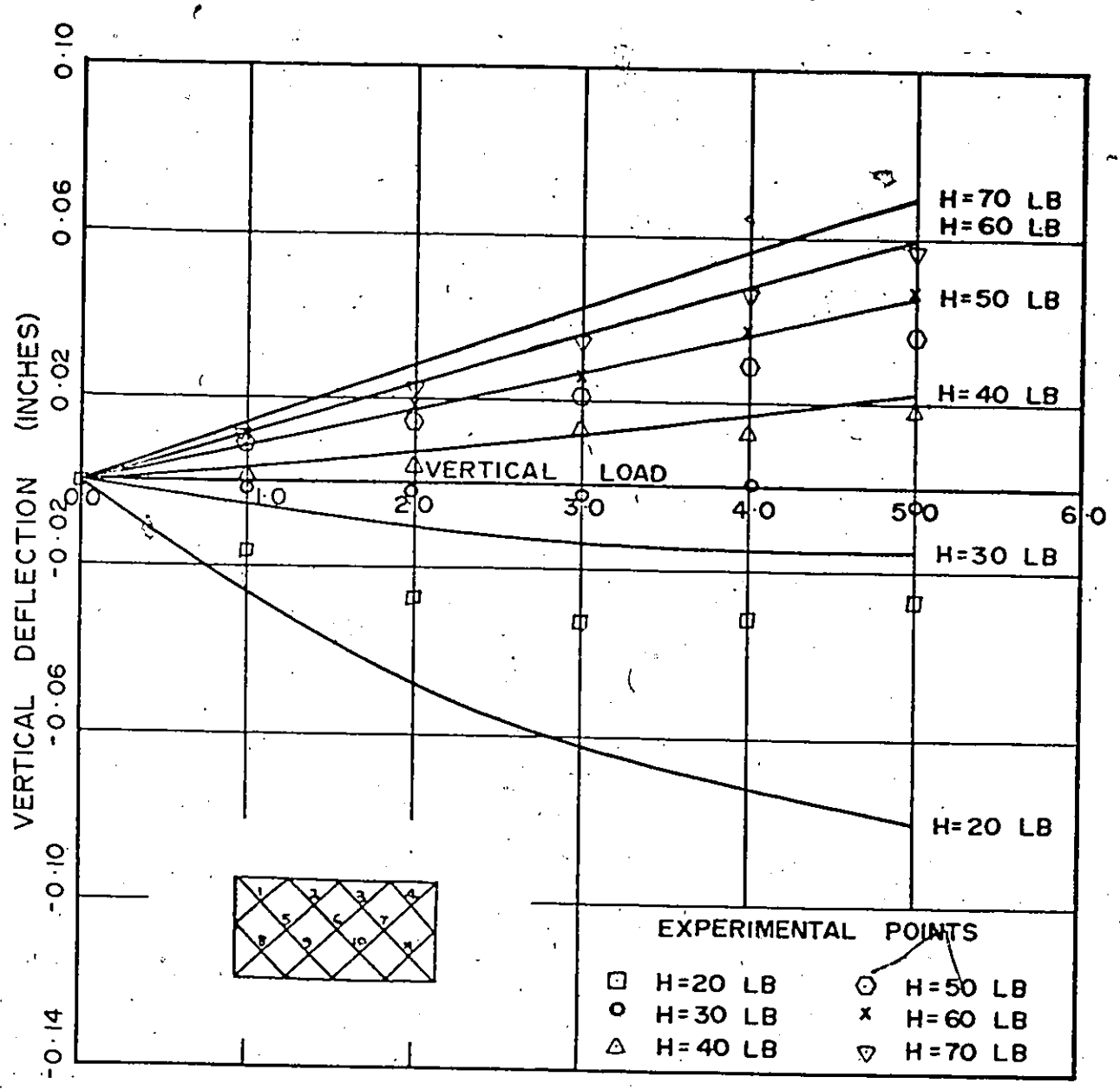

DEFLECTION AT JOINT 5 OF DOUBLE ROOF MODEL
(UNIFORM LOADING)

Fig· (5 - 16)

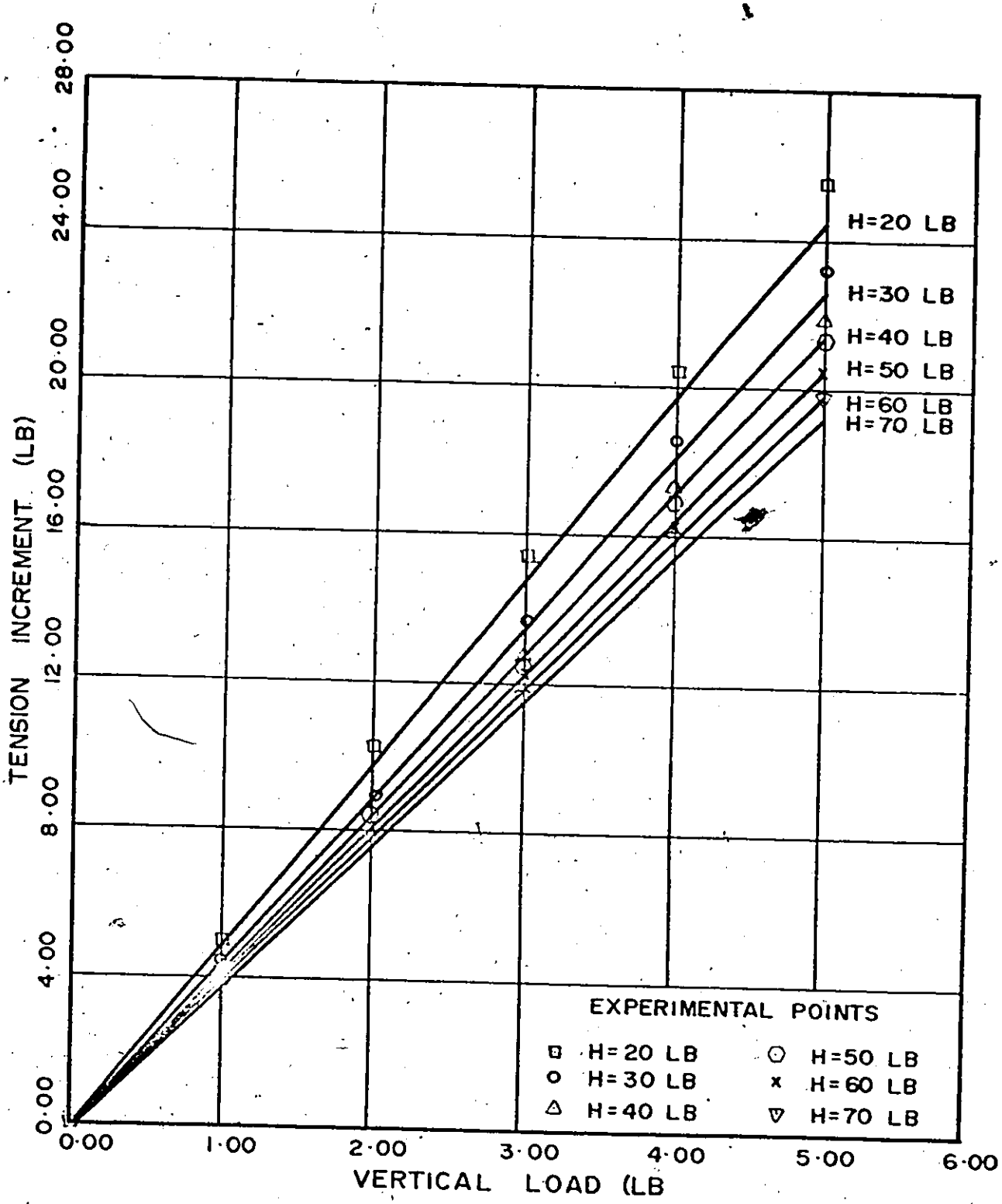

MAX. TENSION INCREMENT IN DOUBLE ROOF MODEL
(UNIFORM LOADING)

Fig. (5-17)

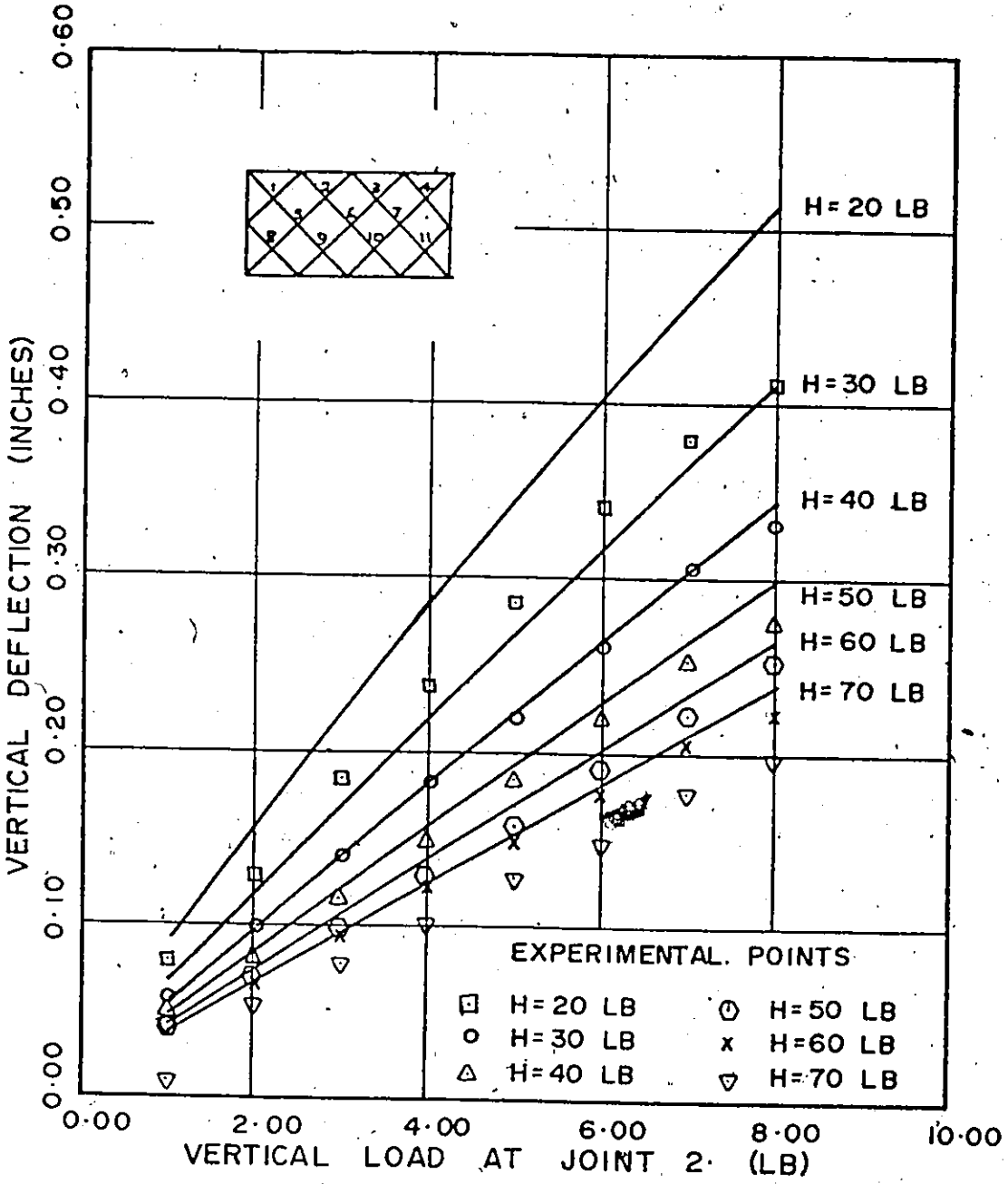

DEFLECTION AT JOINT 2 OF DOUBLE ROOF MODEL
(UNIFORM LOAD OF 1 LB/JT + CONC· LOAD AT THE JT)

Fig· (5 - 18)

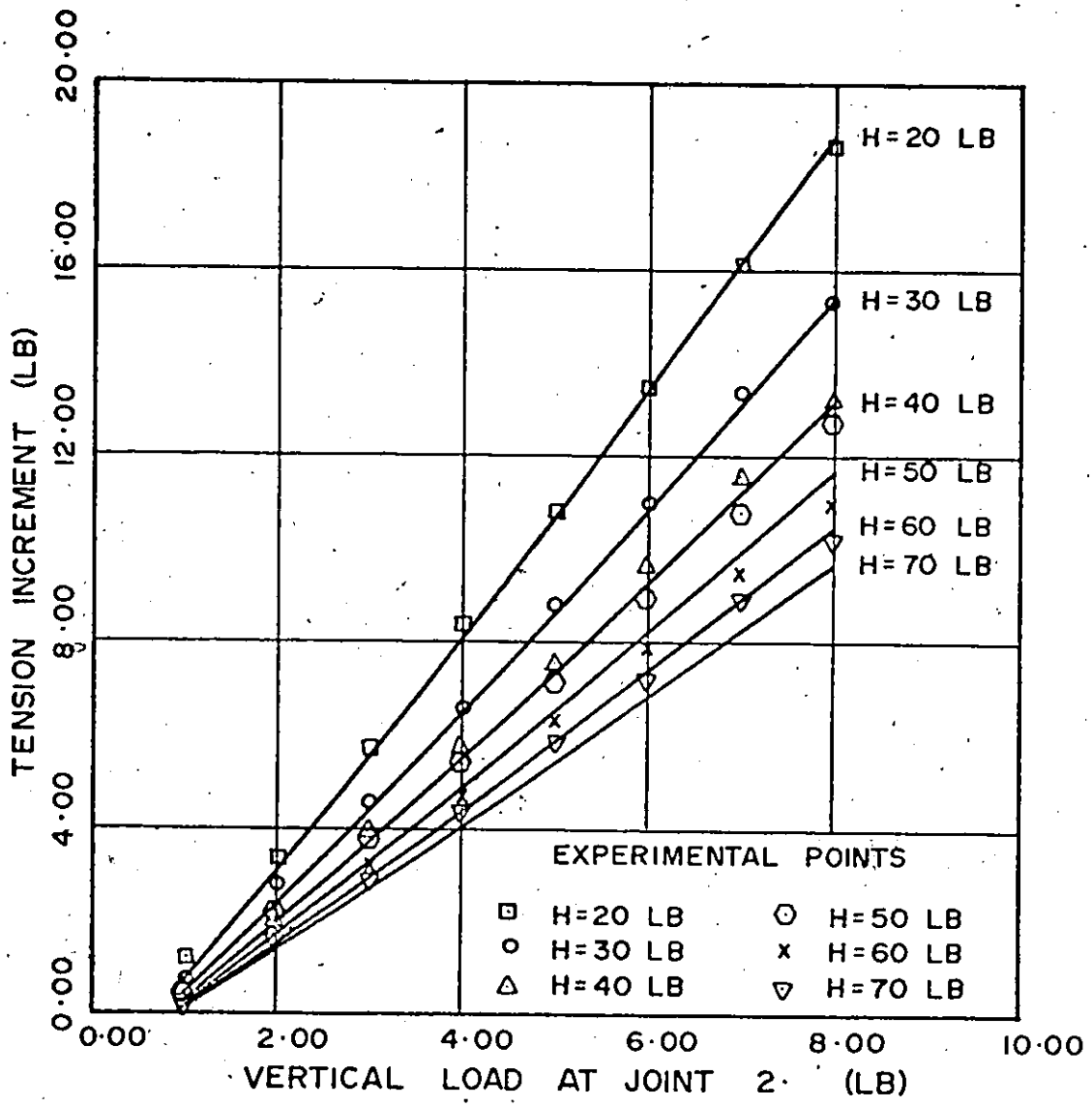

MAX· TENSION INCREMENT IN DOUBLE ROOF MODEL
(UNIFORM LOAD OF 1 LB/JT + CONC· LOAD AT THE JT)

Fig· (5-19)

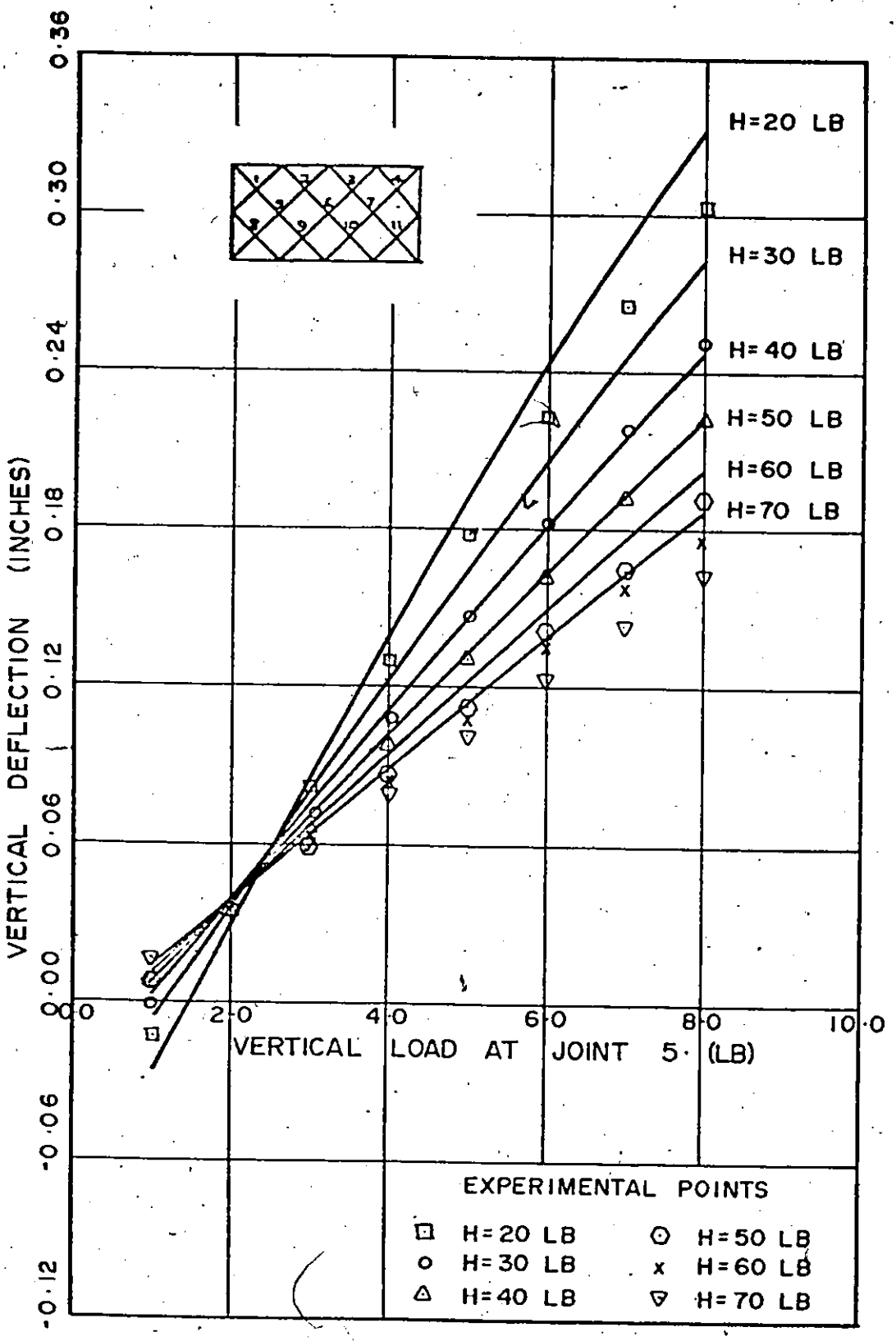

DEFLECTION AT JOINT 5 OF DOUBLE ROOF MODEL
(UNIFORM LOAD OF 1 LB/JT + CONC. LOAD AT THE JT)

Fig. (5-20)

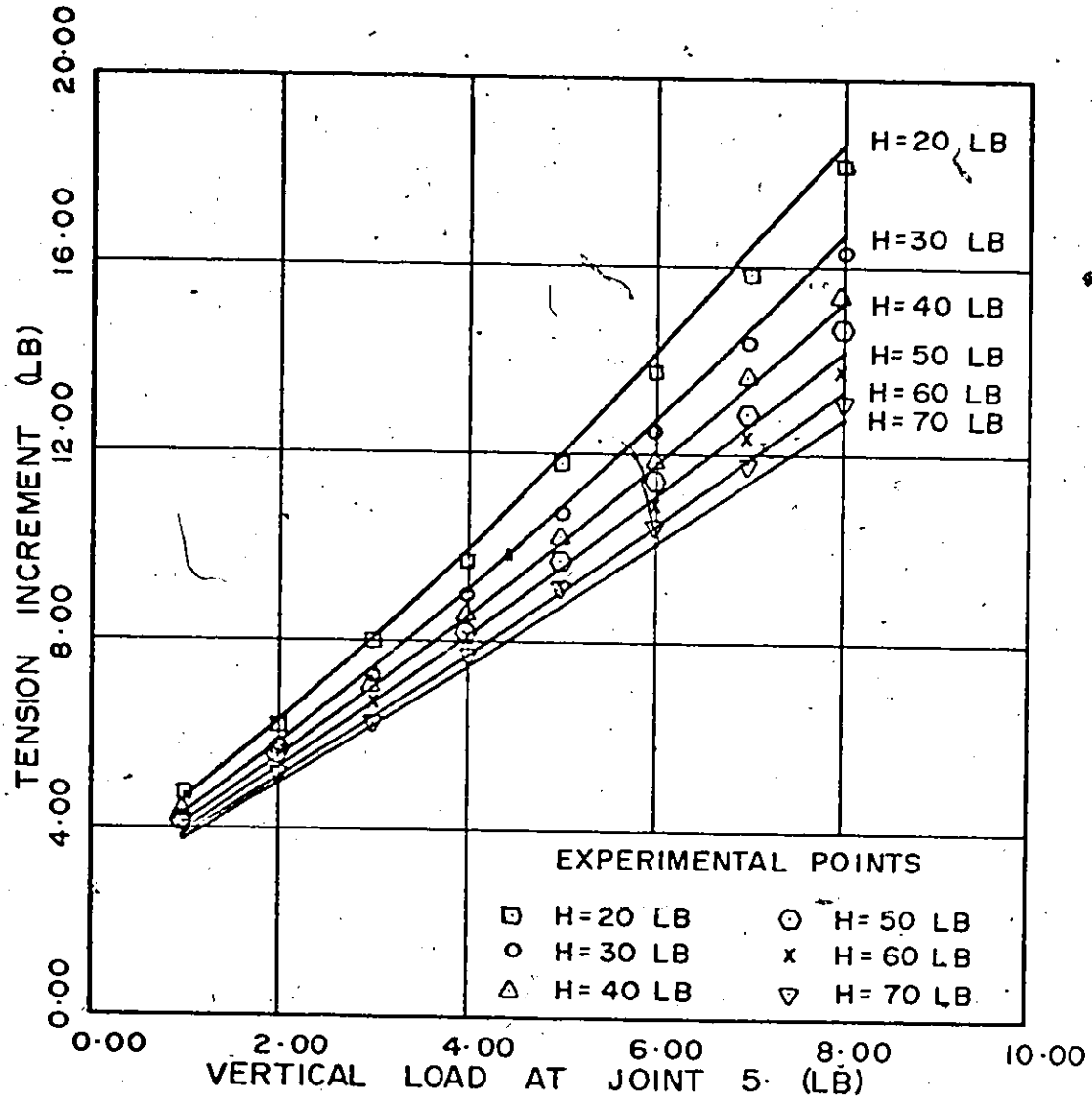

MAX· TENSION INCREMENT IN DOUBLE ROOF MODEL
(UNIFORM LOAD OF 1 LB/JT + CONC· LOAD AT THE JT)

Fig· (5-21)

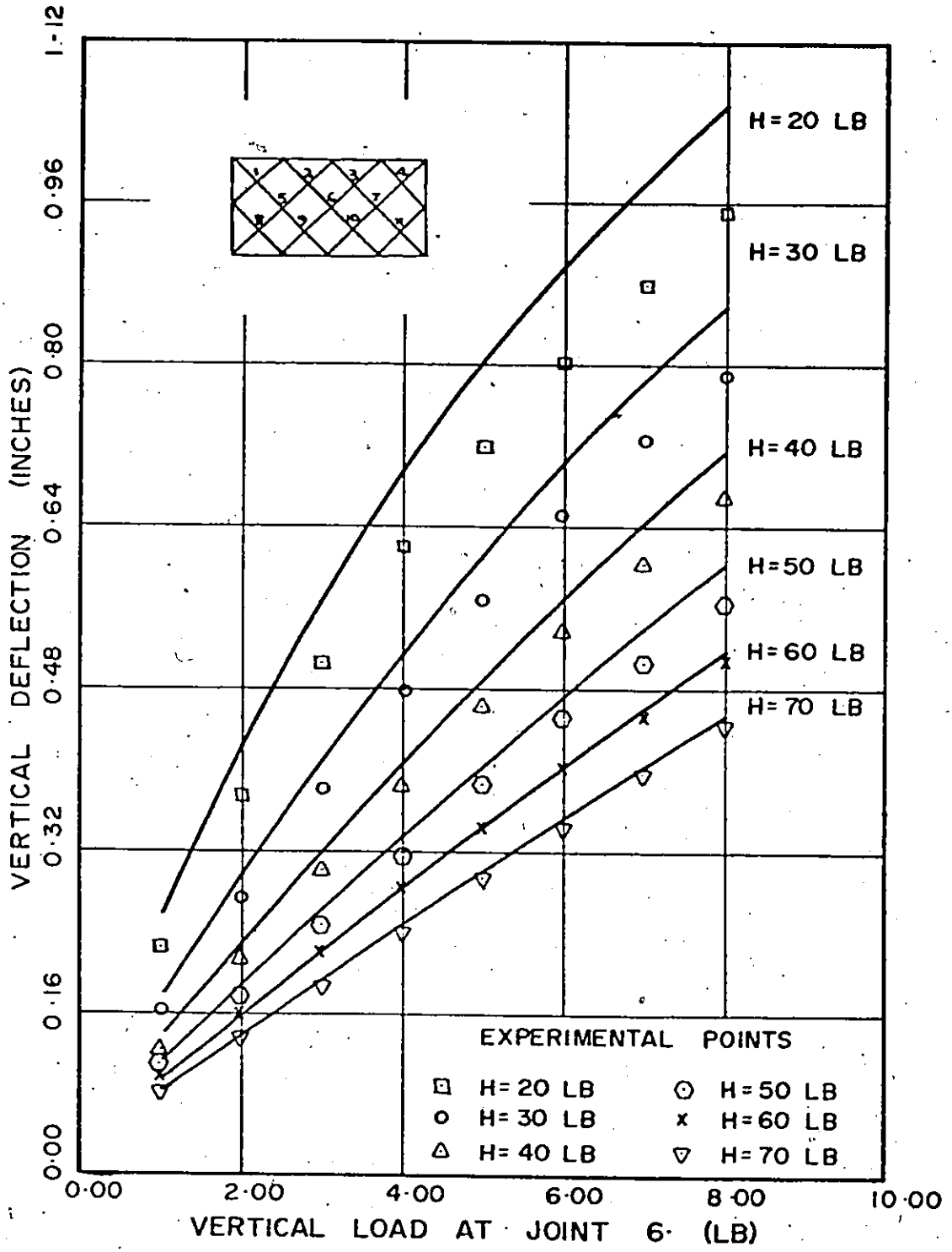

DEFLECTION AT JOINT 6 OF DOUBLE ROOF MODEL
(UNIFORM LOAD OF 1 LB/JT + CONC· LOAD AT THE JT)

Fig· (5-22)

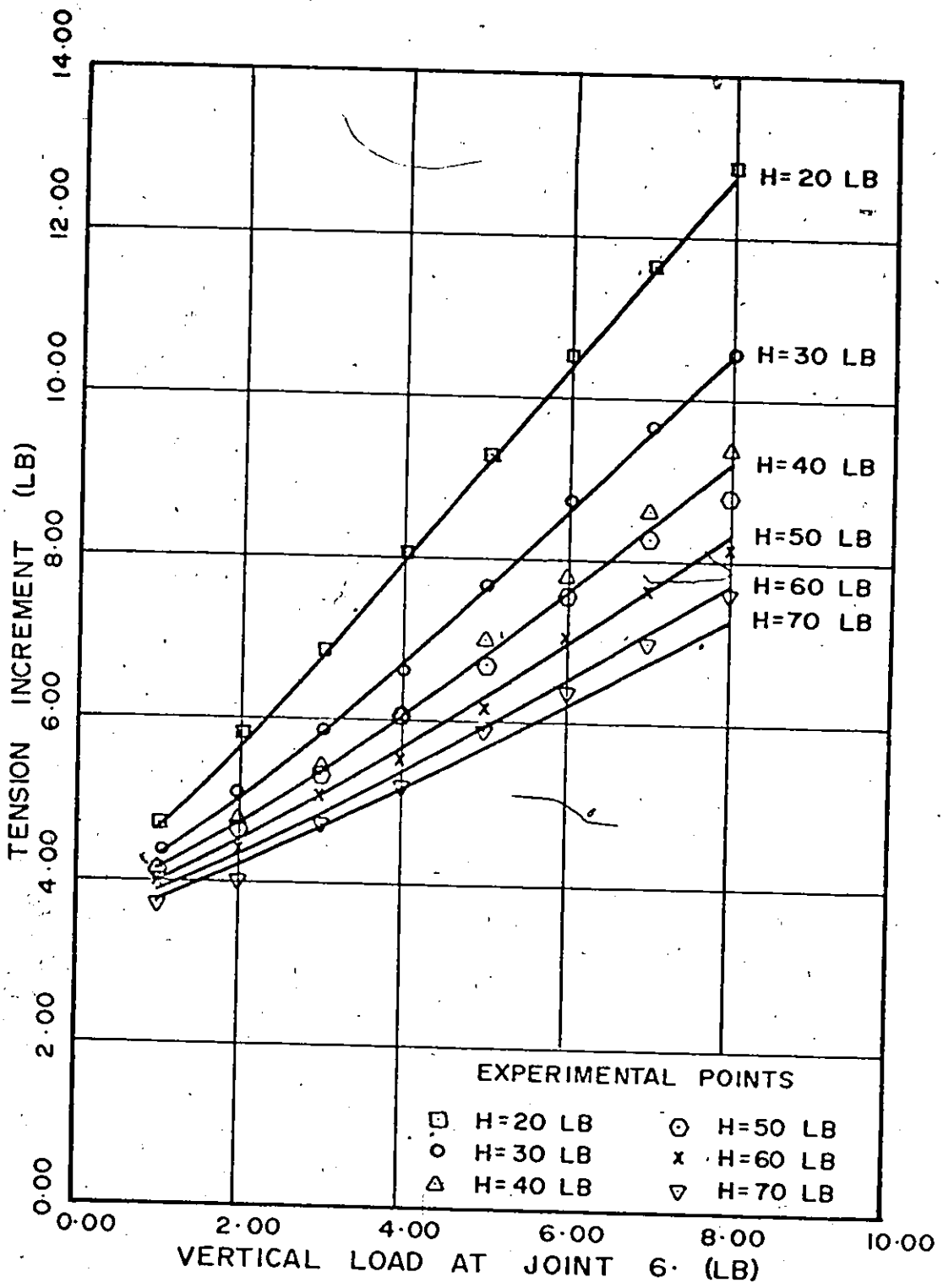

MAX. TENSION INCREMENT IN DOUBLE ROOF MODEL
(UNIFORM LOAD OF 1 LB/JT + CONC. LOAD AT THE JT

Fig. (5-23)

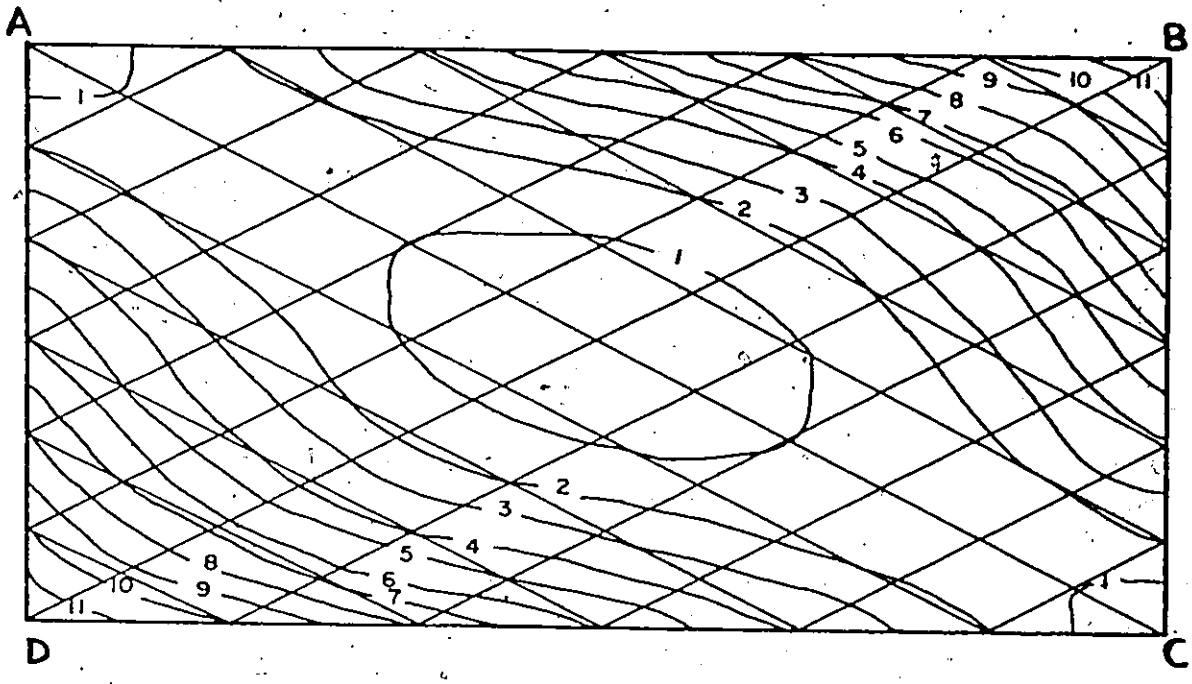

CONTOURS OF DEFORMED SINGLE ROOF

(LOAD = 6 K/J, ROOF HEIGHT = 12 FT)

Fig. (6-1)

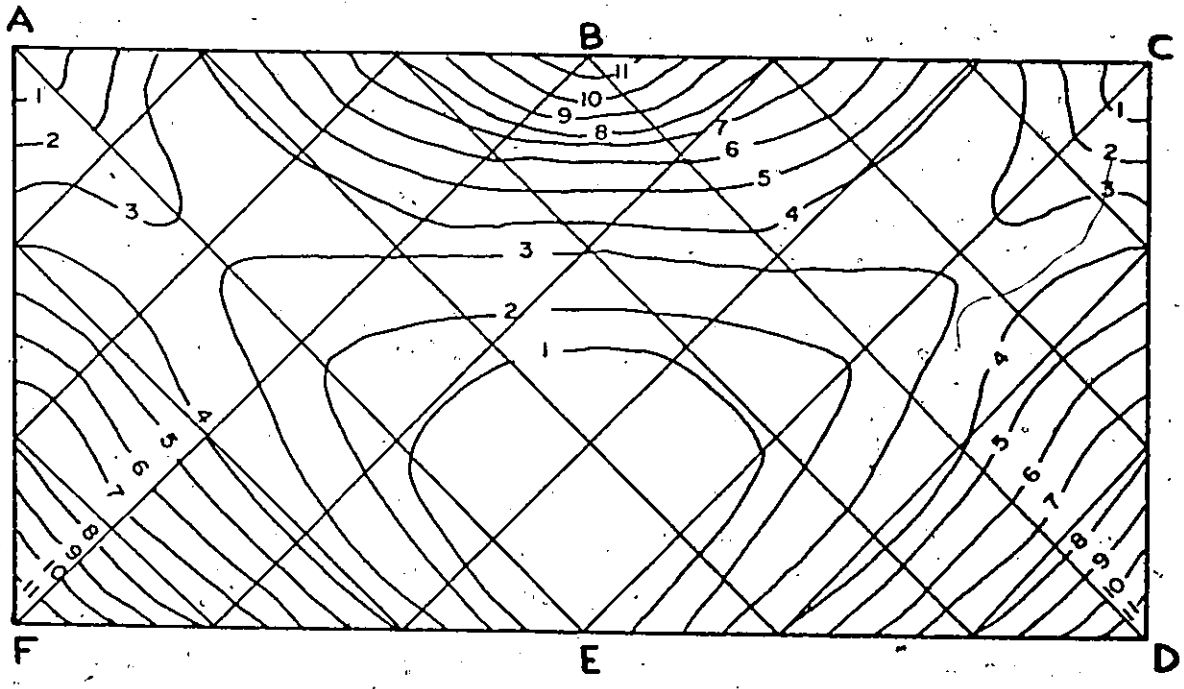

CONTOURS OF DEFORMED DOUBLE ROOF

(LOAD = 12 K/J, ROOF HEIGHT = 12 FT)

Fig. (6-2)

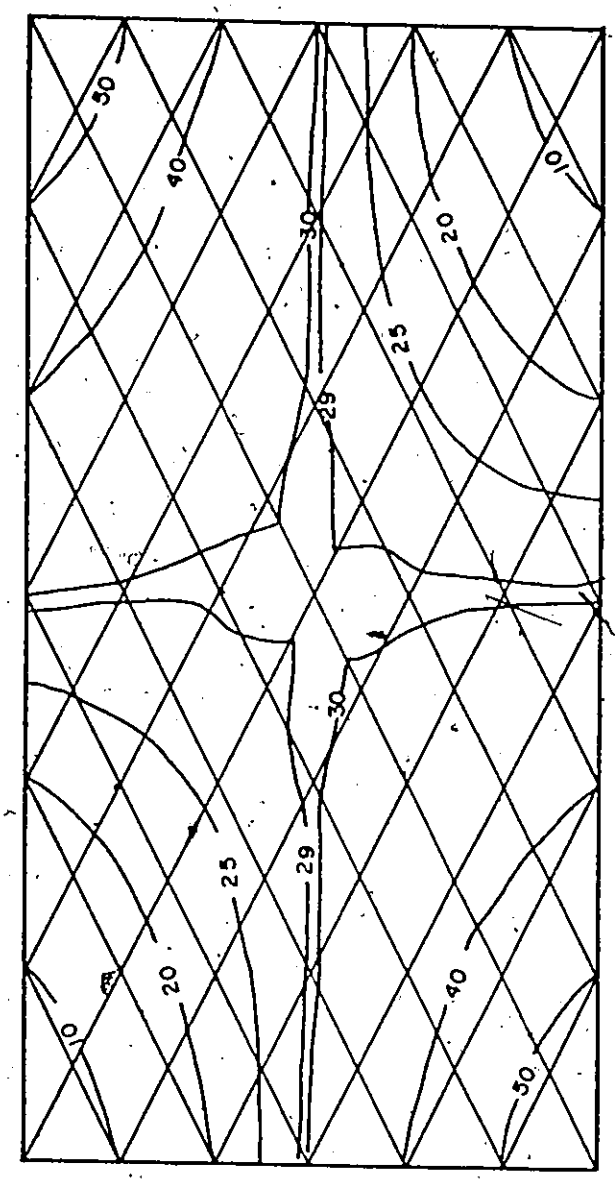

CONTOURS OF DEFORMED SINGLE ROOF

(LOAD = 6K/J, ROOF HEIGHT = 60 FT)

Fig. (6-3).

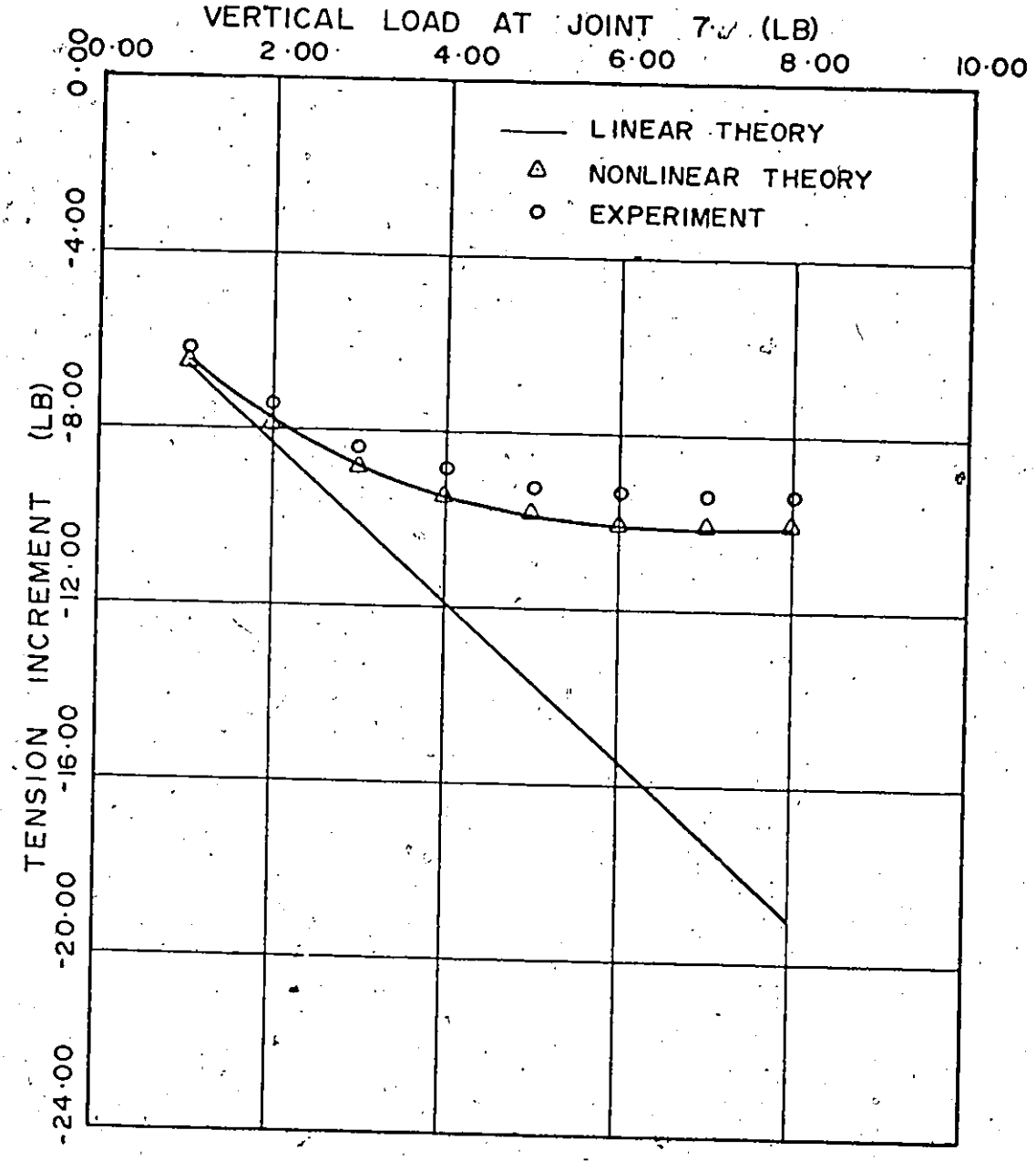

MAX. TENSION DECREMENT IN SINGLE ROOF MODEL
(H=20 LB. UNIFORM LOAD OF 1 LB/JT + CONC. LOAD AT JOINT 7)

Fig. (6-4)

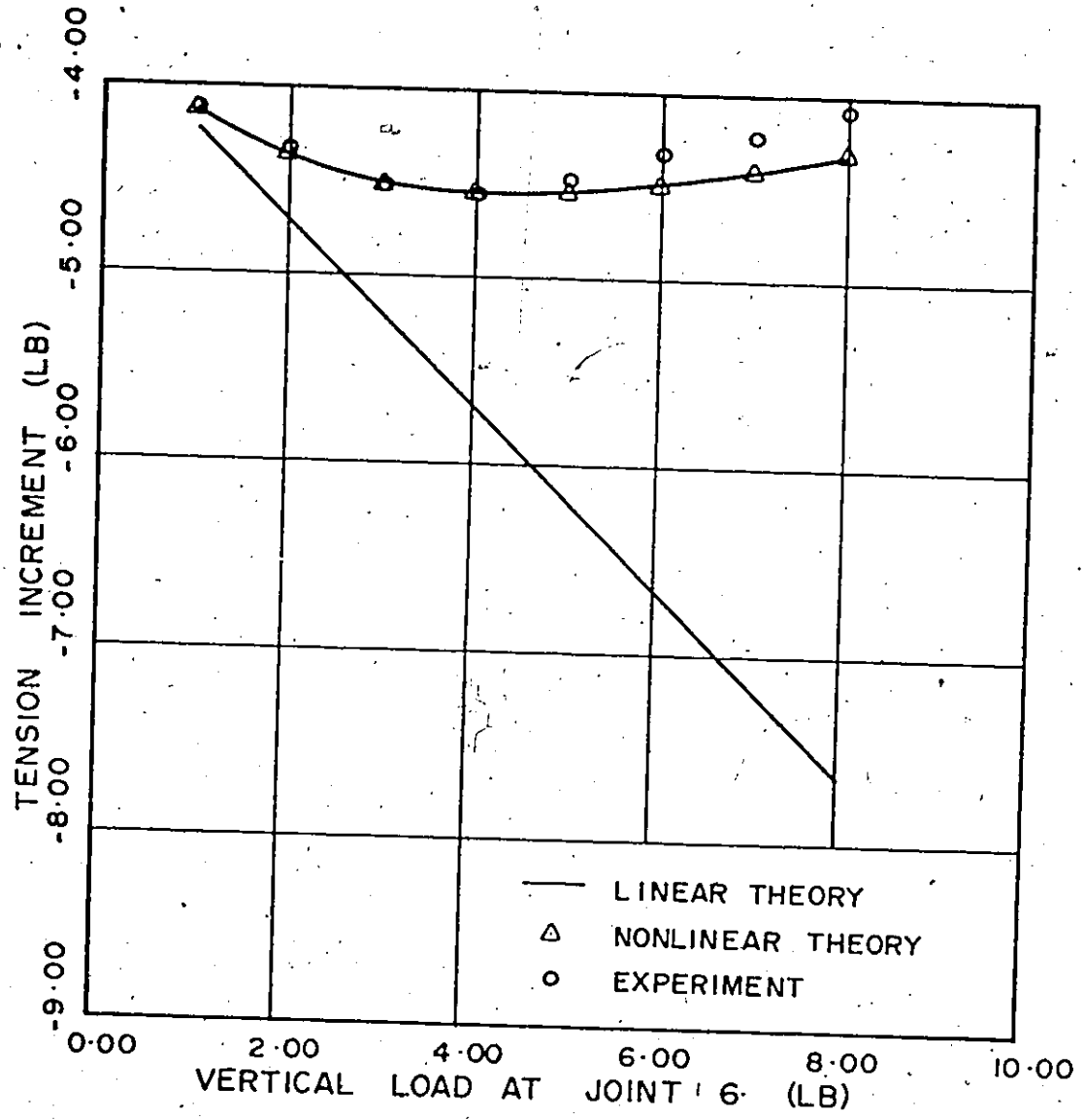

TEN. INC. IN CABLE (3, 1) OF DOUBLE ROOF MODEL
(H = 30 LB. UNIFORM LOAD OF 1 LB/JT + CONC. LOAD AT JT. 6)

Fig. (6-5)

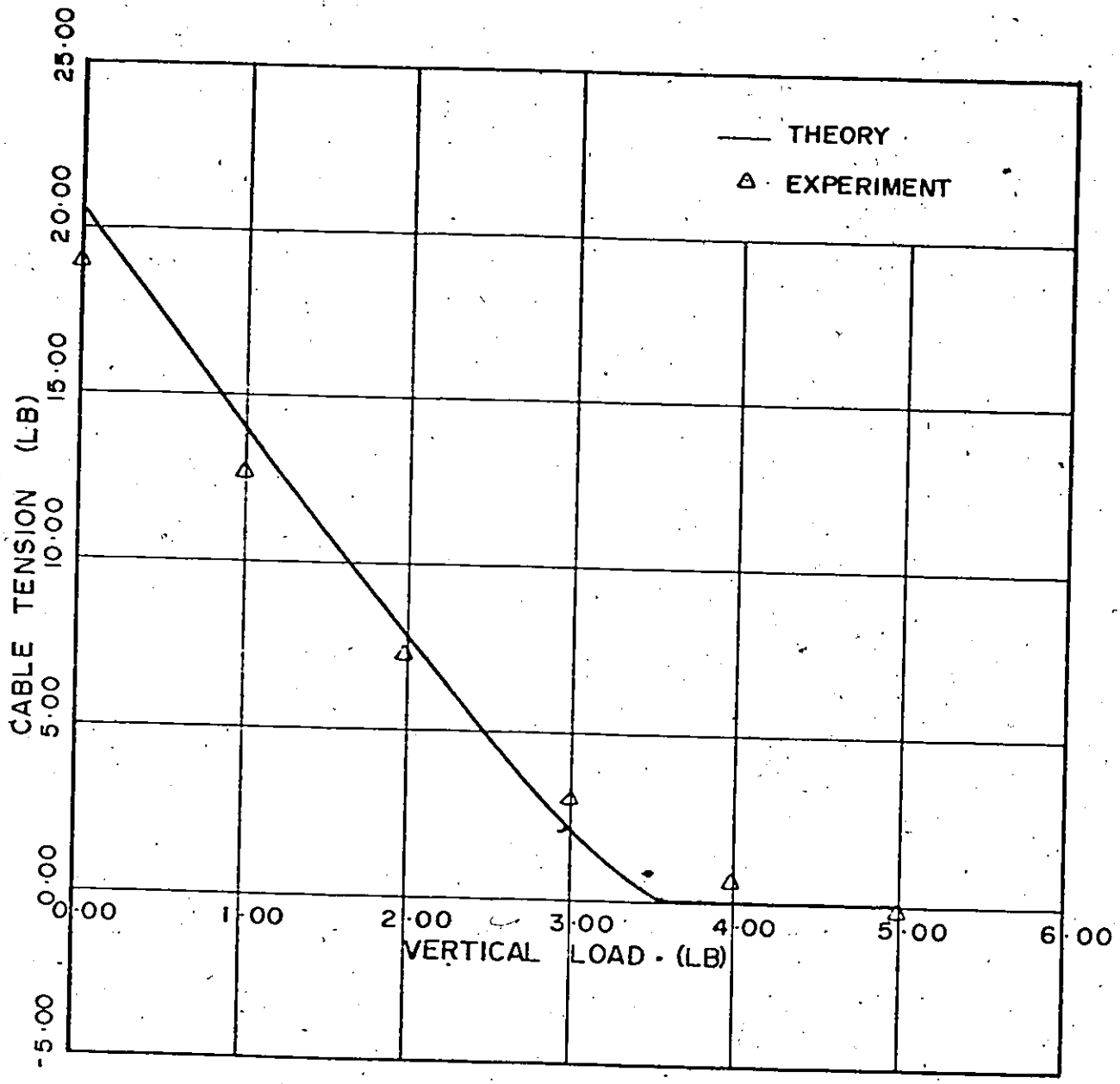

TENSION IN CABLE (3,4) OF SINGLE ROOF MODEL
(H=20 LB. UNIFORM LOADING)

Fig. (6-6)

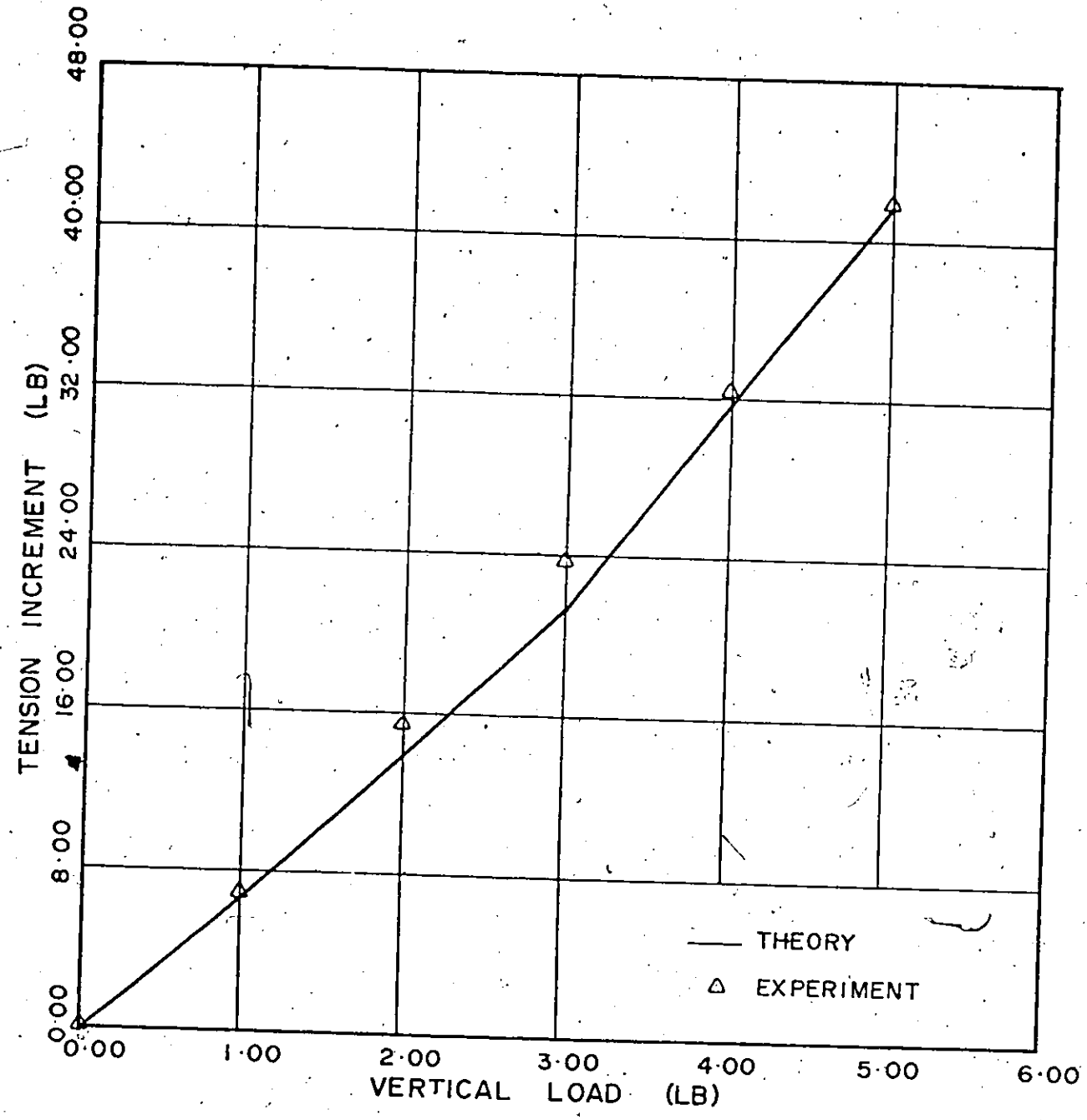

TEN· INC· IN CABLE (1, 1) OF SINGLE ROOF MODEL
(H=20 LB· UNIFORM LOADING)

Fig· (6-7)

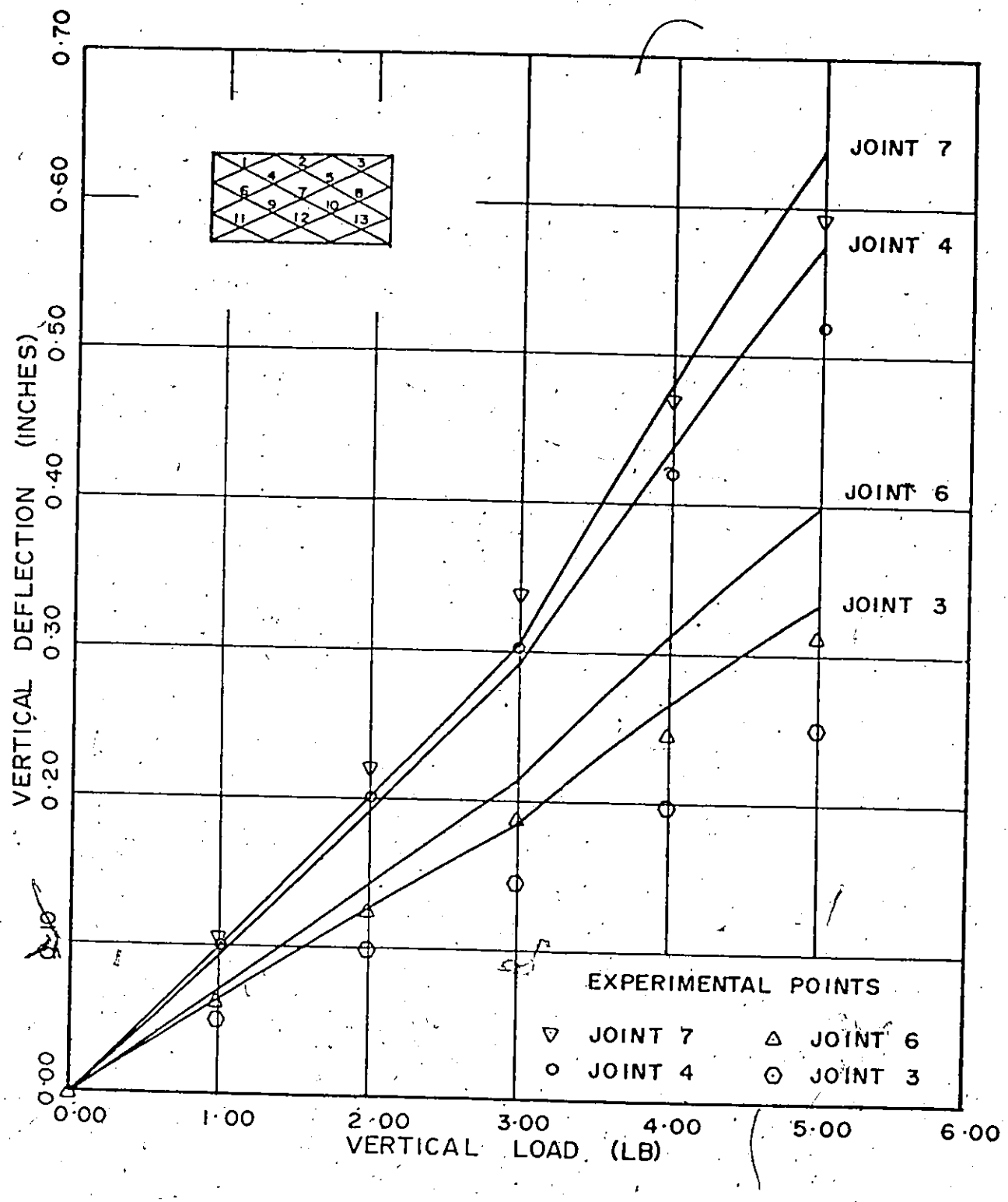

DEFLECTIONS IN SINGLE ROOF MODEL
(H=20 LB. UNIFORM LOADING)

Fig. (6-8)

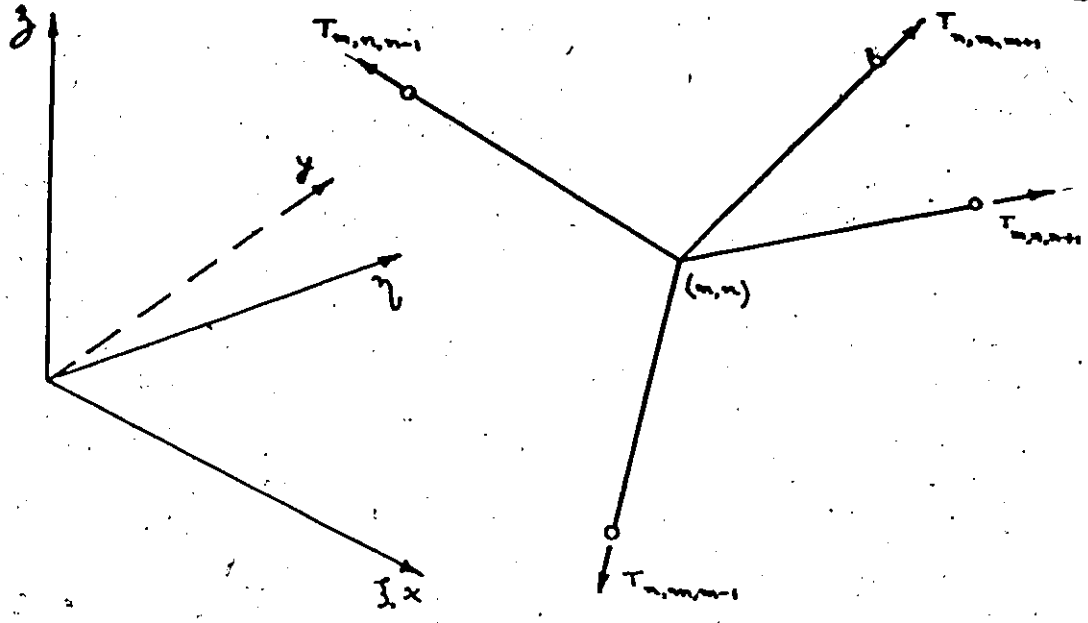

(a) AXONOMETRIC VIEW

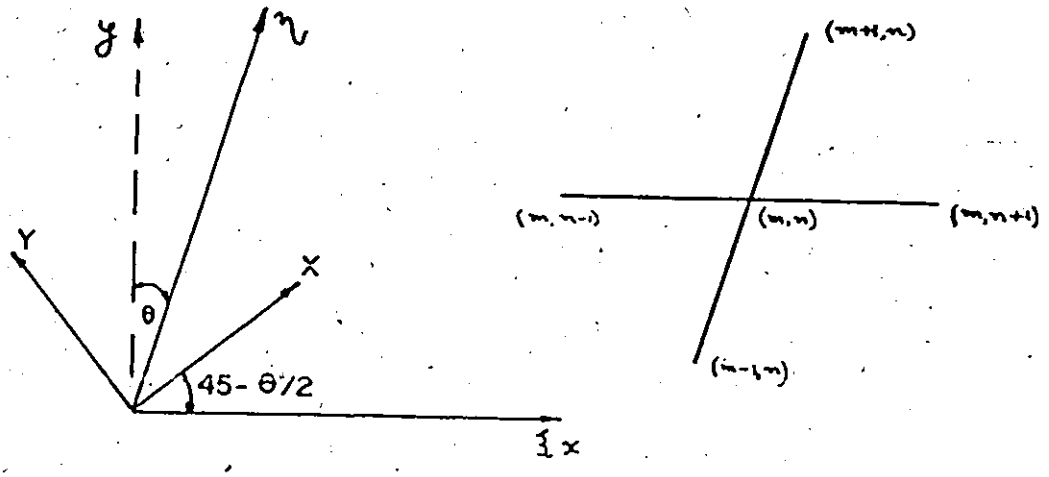

(b) PLAN

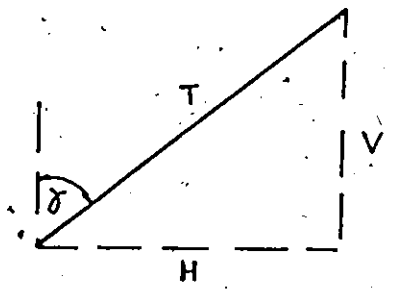

(c) ELEVATION OF A SINGLE SECTION OF CABLE

Fig. (A-1) VIEWS OF CABLE SEGMENTS MEETING AT A JOINT

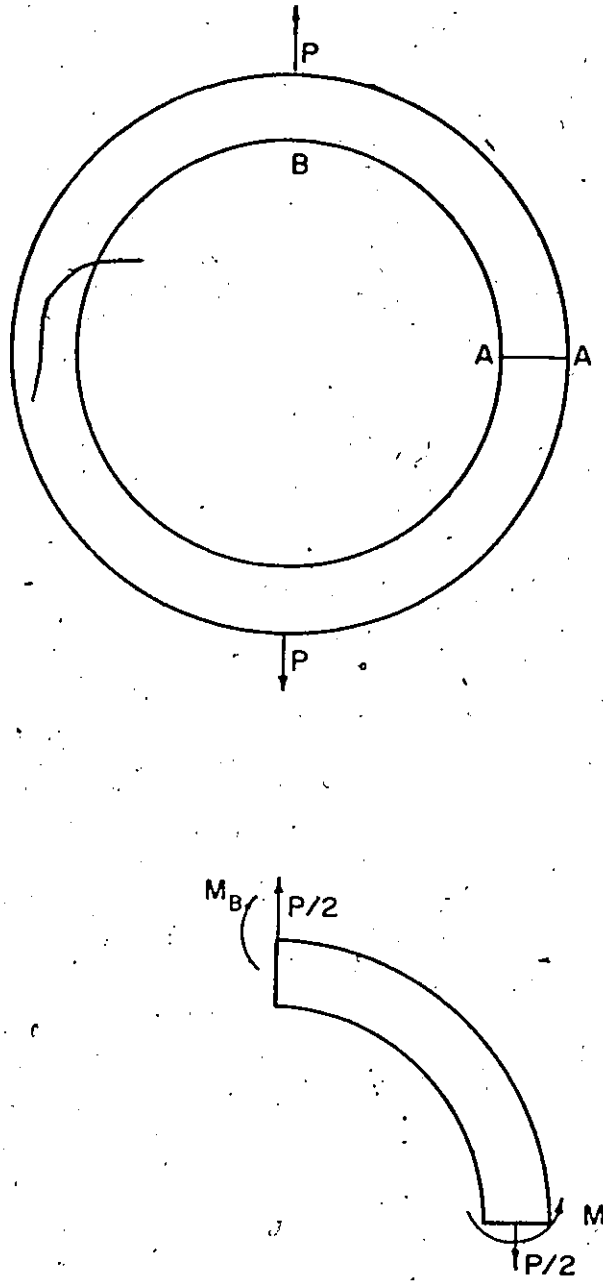

Fig. (B-1) CIRCULAR RING SUBJECTED TO TENSILE LOAD

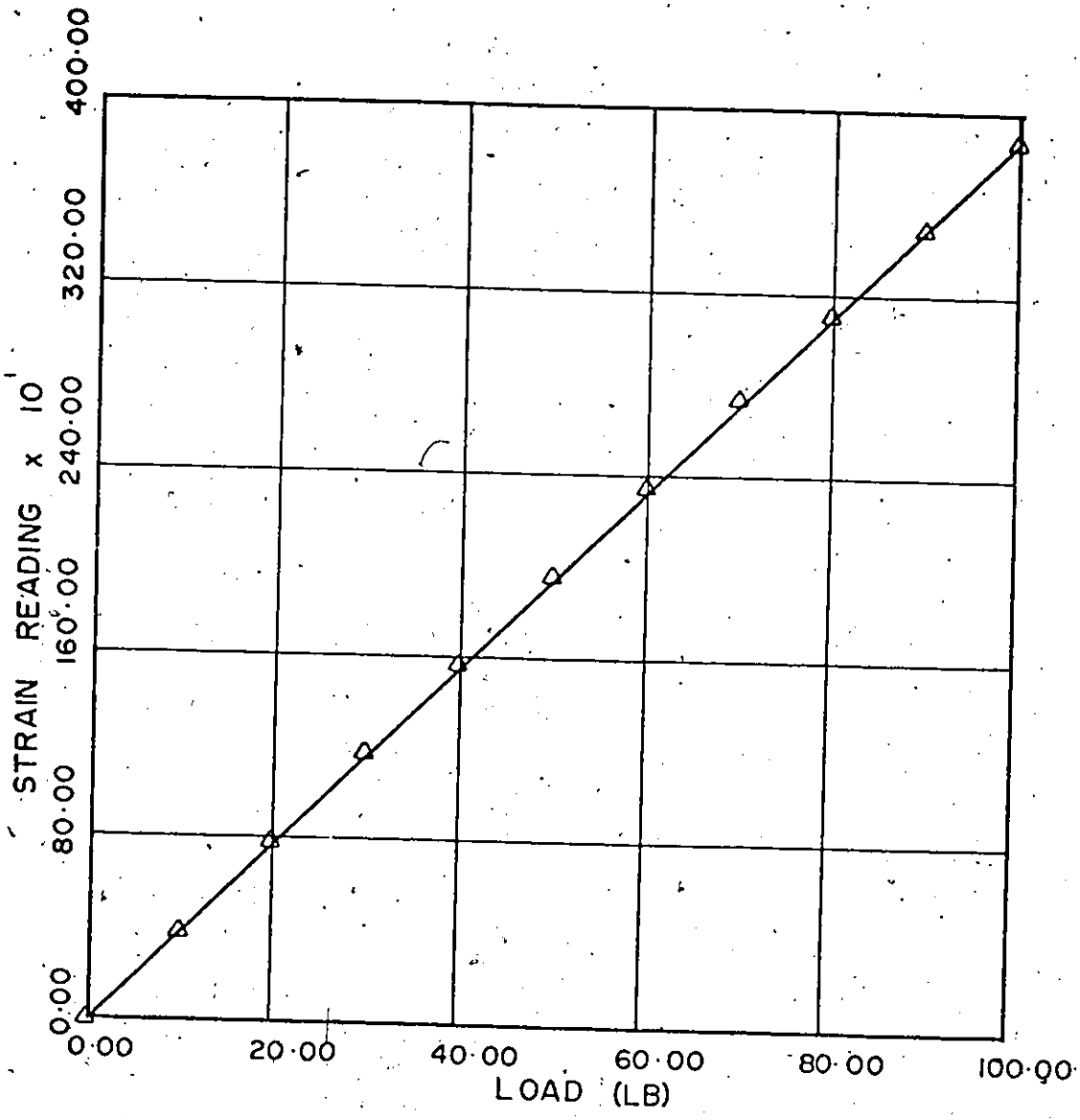

CALIBRATION GRAPH FOR RING NO. 1

Fig. (B-2)

VITA AUCTORIS

1939 Born September 29 in Jaffna, Ceylon.

1960 Entered the University of Ceylon.

1964 Graduated with Bachelor in Science of Engineering (Honours) degree from the University of Ceylon. Joined the Faculty of Engineering, University of Ceylon as an Instructor.

1965 Joined the Public Works Department of the Government of Ceylon as an Assistant Engineer.

1967 Awarded Commonwealth Scholarship by the Government of Canada for graduate study at the University of Windsor.

1968 Elected member of the Institution of Civil Engineers, London, England.

1969 Graduated with Master of Applied Science in Civil Engineering from the University of Windsor.